Sheffield Hallam University

A Sheffield Hallam University thesis

Performance Investigation of a Naturally Driven Building Ventilation Terminal

Ben Richard Hughes

A thesis submitted in partial fulfilment of the requirements of
Sheffield Hallam University
for the degree of Doctor of Philosophy

January 2009

This thesis is dedicated in loving memory of my older brother
Thomas Daniel Hughes, 4th May 1974 - 19th August 2001

Abstract

Naturally driven ventilation terminals (wind vents) offer a way of improving comfort conditions while reducing building carbon emissions. The device sits on top of the building, trapping the air at higher velocity and delivering it into the interior of the building. The current cross-ventilated design combines the velocity, pressure, and density of air to produce wind driven ventilation. Currently there is scarce research investigating the performance of these devices in the United Kingdom (UK).

This thesis provides a performance evaluation and optimisation of a commercially available building ventilation terminal (a benchmark) in the UK. A systematic review and optimisation of the device's geometrical components has been carried out using Computational Fluid Dynamics (CFD) and far-field experimentation.

An extensive literature review was carried out to provide the framework for this investigation. Building on existing (developed) research techniques, the knowledge gaps identified in this subject area, were isolated and examined thoroughly.

A new methodology for creating and dynamically modifying CFD models using complete wind vent geometry was devised. Using this technique the wind vent was subjected to systematic geometrical variation to establish the contribution of each component to the overall performance of the device.

The research used full scale Far field experimentation to validate the CFD models of the wind vent. The Far field experimentation provided greater accuracy (0 - 0.08m/s) for this application, when compared to other validation techniques such as wind tunnel experimentation (0 - 0.15m/s).

A new empirical methodology was devised for predicting the airflow through a wind vent. The empirical method was based on two dimensionless coefficients (0.44 and 0.3) found through the CFD experimentation research carried out.

The investigation established the device is capable of meeting current British Standards Institute (BSI) guidelines, and is therefore suitable for UK applications. The BSI recommended 0.8L/sec of fresh air per m^2 floor area. The benchmark wind vent geometry delivered 1.1L/sec per m^2 of floor area with an external wind speed of 1m/s (UK average was 4.5m/s).

The key geometrical components (in isolation) were identified as the louver angle, distance between louvers and the number of louvers (now subject to patent number 0809311.4). Each of these geometrical variations provided an increase in performance over the benchmark case in the range of 27 - 45%. An optimum configuration of these parameters did not deliver the same increased performance range as the isolated case. However the optimised combination case increased the internal air movement rate using 50% less material than that of the benchmark geometry.

Preface

The work presented in this thesis was carried out between November 2006 and January 2009 in the Materials Engineering and Research Institute, Sheffield Hallam University.

The work described in this thesis is, to the best of my knowledge, original except where reference has been made to others, and no part of it has been submitted for an award at any other College or University

As a result of this research the following journal papers have been published:

HUGHES, B. R. and GHANI, S. A. A. (2008). Investigation of a wind vent passive ventilation device against current fresh air supply recommendations. *Energy and buildings,* 40 (9), 1651-1659.

HUGHES, B. R. and GHANI, S. A. A.(2009) A numerical investigation into the effect of wind vent dampers on operating conditions. *Building and environment,* 44 (2), 237-248.

The author received the following award from the Whitworth Society, under the auspices of the Institution of Mechanical Engineers, in support of the work described in this thesis:

The Whitworth Senior Scholarship Award 2007/08

The unique geometrical configurations devised through this work are subject to UK patent application number 0809311.4.

Acknowledgements

Table of Contents

VII

List of Figures

XI

Nomenclature

A	= cross sectional area of the opening (m^2)
A_w	= effective area of the open window (m^2)
c	= flow coefficient [(m^3/s / Pa^n)]
C_d	= the discharge coefficient
C_p	= static pressure coefficient
C_{p-ww}	= wind pressure coefficient of windward surface location (positive)
C_{p-lw}	= wind pressure coefficient of leeward surface location (negative)
$C_{p-inlet}$	= static pressure coefficient at the inlet
$C_{p-exhaust}$	= static pressure coefficient at the outlet
c_1	= coefficient depending on window opening or position of mass flow rate as indicated
c_2	= buoyancy constant (0.0035 m/s^2 K) or position of mass flow rate as indicated
c_2	= is the pressure-jump coefficient (1/m) in Equation 5-1.
c_3	= wind constant (0.01 m^2/s^2) or position of mass flow rate as indicated
c_4	= position of mass flow rate as indicated
g	= gravitational acceleration (9.81 m/s)
H	= height of the opening (m)
h_L	= head loss (m/s)
k	= turbulence kinetic energy (m^2/s^2)
K_L	= loss coefficient
K_1	= constriction loss coefficient
K_2	= expansion loss coefficient
$\dot{m}$	= mass flow rate (kg/s)

Δm	= thickness of the medium (m)
n	= flow exponent
Δp	= pressure difference across the opening (Pa)
P_0	= standard pressure condition for dry air (101325 Pa)
p_s	= stack pressure (Pa)
p_w	= wind pressure (Pa)
p_{ww}	= positive windward pressure (Pa)
p_{wl}	= negative leeward pressure (Pa)
Δp_{inlet}	= inlet differential pressure (Pa)
$\Delta p_{internal}$	= internal differential pressure (Pa)
$\Delta p_{exhaust}$	= exhaust differential pressure (Pa)
Δp_s	= differential pressure losses of the solar collector (Pa)
Δp_i	= differential inlet pressure (Pa)
Δp_d	= distributed differential pressure (Pa)
Δp_e	= exit differential pressure (Pa)
Q	= mean volume airflow rate (m^3/s)
R	= ideal gas constant (8.3145 J/mol K)
t	= time (s)
T	= thermodynamic temperature (K)
T_0	= standard temperature condition for dry air (273K) or a given outdoor reference temperature
T_i	= indoor temperature (K)
ΔT	= mean temperature difference, outdoor - indoor (K)
u	= x - momentum (kg m/s)
V	= velocity (m/s)

v	= y - momentum (kg m/s)
v_{eff}	= effective wind speed (m/s)
v_r	= site mean wind speed (m/s)
v	= time-mean wind speed at a given level (m/s)
w	= z - momentum (kg m/s)
x	= direction vector
y	= direction vector
z	= direction vector
z	= vertical direction (m)
z_1	= point in the vertical direction (m)
z_2	= point in the vertical direction (m)
Δz	= difference between two vertical points (m)
ρ	= fluid density (kg/m^3)
ρ_0	= standard density condition for dry air (1.29 kg/m^3) or a given outdoor reference density
ρ_i	= indoor density (kg/m^3)
$(\dfrac{\rho v_r^2}{2})$	= kinetic energy per unit volume of reference wind velocity (kg m/s^2)
ε	= dissipation rate
α	= permeability of the medium (m^2)
μ	= fluid dynamic viscosity (kg/ms)

Abbreviations

Sick Building Syndrome	SBS
Display Energy Certificate	DEC
United Kingdom	UK
Home Information Packs	HIP
British Standards Institution	BSI
Building Services Research Information Association	BSRIA
Heating Ventilation and Air Conditioning	HVAC
Computational Fluid Dynamics	CFD
Reynolds Averaged Navier- Stokes	RANS
Japanese Building Research Institute	JBRI
Chartered Institution of Building Services Engineers	CIBSE
Building Research Establishment	BRE
Robust Parameter Design	RPD
Integrated Building Management System	IBMS
Air Handling Unit	AHU
Indoor Air Quality	IAQ
Fog Liquid Glycerin	FLG

Chapter 1 Introduction

Ventilation of occupied spaces places a vital role in the health and well-being of both the occupants and the building itself. Well publicised building related illness such as Sick Building Syndrome (SBS) have increased public awareness of the necessity of a fresh air supply to their places of work.

There are two methods of ventilating occupied spaces, natural ventilation and mechanical ventilation. Typical examples of natural ventilation are windows and doors. Mechanical ventilation uses equipment to generate or move airflow. Typical examples of mechanical ventilation are fans and air conditioning units. Architects in conjunction with building service engineers are charged with the duty of ensuring adequate fresh air supply to buildings.

As shown in Figure 1-1, the most common and widely distributed solution to this issue is the use of mechanical air handling units and air conditioning systems. These systems are effective and reliable and offer reassurance to the designer that the fresh air requirements will be served adequately.

Figure 1-1 Typical cross section of an air handling unit [Iklem circa 2000]

1

Mechanical ventilation systems require a significant proportion of the building's energy supply. Until recently, the energy usage of buildings has not been an issue due to energy being in ready supply and relatively cheap to obtain. However, a combination of diminishing energy supplies and international treaties to cut carbon emissions have seen energy prices soar and government legislation tighten.

The Kyoto protocol came into force on 16th of February 2005 with the United Kingdom (UK) government pledging to reduce its greenhouse gas emissions to 12.5% below 1990 levels by the year 2012.

Museums, galleries, town halls and government buildings must be energy rated and display them to the public in the form of a Display Energy Certificate (DEC). Visitors will be able to see the annual carbon emissions of each building as a measure intended to encourage energy efficiency improvements to public buildings, help cut costs to the public purse and lead the way in cutting carbon emissions. The ratings, based on the consumer-products energy labelling system, apply to all public buildings, shown in Figure 1-2.
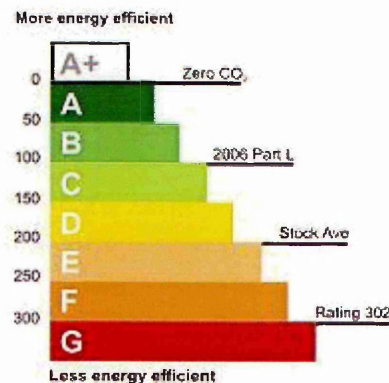
Figure 1-2 Building ratings system [Energy report circa 2005]

2

The regulations stipulate that Energy Performance Certificates for homes must be included in Home Information Packs (HIP), which the government says will help home buyers reduce energy costs by an estimated £300 per year [Energy Performance of Buildings Regulations, 2007].

The UK housing Minister further underlined the government's commitment, "We must all work together to cut carbon emissions. More than 40% of carbon emissions in the UK come from buildings" [Clover 2007].

Mechanical ventilation systems are an integral component of building design and performance. These systems offer a substantial opportunity for reducing energy consumption and increased overall building's performance to engineers and designers.

Natural ventilation refers to the fresh air supply from outdoor (the macro-climate) to indoor (the micro-climate) through non-mechanical methods. The British Standards Institution (BSI) has devised a code of practice for supplying fresh air via non-mechanical means to ensure that this approach is not to the detriment of the building's occupants [British Standards Institution 1991]. Non-mechanical methods are commonly employed in buildings by strategic positioning of openings to allow fresh air to enter and the inclusion of air bricks and roof vents to allow the stale air to exhaust.

The orientation of buildings can be used to gain advantage at the design stage. Spaces prone to over heating, like offices, can be built with a north-facing aspect to reduce the need for air conditioning [Bone, 2007]. Building south-

facing homes maximises so-called "passive solar gain", using the sun to heat rooms wherever possible.

The UK Prime Minister (2007), pledged to build five new "eco-towns" including 100,000 new homes in carbon neutral communities built on old industrial sites. Buyers of new zero carbon homes qualify for tax relief on stamp duty. The government says the regulation is designed to "encourage micro-generation technologies" [BBC News 24 2007A]. House builders are actively seeking to integrate these technologies into new developments to gain a competitive advantage.

Wind vent
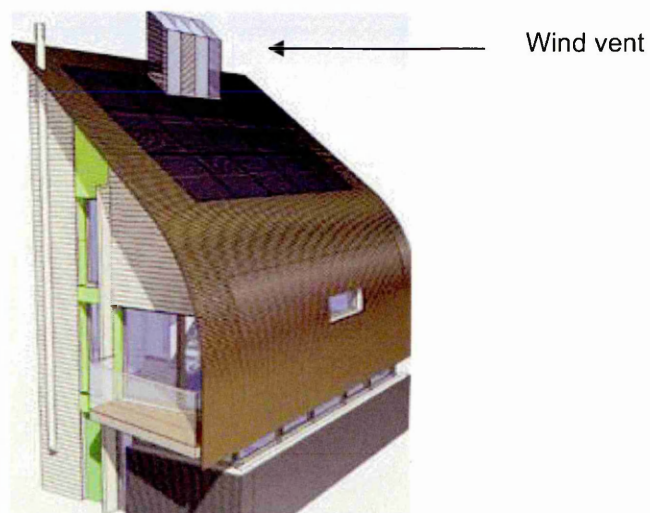
Figure 1-3 Illustration of the United Kingdoms first "Eco-home" [BBC News 24 2007]

In 2007, the UK unveiled its first zero emission home that set the environmental standard for all new homes in the future. The design, unveiled at the offsite exhibition in Watford, meets rules to be applied in 2016 that aim to make UK homes more energy efficient (Figure 1-3). Among the features in the house is a roof mounted wind vent for summer ventilation [BBC news 24 2007B].

4

Eco-technologies are being driven by the government to achieve its Kyoto commitments. The eco-town development includes the use of wind vent devices to provide summer ventilation, a system that is common in hot, arid countries but relatively new in the UK. This could be due to the over reliance on mechanical systems or the climatic differences making the device unsuitable for the UK.

Some places have special climates because they are near a change of surface, as at coasts and near mountains or local water bodies [Lamb 1976]. These sources of topographical modification of the general climate give rise to characteristic differences of climate between eastern and western countries. It is clear that the application of a predominantly eastern eco-technology to the UK climate requires careful consideration and thorough investigation.

1.1 The wind vent

A roof mounted natural ventilation device offers a way of improving comfort conditions while reducing building carbon emissions [Building Services Research Information Association 2005]. The device sits on top of the building, trapping the air at higher velocity and delivering it into the interior of the building. The current cross-ventilated design combines the velocity, pressure, and density of air to produce the wind driven ventilation.

Commercial wind vents are divided into quadrants, which allow fresh air to enter as well as stale (used), air to escape irrespective of the prevailing wind direction. There are two driving forces for the wind vent. The primary force provides fresh air driven by the positive air pressure on windward side, exhausting stale air

5

with the assistance of the suction pressure on the leeward side, shown in Figure 1-4.

+ Windward

- Leeward

Fresh Air In

Stale Air Out
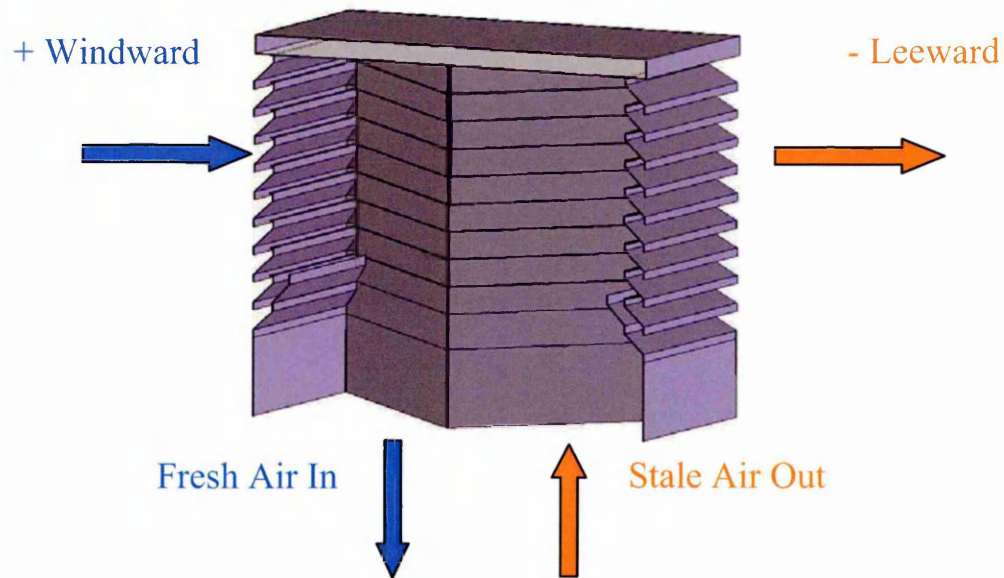
Figure 1-4 Cross section of a wind vent, showing the effect of external wind pressure

The secondary force is temperature driven and termed "the stack effect". The density of air is less as temperature increases causing layers of air to be stacked. The internal and external temperature difference (micro to macro climate) drives the airflow through the ventilator. If the external temperature is lower than the internal temperature, then the buoyancy of the warmer air causes it to rise and exhaust through the unit.

1.2 Research objectives

The main objective of this work is to systematically examine the components of a wind vent and their relative contribution to its effectiveness as a fresh air supply system in the UK. Moreover, it is to assess the ability of a standard

commercially available product to meet BSI guidelines, and to determine a clear methodology for optimising the performance of the unit. Furthermore, to apply this methodology to enhance the capabilities of integrating the system, within building services, and promote its use as a viable eco-technology. This research work will:

- Verify and validate Computational Fluid Dynamic (CFD) model's analysis for the study of a wind vent device

- Collect high quality full-scale experimental data for CFD validation

- Demonstrate the devices ability to meet BSI guidelines

- Determine the key geometrical components to enhance performance of the unit

- Assess the suitability of the wind vent as an eco-technology for the UK

1.3 Methodology

Robust Parameter Design (RPD) is an approach to product realisation activities that emphasises choosing the levels of controllable factors, or parameters, in a process or product to achieve certain objectives [Montgomery, 2005]. This study used this general approach when designing the experiments to generate data in an efficient manner.

The parameters investigated (Figure 1-5) were the control damper angle, external louver angle, the number of external louvers, the distance between the external louvers, the effect of using cross dividers, the use of a low-powered fan, and an optimum configuration based on the preceding investigative results. In

7

each experiment, the measured response of the wind vent with respect to velocity, pressure, and internal air distribution was analysed.
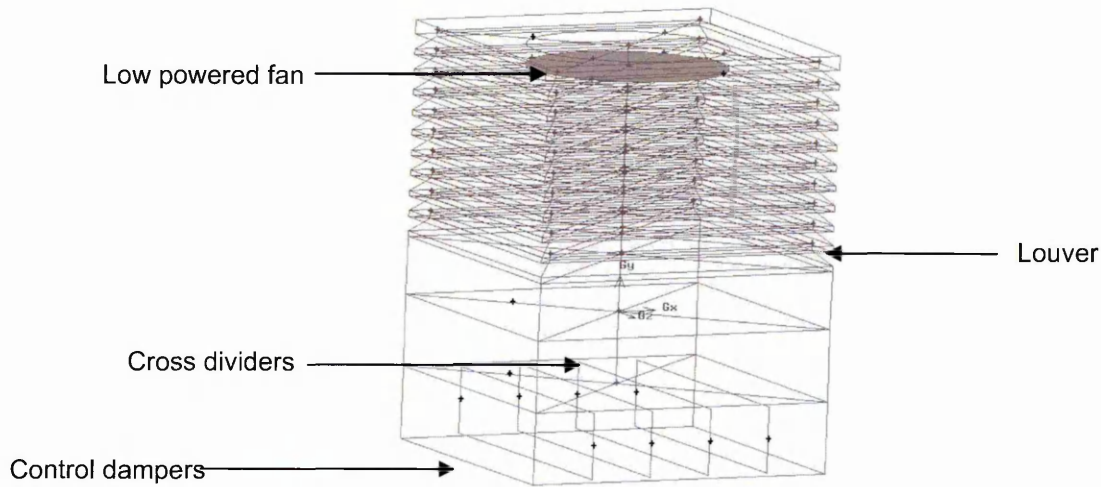
Figure 1-5 Identification of the wind vent component geometry

To achieve the research objectives, and complete the investigations, both CFD and full-scale experimental work were used and structured as illustrated in Figure 1-6.
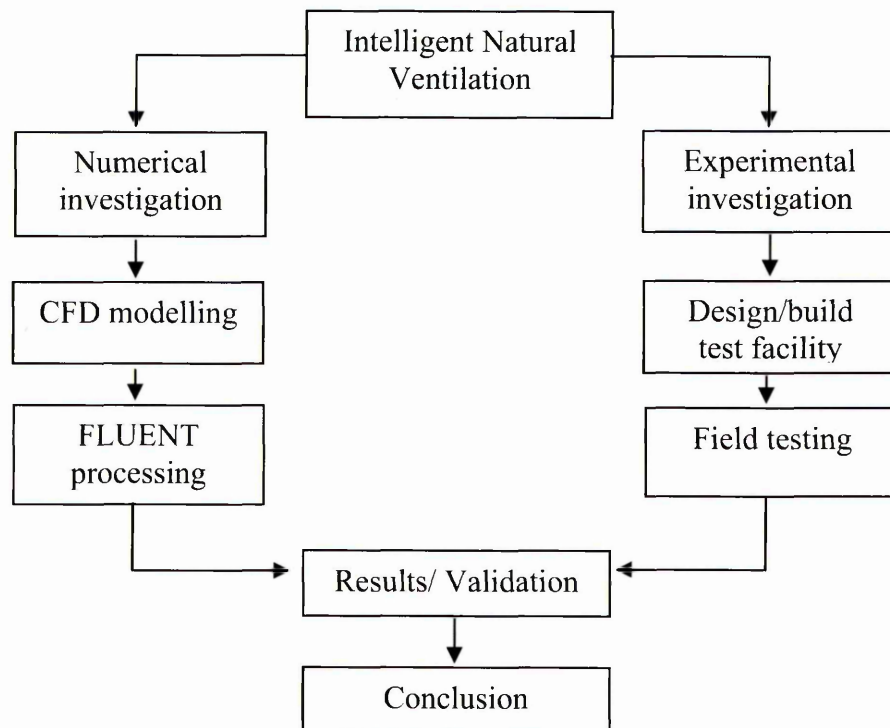
Figure 1-6 Structure of intelligent natural ventilation study

1.4 Thesis structure

The thesis is divided into nine chapters. Each chapter provides detailed information on the relevant subject area and its contribution to the research project as a whole. A summary of each chapter is listed below:

1. Introduction; provides the background to the research, and the requirement for further knowledge in this subject area. The wind vent is introduced with its basic operating principles, research objectives and methodology are defined.

2. Literature review; summarises the available literature in the general subject area, and research specific to wind vent devices. A comprehensive examination of published materials established suitable investigative tools and identified the research gap to be filled.

3. Natural ventilation; examines the physics of natural ventilation. The forces that occur during the process are presented and the empirical formulas to evaluate the effect of these forces are discussed.

4. CFD theory and modelling; describes the numerical algorithms used in CFD modelling and presents the simulation process. Introduces the computational domain, boundary conditions, and CFD techniques employed for this application.

5. CFD results; presents the results from the CFD investigations in tabular and graphical forms. The CFD results and the findings of each geometrical variation examined are discussed thoroughly.

6. Experimental set-up; describes the experimental work carried out, including the instrumentation, and the complete experimental model.

7. Experimental results; presents the results from the experimental investigations in tabular and chart forms. The experimental results and the findings of each geometrical variation examined are discussed thoroughly.

8. Validation of CFD model; compares the CFD results and experimentation work carried out. The accuracy of the CFD simulations is established. The level of accuracy is validated against other published work in this area.

9. Conclusion and recommendations; the research objectives are evaluated against the research findings. Potential future research in this subject area is identified and presented.

1.5 Summary

This chapter presented the background to this research, and introduced the wind vent device under investigation. The research objectives were clearly identified as was the methodology. The thesis structure has been introduced with a brief summary of each chapter.

2.1 Introduction

The aim of this chapter is to review previous research and literature relevant to the current study of a natural ventilation device, the wind vent. This chapter is followed by a discussion of the physics associated with natural ventilation and the fundamentals of computational fluid dynamics in Chapter three and Chapter four respectively. The literature review consolidates methodically, related work in the field on natural ventilation and in particular the wind vent device. In order to identify the research gap to be filled through this investigation, a review has been conducted to establish proven simulation and experimental techniques.

2.2 Natural ventilation in buildings

Traditionally natural ventilation was the way all buildings were ventilated. The use of windows and doors and also the air leakage rate, due to the materials of construction, provided adequate fresh air supply. However, as insulation and construction materials improved the air tightness of the building envelope, a mechanical solution became a requirement. Mechanical ventilation has numerous drawbacks leading engineers and architects to revisit natural ventilation techniques.

"Natural ventilation seems to provide an answer to many complaints from users concerning mechanical ventilation. The main complaints are that mechanical systems appear to be noisy, to create health problems (sick building syndrome is usually associated with mechanical Heating Ventilation and Air Conditioning HVAC systems), to require routine maintenance and to consume energy. In contrast, natural ventilation is preferred by the occupants, since it is energy

efficient (no need of a mechanical system), it can be easily integrated into buildings and it provides a healthier and more comfortable environment if integrated correctly" [Santamouris and Allard, (2002)].

The British Standards Institution (1991) gives recommendations on the principles which should be observed when designing for the natural ventilation of buildings for human occupation. The standard does not attempt to address thermal comfort aspects of ventilation such as indoor air movement, temperature stratification, or exact position of ventilation openings. However, it does provide recommended ventilation rates/fresh air supply according to occupancy levels and floor area.

Letan *et al.* (2003), investigated the use of natural convection in a vertical heated duct, as part of a multi-storey structure. Experimental and computer simulations were performed in a scaled-down laboratory model with an electrically heated plate used as the transfer medium. The authors compared both simulation and experimentation measurements of both temperature and velocity within the duct and achieved good correlation. Following this experimentation and validation a simulation model was developed of a full scale five storey building with a duct heated by solar irradiation (Figure 2-1).
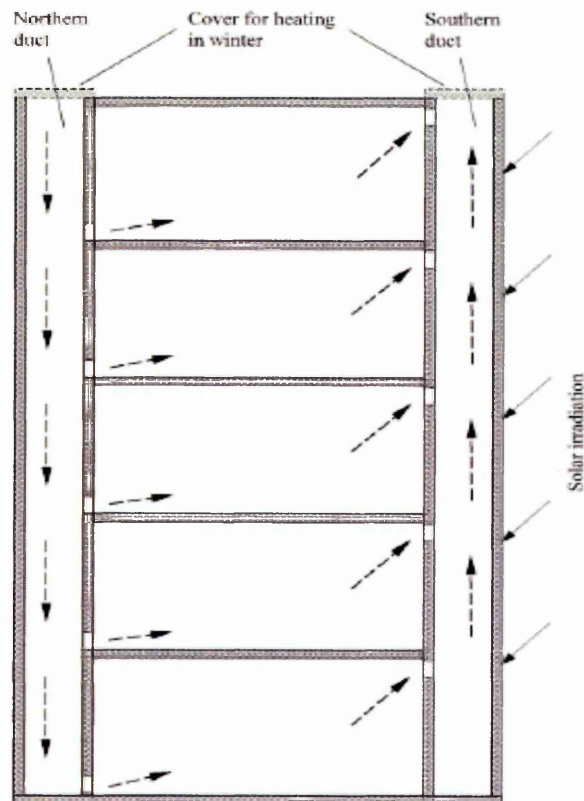
Figure 2-1 Five storey building configuration [Letan *et al.* (2003)]

The results of this study showed that, even at low solar irradiation fluxes, ventilation was achieved in summer and heating in the winter. This investigation concluded that utilising natural convection as a ventilating and heating method was achievable.

Gratia *et al.* (2004), investigated the use of natural ventilation to cool narrow office buildings. The study used simulation to compare different window sizes and locations to the airflow rates throughout the space. Different types of ventilation strategies were analysed, namely single sided and cross ventilation, (discussed in more detail in Chapter 3). Gratia *et al.* (2004) showed that the type of ventilation strategy employed must be matched to the environment in which the building is situated. Furthermore, the employment of single-sided

14

ventilation during the day reduced the cooling load by 30% with cross-ventilation only achieving a 10% reduction.

Priyadarsini *et al.* (2004) assessed the status of natural ventilation in a typical four-room flat in a high rise residential building. The authors created a scale model of the flat and conducted wind tunnel testing (Figure 2-2).
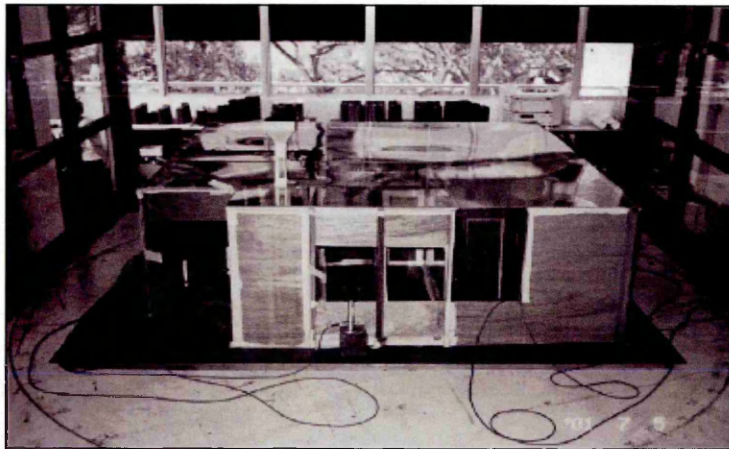
Figure 2-2 Apartment model for the study, scale 1:5 [Priyandarsini *et al.* (2004)]

The natural ventilation of the model was provided using two different stack techniques, passive and active, (which are discussed in Chapter 3), the active stack ventilation utilised a low powered fan. The study showed that the passive stack, incorporating the principle of airflow due to buoyancy, does not enhance the air velocity within the flat. The active stack, (Figure 2-3) which operates on the suction effect induced by the fan fixed at the top of the stack, substantially increased the air velocity within the flat.
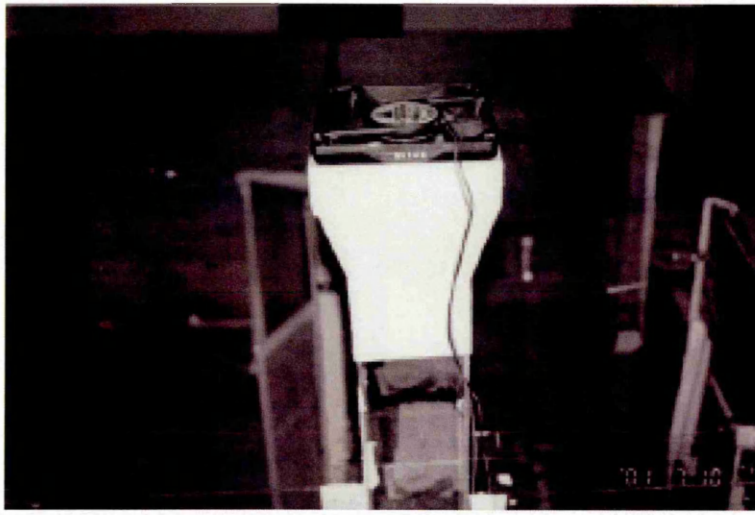
Figure 2-3 Extract fan at the top of the active stack [Priyadarsini *et al.(*2004)]

In his research, Yang (2004), carried out CFD and field testing on a full-scale naturally-ventilated building. The natural ventilation was provided by the careful positioning of openings (windows and doors) to capture the effects of the prevailing wind and enhance the internal air movement rate. The work used extensive CFD modelling for natural ventilation which was successfully validated during the field testing element of the research project.

Graca *et al.* (2005), presented an analysis of the thermal behaviour of the San Diego children's museum. To determine a ventilation strategy the building was analysed using CFD software in conjunction with weather analysis software. The museum is designed as a naturally ventilated building with no mechanical heating or cooling. The exhibition space consists of two galleries on the first floor and an atrium that extends over the two floors (Figure 2-4).
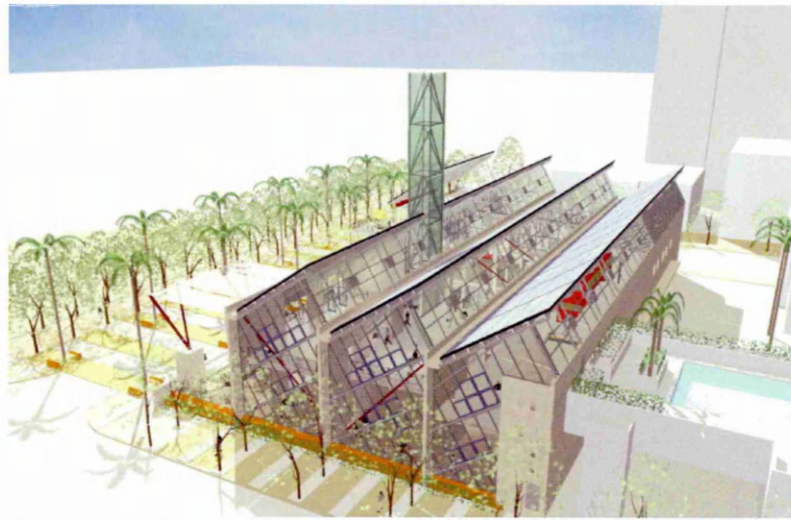
Figure 2-4 Illustration of the San Diego Children's Museum [Urban living (circa 2000)]

Initial CFD simulations of this solar stack-driven arrangement compared with climatic data led to predictions of significant periods of overheating in the museum. It was decided to use wind as a supplement to the stack driven flow. Additional openings were placed in the facade facing the predicted prevailing wind (sea breeze in this case). The second analysis led to a decrease in predicted hot hours and the results suggested that the building would operate satisfactorily.

Shun and Ahmed (2007), investigated the use of a hybrid roof mounted ventilation device. The device combined solar and wind energy to provide natural ventilation. The authors used wind tunnel testing to compare the ventilation capabilities of three devices. The hybrid device consisted of a wind driven turbine ventilator combined with a single stage axial fan, driven by an electric motor, which received power from a solar cell.

The hybrid device was compared to the wind driven and the solar driven devices to determine its effectiveness in a wind tunnel. The results showed that the hybrid device had increased the performance against both the standard

17

devices. The work concluded that a combination of wind and solar power presents the most effective strategy in this application.

2.3 Mathematical models for natural ventilation of buildings

Hunt and Linden (1999), used experimental and theoretical investigations to analyse the fluid mechanics of natural ventilation-displacement by buoyancy-driven flows. A major result of this work was the identification of the form of the non-linear relationship between the buoyancy and wind effects. The study showed that there is a Pythagorean relationship between the combined buoyancy and wind-driven velocity. The velocities which are produced by buoyancy and wind forces act in isolation (Figure 2-5).
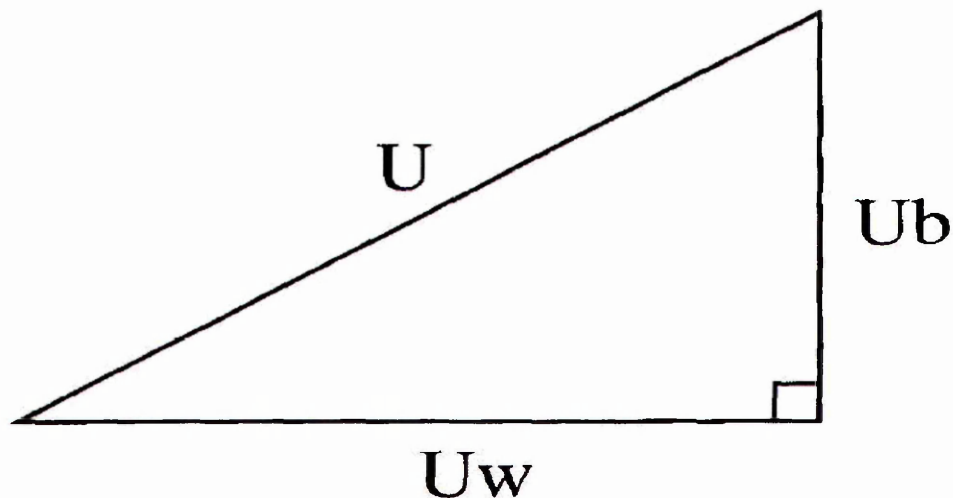
The 'natural ventilation triangle' for buoyancy-driven displacement flows assisted by wind. The base and vertical sides of the triangle are set by the magnitudes of the wind and buoyancy produced velocities, U_w and U_b, respectively. The length of the hypotenuse determines the total fluid velocity U produced by buoyancy forces reinforced by wind.

Figure 2-5 The natural ventilation triangle [Linden and Hunt (1999)]

This relationship enables the prediction of airflow capabilities in buildings using natural ventilation.

18

Li and Delsante (2001), derived analytical solutions for calculating natural ventilation flow rates and air temperatures in a single-zone building. The solutions are based on two independent variables, heat source strength and wind speed. The indoor air temperatures were neglected. Li and Delsante introduced three air change parameters to characterise the effects of the thermal buoyancy force, the envelope heat loss, and the wind force respectively (Figure 2-6).
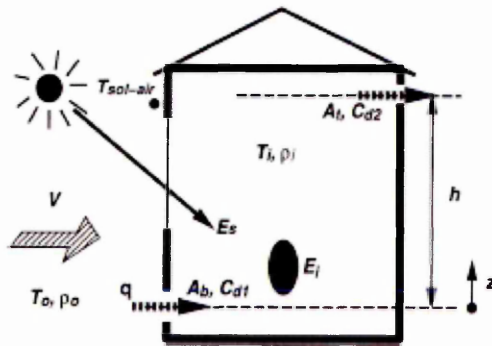
Figure 2-6 Illustration of the three air change parameters [Li and Delsante (2001)]

The work presented non-dimensional graphs for calculating ventilation flow rates, air temperatures, and for sizing ventilation openings. However, the wind force can either assist the buoyancy force or oppose the airflow. For assisting wind the flow is always upwards and the analytical solutions are less complex. For opposing winds, the flow can be either upwards or downwards depending on the relative strengths of the two forces. The opposing force from the wind introduces severe complexities to the analytical solutions, to an extent where they may no longer be considered stable.

Parker and Teekaram (2005), produced a guide to wind driven natural ventilation systems. This work was carried out by the Building Services Research and Information Association (BSRIA). The guide presents a

19

methodology for sizing wind vent devices for the application of building ventilation. The presented formulae are based on the British Standards Institution (1991). In the BSRIA guide, additional formulae are presented for building characteristics such as heat gains and air leakage. The formulae use assumed values for the pressure distribution, and are applied in isolation to combat heat gain and air leakage. Although the guide presents a series of case studies, the mathematical formulae are not evaluated and no indication is given as to the accuracy of the results.

Lomas (2007), presented a methodology of simple equations which may be used at the design stage of a naturally ventilated building. The equations were developed through practice-based research to design three large educational buildings (Figure 2-7). The buildings evolved through three stages: naturally ventilated, passive down-draught cooling, and finally additional HVAC support.
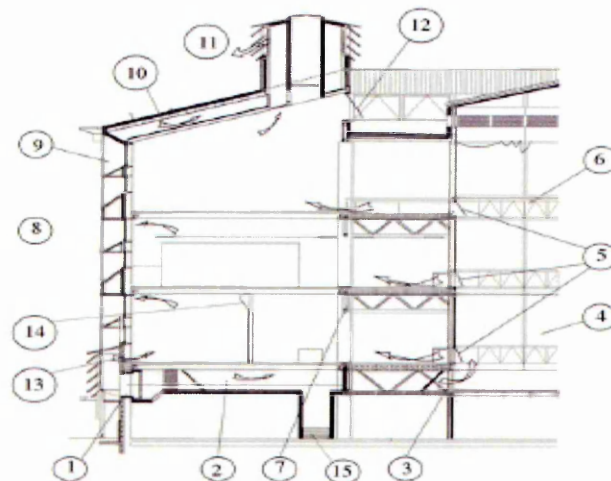
1   Fresh air inlet to plenum.
2   Fresh air supply plenum.
3   Plenum outlet into lightwell.
4   Lightwell supplies fresh air.
5   Low-level, top hung windows provide air to floors.
6   Horizontal glass lens seals lightwell.
7   Open truss permits airflow.
8   Air outlets at high level with dampers.
9   Insulated steel exhaust duct in deep façade.
10 Plenum connects ducts to terminations.
11 Air exhausts via louvered terminations with damper.
12 Clerestory windows provide additional top floor ventilation.
13 Dedicated supply from plenum to perimeter offices.
14 Operable windows for office occupants.
15 Downfeeds from plenum to basement area.

Figure 2-7 The Harm A Weber Library natural ventilation strategy [Lomas (2007)]

The case studies showed that, with the proposed calculation methods used at the design stage of the building, that the ventilation strategy may be adequately predicted. The strategy then implements a more efficient usage of mechanical assistance.

Elmualim (2006A), investigated the use of equations proposed by British Standards Institution (1991) for the application of a wind vent device. The equations were evaluated against experimental testing in a seminar room in the University of Reading UK (Figure 2-8).

Figure 2-8 Position of wind vent device in seminar room [Elmualim (2006A)]

The wind vent was also evaluated against the use of a standard openable window. The window and wind vent had equivalent opening areas to determine the advantage over traditional natural ventilation techniques. The results of the experimental testing showed the mathematical formula consistently over-estimated the ventilation rate. Elmualim also concluded that the wind vent device provided a substantially greater ventilation rate than an equivalent area of openable window.

2.4 Simulation models for wind vent device

Ayad (1999), investigated the use of CFD, specifically the k-ε turbulence model (discussed in Chapter 4), to evaluate the natural ventilation properties of a room with different opening configurations. The positioning of openings in relation to one another (single sided/cross ventilation) enhances or reduces the mean velocity at certain locations within the room. The results of this study were validated against experimental results. The results showed the importance of methodical ventilation design and the suitability of the k-ε model as a CFD tool in natural ventilation evaluation.

Chen (2004), investigated the suitability of available computational tools for studying the wind effect in building design. The techniques compared in this study were model mock-up using a wind tunnel, nodal/zonal models, and CFD. From the available techniques Chen concluded that CFD was the most efficient tool for building environmental design. This conclusion was based on affordability, accuracy and informative display method (Figure 2-9).
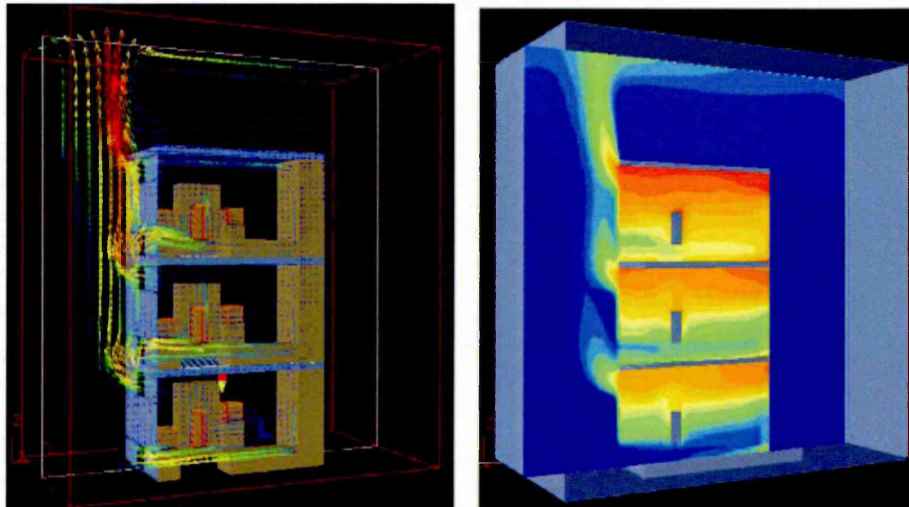
Figure 2-9 CFD results of stack effect in a high rise building [Chen (2004)]

The work also illustrates a number of applications where CFD has been utilised in environmental building design. These include, airflow around a building complex, cross-ventilation in a building, single-sided ventilation in a building, and using building shape to prevent draft (due to cold winds) in a high rise building site.

Ahmed (2004), used FLUENT, a commercially available CFD package, to study the thermal behaviour of a middle-eastern wind tower house. For the investigation, a simulation model of the Al-Bastakia tower house in Dubai was created. The cooling performance of the house is affected by two main parameters, strength and direction of the wind. Full scale 3D models of the tower were simulated using varying wind speed and directions. The purpose was to determine the flow path through the building. The CFD results showed that the positioning of windows and the tower itself, with respect to wind direction, must be carefully considered. The cooling of these houses utilises the wind energy. The strategic location of the tower and windows utilises this energy in the most efficient manner.

Evola and Popov (2006), investigated two different CFD turbulence modelling approaches to evaluate natural ventilation in buildings. The two turbulence models compared are the k-ε model and the Reynolds Averaged Navier- Stokes equation (RANS). The results of both models were compared with experimental work and found to be in agreement with good correlation between both sets of results. The work found that the k-ε model was less accurate than the RANS model in areas close to vertical planes (wall areas). The authors concluded that the RANS model was more suitable for this application (natural ventilation in

23

buildings). However, wall theory in CFD is well documented and careful considerations must be made when applying the boundary conditions for this application. Incorrectly applied boundary conditions may explain the increased error when using the k-ε model.

Elmualim (2006B), used CFD modelling to evaluate the performance of a wind vent device and compared the results to wind tunnel experimentation. The study constructed a computational model of a commercial wind vent device. Due to the complexity of the geometry, the louver sections were reduced to porous flat surfaces, with an orifice flow calculation used in the solver to represent resistance to airflow. In addition, the damper and diffuser sections were omitted for the same reason. No compensating calculation was used in the solver (Figure 2-10).
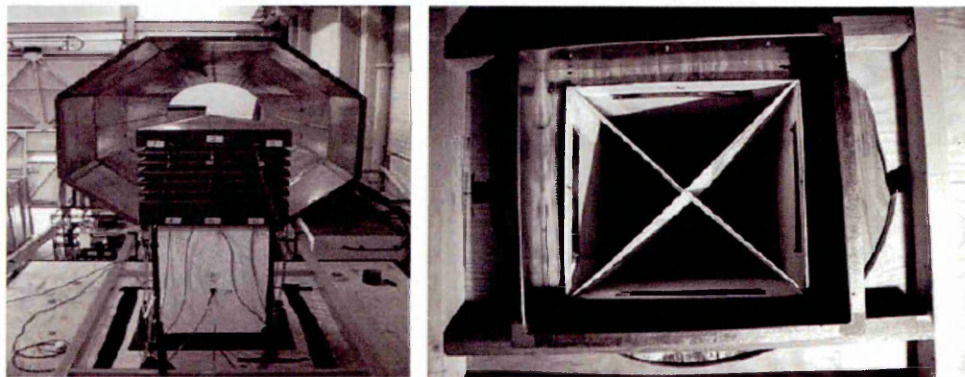
Figure 2-10 Wind tunnel testing wind vent device without dampers and diffuser [Elmualim (2006B)]

The investigation used various turbulence modelling techniques available and found no noticeable difference in the reported solution. Comparing the CFD solution to the wind tunnel experimentation, it was found that the results showed "reasonable" correlation. The CFD code consistently over estimated the flow. This was attributed to the lack of louver geometry used in the modelling.

Liu and Mak (2007), used CFD to investigate the ventilation capabilities of a wind vent system connected to a room. The study used louver geometry but omitted the damper and diffuser sections (Figure 2-11).
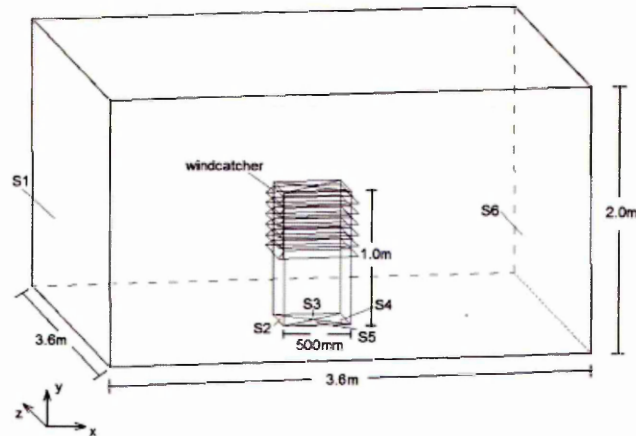
Figure 2-11 3D Model of the wind vent device [Liu and Mak (2007)]

The turbulence model used in this work was the standard k-ε model, (discussed in Chapter four). The computational model was run for external wind speeds of the range 0.5 - 6m/s. The results were compared to previous published wind tunnel results [Elmualim 2006B]. The results of this numerical work showed that the CFD predictions correlate with the wind tunnel testing results. This work demonstrated the predictive capabilities of CFD for wind vent applications.

Hughes and Ghani (2008) used a standard k-ε CFD model to investigate the capability of a wind vent device to meet the British Standards Institution (1991) recommendations. The investigation simulated a current commercially available wind vent installed in a classroom. The full geometry of the wind vent was recreated including louvers and dampers (Figure 2-12).

25
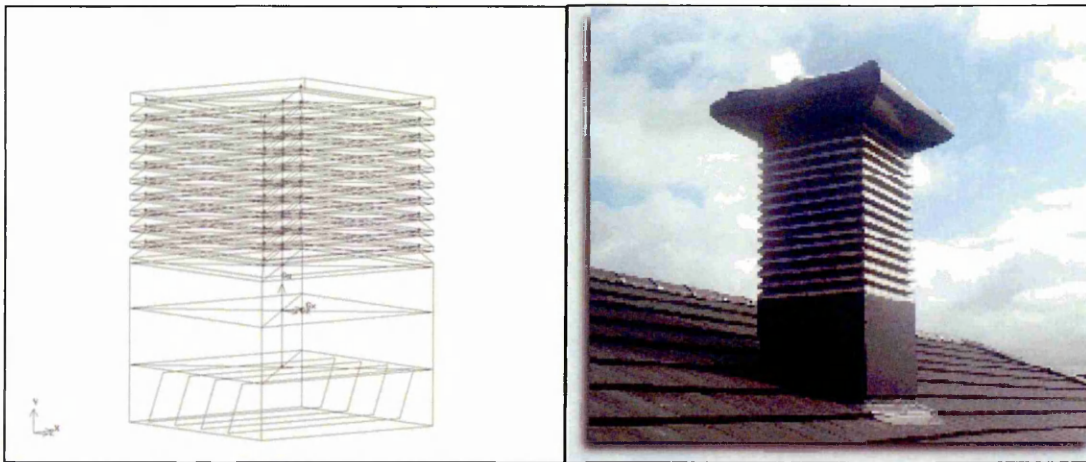
Figure 2-12 Full Geometry recreated from a commercially available wind vent

The CFD results of this investigation showed that the wind vent device met the BSI recommendations. At low levels of external wind, regardless of wind direction, the device is capable of meeting BSI recommendations. The work demonstrated the effectiveness of this technique for predicting airflows through the device. However, the lack of experimental data required that this work must be validated through wind tunnel/ full scale experimentation.

Hughes and Ghani (2009), used CFD to investigate the effect of the control dampers from a wind vent on the indoor air distribution. The purpose of this study was to ascertain an operating range for the control dampers; to deliver the maximum internal air movement rate. A total of 19 CFD models were created using the full geometry of the wind vent device installed in a classroom, with the damper angle varied in each case by five degrees (Figure 2-13).

Contours of Velocity Magnitude (m/s)

Nov 22, 2007
FLUENT 6.2 (3d, segregated, ske)
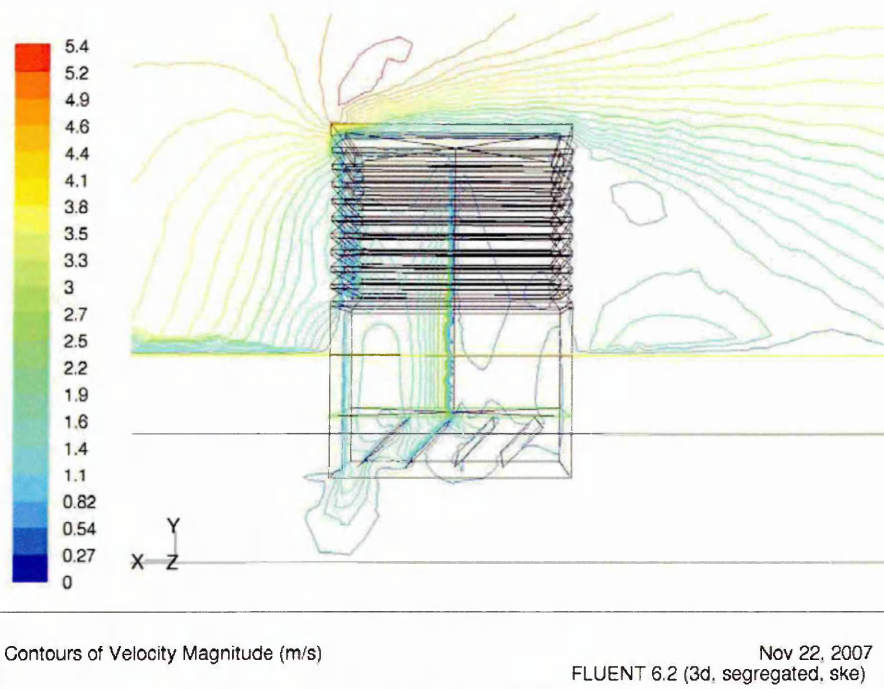
Figure 2-13 Illustration of the CFD simulation with angled control dampers

The CFD results showed that the optimum operating range for the control
dampers was in the region of 45 - 55°. To quantify the validity of these
computational results, the authors compared them to previous published CFD
and experimental work of Elmualim (2006B). Good correlation between both
sets of data validated the CFD work.

2.5 Empirical models for wind vent devices

Drori and Ziskind (2004), experimentally induced natural ventilation into a one-
story detached real-size building. The investigation used an element mounted
above the roof, heated by solar radiation to form a duct, connecting to the inner
space of the building. The attained temperature difference, allowed the heated
air to flow out of the duct, with fresh air suction at the opposite end of the duct,
which created flow into the constructed building (Figure 2-14).

27

Figure 2-14 Experimental setup of induced ventilation building [Drori and Ziskind (2004)]

The study used extensive experimental work with continuous monitoring. Both temperature and velocity, inside and outside the building, were monitored. The results show that the generated temperature difference produced effective induced ventilation. The indoor temperature followed the ambient temperature. In contrast, the building without the element showed considerably higher indoor temperatures than the ambient. Simulations of the experiment were carried out using the k-ε CFD model and were compared to the experimental work and found to be in good agreement.

Elmualim (2006C), investigated the use of dampers in a wind vent device using smoke visualisation and wind tunnel testing. A commercially available wind vent device connected to a specially constructed room, beneath an open-ended wind tunnel was tested at BSRIA. Tests were performed for various external wind speeds in the range 0 - 6m/s. The results were compared to the author's previous simulation results [Elmualim (2006B)] and found to show good correlation. In addition, smoke visualisation testing was carried out to establish the effectiveness of the wind vent device as a fresh air-exchange unit.

Smoke pellets were ignited inside the test room, and smoke extraction through the device was observed. The observations showed that the smoke was visibly cleared within 3 minutes at an average wind speed of 3m/s. The smoke visualisation results demonstrated the device is effective in mixing and distributing the supplied fresh air within the test room, whilst simultaneously extracting the stale air.

Larsen and Heiselberg (2007), investigated the effect of wind pressure and temperature difference on natural ventilation using wind tunnel experimentation. The aim of the work was to develop a new mathematical expression for calculating airflow rates in single sided natural ventilation applications. A full scale model house was created and placed inside a wind tunnel at the Japanese Building Research Institute (JBRI) as shown in Figure 2-15.
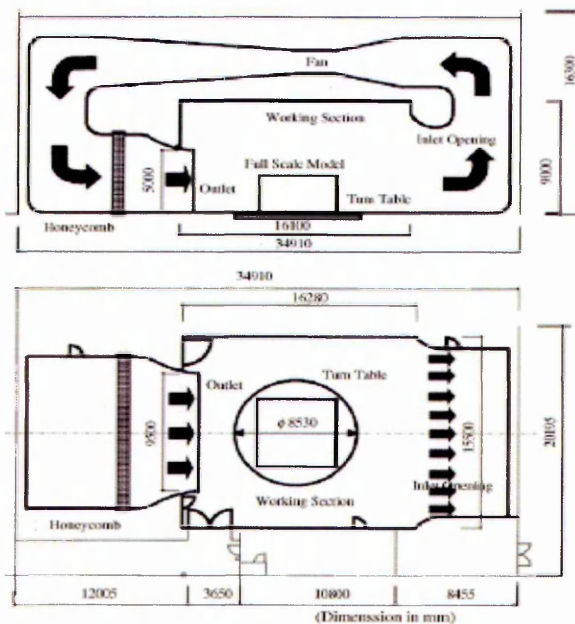
Figure 2-15 Experimental set-up in Japanese BRI [Larsen and Heiselberg (2007)]

The wind tunnel experiments found the dominating driving force between wind speed and temperature difference differs, depending on the ratio between the forces and wind direction. Furthermore, the study found that the wind incident angle is the overriding factor in the air-change rate. The study developed new expressions based on three incident angle cases: windward, leeward, and parallel flow, and found them to be an improvement on previous expressions. However, the mathematical expression developed retained a 23% error margin.

Su *et al.* (2007), studied the ventilation flow rate through a commercially available wind vent using a blower fan in a specially constructed test room (Figure 2-16). The results were compared to CFD results generated using the k-ε turbulence model. Using a series of manometers the authors measured experimental air velocities to calculate the ventilation rates of the device.
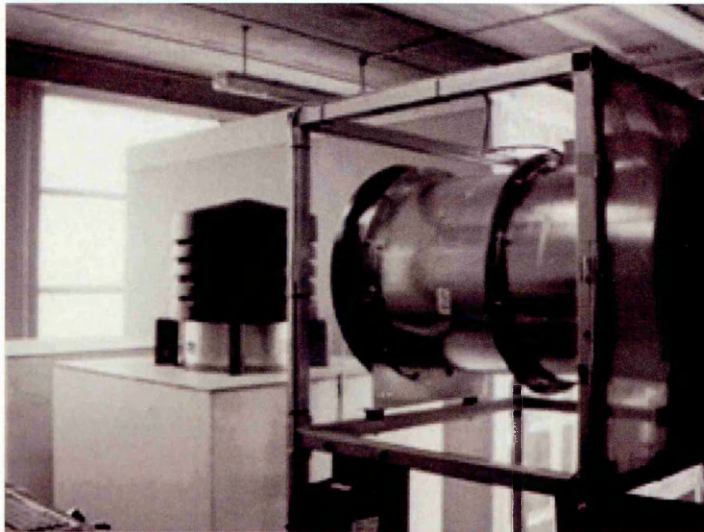
Figure 2-16 Experimental set-up using blower fan [Su *et al.* (2007)]

The CFD simulation used a blower fan as an air supply, as opposed to previous studies which used a far-field wind. The experimental and CFD results showed good agreement and underlined the potential of CFD for this application. A comparison was made between the use of a far-field wind and a blower fan wind in the CFD simulation. The study found that the two different simulation

30

techniques show a difference in predicted flow rates. The far-field method showed double the internal flow rates of the blower model. This investigation highlighted the need for accurate computational domain to be developed in line with the experimental methods employed. The far-field experimentation work carried out for this investigation relates to the use of a far field wind as opposed to a mechanical fan or blower.

Montazeri and Azizian (2008), studied the aerodynamic performance of a one-sided wind catcher using smoke visualisation and wind tunnel testing. The one-sided wind catcher is of traditional Iranian stone/adobe construction and orientated towards prevailing wind (Figure 2-17).
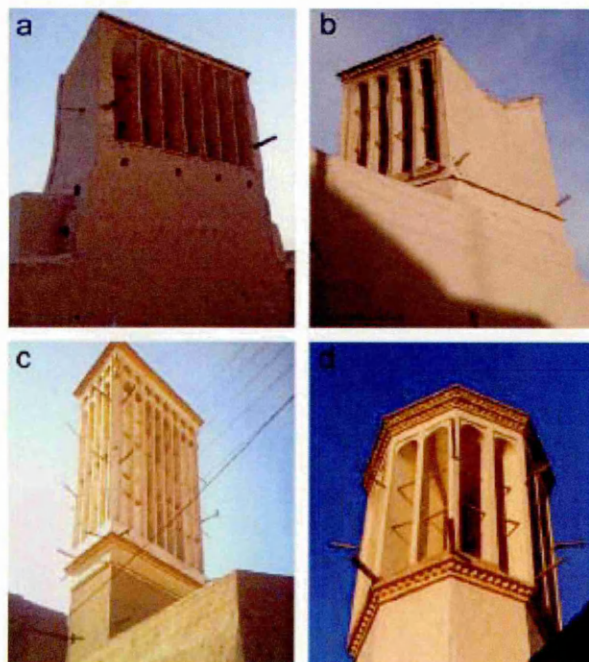
Figure 2-17 Traditional Iranian wind catcher [Montazeri and Azizian (2008)]

In this study, a 1:40 scaled model of a wind catcher was constructed and attached to a test room with an external wind induced via a wind tunnel (Figure 2-18).

31
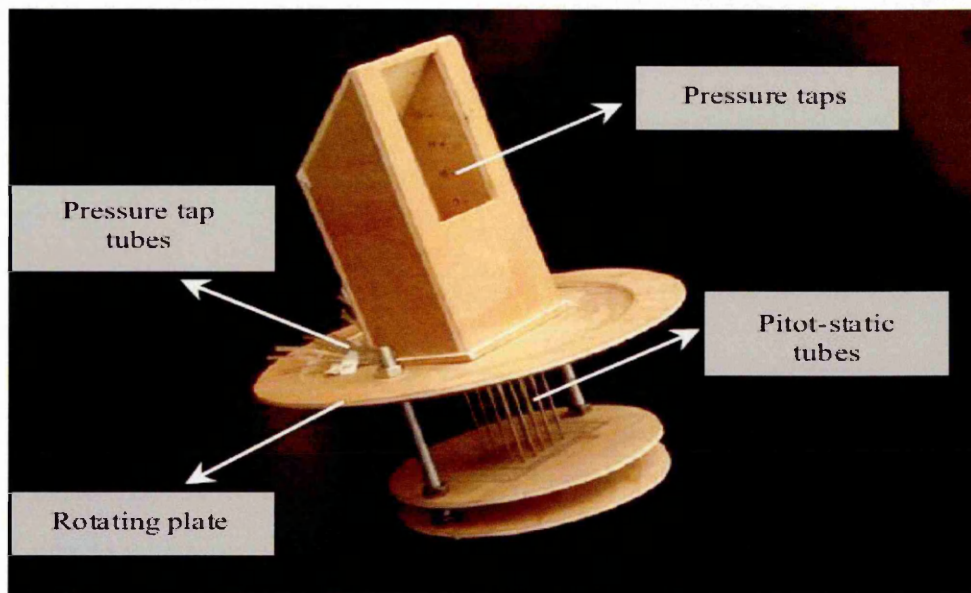
Figure 2-18 The Scale model of Iranian wind catcher [Montazeri and Azizian (2008)]

In addition, scale models of adjoining buildings were placed upstream of the airflow. The purpose was to determine the effect of flow rate and direction the urban environment has on the wind catcher. The results of this investigation showed that the wind incidence angle, urban environment, and the blowing of atmospheric wind influenced the rate and direction of ventilation airflow. It was concluded that for an isolated wind catcher model, the maximum efficiency is achieved at zero air incident angle.

2.6 Post occupancy studies of wind vent device

Battle McCarthy (1999), presented a comprehensive review of the usage of wind towers through-out the world. The work presents methodologies for sizing and locating wind towers in buildings. The basic principles of operation for wind towers systems are outlined and various combination strategies of multiple towers are presented. Finally, a collection of case studies of various applications of the technologies is presented both in the UK and around the world (Figure 2-19).

32

Figure 2-19 Typical wind tower in Dubai [data dubai (2007)]

However, this work does not examine the geometry of the device and its effect

on the performance. Furthermore, it does not evaluate the use of wind vent

devices in the UK climate.

Elmualim and Awbi (2003), evaluated the performance of a wind vent device

using experimental methods and a post occupancy questionnaire survey. A

wind vent device was installed in a seminar room in the University of Reading.

Monitoring was carried out on the indoor environment in real weather conditions.

In addition, a subjective occupancy survey was carried out to determine the

occupant's comfort level within the room.

The seminar room contained windows and these were used in conjunction with

the ventilation device to create four different operating conditions. The results

obtained through the monitoring process, over a period of four months

demonstrated the combination strategies of all four cases. Each strategy

provided adequate air exchange rate, in the range of 1.5 to 6.8 air-changes per

hour. The investigation concluded that the wind vent helped in removing

33

accumulated heat gains during the day through night ventilation, this however was not quantified. The survey revealed that 75% of the occupants welcomed the use of the combined strategies to provide cooling and ventilation. However, the published results show a small sample size (12 people) and therefore the validity of this survey must be questioned, as a cross-section of the general population was not represented.

Elmualim (2006D), investigated the control strategy for a combined wind vent and Air Handling Unit (AHU) solution at Bluewater shopping mall in Kent, UK (Figure 2-20). The primary purpose of this post-occupancy evaluation was to determine the contribution of the wind vents to the indoor air environment. The secondary aim was to assess any possible energy savings.

Figure 2-20 Bluewater shopping mall, Kent UK [Hugh pearmen (circa 2005)]

The building ventilation system is managed via an Integrated Building Management System (IBMS). A total of 39 wind vent devices are in place. The devices are automatically controlled in conjunction with a mechanical ventilation system. The wind vents are opened if external wind speeds are within the range of 1- 3m/s. The number of wind vents opened is reduced in line with the rise in external wind speed, with a maximum of 7m/s before total closure. The work

showed that the mechanical and natural systems (wind vent device) were not integrated effectively via the IBMS. The natural ventilation devices were continually isolated as the AHU over-rode the system. The results were impossible to evaluate as no recorded data for the ventilation device exist. The lack of integration showed that a control strategy for this device was not in place and that a new system needed to be identified.

The conclusion of this study was that natural ventilation devices should be the primary ventilation provider. Additional AHU systems should be deployed when external wind conditions render wind vents inoperable (low or excessive wind speeds).

2.7 Research gap

The review of the existing literature and research covered a wide range of different analytical and experimental tools, to address the effectiveness of natural ventilation. The significant unresolved issues in the literature review are:

- There is little data on natural ventilation devices tested in the natural environment (far-field testing)
- There is little attempt to use complete geometry for wind vent devices in CFD simulation
- There is no variation in specific device geometry, and data regarding the effects on both flow and air movement
- There is no attempt to optimise the performance of the device through geometrical variation
- There is no work that involves the validation of CFD techniques using far-field experimental methods on wind vent devices.

35

This work will use the experimental techniques, identified through the literature review, to fill the research gap. This will contribute to the knowledge and understanding in this area. In summary this work will utilise:

- CFD simulation models, specifically the k-ε model function
- Smoke testing for flow visualisation
- Full scale experimental testing in the natural environment (far-field)

In order to achieve the following:

- Validation of CFD techniques using experimental methods for wind vent devices
- The use of complete wind vent geometry for CFD simulation
- Geometrical variation of the wind vent to establish the effect on flow and performance
- Systematic geometrical variations to optimise the performance of the wind vent
- Establish the suitability of the wind vent to meet British Standards for natural ventilation rates

2.8 Summary

In reviewing the previous published work, the following points were concluded:

- British Standards are established for natural ventilation [British standards Institution (1991)]
- Mathematical models have proved unreliable for wind vent devices [Elmualim (2006A); Li and Delsante (2001)]

36

- CFD techniques are well established in this field [Yang (2004); Graca *et al.* (2005); Chen (2004); Ahmed (2004); Evola and Popov (2006); Elmualim (2006A)]

- The k-ε simulation model is appropriate for this application [Ayed (1999); Liu and Mak (2007); Drori and Ziskind (2004); Elmualim (2006A)]

- Smoke testing is used for flow visualisation [Montazeri and Azizian (2008); Elmualim (2006B)]

- Far-field testing vastly improves micro climate ventilation rate [Su *et al.* (2007)]

Chapter 3   Natural ventilation

3.1 Introduction

The role of ventilation in buildings is to maintain acceptable levels of oxygen in the air, to remove odours, moisture, and internal pollutants. It can also remove excess heat by direct cooling or by using the building's thermal mass.

There are many different techniques to achieve natural ventilation in buildings. "Traditional architecture shows how carefully designed passive cooling systems did not make use of any mechanical energy to operate, such as, ground cooling, wind towers, fountains and whitewash. These techniques have been termed natural ventilation" [Santamouris and Allard (2002)].

Natural ventilation may be used to cool or dissipate heat loads from buildings. However, this is not the focus of this investigation. This chapter presents the main physical concepts and basic techniques for natural ventilation, with respect to airflow and distribution in and around buildings.

3.2 Performance criteria

Performance criteria are related to the objectives of ventilation, air quality control and thermal comfort. The criteria for air quality control are defined in terms of minimum ventilation rates or alternatively restricting the contaminant concentration to acceptable levels. The current standard of fresh air supply rates in the UK are based on the British Standards Institution (1991) as reviewed in Chapter 2.

Designing for minimum ventilation rate is less complex when compared to designing for restriction of air contamination. Hence, most often the minimum

ventilation rate is the approach taken in the design of natural ventilation systems.

Minimum ventilation rates are defined by the intended usage of the occupied space. The building's usage also dictates the recommended ventilation rate standards as regulatory bodies introduce their own requirements for ventilation. For example, school buildings must follow the guidance set out by the Department for Education and Skills (2005), in addition to British Standards Institution (1991).

Various other types of non-domestic buildings are covered by the Chartered Institution of Building Services Engineers (CIBSE 2005). CIBSE further defines the natural ventilation rates for occupied spaces, and introduces design strategies for contamination restriction.

However, all three guides share a commonality between the recommended ventilation rates. Specifically they are expressed in terms of velocity flow rate (L/sec) per occupant or per floor area (L/sec/m^2). Synchronising of the correct legislative recommendations with the occupied spaces usage will determine the success of the buildings ventilation strategy.

3.3 Physics of natural ventilation

Determining the rate of airflow when using natural ventilation is difficult due to the frequency of variation in external conditions. "The calculation of airflow through large openings, through natural ventilation is a complicated task. The random nature of the wind makes estimation of airflow characteristics much

40

more complicated than that in the case of mechanical ventilation" [Vollebregt *et al.* (1998)].

The airflow behaviour is described by a set of differential equations for mass, momentum, and energy conservation. These equations are solved using CFD techniques that are discussed in Chapter 4.

3.3.1 Eddy, turbulent and mean description of flow

As the direction and velocity of the airflow is changing with such frequency, the behaviour may be considered as turbulent. Turbulent flow distorts in complex patterns, containing both coarse and fine features. The flow is said to contain eddies, which are regions of swirling flow that for a time retain their identities as they drift with the flow, which ultimately break up into smaller eddies (Figure 3-1).
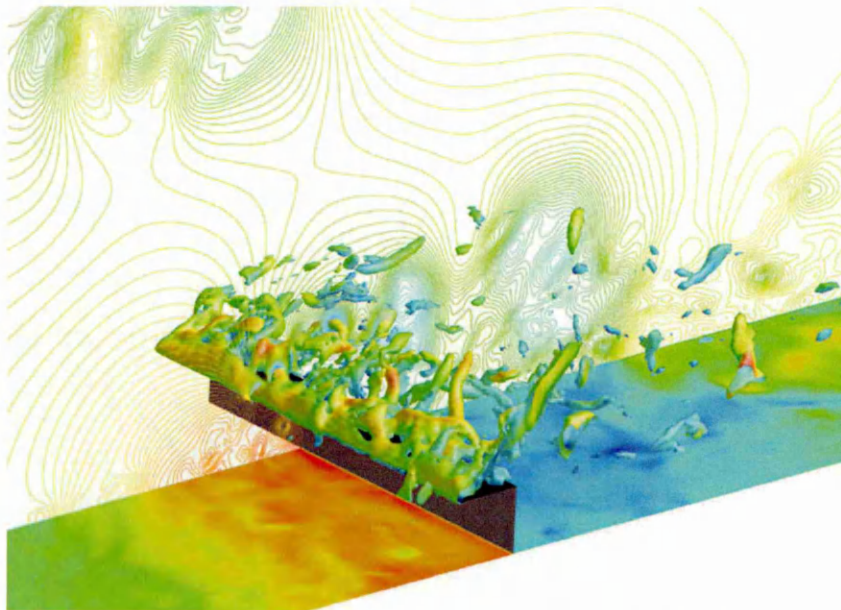
Figure 3-1 Simulation of turbulent flow [FLUENT, 2006]

The velocity field of turbulent flow is regarded as the super position of a large number of eddies of various sizes. The largest eddies are limited by the

transverse dimension of the flow. The smallest eddies are rapidly damped out by viscous forces.

Mathematical analyses of steady laminar viscous flows show minor disturbances to the flow grow exponentially with time whenever the Reynolds number is significantly large. Under these conditions, the flow is unstable and cannot remain steady under practical circumstances. This is because there are always some flow disturbances that may then grow spontaneously.

The generation and break-up of eddies provides a mechanism for converting the energy of the mean flow. The mean flow is converted into the random energy of molecules by viscous dissipation in the smallest eddies. Compared to a laminar flow, of the same Reynolds number, a turbulent flow is like a short circuit in the flow field, it increases the rate at which energy is lost. Therefore, a turbulent flow produces higher drag forces and pressure losses in comparison with a laminar flow under the same conditions.

When the unsteadiness of the flow is a small disturbance of the average flow, the velocity field can be expressed as the sum of a mean value. This value is obtained by averaging the velocity in time and a variable component. The variable component has the characteristics of a random noise signal of zero-mean.

The turbulent kinetic energy is a measure of how much kinetic energy has been invested in the random turbulent motion of the flow. It amounts in general to only a few percent of the kinetic energy of the time-averaged flow. The random

velocity field produces large shear stresses in the flow in comparison to those of laminar flow. The largest eddies contribute most to the turbulent energy while the smallest eddies contribute most to the energy dissipation [Ghiaus and Allard (2005)].

3.3.2 Flow through openings

Considerable volumes of air are induced by natural convection using small temperature differences. The up-flow of air is caused by density differences due to the change in temperature of air. Glover (1974) used this knowledge to demonstrate the principle of convective air ventilation. Using the occupant's body heat to generate the temperature differential within the test-chamber, he successfully created convective airflow (Figure 3-2).
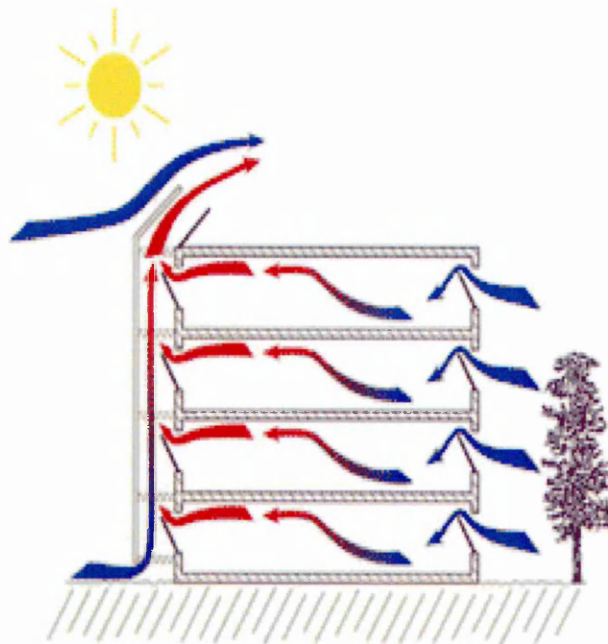
Figure 3-2 Convective airflow in a building [Dyer environmental (circa 2001)]

Assuming steady fully developed flow, the pressure drop for a flow between infinite parallel plates, impinging on a hole, nozzle, or orifice in a thin plate is [Santamouris and Allard (2002)]:

$$\Delta p = 0.5 \rho Q^2 / (C_d A)^2 \qquad\qquad (3\text{-}1)$$

Where:

Δp = pressure difference across the opening (Pa)

ρ = air density (kg/m^3)

Q = mean volume airflow rate (m^3/s)

C_d = the discharge coefficient

A = cross sectional area of the opening (m^2)

The discharge coefficient depends on the opening geometry and Reynolds number. The openings in a building are much less uniform in geometry and generally the flow is not fully developed [Santamouris and Allard (2002)]. Therefore, an empirical power law equation is used:

$$\Delta p = (Q / c)^{1/n} \qquad\qquad (3\text{-}2)$$

Where:

Δp = pressure difference across the opening (Pa)

Q = mean volume airflow rate (m^3/s)

c = flow coefficient [m^3/s / Pa^n)]

n = flow exponent

In this equation the flow coefficient and flow exponent are determined experimentally and do not have physical meanings. For laminar flow n = 1, for

turbulent flow n = 0.5 and for transient flow n is between 0.6 - 0.7 [Santamouris and Allard (2002)].

3.3.3 Wind pressure

The time-mean pressure due to wind flow on to or away from a surface is given by [Ghiaus and Allard (2005)]:

$$p_w = C_p \rho v^2 / 2 \qquad\qquad (3-3)$$

Where:

p_w = wind pressure (Pa)

C_p = static pressure coefficient

v = time-mean wind speed at a given level (m/s)

Pressure coefficients are experimentally measured in wind tunnels or calculated using CFD methods. The coefficients have positive or negative values that depend on the building shape or location. The wind direction and velocity vary with time as a result of wind turbulence and effects of obstacles. Therefore, the pressure coefficients are difficult to estimate in the urban environment and for complex-shaped buildings [Ghiaus and Allard (2005)].

3.3.4 Buoyancy pressure

Buoyancy pressure or stack pressure depends on air density differences and the height of the opening above or below the neutral level (Figure 3-3). Assuming that the air has the same composition indoors and outdoors, the density depends on air temperature only [Mansouri et al. (2003)].

45
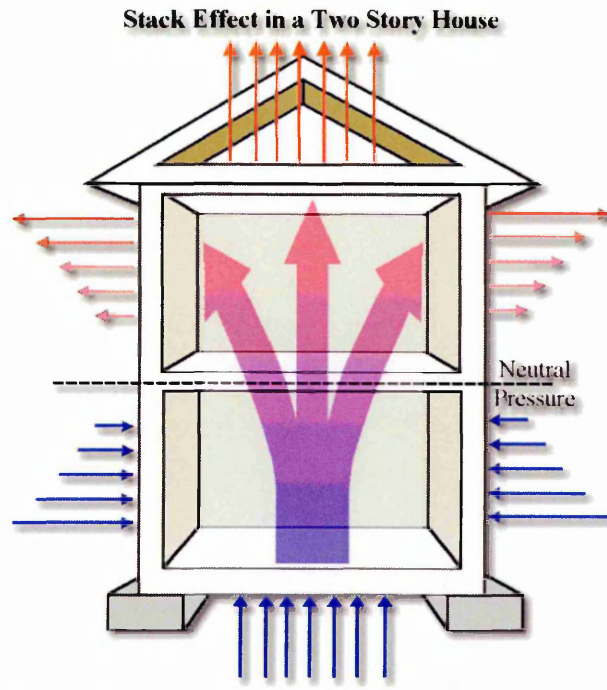
Figure 3-3 Buoyancy pressure above and below the neutral plane [Department of Housing and Development (circa 2002)]

The static pressure difference between two points separated on vertical direction by a distance $z = z_2 - z_1$ is:

$$p_2 - p_1 = g(\rho_2 z_2 - \rho_1 z_1) \qquad (3\text{-}4)$$

Where:

z = vertical direction (m)

z_1 = point in the vertical direction (m)

z_2 = point in the vertical direction (m)

The air density depends on temperature. From the gas law, $p = \rho RT$ we have:

$$\rho = \frac{\rho_0 T_0}{p_0} \bullet \frac{p}{T} \qquad (3\text{-}5)$$

Where the subscript 0 designates conditions for dry air ($\rho_0 = 1.29$ kg/m^3, $T_0 = 273$K, $p_0 = 101325$ Pa). Since the pressure differences in ventilation systems

are of three or four order of magnitude lower than ρ_0, the density variation with temperature may be written as:

$$\rho = \frac{\rho_0 T_0}{T} = \frac{1.29 x 273}{T} = \frac{352.9}{T} \qquad (3\text{-}6)$$

For an increase in temperature with height, there will be a corresponding decrease in pressure. The pressure difference between two points vertically separated by a distance Δz, also known as stack pressure p_s is given by:

$$p_s \equiv p_2 - p_1 = (\rho_2 - \rho_1)g\Delta z = \rho_0 T_0 [1/T_2 - 1/T_1]g\Delta z \qquad (3\text{-}7)$$

Where T_0 is the temperature at a reference point.

3.4 Urban environment

Although eddies and turbulence are important in an urban environment, the mean velocity of wind is reduced significantly by about an order of magnitude. Hence, the wind-induced pressure on a building surface is also reduced. For example, a building with a height of 20m and a much larger length exposed to a perpendicular wind velocity of 4m/s, at 10m over the building. The pressure difference between the two opposing facades is then about 10-15Pa in the case of an isolated or exposed building and about zero for a building located in a dense urban environment.

3.4.1 Wind variation-induced single-sided ventilation

In a naturally ventilated building air is driven in and out due to pressure difference produced by wind or buoyancy forces. The airflow through an opening is due to both wind and buoyancy [Jiang and Chen (2003)]. The wind

has a mean and a fluctuating component which may vary over the opening and produce a pumping effect. When the indoor temperature is higher than the outdoor, the buoyancy makes the cold air enter at the lower part and the hot air exit at the upper part of the opening.

An empirical model (a mathematical equation based on experimental data) to describe these phenomena is as follows [deGidds and Phaff (1982)]:

$$v_{eff} = (c_1 v_r^2 + c_2 H \cdot \Delta T + c_3)^{\frac{1}{2}} \qquad (3\text{-}8)$$

Where:

v_{eff} = effective wind speed (m/s)

v_r = site mean wind speed (m/s)

c_1 = coefficient depending on window opening

c_2 = buoyancy constant (0.0035m/s^{2}K)

c_3 = wind constant (0.01m^2/s^2)

H = height of the opening (m)

ΔT = mean temperature difference, outdoor - indoor (K)

The flow rate through the opening is given by:

$$Q = 0.5 A_w v_{eff} \qquad (3\text{-}9)$$

Where A_w is the effective area of the open window in m^2.

3.4.2 Wind-driven cross ventilation

Wind airflow over a building induces positive (inward-acting) pressures on windward surfaces and negative (outward-acting) pressures on leeward surfaces. Therefore, creates a net pressure difference across the section of the

48

building that drives cross-ventilation airflows. Two-sided (or cross-ventilation) takes place when air enters the building on one side sweeps the indoor space, and leaves the building on another side. An example of this is the Building Research Establishment (BRE) headquarters in Watford, UK (Figure 3-4).

Figure 3-4 BRE headquarters Watford, UK. [London Metropolitan University (circa 2005)]

The positive (wind-ward) pressure and the negative (lee-ward) pressure are pressure differences from the ambient air pressure of the free-field airflow. These pressure differences vary rapidly with time due to turbulence in the wind airflow and position due to the aerodynamic effects of the building form [Ghiaus and Allard (2005)].

They are related to a reference time-averaged approach-wind velocity:

$$p_{ww} = C_{p-ww}(\frac{\rho v^2_r}{2})$$ (3-10)

$$p_{wl} = C_{p-lw}(\frac{\rho v^2_r}{2})$$
(3-11)

Where:

p_{ww} = Positive windward pressure (Pa)

p_{wl} = Negative leeward pressure (Pa)

$(\frac{\rho v^2_r}{2})$ = Kinetic energy per unit volume of reference wind velocity

(kg m/s^2)

C_{p-ww} = Wind pressure coefficient of windward surface location (positive)

C_{p-lw} = Wind pressure coefficient of leeward surface location (negative)

The reference wind velocity is most commonly, but not in every instance, taken as the time-averaged wind velocity at 10m above the building height. The wind pressure difference between the facades is given by:

$$\Delta p_w = p_{ww} - p_{wl} = (C_{p-ww} - C_{p-lw})\frac{\rho v_r^2}{2}$$
(3-12)

The pressure changes along a given cross-ventilation airflow path:

$$\Delta p = \Delta p_{inlet} + \Delta p_{internal} + \Delta p_{exhaust}$$
(3-13)

The typical driving pressure is small compared to similar fan-driven pressure difference, in the order of one or two magnitudes higher. Hence, to achieve similar ventilation rates the resistance offered by the natural ventilation system must be small relative to ducted mechanical systems. This natural ventilation scheme suffers from critical shortcomings, as it depends on wind direction and intensity. As wind direction changes so does the wind pressure coefficients.

Therefore, the driving wind pressure can drop to low values even when wind conditions are good. Which in turn means the ventilation rates drop. When wind speeds drop to low values, the driving wind pressure will diminish and ventilation rates drop regardless of wind direction.

3.4.3 Buoyancy-driven stack ventilation

Natural convection in enclosures, partial enclosures and vented enclosures occur in a wide range of engineering applications. The convective flow occurs due to both vertical and horizontal surfaces heating the air which creates instability in the flow field and therefore is difficult to predict. Baskaya and Gilchrist (1996) investigated this phenomenon using both experimental and simulation techniques. They concluded that simulation accurately predicted the flow. In particular the k-ε model offered the best compromise between accuracy and computational effort. Warm air within a building will move up and flow out of upper level exhausts. Cooler outdoor air will flow in through lower inlets to replace it (Figure 3-5).
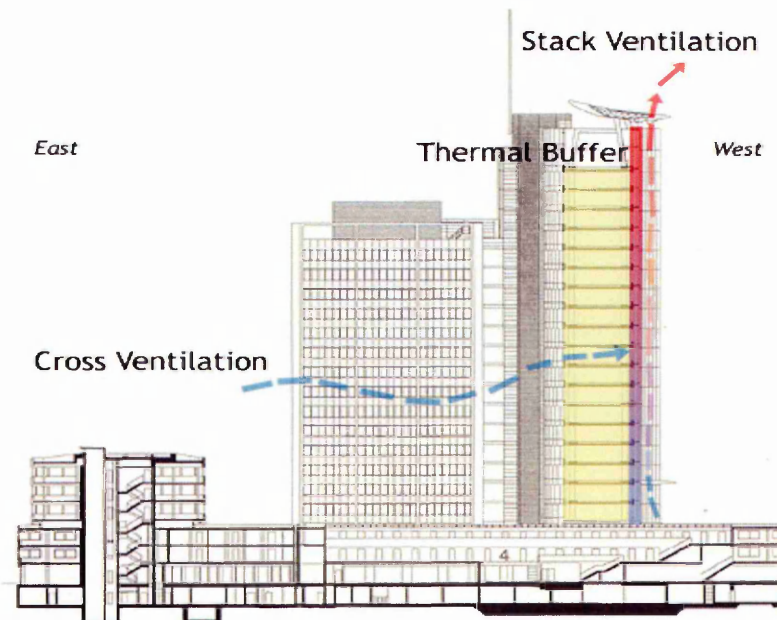
Figure 3-5 Illustration of stack ventilation [High performance building facades (circa 2007)]

The pressure loop this creates may be expressed as:

$$\rho_0 g \cdot \Delta z - \Delta p_{inlet} - \Delta p_{internal} - \rho_i g \cdot \Delta z - \Delta p_{exhaust} = 0 \qquad (3\text{-}14)$$

The stack pressure is given by:

$$p_s = (\rho_0 - \rho_i) g \cdot \Delta z \qquad (3\text{-}15)$$

And is equal to the pressure losses:

$$\Delta p_s = \Delta p_{inlet} + \Delta p_{internal} + \Delta p_{exhaust} \qquad (3\text{-}16)$$

The driving pressure stack varies with building height, h, and the temperature difference between indoor and outdoor expressed as:

$$\Delta p_s = (\rho_0 - \rho_i) g \cdot \Delta z = 352.9 [\frac{1}{T_0} - \frac{1}{T_i}] g \cdot \Delta z \qquad (3\text{-}17)$$

During warm periods, as outdoor temperatures approach indoor air temperatures, the stack pressure differences for all but very tall multi-story buildings may be expected to be small relative to typical wind-driven pressure difference. For example, a 10m high building would require a temperature difference between indoor and outdoor of 23°C in order to obtain a pressure differential of 10Pa, typical for wind-driven pressure. For a taller building of 25m, the temperature difference only need be 10°C to achieve the same pressure differential [Ghiaus and Allard (2005)].

3.4.4 Combined wind and buoyancy-driven ventilation

McGowan and Holmes (1997) investigated the effect of wind and buoyancy-driven ventilation using CFD simulation models. The investigation showed that the complexity of the forces within the building made predicting the airflow

extremely difficult. Empirical methods provided just as good accuracy as the developed CFD methods.

Stack ventilation systems use both wind and buoyancy-driven pressure difference. They include a stack terminal device, described in section 3.5, that can respond to prevailing wind direction in order to maximise the negative pressure induced by the wind. A pressure loop which includes both buoyancy-driven and wind-driven pressure differences can be expressed as a simple sum:

$$\Delta p_s + \Delta p_w = \Delta p_{inlet} + \Delta p_{internal} + \Delta p_{exhaust} \qquad (3\text{-}18)$$

Where:

$$p_s = (\rho_0 - \rho_i)g \cdot \Delta z \qquad (3\text{-}19)$$

$$\Delta p_w = (C_{p-inlet} - C_{p-exhaust})\frac{\rho v_r^2}{2} \qquad (3\text{-}20)$$

Ventilation stacks that extend above nearby roofs, when equipped with properly designed stack terminal devices, create suction pressures that are independent of wind direction. Therefore, these devices overcome the major limitation of simple cross-ventilation strategies.

3.4.5 Solar-assisted ventilation

Although not considered in this study, solar assisted ventilation is a natural ventilation technique which may be used to assist stack ventilation strategies. Papaefthimiou *et al.* (2007) investigated the empirical prediction methods of solar chimneys and compared to experimental results. The study showed that

the empirical methods showed good correlation with the experimental results, and gave confidence that the airflow behaviour may be accurately predicted.

When buoyancy pressure, resulting from internal to external temperature differences, is not sufficient then solar induced temperature difference may be used as an alternative.

The pressure losses for a solar collector are:

$$\Delta p_s = \Delta p_i + \Delta p_d + \Delta p_e \qquad (3\text{-}21)$$

Where:

Δp_s = Pressure losses of the solar collector (Pa)

Δp_i = Inlet pressure drop (Pa)

Δp_d = Distributed pressure drop (Pa)

Δp_e = Exit pressure drop (Pa)

Depending on the position of the control dampers, Δp_i and Δp_e include the control damper pressure losses [Ghiaus and Allard (2005)].

3.5 Stack terminal devices - the wind vent

Wind vents are situated on top of buildings to take advantage of higher wind velocities. The role of the wind vent is to ensure a depressurisation, which does not depend upon wind direction, together with protecting the ventilation duct against rain. "Wind vent devices have been in existence for hundreds of years, and modern day equivalents have been commercially available in the UK for

54

over a century" [Axley (2001)]. The purpose of this study is to systematically examine and optimise such a device (as detailed in Chapter 2).

3.5.1 Principle of operation

The ventilation principles of the wind vent are illustrated in Figure 3-6. The sections on the windward side of the wind vent provide a supply of air to rooms below, due to the pressure of the wind blowing at the ventilator. The remaining sections which act as extracts are subjected to a suction force, created by the low pressure region downstream of the ventilator.
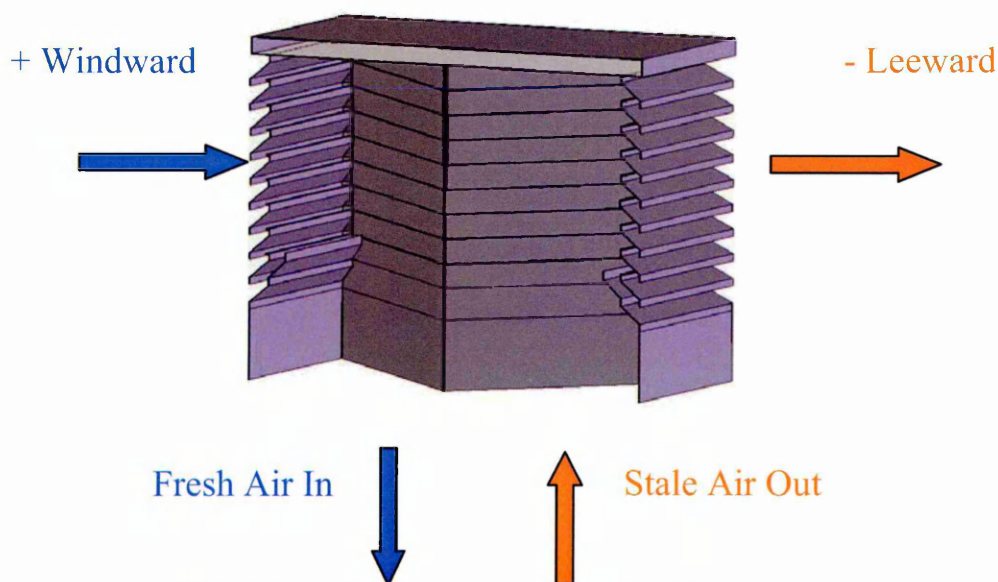
Figure 3-6 The principle of operation of a wind vent

This low pressure region is formed as a result of the detachment of the streamlines around the ventilator. The primary driving force therefore is the pressure difference between the inlet and outlet quadrants of the device. The difference between internal and external temperature is a secondary force which will also drive the airflow through the ventilator. If the external

temperature is lower than the internal temperature, then the buoyancy of the warmer air will cause it to rise up and exhaust through the ventilator. This is termed passive-stack ventilation and will occur with little or no wind.

Combined inlet and outlet static roof-mounted natural ventilation systems are typically made up of a louvered terminal, a base and a damper assembly. The terminal can be manufactured in a variety of shapes, commonly square or circular (a square terminal was used in this study).

3.5.2 System components

The square louvered terminal consists of a sheet metal exterior with horizontally mounted louvers on all sides of the terminal (Figure 3-7). A mesh is also installed inside the louvers to stop birds from entering the ventilator.

Figure 3-7 A square louvered wind vent terminal

The inside of the terminal is divided into quadrants, which act as the inlet/outlet ducts (Figure 3-8). These ducts are typically an integral part of the base of the unit and terminate with control damper assemblies that allow the user to control the ventilation.
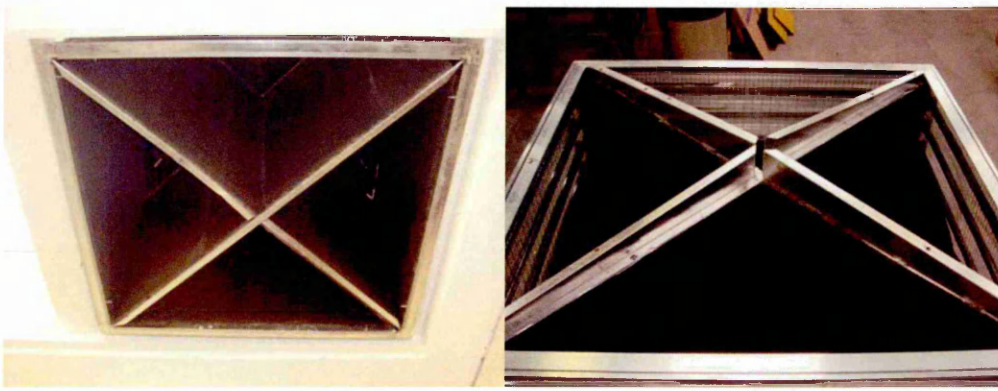
Figure 3-8 Inlet and extract ducts of typical wind vent without damper unit attached

The control dampers are an integral part of the air distribution system and are attached to the ventilator (Figure 3-9). The control dampers are used to control the rate of fresh air entering the occupied space. The dampers are controlled electrically using an actuator and Direct Current (DC) motor. For the purpose of this study the dampers were controlled manually.

Figure 3-9 A wind vent control damper unit

Attached directly below the damper unit is an "egg-crate" diffuser grille that is mounted in the ceiling of the room (Figure 3-10). The purpose of this diffuser is to evenly distribute the flow from the terminal across the area of the occupied space.

Figure 3-10 A wind vent with egg crate grille

3.5.3 Application

Roof-mounted ventilation devices offer a secure and weather-resistant option. They are typically used on the top or next floor down, as longer runs create adverse pressure losses reducing the system performance. No additional openings are required to use this type of ventilator as it provides both a supply and extract function.

3.5.4 Aerodynamic properties

As the device sits at roof level and is subjected to prevailing wind, the louvers and specifically the louver angle have an important role in the air movement within the inlet and exhaust ducts.

The louvers are angled against the prevailing wind, and may be considered as airfoils as they are subjected to the same lift and drag forces. However, from aerodynamic theory, flow separation occurs over the top surface of the airfoil when the angle of the airfoil, known as attack angle, exceeds a certain value. This is termed the stalling angle of attack [Anderson (2007)].

Louvers are constructed from sheet metal, or flat plate extrusion of 2 - 3mm thick metal. The type of stall behaviour associated with the extreme thinness of an airfoil is termed thin airfoil stall. Inviscid, incompressible flow theory shows that the velocity becomes infinitely large at a large convex corner. The leading edge of a flat plate or louver at an angle of attack is such a case.

In the flow over the plate, nature addresses this singular behaviour by having the flow separate at the leading edge, even for very low angles of attack. As illustrated in Figure 3-11, there is a small region of separated flow at the leading edge at 0°. This flow re-attaches itself further downstream, forming a separation bubble in the region near the leading edge [Houghton and Carpenter (2003)].
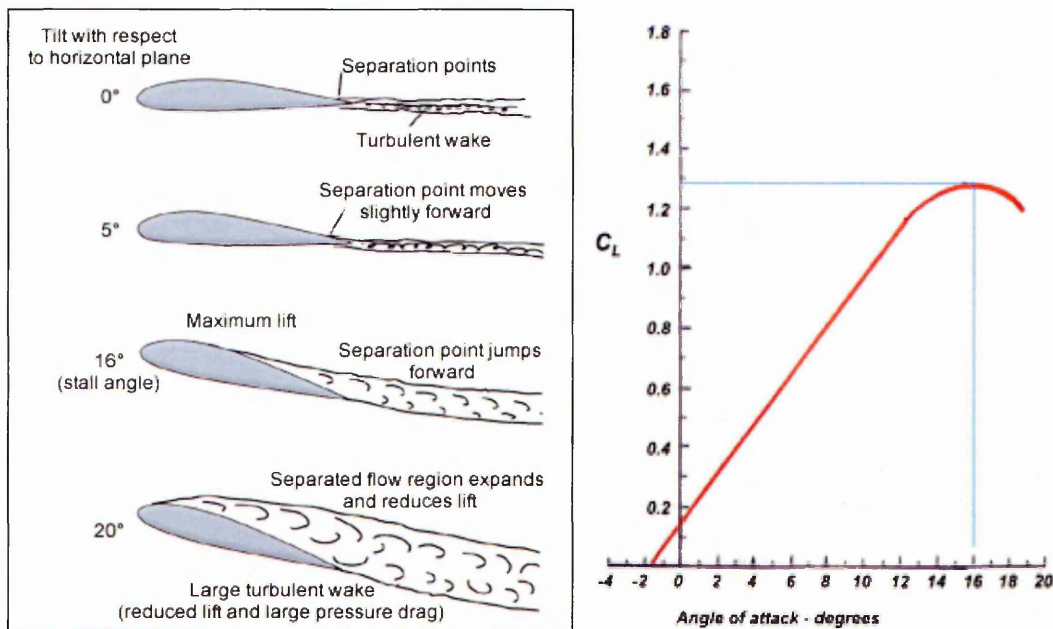
Figure 3-11 Thin air foil stall and associated lift coefficient [US centennial of flight commission (circa 1999)]

As the attack angle is increased, the re-attachment point moves further downstream and the separation bubble becomes larger. The lift curve illustrates the effect of increasing this attack angle. The lift curve follows a linear path up until the angle of stall, at which point the curve peaks and falls. The angle of the

louvers, with respect to the prevailing wind, follows the same pattern (detailed in Chapter 6). Therefore, the phenomena of thin airfoil stall must be overcome to ensure efficient air delivery rates.

3.5.5 Physics of the wind vent

As described in this chapter, there are numerous approaches to predict the airflow within buildings. However, the wind vent has unique geometry and therefore requires comprehensive investigation to ascertain the correct empirical methodology to use when employing this type of device. To establish the basic forces acting upon the device, a simple diagram was constructed (Figure 3-12).

3.5.6 Wind vent free body diagram

Macro climate

F_1 + density (ρ)

F_2 - density (ρ)

F_3 + velocity (V)

F_4 - velocity (V)

F_5 + pressure (p)

F_6 - pressure (p

F_7 + velocity (V)

F_8 - velocity (V)

F_9 + pressure (p)

F_{10} - pressure (p)

F_{11} + density (ρ)

Micro climate

F_{12} - density (ρ)
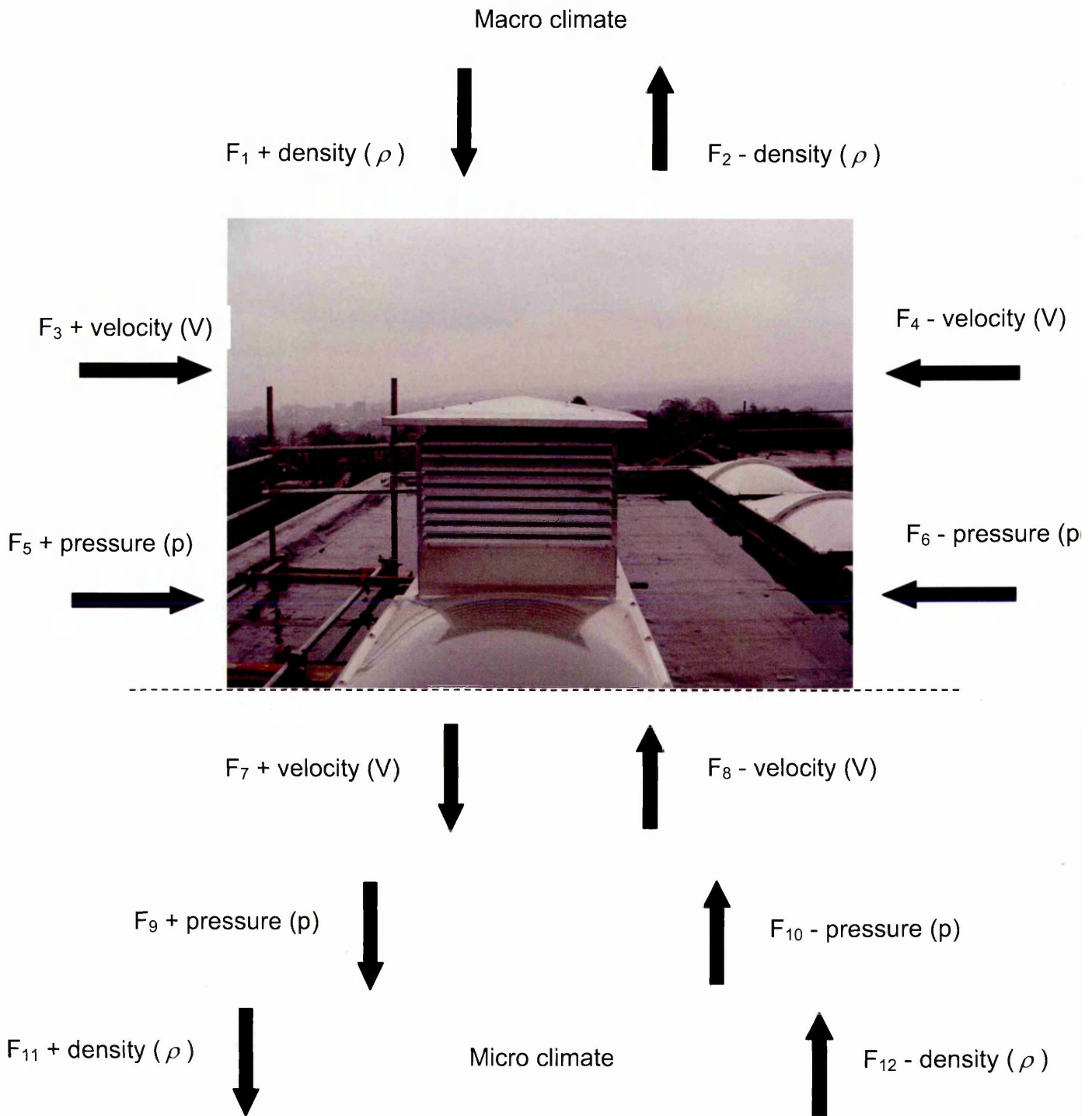
Figure 3-12 Free body diagram of the wind vent

The free body diagram (Figure 3-12) illustrates the specific influencing forces

acting upon the wind vent device. In addition gravity and the variable z, distance

from top of device to a point within the micro climate in metres, must also be accounted for. All of these variables may be accounted for in one formula:

$$\frac{P_1}{\rho} + gz_1 + \frac{V_1^2}{2} = \frac{P_2}{\rho} + gz_2 + \frac{V_2^2}{2}$$ (3-22)

This is the Bernoulli equation, first presented by Daniel Bernoulli (1700 - 1782). It applies for a steady, incompressible, inviscid and isothermal flow with no work done [Kaminski and Jensen (2005)].

3.5.7 Empirical formula to determine fresh air delivery rate of the wind vent

In order to determine an estimate of flow through the wind vent, a simple formula has been used based on CFD determined loss coefficients. By treating the airflow from macro-climate to micro-climate through a wind vent in the same way as fluid flow between two large reservoirs via a pipe. The purpose was to determine a quick and accurate empirical formula for estimating the flow through a wind vent from macro-climate to micro-climate.

The head loss, h_L due to minor losses can be determined experimentally and correlated, where K_L is called the loss coefficient, which is dimensionless [Kaminski and Jensen, 2005].

$$h_L = K_L \frac{V_1^2}{2g}$$ (3-23)

The head loss due to minor losses is added to the head loss in straight pipe sections so that the steady-flow equation becomes:

$$\frac{P_1}{\rho} + gz_1 + \frac{V_1^2}{2} + h_{L1} = \frac{P_2}{\rho} + gz_2 + \frac{V_2^2}{2} + h_{L2} \qquad (3\text{-}24)$$

In the case of the wind vent there are two loss coefficients, one at the entrance to the vent from the macro climate, a constriction loss K_1. The second coefficient is at the exit of the vent to the micro climate, an expansion loss K_2. CFD experimentation (as detailed in Chapter 5) has been used to determine these two coefficients.

3.5.8 Determining the loss coefficients for the wind vent

The wind vent is a 1m x 1m square louvered terminal with an overall height of 1m (Figure 3-13). The wind vent was modelled in CFD simulation and also subjected to extensive far-field experimental testing.

1.0 m

C_1

C_2

0.5 m
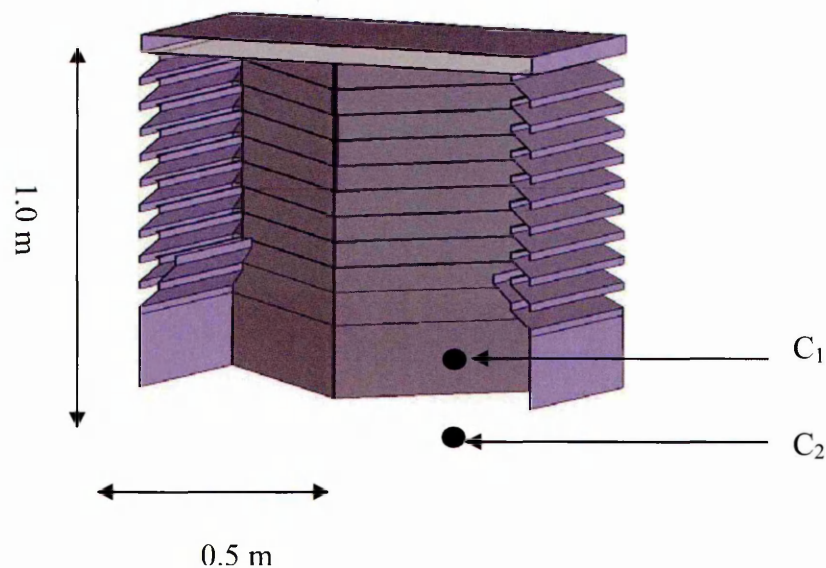
Figure 3-13 Wind vent geometry and location of C_1 and C_2

The results of this research have been used to ascertain the loss coefficients as follows:

Cross sectional area (A) = 1 x 0.5 = 0.5m^2

Density (ρ) = 1.225kg/m^3 [FLUENT (2006)]

External velocity = 4.5m/s [UK average wind speed, BSI (1991)]

Mass flow rate through the wind vent assuming no loss coefficients:

$$\dot{m} = v \times \rho \times A \qquad\qquad\qquad (3\text{-}25)$$

$\dot{m}$ = 4.5 x 1.225 x 0.5 = 2.75kg/s

CFD analysis within the wind vent gives C_1 = 1.97m/s, thus the mass flow rate at C_1 is:

$\dot{m}$ = 1.97 x 1.225 x 0.5 = 1.21kg/s

Therefore, the loss coefficient at C_1 is:

$$K_1 = \frac{1.21}{2.75} = 0.44$$

CFD analysis within the wind vent gives C_2 = 0.59m/s, thus the mass flow rate at C_2 is:

$\dot{m}$ = 0.59 x 1.225 x 0.5 = 0.36kg/s

Therefore, the loss coefficient at C_2 is:

$$K_2 = \frac{0.36}{1.21} = 0.3$$

3.5.9 Comparison of empirical and CFD prediction of flow rate through the wind vent

To compare the empirical model with the CFD prediction of the airflow through the wind vent, two sample calculations were carried out with external velocities of 5 and 3m/s respectively

- Sample calculation 1

$A = 1 \times 0.5 = 0.5m^2$

$\rho = 1.225kg/m^3$

External velocity = 5m/s

$$C_1 \text{ mass flow rate} = \overset{\bullet}{m} = v \times \rho \times A \times K_1 \tag{3-26}$$

$$= 5 \times 1.225 \times 0.5 \times 0.44$$

$$= 1.35kg/s$$

$$C_2 \text{ mass flow rate} \quad \overset{\bullet}{m} = C_1 \times K_2 \tag{3-27}$$

$$= 1.3475 \times 0.3$$

$$= 0.404kg/s$$

$$\text{Velocity at } C_2 = \frac{C_2}{\rho A} \tag{3-28}$$

$$= \frac{0.404}{\rho A}$$

$$= 0.66m/s$$

CFD prediction = 0.65m/s

The difference between the validated CFD prediction of 0.65m/s and the empirical prediction of 0.66m/s using the calculated coefficients is 1.5%.

- Sample calculation 2

$A = 1 \times 0.5 = 0.5m^2$

$\rho = 1.225kg/m^3$

External velocity = 3m/s

C_1 mass flow rate = $\qquad \dot{m} = v \times \rho \times A \times K_1$

$\qquad\qquad\qquad = 3 \times 1.225 \times 0.5 \times 0.44$

$\qquad\qquad\qquad = 0.8085kg/s$

C_2 mass flow rate $\qquad \dot{m} = C_1 \times K_2$

$\qquad\qquad\qquad = 0.8085 \times 0.3$

$\qquad\qquad\qquad = 0.243kg/s$

Velocity at $C_2 = \dfrac{0.243}{\rho A}$

$\qquad\qquad = 0.39m/s$

CFD prediction = 0.34m/s

The difference between the validated CFD prediction of 0.34m/s and the empirical prediction of 0.39m/s using the calculated coefficients is 12%.

3.5.10 Comparison of empirical and experimental flow rate through the wind vent

Experimental testing was carried out to determine the airflow rates through a wind vent (detailed in Chapter 7). Values recorded during the experimental work were compared to empirical predictions to ascertain their accuracy.

$A = 1 \times 0.5 = 0.5\text{m}^2$

$T_{External} = 10° \text{C} = \rho = 1.249\text{kg/m}^3$

External wind speed (v) = 3.9m/s

C_1 mass flow rate $\qquad \dot{m} = v \times \rho \times A \times K_1$

$\qquad\qquad\qquad = 3.9 \times 1.249 \times 0.5 \times 0.44$

$\qquad\qquad\qquad = 1.0716\text{kg/s}$

C_2 mass flow rate $\qquad \dot{m} = C_1 \times K_2$

$\qquad\qquad\qquad = 1.0716 \times 0.3$

$\qquad\qquad\qquad = 0.32\text{kg/s}$

Velocity at $C_2 = \dfrac{0.32}{\rho A}$

$\qquad\qquad\qquad = 0.53\text{m/s}$

Experimental recording $\qquad = 0.44\text{m/s}$

The difference between the experimental record of 0.44m/s and the empirical

prediction of 0.53m/s using the calculated coefficients is 17%.

3.5.11 Distribution of airflow in the microclimate

As the flow of air is now being treated as a fluid flow between two large

reservoirs, at the point of entry to the micro-climate (second reservoir)

maximum velocity will occur. Assisted by a constant external head pressure, the

flow spreads into the reservoir area where its velocity diminishes (Figure 3-14).
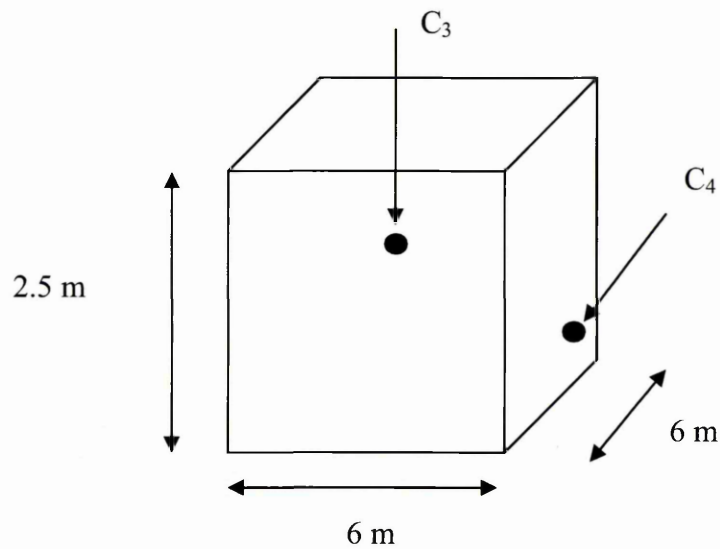
Figure 3-14 Position of C₃ and C₄ within the microclimate (not to scale)

3.5.12 Empirical method for determining the air distribution within the micro climate

At point C_3, the delivered velocity from point C_2 must be divided by the cross sectional area of the microclimate to determine the velocity at that point. At point C_4, the delivered velocity from point C_2 must be divided by the floor area of the microclimate to determine the velocity at that point.

3.5.13 Comparison of empirical formula with experimental data, and CFD prediction

To determine the accuracy of the empirical method of airflow estimation within the microclimate, a comparison was made using an external wind velocity of 5m/s.

External wind speed = 5 m/s

C_2 = 0.66m/s (sample calculation 1)

Cross sectional area = 2.5 x 6 = 15m^2

Floor area = 6 x 6 = 36m^2

Velocity at C_3 = $\dfrac{0.66}{15}$ = 0.044m/s

CFD prediction   = 0.033 m/s   Difference (empirical vs CFD) = 25%

Experimental data   = 0.05 m/s   Difference (empirical vs exp.) = 13%

Velocity at C_4 = $\dfrac{0.66}{36}$ = 0.018m/s

CFD prediction   = 0.010m/s   Difference (empirical vs CFD) = 45%

Experimental data   = 0.010m/s   Difference (empirical vs exp.) = 45%

3.5.14   Conclusion

The use of the two loss coefficients K_1 and K_2 found through CFD investigation gave an accurate prediction of the airflow within the range 1.5 - 17% difference. This error range must be quantified further. When dealing with such low velocities of airflow, the degree of velocity variation is low and must be quantified against other work in the field. Previous work using assumed values for the coefficients have yielded results with the range of 20 - 100% [Elmualim (2006B)] and 2- 22% [Liu and Mak (2007)]. Therefore, the presented empirical methodology for predicting airflow through the wind vent is more accurate. The empirical formula, when predicting the microclimate velocity at point C_3, is in agreement and gives greater accuracy compared to the equivalent CFD

prediction. The accuracy at point C_4, using the empirical method, is less accurate in comparison to the equivalent CFD prediction with a difference margin of 45%. However, this error must be put into context when working with such low velocities of airflow rates. The under and over prediction of the two points, is 0.006 and 0.008m/s respectively. It is concluded that the empirical solution proposed gives an accurate and quick prediction of the airflow rates in the micro-climate achievable using a wind vent device.

3.6 Summary

This chapter presented the main physical concepts, and basic strategies for natural ventilation, and provided where appropriate orders of magnitude that allow for relative comparison. The available empirical methods for each of the natural ventilation components have been illustrated. The specific device related to this study was described in detail including principle of operation, system components, application and aerodynamic properties. A methodology was presented and demonstrated for using empirical formula to accurately predict the airflow rate through the device. The understanding of these concepts and strategies forms the basis for the study of the wind vent.

Chapter 4   CFD theory and modelling

4.1 Introduction

CFD is used for analysis of large amounts of data in a cost effective manner. CFD is a prominent tool in aerodynamic design due to advancements in computational capabilities, along-side traditional methods such as wind tunnels. Wind tunnels and CFD are both simulators. Wind tunnels are analogue and CFD is digital. Any simulation tool requires validation through experimentation. This study validated the simulation work with full scale far-field testing (detailed in Chapter 8).

The three basic steps of a CFD computation are the same irrespective of the method. Once the choice of the appropriate method is made, the steps followed are:

- Discretisation of the body surface or the computational domain, termed "pre-processing"

- Computation, termed "solving"

- A suitable graphical representation of the numerical results, termed "post processing"

A commercially available wind vent was used as the benchmark geometry for this research. The wind vent was of standard 1 x 1 x 1m dimensions (length x width x height). The unit comprised of ten louvered sections, eight opening louvers with one louver at each end of the section used as a joining piece and did not allow airflow through, a terminal roof or hat, and a 1 x 1 x 0.5m spacer acting as link piece between external roof and internal ceiling and a 1 x 1 x 0.25m control damper unit. The internal space, the micro-climate, was determined as a small classroom of 6 x 6 x 2.5m dimensions [Department for

Education and Skills (2004)]. This chapter describes the process of translating the pre-determined physical domain to a computational domain (pre-processing), which is solved and post-processed, using the FLUENT software package.

4.2 Physical domain

Gambit, FLUENT pre-processor, has the ability to create a physical domain directly from user defined co-ordinates. The other option for creating pre-processor geometry is to import geometry from a Computer Aided Design (CAD) software package. Gambit does not have the same dedicated CAD tools as a purely geometric modelling programme, thus the creation of complex geometry is severely limited. An additional advantage of CAD packages is the ability to "dynamically modify" a model. The complete model is an assembly of many parts, when any of the parts are edited or modified, the model automatically regenerates a new model to reflect these adaptations, termed "dynamic modification". This research required geometrical investigation. Therefore, the ability to dynamically modify the physical domain was desirable. Thus, the secondary option of using a CAD modelling package was engaged.

The wind vent geometry, the louvered sections and hat, was created using 3D CAD software, namely Pro/ENGINEER Wildfire 2.0 [PTC (2008)]. Replicating the physical geometry of the wind vent does not represent a computational domain. To achieve this, the fluid volume must be defined prior to exporting the model to Gambit. The fluid volume, where the fluid should flow, is the area within the geometry which is under investigation. Translating a Pro/ENGINEER model to a fluid volume prior to Gambit pre-processing is a common procedure

[Fluent (2006)]. This procedure requires a new fluid volume to be created with each regenerated model after dynamic modification. Therefore, a new procedure was devised during this stage of the investigation whereby each regenerated model created a regenerated fluid volume [Appendix A]. The remaining geometry namely micro-climate, damper unit, spacer and macro-climate, external wind velocity domain, were created using Gambit version 2.0 as illustrated in Figure 4-1.
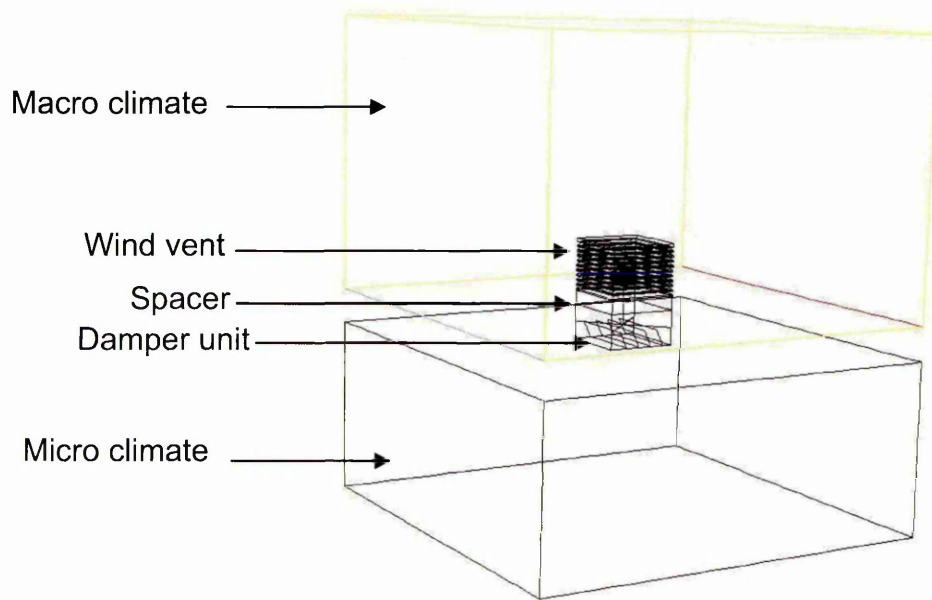
Figure 4-1 Gambit physical representation of geometry under investigation

The macro-climate, which contained the simulated external velocity, was determined by setting the perimeters at a minimum of 2.5 times the distance of the fluid volume wall under investigation to the external boundary (a general modelling guideline from CFD tuition). For example, the wind vent fluid volume to the horizontal plane of the macro-climate was determined as 2.5 x 1m = 2.5m wall to wall distance. The complete macro-climate dimensions were 6 x 6 x 4m.

4.3 Computational domain

Defining the computational domain from the physical domain consists of four key stages. These are:

a) Defining boundary conditions

b) Creating the volume mesh

c) Examining the mesh

d) Establishing mesh independency or grid adaption

4.3.1 Boundary conditions

The boundary conditions define the physical and operational characteristics of the model at its boundaries and within specific regions of its domain. The boundary types available in FLUENT are classified as follows:

- Flow inlet and exit boundaries: pressure inlet, velocity inlet, mass flow inlet, inlet vent, intake fan, pressure outlet, pressure far-field, outflow, outlet vent, exhaust fan

- Wall, repeating, and pole boundaries: wall, symmetry, periodic, axis

- Internal cell zones: fluid, solid (porous is a type of fluid zone)

- Internal face boundaries: fan, radiator, porous jump, wall

The physical domain contained three fluid volumes namely, macro-climate, wind vent and micro-climate. A wall boundary condition was used to clearly define the flow limitations in each region. The macro-climate fluid volume, used to simulate the external velocity flow field, generates a velocity into the wind vent and accepts an exhaust air out-flow from the wind vent. To generate a velocity flow field one horizontal plane was named as a velocity inlet, with the opposite

horizontal plane named as a pressure outlet. Unless otherwise stated, the velocity inlet was set to 4.5m/s, as this is the UK average wind speed [British Standards Institution (1991)]. The remaining planes of the macro-climate were named as symmetry planes, used to model zero shear-slip walls, thus alleviating potential distortion of the macro-climate flow.

The wind vent fluid volume contained two boundary conditions, wall and porous jump. The wall condition was used to simulate any geometrical obstruction to the fluid flow. For example the cross-dividers and dampers. The porous jump was used to simulate the fluid flow through the diffuser egg crate grille of the unit shown in Figure 4-2.
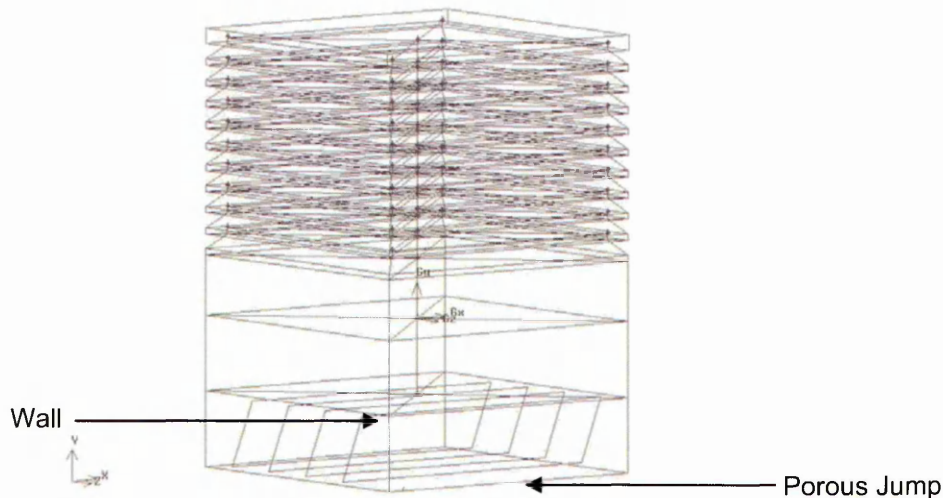
Figure 4-2 Wind vent fluid volume

The porous jump acts as a thin membrane or filter with user defined inputs of permeability and medium thickness. A tertiary term of pressure-jump coefficient is available to the user for this type of boundary condition (Equation 4-1). As a

reliable coefficient determined by experimentation was unavailable, the
equation reduced to the Darcy's law in the absence of this input [Fluent (2006)].

$$\Delta p = -\left(\frac{\mu}{\alpha}v + C_2\frac{1}{2}\rho v^2\right)\Delta m$$

<div align="right">(4-1)</div>

Where:

α	=	the permeability of the medium	(m^2)
C_2	=	the pressure-jump coefficient	$(1/m)$
Δp	=	the pressure change	(Pa)
μ	=	the laminar fluid viscosity	(kg/ms)
Δm	=	the thickness of the medium	(m)
ρ	=	the fluid density	(kg/m^3)
υ	=	the fluid velocity	(m/s)

The permeability, or the area of restricted flow and medium thickness were
calculated from actual physical measurements of an egg crate grille as shown in
Figure 4-3.

Figure 4-3 Wind vent diffuser (egg crate grille)

The calculations are:

Length of each side = 1m

Each side contained 86 dividers at 0.5 mm thick, 1 – 0.043 = 0.957m

Total area of unrestricted flow = 0.957 x 0.957m = 0.92m^2

Total depth of the grille = 0.01m

The third and final fluid volume, the micro-climate, contained only the wall boundary condition used to simulate the horizontal walls and the ceiling of the classroom.

4.3.2 Volume mesh

The macro and micro-climate, were subdivided into smaller blocks to facilitate grid refinement. The "mesh volumes" command creates a mesh for one or more volumes in the model. Gambit creates mesh nodes throughout the volume according to the specified meshing parameters.

The following parameters were specified to mesh the volumes:

- Volume(s) to be meshed
- Meshing scheme
- Mesh node spacing
- Meshing options

The meshing scheme used in this investigation was the tet/hybrid element combined with the tgrid type. This scheme specifies that the mesh is composed primarily of tetrahedral elements. The model also includes hexahedral, pyramidal and wedge elements where appropriate. The selection of this scheme was due to the nature of the investigation, whereby geometrical variations would be performed requiring a variation of element types to produce an accurate mesh. Mesh node spacing and meshing options were varied to achieve grid independency or grid adaption.

4.3.3 Grid adaption

The basic concept of grid or mesh adaption methods is to refine the elements in which a priori or posteriori error indicator, measure of error based on solution gradients is larger than the preset criterion. Adaptive methods are divided into structured and unstructured grid methods. This study used unstructured grid methods as a priori error indicator was unavailable.

Unstructured adaptive methods have been extensively developed by Oden and Babuska. Some of their later work is summarised in Babuska,*et al.*(1986) and Oden,*et al.* (1986). Selection of the appropriate adaptive method for the mesh results in increased accuracy in the final solution. Selecting the appropriate

method requires a compromise between computational time, cost and solution accuracy.

This study used an *hp* adaptive strategy for the unstructured mesh. "The three-step *hp* adaptive strategy, provides an accurate approximate solution while keeping the computational costs under control" [Oden and Legat (1995)].

The *hp* method is a combination of two adaptive methods, mesh refinement (*h* method) and mesh enrichment (*p* method). Mesh refinement refers to the targeting of areas of the mesh which have high levels of skewness and replacing them with an increased number of elements or cells, or a different element type. Mesh enrichment refers to an increase in the degree of the polynomials or higher order approximations [Chung (2006)].

Each method is applied until a posteriori error indicator shows no improvement from the previous adaption, thus the solution is deemed stable. At each stage of the adaption, a decision is taken as to whether an *h*-refinement or a p-enrichment should be performed. One technique is to apply h-refinements until a certain level is reached, then begin *p*-enrichments to establish a satisfactory posteriori error. Thus, the mesh may be considered independent of adaption.

The complete computational domain was split and refined in three areas corresponding to the three fluid volumes:

1) The wind vent and immediate surrounding zone

2) Remaining macro-climate

3) The micro-climate

The *hp* method required a posteriori error indicator which was defined as the diffuser average area-weighted velocity result. Gambit allows for two types of element node patterns to be selected with increased number of nodes (*p*-enrichments). The variation of these two types had insignificant effect on the posteriori error indicator. The *h*-refinements were applied to the three areas in three correlating stages shown in Figure 4-4.
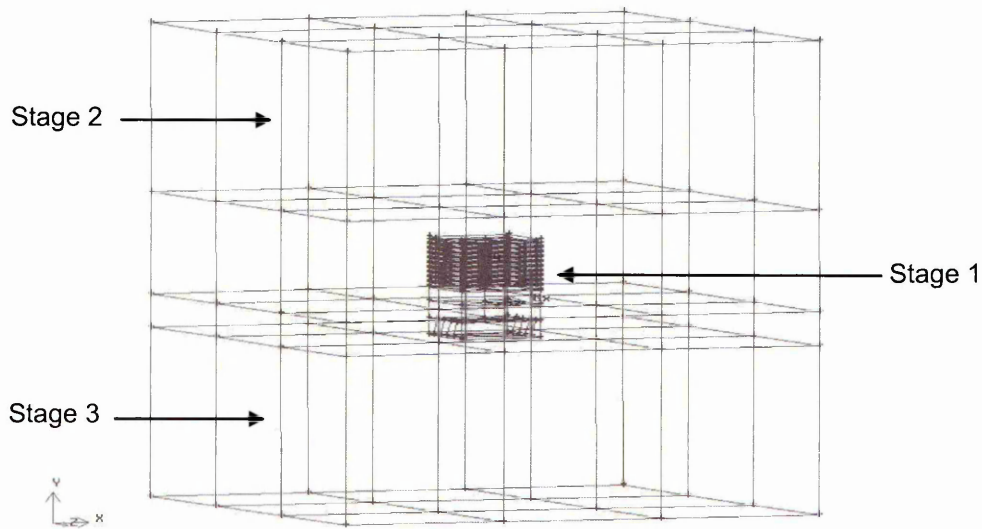
Figure 4-4 Grid adaption areas (identified by stage of adaption)

The initial model consisted of 750,210 elements. Stage one of the *h*-refinement increased the number of elements by 263,039 with an error indicator of 2.8%. As depicted in Table 4-1, at the third refinement no change was evident, thus this stage of the process was complete.

Table 4-1 Stage 1 *h*-refinement

Grid spacing				Posteriori error indicator		
Wind vent	Surround	Stage 2	Stage 3	Diffuser (m/s)	Error %	Total Elements
32	110	200	200	0.830	N/A	750,210
28	100	200	200	0.807	2.8	860,166
25	85	200	200	0.807	0	1,013,249

Stage two increased the number of elements by 335,837 with an error indication of 11.5% between refinements (Table 4-2).

Table 4-2 Stage 2 *h*-refinement

Grid spacing				Posteriori error indicator		
Wind vent	Surround	Stage 2	Stage 3	Diffuser (m/s)	Error %	Total Elements
28	100	200	200	0.807	N/A	860,166
28	100	175	200	0.693	16.3	899,431
28	100	150	200	0.584	18.8	998,050
28	100	125	200	0.523	11.5	1,196,003

The final stage of the h-refinement increased the number of elements by 92,752 with an error indication of 0.01% between refinements as seen in Table 4-3. The third refinement at this stage showed no change in the error indicator, thus the process was complete.

Table 4-3 Stage 3 *h*-refinement

Grid spacing				Posteriori error indicator		
Wind vent	Surround	Stage 2	Stage 3	Diffuser (m/s)	Error %	Total Elements
28	100	125	200	0.523	N/A	1,196,003
28	100	125	175	0.527	0.01	1,216,987

The grid adaption process increased the number of elements by 445,793. Each stage continued until an acceptable compromise was reached between the number of elements, computational time to solve and the posteriori error indication, as depicted in Figure 4-5. At 1,196,003 elements, the error indication between refinements was at its lowest in the final two stages. This coupled with the computational time made it an acceptable compromise. These node spacings were then applied to each investigation.
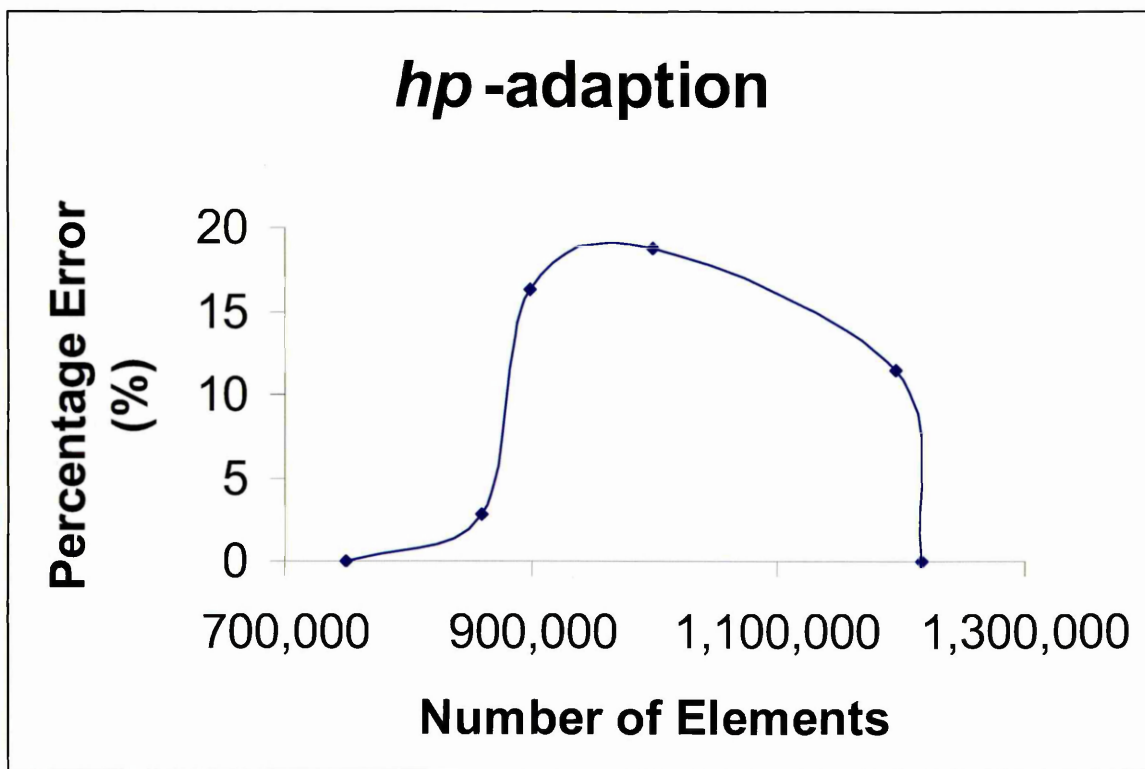
hp-adaption

Figure 4-5 Error reduction through successive *hp*-adaption stages

4.3.4 Examining the mesh

Examination of the mesh was done computationally. The computational

examination is carried out by a skewness tool provided by the software. The

skewness (range 0 -1) is the distribution relationship between the mesh nodes.

In statistical terms, a normal distribution has a skewness of zero. Hence, data

points are symmetrical about a mean. A high level of skewness indicates that

the distribution is "stretched". Consequently the model under-estimates the

solution variables which leads to an inaccurate solution. The default maximum

allowable skewness from the FLUENT software is 0.97 for the meshing scheme

applied. If the skewness factor is above this level, the accuracy of the solution is

deemed unacceptable.

The mesh was examined to eliminate any potential problems prior to exporting

to the FLUENT solver. The mesh was examined using the skewness tool

provided. The first examination consisted of examining the mesh and looking for any signs of high density clusters of elements in geometrically important areas, shown in Figure 4-6.
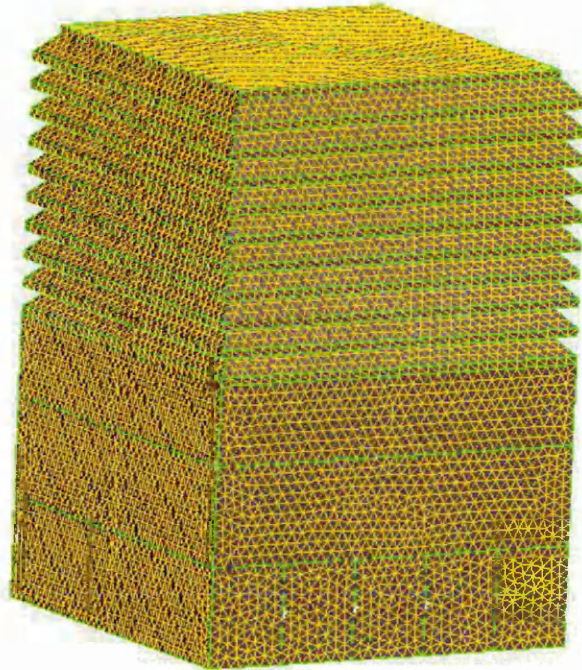
Figure 4-6 Meshed wind vent geometry

Any elements with a high skewness value would be highlighted. According to colour map red is the highest level of skewness. At this point the mesh was refined in that particular area to remove these potential solving problems. A further examination was carried out using the software's grid check function, which gives the overall skewness of each mesh. The maximum recorded skewness during this investigation was 0.79 with typical values being 0.6 - 0.7.

4.4 Solving the model

The k-ε model is the most widely used and validated turbulence model (as detailed in Chapter 2). It is the simplest turbulence model for which only initial

and/or boundary conditions need to be supplied. The two-equation k-ε model was used to carry out the computational work reported in this study with the following equations solved:

- Continuity or mass conservation equation

- Momentum conservation equation

- Navier-Stokes equation

- Kinetic and epsilon transport equation

These equations are established and widely used, full description and derivation is available [Ahmed (1998), Chung (2002), Fluent (2006), Appendix A]. No attempt was made during this study to modify any of these standard equations. In addition the defined boundary conditions require value inputs to accurately define the model as depicted in Table 4-4.

Table 4-4 Boundary conditions requiring input

Boundary condition	Input
Velocity inlet	4.5 m/s
Pressure outlet	Default (atmos)
Porous jump permeability	$0.91\ m^2$ (section 4.3.1)
Porous jump thickness	0.01m (section 4.3.1)

4.5 Solution algorithms

Solution algorithms are tools used to dictate the method in which the progressive iterations are carried out. FLUENT provides three methods for pressure-velocity coupling in the solver:

1) SIMPLE (Semi-Implicit Method for Pressure-Linked Equations) Figure 4-7.

2) SIMPLEC (SIMPLE-Consistent).

3) PISO (Pressure-Implicit with Splitting of Operators).

The SIMPLE algorithm is used in FLUENT as a default algorithm and was used in performing the numerical work reported in this study. The SIMPLE algorithm, illustrated in Figure 4-7 (derived and detailed in Appendix A) provides a method of calculating pressures and velocities.

```
                          ┌──────────────┐
                          │    Start     │
                          └──────┬───────┘
                                 │          Initial guess p*, v*, φ*
   ┌──────────────────┐          ▼
   │                  │   ┌──────────────────────────────────┐
   │                  │   │ Step 1: solve discretised momentum│
   │                  │   │ equations                         │
   │                  │   └──────────────┬───────────────────┘
   │                  │                  │         u*, v*
   │                  │                  ▼
   │                  │   ┌──────────────────────────────────┐
   │   Set:           │   │ Step 2: Solve pressure correction │
   │   p*=p, u*= u    │   │ equation                          │
   │                  │   └──────────────┬───────────────────┘
   │                  │                  │         p'
   │                  │                  ▼
   │                  │   ┌──────────────────────────────────┐
   │                  │   │ Step 3: correct pressure and      │
   │                  │   │ velocities using under-relaxation │
   │                  │   └──────────────┬───────────────────┘
   │                  │                  │       p, u, v, φ*
   │                  │                  ▼
   │                  │   ┌──────────────────────────────────┐
   │                  │   │ Step 4: solve all other discretised│
   │                  │   │ transport equations               │
   │                  │   └──────────────┬───────────────────┘
   │                  │                  │
   │    No            │                  ▼          φ
   └──────────────────┘◄───────◇ Convergence ◇
                                         │
        p= p*+p'                         │ Yes
                                         ▼
                              ┌──────────────────┐
                              │  Stop iterations │
                              └──────────────────┘
```
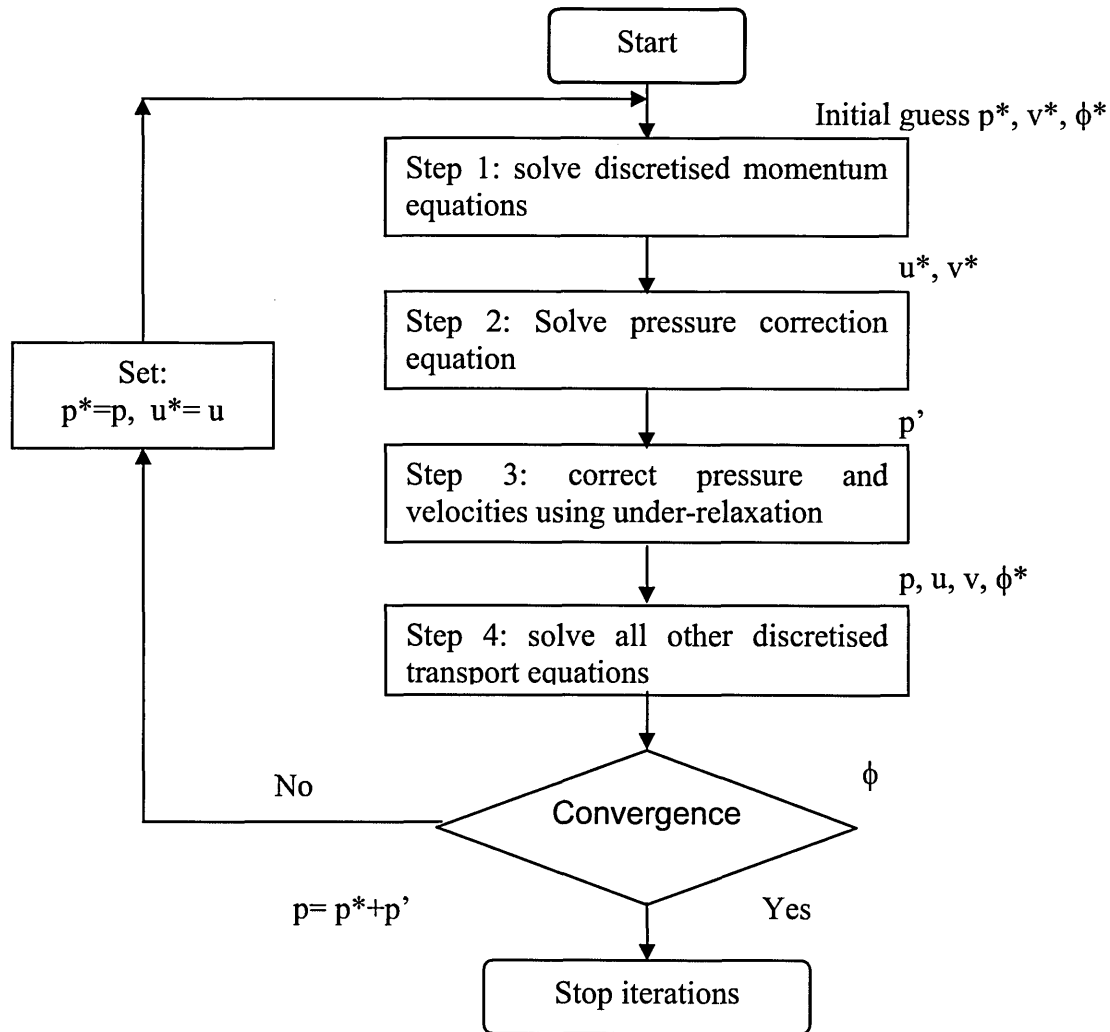
Figure 4-7 SIMPLE algorithm flowchart [Ahmed (2008)]

The method is iterative and, when other scalars are coupled to the momentum equations, the calculation needs to be done sequentially.

4.6 Solution convergence

Convergence is the term for a numerical method using iterations to produce a solution of the grid, whereby the error approaches zero. Solutions are based on iterations against pre-defined convergence criteria. After initialising the solution, setting all residual values to zero, the iteration process is commenced. An online plot of scaled residuals versus iterations was used to assess the status of the convergence. When the set convergence criterion is met the iteration process is complete.

There are no universal metrics for judging convergence. Residual definitions that are useful for one class of problem are sometimes misleading for other classes of problems. Therefore, it is useful to judge convergence not only by examining residual levels, but also by monitoring relevant integrated quantities such as volume averaged velocities. For most problems, the default convergence criterion in FLUENT is sufficient. This criterion requires that the scaled residuals defined by the equations selected decrease to 10^{-3} [Fluent (2006)]. Initial models, the benchmark geometry, were solved within 90 iterations using the default criteria, as illustrated in Figure 4-8.
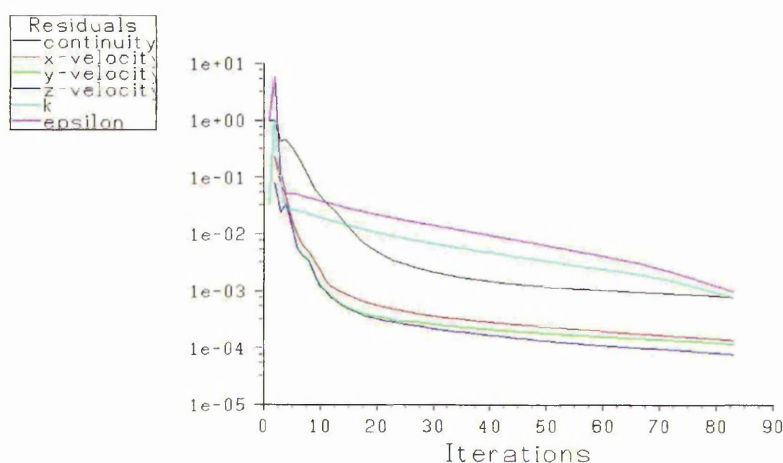
Figure 4-8 Converged solution residuals

87

To ascertain the accuracy of the default convergence criteria, the set-point was altered to 10^{-4}, and 10^{-5} respectively. The new criteria increased the number of iterations to 750 for the 10^{-4} case, with the 10^{-5} case not converging after 2000 iterations but remaining constant. Comparing the posteriori error indicator, used for grid adaption, no significant difference (0.001) between any of the cases was found. Due to the increased computational time for relatively small increased accuracy, the default convergence criterion was used for the remaining computational models used in this investigation.

4.7 Post processing

To obtain an accurate picture of the airflow behaviour through the wind vent and into the micro-climate a series of data points, vertices, were created. From these points, the average vertex velocity (m/s) was obtained and recorded for comparison with experimental results (Chapter 8). In total, ten data points were created. Nine of the data points were positioned at a height of 1.5m, with a tenth point centrally positioned at the diffuser entry and exit face. By joining these data points about a 1.5m high, horizontal plane, velocity and pressure profiles within the micro-climate were obtained (Figure 4-9).
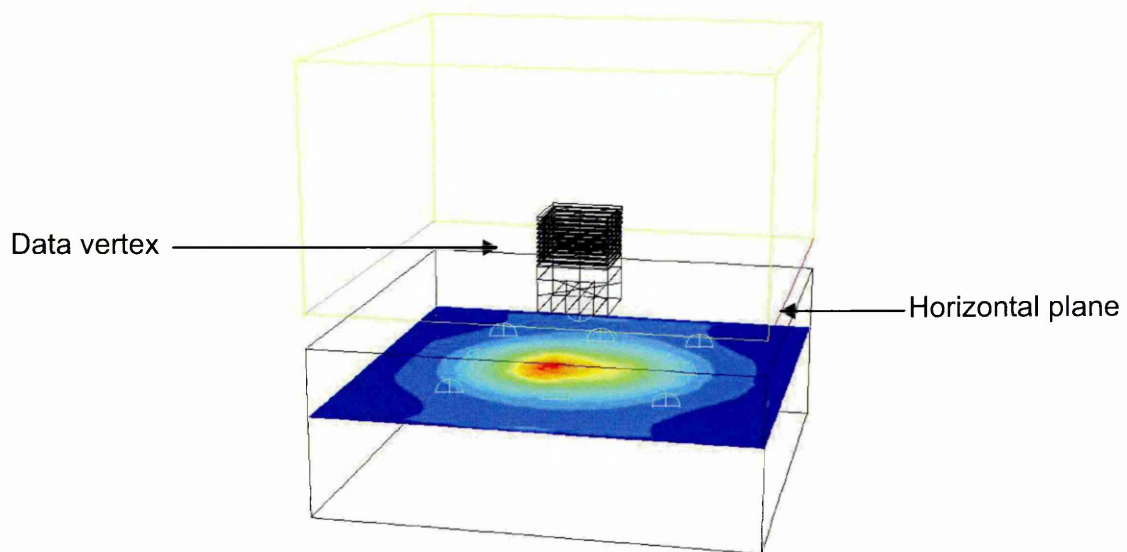
Figure 4-9 Velocity contour profile within the micro climate

4.8 Computational uncertainties

Any computational method contains some unknowns or uncertainties. It is

necessary to identify these and eradicate where possible. "Computational

uncertainties inevitably arise due to equivalence of a continuum phenomenon

by a discrete model, and the subsequent numerical solution of the model which

gives rise to a loss of accuracy" [Hamdan (1998)].

Quantifying the uncertainties that arise in the study of any scientific problem

requires that the sources of uncertainties must be identified. In the type of

physical problems that require modelling followed by solving, the following

sources/factors of uncertainties have been identified and discussed in detail by

Mehta (1991):

- The physical phenomenon being studied and the associated uncertainties due to isolation of the physical phenomenon; the effects of extraneous phenomenon; modelling of the physical problem and underlying simplification of the models; modelling the physical parameters inaccurately; lack of understanding of the physical phenomenon and the lack of confirmation measures.

- The human factors involved are manifested in creative over belief; uncertainties about definitions; uncertainties about risk assessment; and uncertainties in decision making.

- Computational uncertainty and its sources of equivalence and accuracy.

4.9 Quantification of CFD uncertainties

Quantification of uncertainty, as opposed to qualitive assessments, involves more than just obtaining a good error estimate. A more conservative procedure, based on the grid-convergence procedure index, reports an error band equal to three times an error estimate. Roache (1997) considers only *a posteriori* error estimate, being of the opinion that useful *a priori* estimation is not possible for non-trivial fluid mechanics problems. This study used a posterior error estimate based on the *hp* grid-convergence procedure (Section 4.3.3).

In addition to verification of the calculation through convergence techniques, independent validation of the model must be made through experimentation, to minimise potential modelling errors. For example, the equations set may not accurately represent the intended application, regardless of the accuracy of the grid, which would only become apparent through comparison with full-scale testing. The simulation model used in this study has been validated against far-field experimental testing and flow visualisation (Chapter 8).

4.10 Summary

This chapter presented the specific CFD theory and modelling used for the purpose of this investigation. The three main areas of the CFD process were described namely pre-processing, solving, and post-processing. The pre-processing area detailed the creation of the physical domain and computational domain (Sections 4.2 and 4.3). The solving area detailed the selection of solvers and equations; and solution convergence (Sections 4.4 and 4.6). The final topic area, post-processing, detailed results analysis and display (Section 4.7).

5.1 Introduction

Robust Parameter Design (RPD) is an approach to product realisation activities that emphasises choosing the levels of controllable factors or parameters in a process or product to achieve certain objectives [Montgomery (2005)].

This study used this general approach when designing the CFD experiments to maximise the generated data in the most efficient manner, shown in Table 5-1.

Table 5-1 Design of CFD experiments

Experiment	Measured response		
	Velocity (m/s)	Pressure (Pa)	Internal air distribution (m/s)
Benchmark	✔	✔	✔
Control damper angle	✔	✔	✔
External louver angle	✔	✔	✔
Amount of external louvers	✔	✔	✔
Distance between external louvers	✔	✔	✔
Use of cross dividers	✔	✔	✔
Use of internal fan	✔	✔	✔
Optimum external geometrical configuration	✔	✔	✔

To determine which type of parameters to examine and responses to measure for the purpose of the device, this study was broken down into a simple flow chart (Figure 5-1).

Maximise the flow

Control the flow

Regulate the flow

Figure 5-1 Flow chart of design procedure

The parameters are all geometrical features which may influence the performance of the device. The measured responses are factors which contribute to the effectiveness of the wind vent as a ventilation device.

5.2 Benchmark model

The macro and micro climates geometry remained constant in each CFD model. The wind vent geometry (described in Chapter 4) was used as a benchmark for the CFD investigations, shown in Figure 5-2, the standard geometry is detailed in Table 5-2.

External louver

Counter -current flow

Cross divider

Control damper

Con -current flow
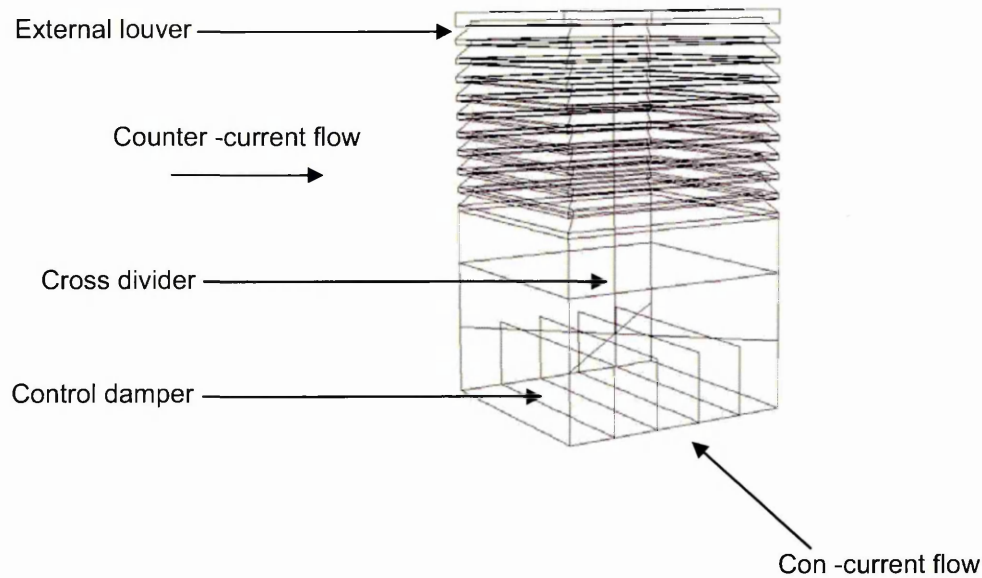
Figure 5-2 Benchmark wind vent geometry

Table 5-2 Geometry used for the benchmark case

Geometry	Dimension/Position
Damper angle	0° (fully open)
External louver angle	45°
Number of external louvers	8 (8 opening louvers, 2 fixed with no flow through)
Distance between external louvers	50 mm
Number of cross dividers	1
Internal fan position	No fan

The benchmark model was solved for a range 1, 2, 3, 4 and 5m/s of inlet velocities, and a BSI standard velocity of 4.5m/s [British Standards Institution (1991)]. The inlet and outlet boundary wall positions were varied through 90° to examine con-current flow, in line with control dampers and counter-current flow in opposition to control dampers. Figures 5-3 and 5-6 illustrate the flow path predicted in the FLUENT model for both the con-current and counter-current flow paths. The left hand side of the CFD plot shows the scale of velocity (m/s) or pressure (Pa) where applicable. The lines within the fluid domain are colour coded and relate to the colour map on the left hand side. The distribution within

the micro climate is shown. Figure 5-3 shows the con-current flow entering from the left velocity inlet boundary. The flow splits at the wind vent face with air entering the macro to micro climate interface (wind vent) and the remaining flow passing over and exiting to the right pressure outlet boundary. The geometry shown includes a supplementary vertical plane created to assist in the illustrative analysis of the model.
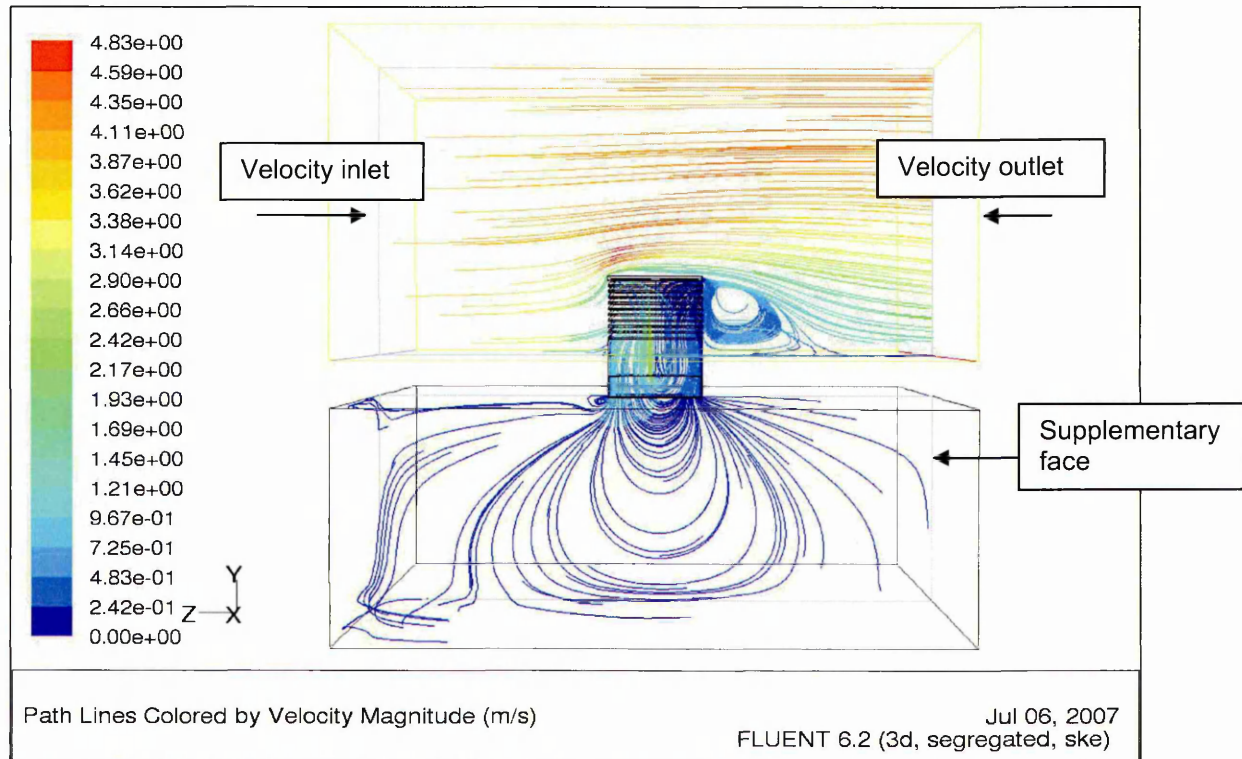
Figure 5-3 Velocity vectors simulating the con-current flow at 4.5m/s through the wind vent

Figure 5-4 shows a supplementary face without the surrounding geometry. The vertical face through the centre of the model shows an accurate cross-section of the model to assist the illustrative analysis. The flow is con-current with the direction of the dampers.
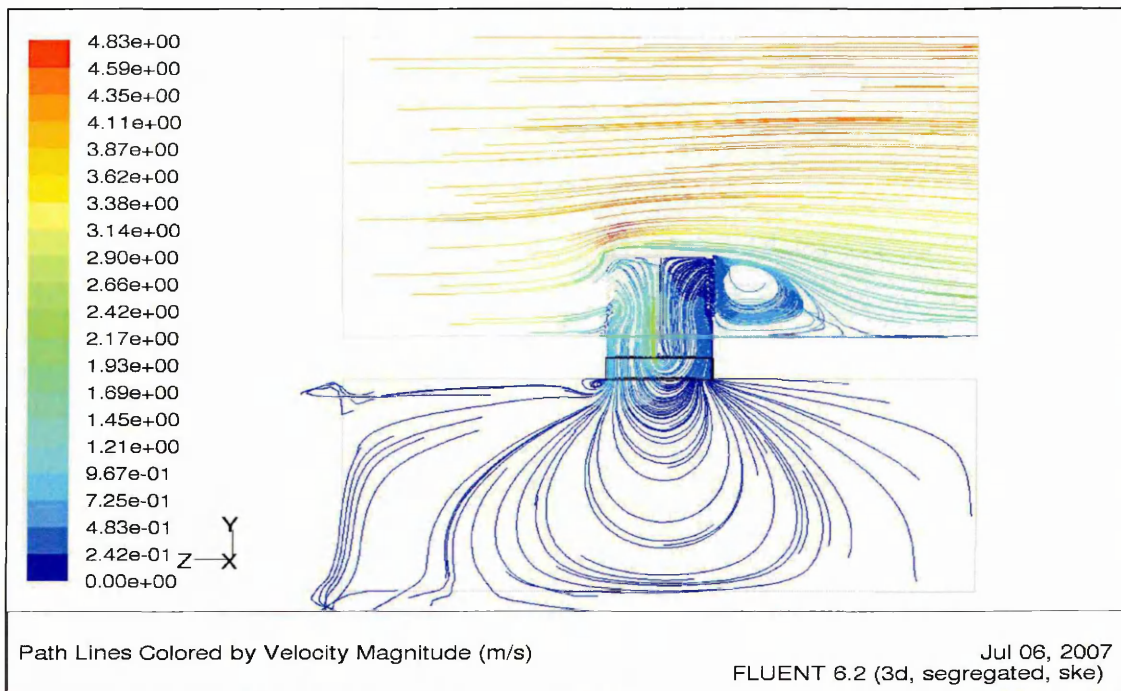
Figure 5-4 Supplementary plane view of velocity vector results

Figure 5-5 is a zoom view of the wind vent air distribution with con-current flow.
Some of the airflow exits the wind vent without entering the micro climate, a
phenomena known as short-circuiting. For this reason natural ventilation is
described in terms of delivery rates (L/sec) as opposed to air changes per hour
for mechanical systems.
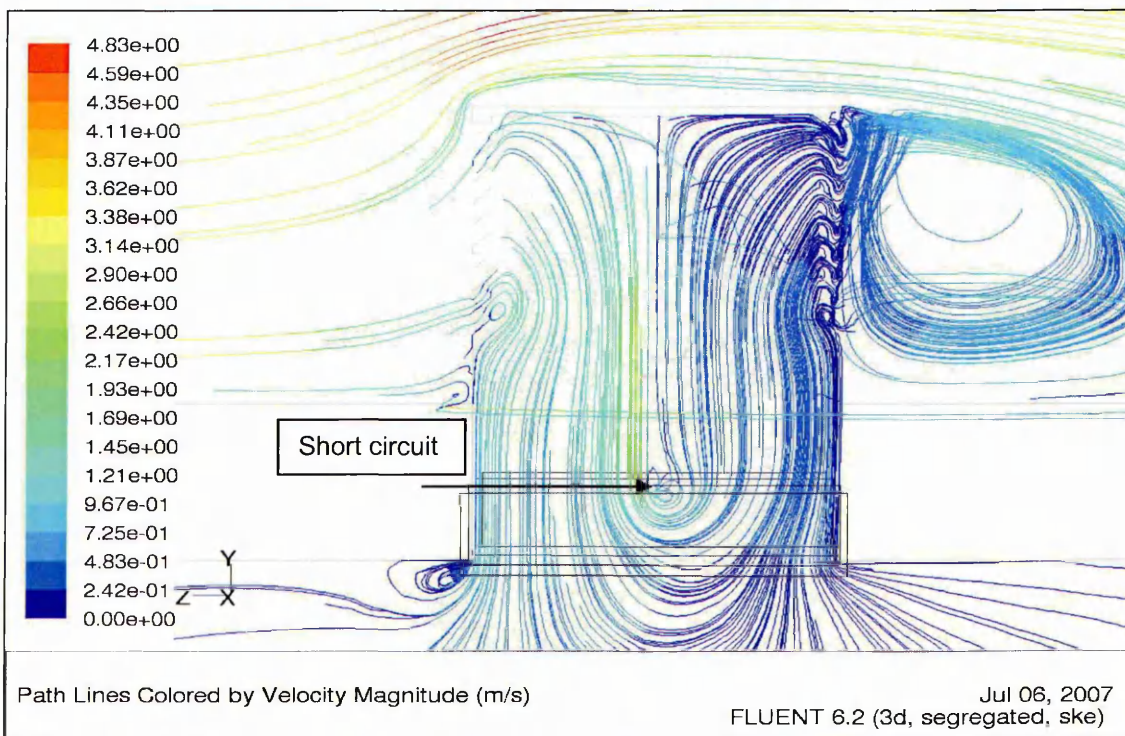
Figure 5-5 velocity vectors to illustrate the short circuit phenomena in con-current flow

Figure 5-6 shows the geometry and supplementary face, with the airflow in the counter-current direction of the dampers.

Path Lines Colored by Velocity Magnitude (m/s)   Jul 06, 2007
FLUENT 6.2 (3d, segregated, ske)
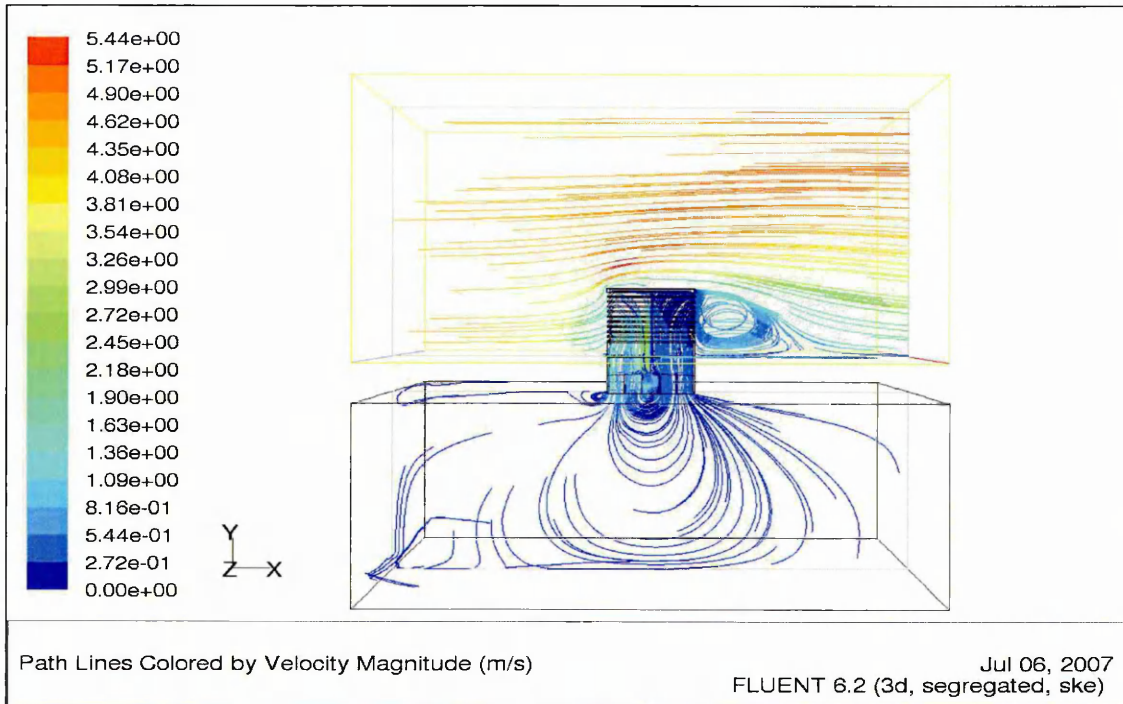
Figure 5-6 Velocity vectors for the counter-current simulation model with external velocity of 4.5m/s

Figure 5-7 shows the supplementary plane. The velocity scale on the left hand side of the Figure suggests an increased velocity range is experienced in comparison to Figure 5-4.

Path Lines Colored by Velocity Magnitude (m/s)   Jul 06, 2007
FLUENT 6.2 (3d, segregated, ske)
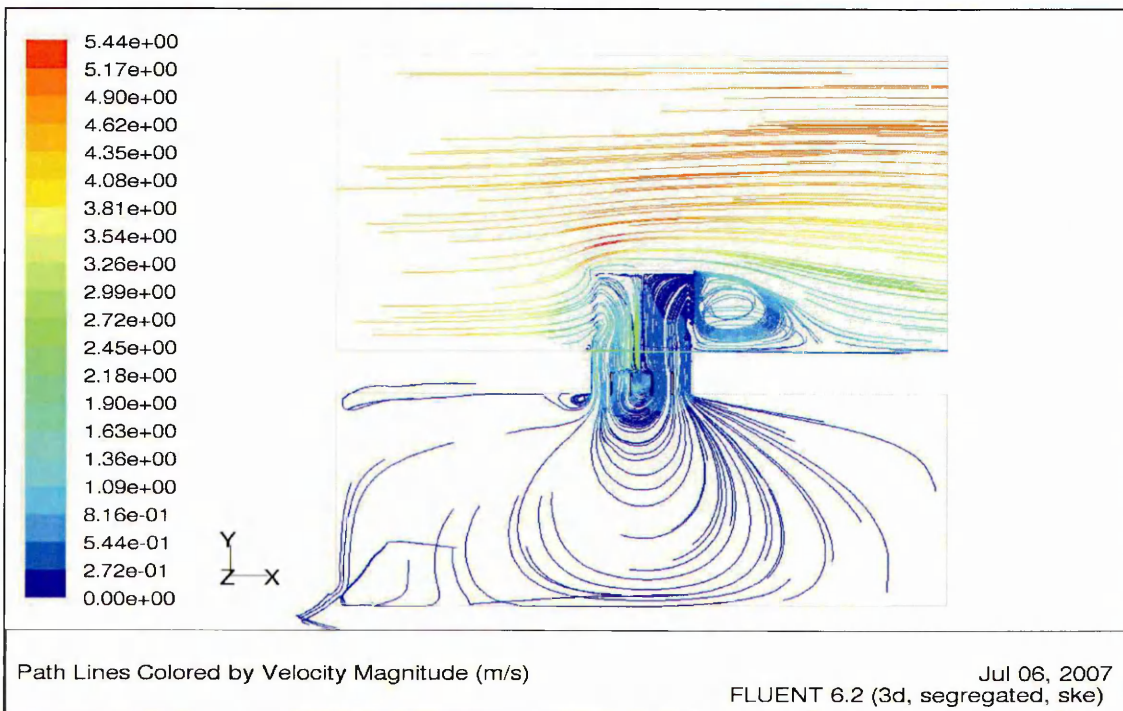
Figure 5-7 Supplementary face to illustrate the velocity vectors in the counter-current flow model with external velocity of 4.5m/s

Figure 5-8 is a zoom view of the velocity distribution inside the wind vent. The flow short-circuits. However, it is reduced in comparison with Figure 5-5.

Path Lines Colored by Velocity Magnitude (m/s)

Jul 06, 2007
FLUENT 6.2 (3d, segregated, ske)
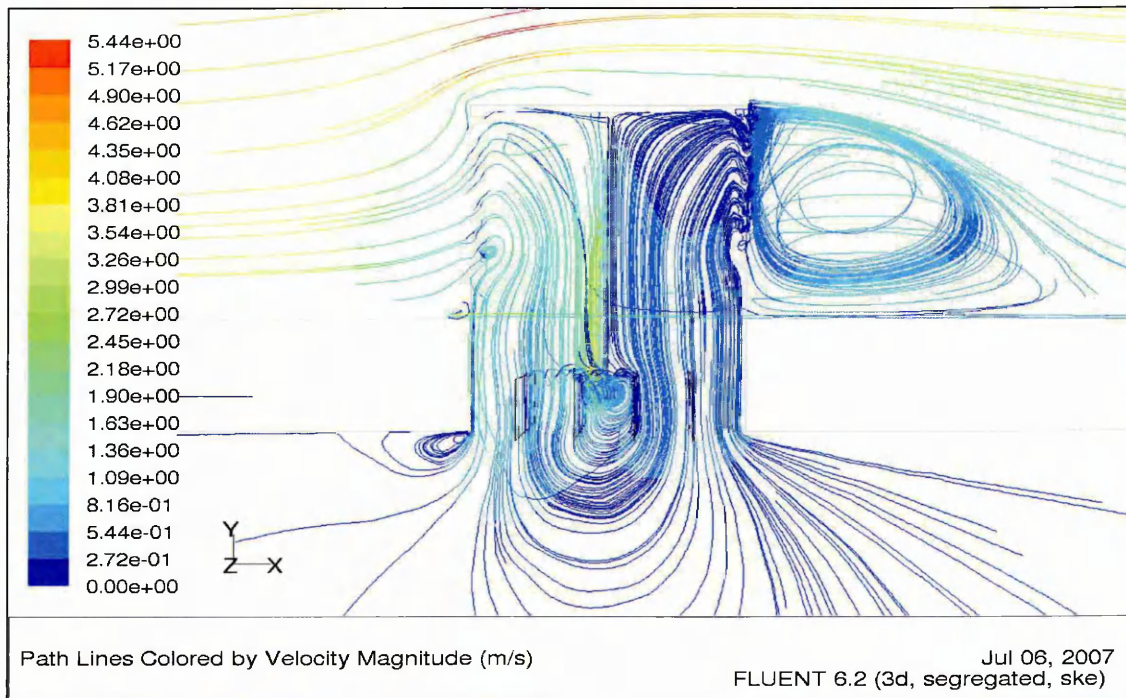
Figure 5-8 Illustration of the short circuit phenomena in the counter-current flow

Post-processing of the results from the 4.5m/s counter-current simulation was done by using contour plots of the internal, micro-climate, pressure and velocity. Figure 5-9 shows the static pressure contours of the micro-climate.

Contours of Static Pressure (pascal)

Dec 01, 2008
FLUENT 6.3 (3d, pbns, ske)
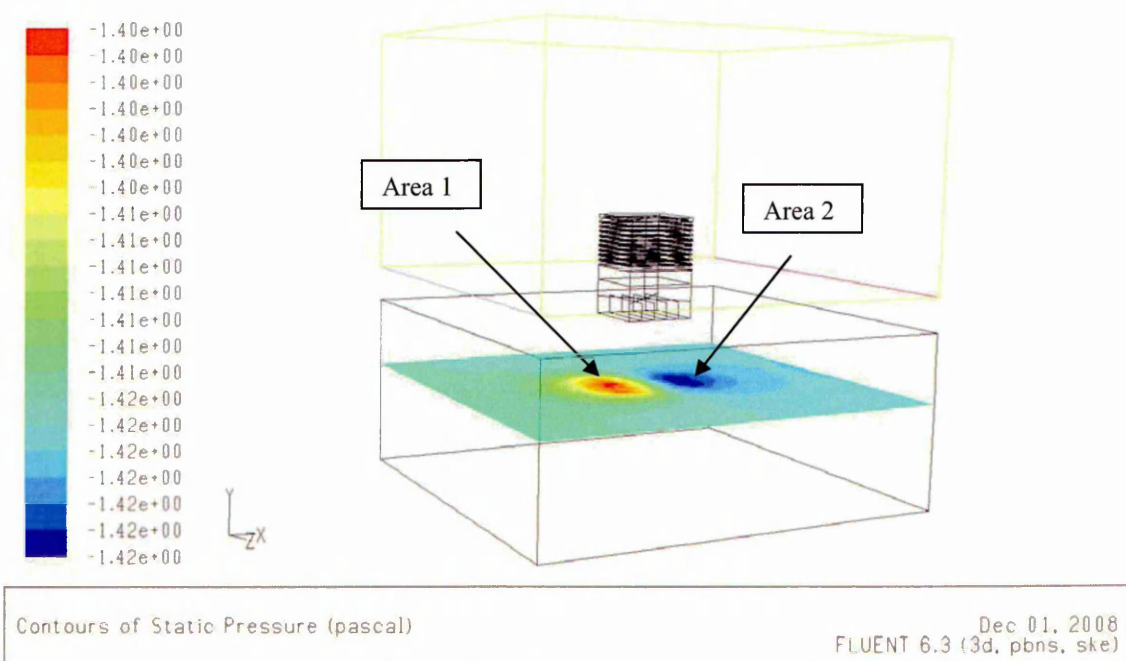
Figure 5-9 Contour plot of the internal static pressure at 4.5m/s external velocity

The results show two distinct areas of static pressure directly below the wind vent. The red area (area 1) showing a higher static pressure is on the velocity inlet side of the wind vent. The dark blue area (area 2) shows a lower static pressure on the wind vent exit side.

The velocity contour plot (Figure 5-10) shows a distinct area of higher velocity directly below the wind vent. This was expected, due to the displacement effect between inlet and outlet (detailed in Chapter 3).

Contours of Velocity Magnitude (m/s)

Dec 01, 2008
FLUENT 6.3 (3d, pbns, ske)
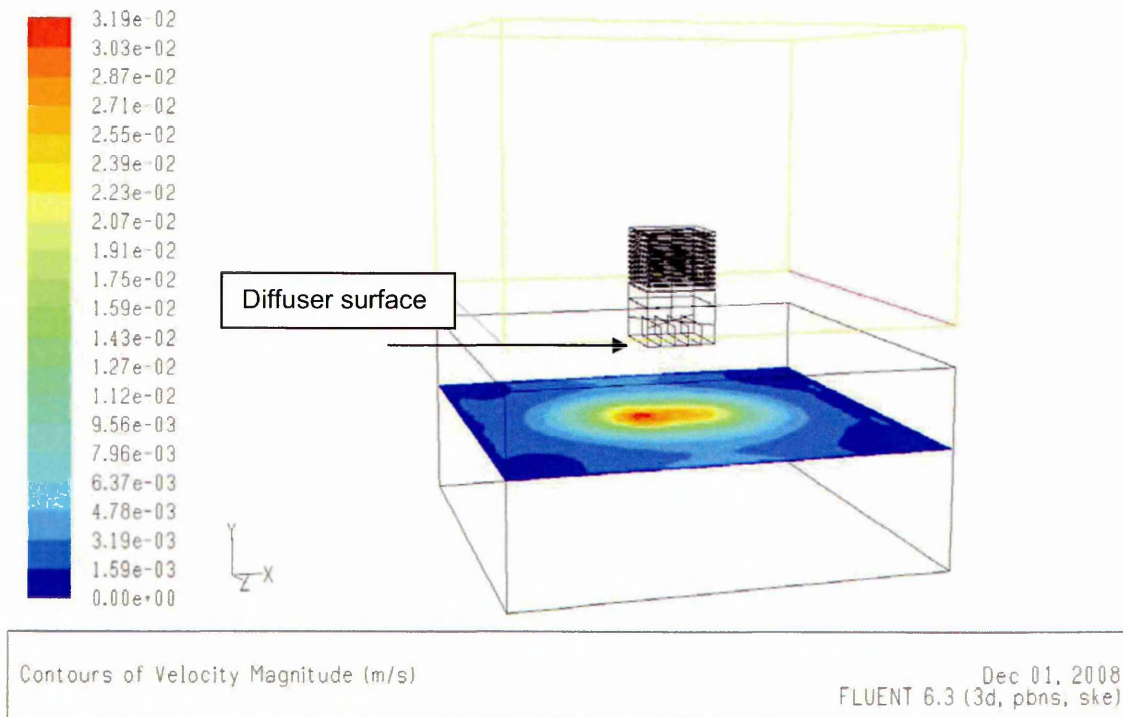
Figure 5-10 Contour plot of internal velocity at external velocity of 4.5 m/s

As expected, the maximum velocity and pressure differential was around the inlet and outlet areas of the wind vent as this is the point of air exchange. Therefore, the connecting surface (diffuser surface) was used as a performance indicator. The simulation model was solved for the full range of velocities in both directions. The velocity and dynamic pressure readings were taken from the weighted-average of the diffuser surface. The volume average internal velocity

100

was used to determine the average internal air distribution rate, as a second performance indicator. The full results for the con-current simulations are shown in Table 5-3. The counter-current simulation results are shown in Table 5-4.

Table 5-3 Simulation results of benchmark with con-current flow

Velocity inlet speed (m/s)	Diffuser velocity (m/s)	Diffuser pressure drop (Pa)	Average internal air velocity (m/s)
1	0.08	0.01	0.08
2	0.20	0.03	0.15
3	0.33	0.09	0.23
4	0.45	0.16	0.31
4.5	0.50	0.21	0.35
5	0.60	0.30	0.38

Table 5-4 Simulation results of benchmark with counter-current flow

Velocity inlet speed (m/s)	Diffuser velocity (m/s)	Diffuser pressure drop (Pa)	Average internal air velocity (m/s)
1	0.09	0.01	0.07
2	0.21	0.04	0.14
3	0.34	0.09	0.20
4	0.47	0.17	0.27
4.5	0.54	0.23	0.31
5	0.65	0.32	0.34

Tables 5-3 and 5-4 show that the direction of external wind has a nominal effect on the performance of the wind vent. The counter-current external flow has a marginal 2.4 - 8.3%, increase in diffuser velocity (Figure 5-12). The internal air distribution shows little relation to the external wind direction with a marginal increase 7.2 - 14.1% with con-current flow.

Increased wind vent performance with counter-current flow
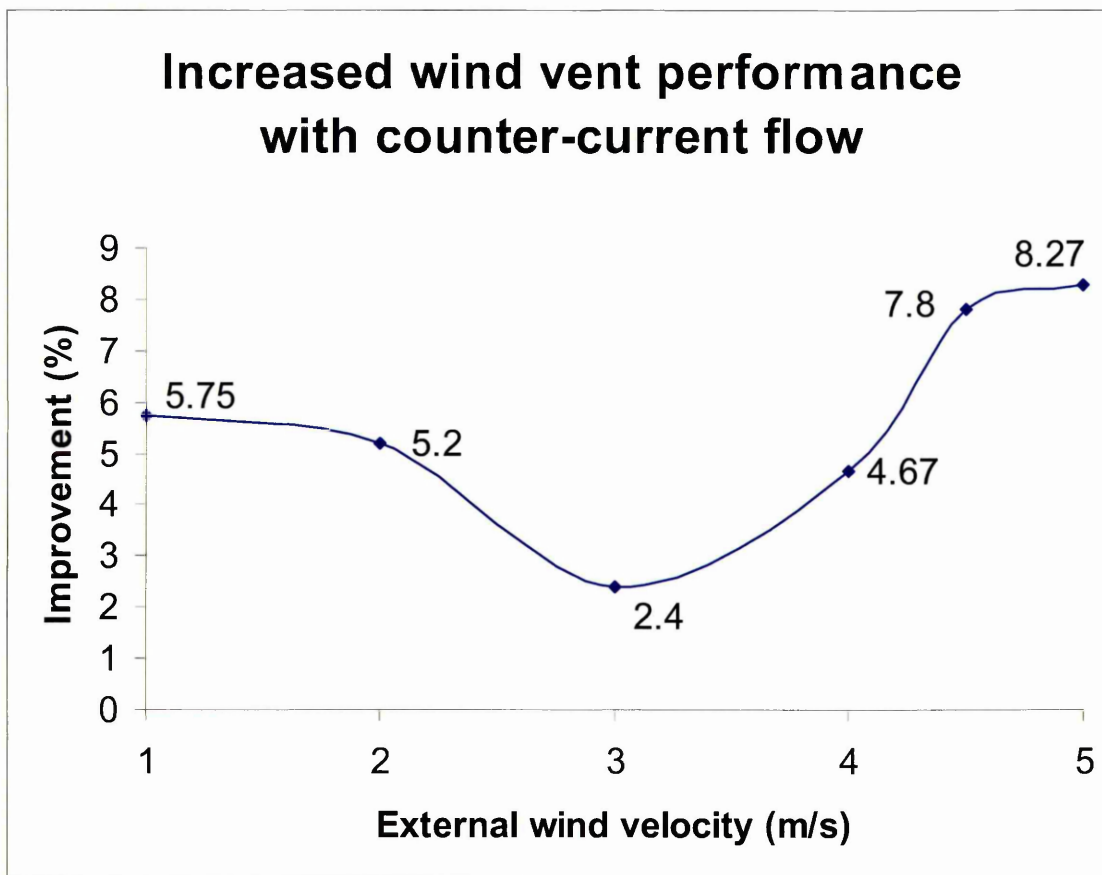
Figure 5-11 The effect of external wind direction on the diffuser velocity

Results from both simulations show the same trend with velocity, pressure and internal air distribution, increasing in proportion with an increased external wind velocity. This was as expected as the influencing forces (discussed in Chapter 3) acting upon the wind vent increase, as does the air exchange within the micro-climate. Figure 5-12 shows the increased air-exchange across the diffuser and within the micro-climate as a direct result of an increased external wind velocity.

External VS internal velocity for counter current flow
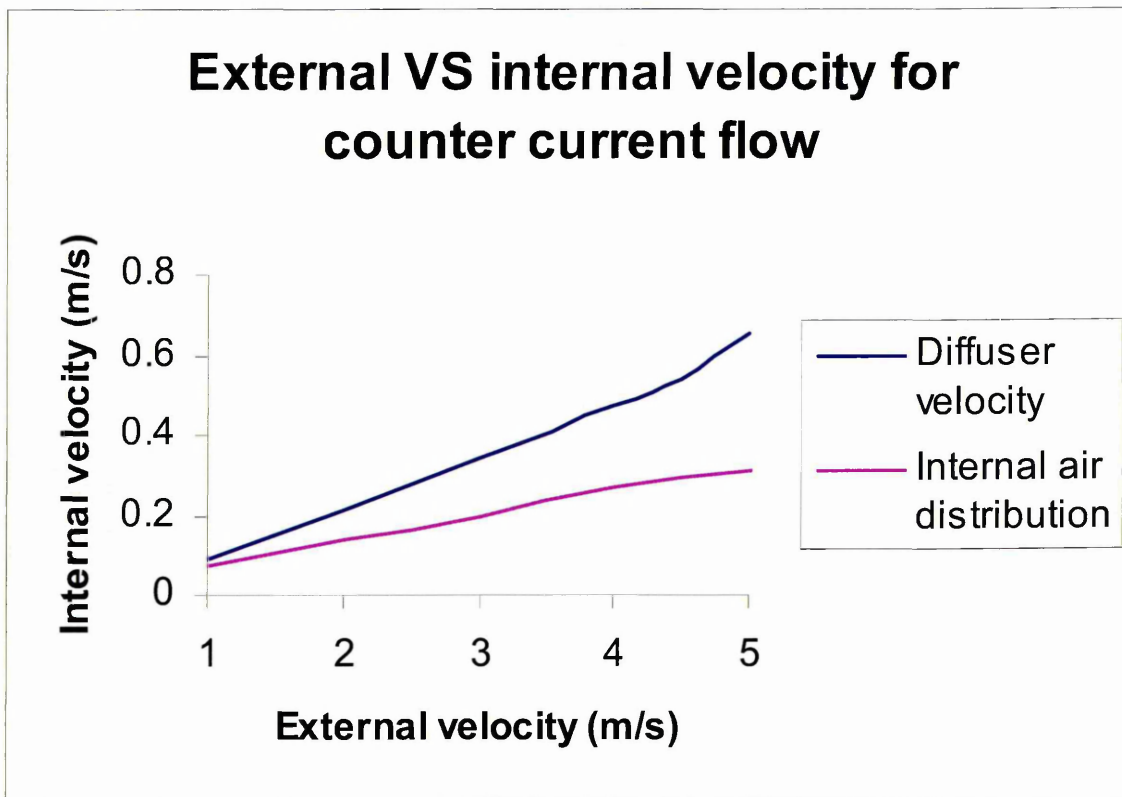
Figure 5-12 Effect of external velocity on the internal velocity for the benchmark simulation model

The objectives of this study were clearly defined in Chapter 1. One of the key objectives was to demonstrate the wind vent capabilities with respect to the BSI guidelines [BSI (1991)]. The guidelines stipulate a minimum fresh air delivery rate of 0.8L/sec per m^2 of floor area. Converting the benchmark case results to L/sec of fresh air delivery, which equates to half the diffuser rate, demonstrated the device ability to meet the BSI criteria (Table 5-5).

Table 5-5 Fresh air delivery rates of the benchmark wind vent geometry

Velocity Inlet Speed (m/s)	Diffuser Velocity (m/s)	Delivered rate (L/sec per m^2)
1	0.08	1.1
2	0.2	2.8
3	0.33	4.6
4	0.45	6.3
4.5	0.5	6.9
5	0.6	8.3

From Table 5-5 at low external velocities of 1m/s the wind vent exceeds the required minimum. The UK average wind speed is 4.5m/s [BSI (1991)]. Therefore, the wind vent has been shown to have the capability to meet the BSI guidelines.

5.3 *Control damper angle*

The geometrical variation of the control damper angle was investigated for a range of angles, fully open (0°) to fully closed (90°) (Figure 5-13).
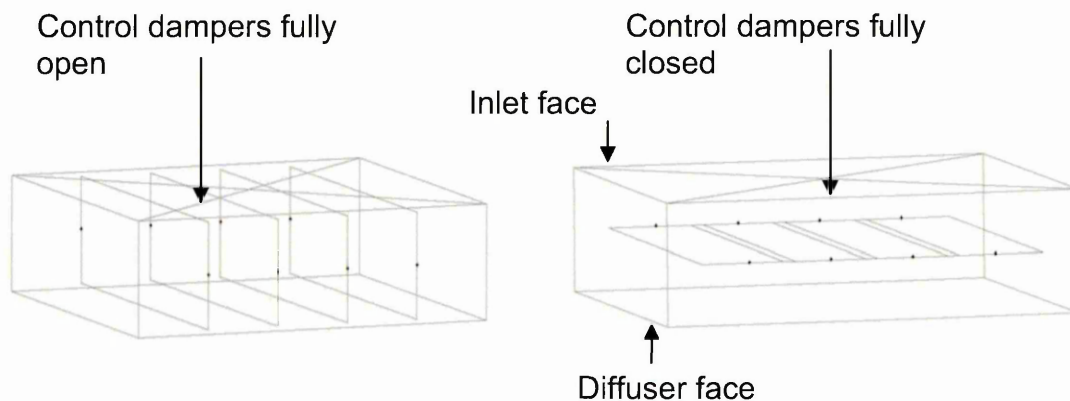
Figure 5-13 Control damper geometry for 0° and 90° simulation models

The control dampers were rotated in the clockwise direction with a new model created every 5° step. A total of 19 simulation models were created and analysed to determine the effect of the control damper angle on the wind vent performance. Unless otherwise stated a fixed external velocity of 4.5m/s at counter-current direction for all models was used. From the geometry it is noted that increasing the damper angle should restrict the velocity and increase the pressure drop across the diffuser. The control dampers regulate the flow entering the micro-climate and provide an even distribution to the internal air movement. The CFD simulations were used to determine the angle at which the

control dampers provide the most effective control of the velocity and pressure drop across the diffuser, and evenly distribute the air movement rate within the micro climate. Restricting the flow entering the diffuser has the effect of reducing the pressure on the diffuser face, whilst increasing the pressure on the inlet face, (Figure 5-13). Therefore, the pressure drop across these two faces in combination with the diffuser velocity was used to determine the most effective angle for the control dampers. The full results are shown in Table 5-6.

Table 5-6 Simulation results for control damper angle range 0° - 90°.

Damper angle	Diffuser velocity (m/s)	Inlet face pressure drop (Pa)	Diffuser face pressure drop (Pa)	Pressure drop (Pa)	Internal air distribution (m/s)
0	0.53	0.57	0.23	0.34	0.31
5	0.54	0.59	0.24	0.35	0.31
10	0.53	0.57	0.23	0.34	0.31
15	0.52	0.57	0.24	0.33	0.31
20	0.51	0.58	0.24	0.34	0.31
25	0.5	0.59	0.24	0.35	0.31
30	0.5	0.61	0.25	0.36	0.31
35	0.47	0.60	0.24	0.36	0.31
40	0.46	0.61	0.24	0.37	0.31
45	0.42	0.62	0.22	0.40	0.33
50	0.4	0.62	0.21	0.41	0.31
55	0.38	0.63	0.21	0.42	0.31
60	0.36	0.63	0.19	0.44	0.33
65	0.34	0.63	0.18	0.45	0.31
70	0.32	0.64	0.16	0.48	0.31
75	0.31	0.64	0.15	0.49	0.31
80	0.28	0.62	0.12	0.50	0.28
85	0.26	0.64	0.1	0.53	0.25
90	0.23	0.67	0.08	0.59	0.23

The simulation results showed little variation in the internal air movement rate compared to the control damper angle. The highest rates were at 45° and 60° angles. This 6% marginal increase corresponds to a drop in diffuser velocity of 26% and 47% respectively. Figure 5-14 compares the pressure-drop across the control dampers with the average-weighted diffuser velocity. The point of inter-

section, the damper angle of 45°, is the optimum to balance the air-exchange rate with internal air movement rate. The 60° angle has been discounted due to drop in velocity. By using the control damper to remove the short-circuiting phenomena the internal air movement performance of the wind vent has been increased. The velocity is attributed to air exchange, with pressure drop to direction of velocity, hence a positive pressure drop indicates a higher level of air leaving the micro climate.
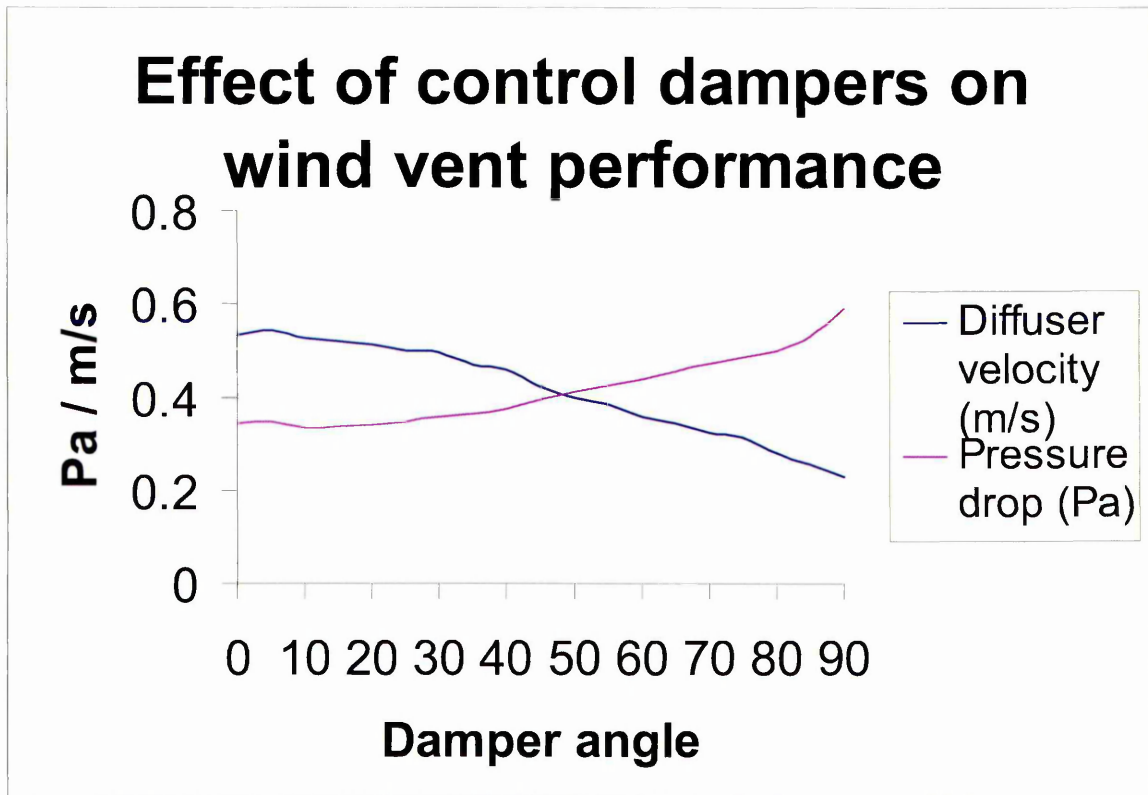
Figure 5-14 Pressure drop against diffuser velocity to establish optimum control damper angle

This investigation established the most effective damper angle to provide an even distribution of the internal air movement rate. The air movement rate was analysed using the internal velocity contours plane (Figure 5-15). With the dampers at the fully open position air enters the micro-climate centrally at its highest velocity. The velocity decreases as it distributes within the micro-climate with no pattern to the distribution.
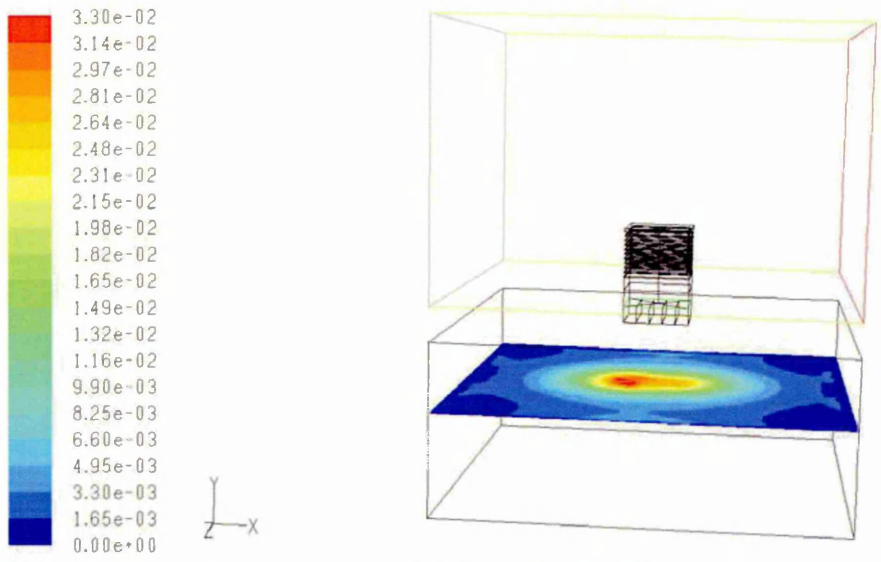
Figure 5-15 Velocity contours within the micro climate with the control dampers in the fully open position with external velocity of 4.5m/s

The velocity contours with the dampers angled at 45°, are shown in Figure 5-16. The velocity peaks centrally beneath the diffuser. When the dampers are angled at 45° the flow decreases in concentric circles within the micro-climate. The angling of the control dampers has dampened the erratic internal air movement (Figure 5-15).
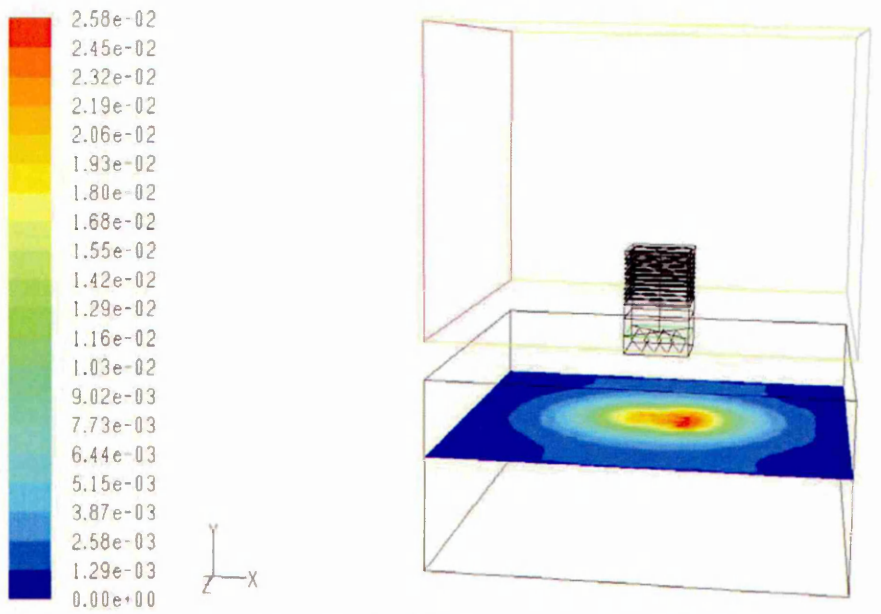
Figure 5-16 Velocity contours within the micro climate with the control dampers at 45°

Analysis of the results showed the optimum control damper angle for this application is at 45°. Using this angle produced a smooth evenly distributed flow within the micro-climate.

5.4 External louver angle

Geometrical variation of the external louver was investigated to determine its effect on the wind vent performance. The predominant geometrical dimension of the external louver is the angle of inclination, with respect to the prevailing external wind. A range of 10° to 60° louver angles were modelled. However, during the course of this experiment it was found unnecessary to investigate beyond the 45° model, the benchmark louver angle, shown in Figure 5-17.

Figure 5-17 Range of external louver angles created from 10° to 45°

Variation of the louver angle reduces the internal air volume. Therefore, the results were normalised against the benchmark volume to facilitate accurate comparison (Table 5-7).

Table 5-7 Normalising factor for louver angle investigation

Louver angle	Volume (m^3)	Factor
10	0.0122	1.34
15	0.01377	1.18
20	0.01467	1.11
25	0.01526	1.07
30	0.01568	1.04
35	0.016	1.02
40	0.01626	1.002
45	0.01629	1

The eight models were solved with an external wind speed of 4.5m/s. The resulting diffuser velocities and pressure were normalised according to Table 5-7. As the wind vent was normalised to accurately compare the results a vertical line was created in Fluent (CFD post-processor), running along the length of the inside of the vent from the highest louver to the diffuser. Hence the results are line average values as opposed to face average values. The full results are shown in Table 5-8.

Table 5-8 Normalised results for external louver angle simulation

Louver angle	Line pressure drop (Pa)	Line velocity (m/s)	Average internal air velocity (m/s)
10	4.39	1.89	0.37
15	2.67	1.69	0.34
20	1.67	1.38	0.35
25	1.66	1.42	0.36
30	1.18	1.22	0.36
35	1.29	1.29	0.45
40	5.57	2.84	0.35
45	2.88	1.99	0.31

Table 5-8 showed that at an external louver angle of 40°, the recorded velocity and pressure across the diffuser showed anomalies in comparison to the other simulation models.

Figure 5-18 illustrates the pressure build-up around the bottom louver at 35°
caused by the angle variation. The pressure had increased around this area
throughout the various increments of louver angle. This is referred to as the
attack angle as it is in direct opposition to the wind direction (detailed in Chapter
3). "Inviscid, incompressible flow theory shows that the velocity becomes
infinitely large at a sharp convex corner" [Anderson (2007)]. The leading edge of
a flat plate at an angle of attack is such a case and the wind vent louver similar
to a sharp convex corner. When the angle of attack exceeds a critical value, the
flow separation occurs over the top surface of the louver. This is termed "the
stalling angle of attack". Behaviour associated with the extreme thinness of an
airfoil, (or in this case wind vent louver), is labelled as thin airfoil stall.

8.00e+00	
7.55e+00	
7.10e+00	
6.65e+00	
6.20e+00	
5.75e+00	
5.30e+00	
4.85e+00	
4.40e+00	
3.95e+00	
3.50e+00	
3.05e+00	
2.60e+00	
2.15e+00	
1.70e+00	
1.25e+00	
8.00e-01	
3.50e-01	
-1.00e-01	
-5.50e-01	
-1.00e+00	

Contours of Dynamic Pressure (pascal)   Sep 12, 2007
                                        FLUENT 6.2 (3d, segregated, ske)
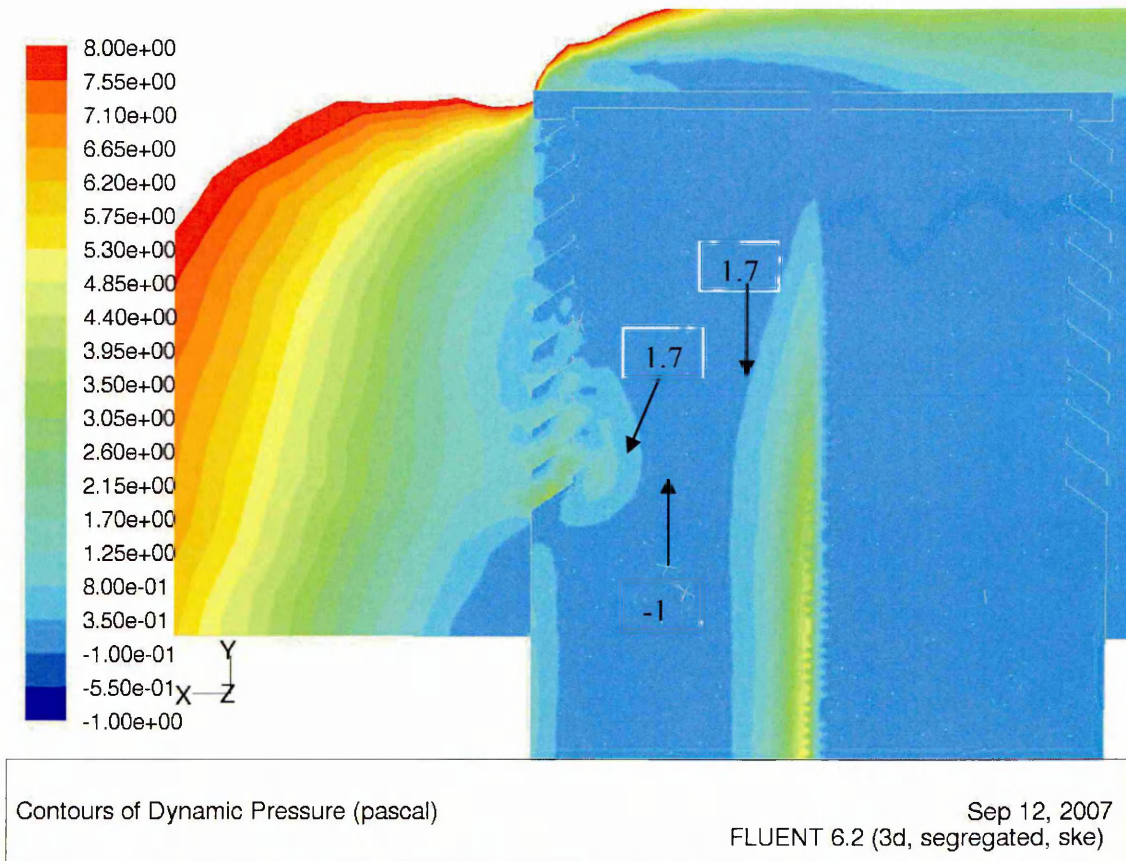
Figure 5-18 CFD prediction of pressure contours at louver angle of 35°

Figure 5-19 illustrates the increased pressure caused by increasing the louver

angle from 35 to 40°. Comparison of the pressure contours at 35° shows the

pressure has increased from 1.1 to 5 Pa, causing a restriction within the wind

vent. At the louver angle of 40°, the flow has stalled and as such the results are
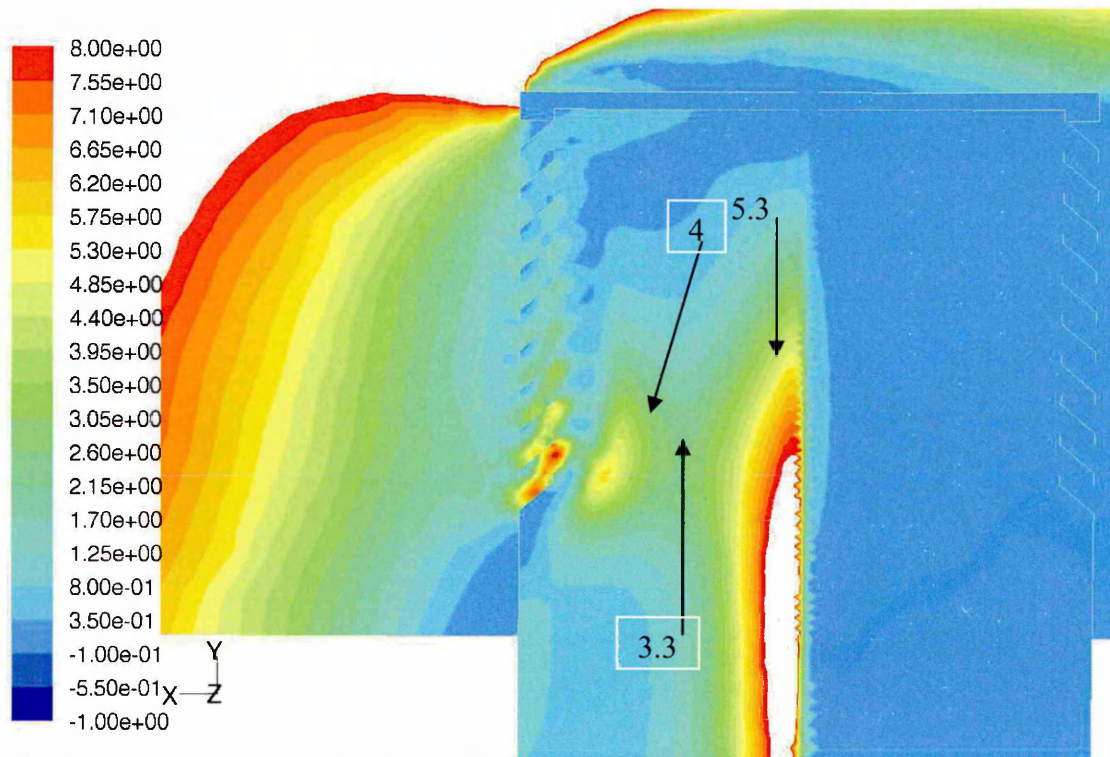
unreliable.

Figure 5-19 CFD predicted pressure contours at louver angle of 40°

Contours of Dynamic Pressure (pascal)

Sep 12, 2007
FLUENT 6.2 (3d, segregated, ske)
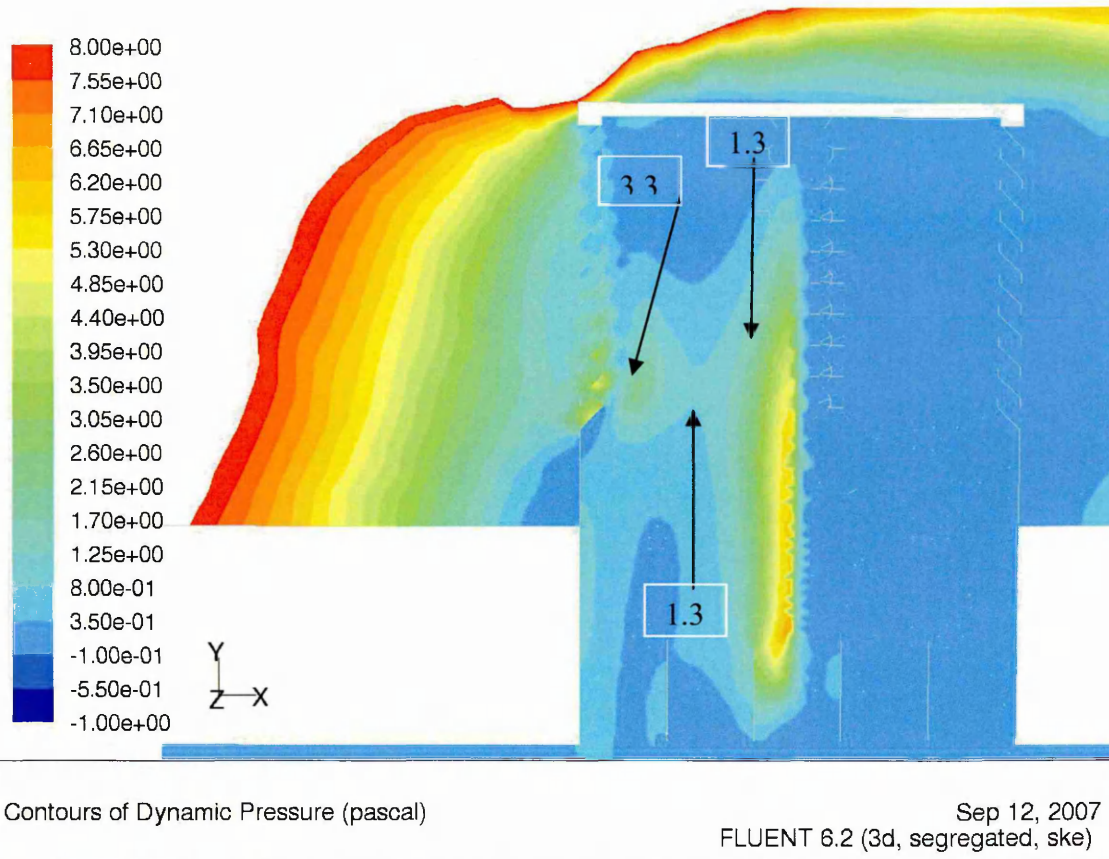
Figure 5-20 CFD predicted pressure contours at louver angle of 45°

A close scrutiny of Figures 5-19 and 5-20 shows a decrease in pressure within

the wind vent. The louver angle has now passed the critical stall point. This

demonstrated known aerodynamic theory regarding trailing-edge stall (as

detailed in Chapter 3). Lift coefficient curves for thin airfoil plates show a linear

rise up until the point of stall. After this peak the curve regresses and the

behaviour is no longer linear. The louver angle at 45°, compared to the 30° and

35° angles, showed that the pressure restriction had been overcome. Thus,

confirming that the stall angle had been surpassed. The simulation of external

louver angles greater than 45° was unnecessary, as the anticipated velocity and

pressure increase had peaked. Comparison of average diffuser velocity and

dynamic pressure showed that the external louver angle was significant on

these RPD parameters (Figure 5-21). The graph shows two points of

intersection, the 30° and 35° cases. The intersections demonstrated the

pressure, equated to flow direction and velocity, equated to air-exchange, are working in tandem representing potential for an optimised external louver angle.

Effect of external louver angle on diffuser velocity and pressure drop
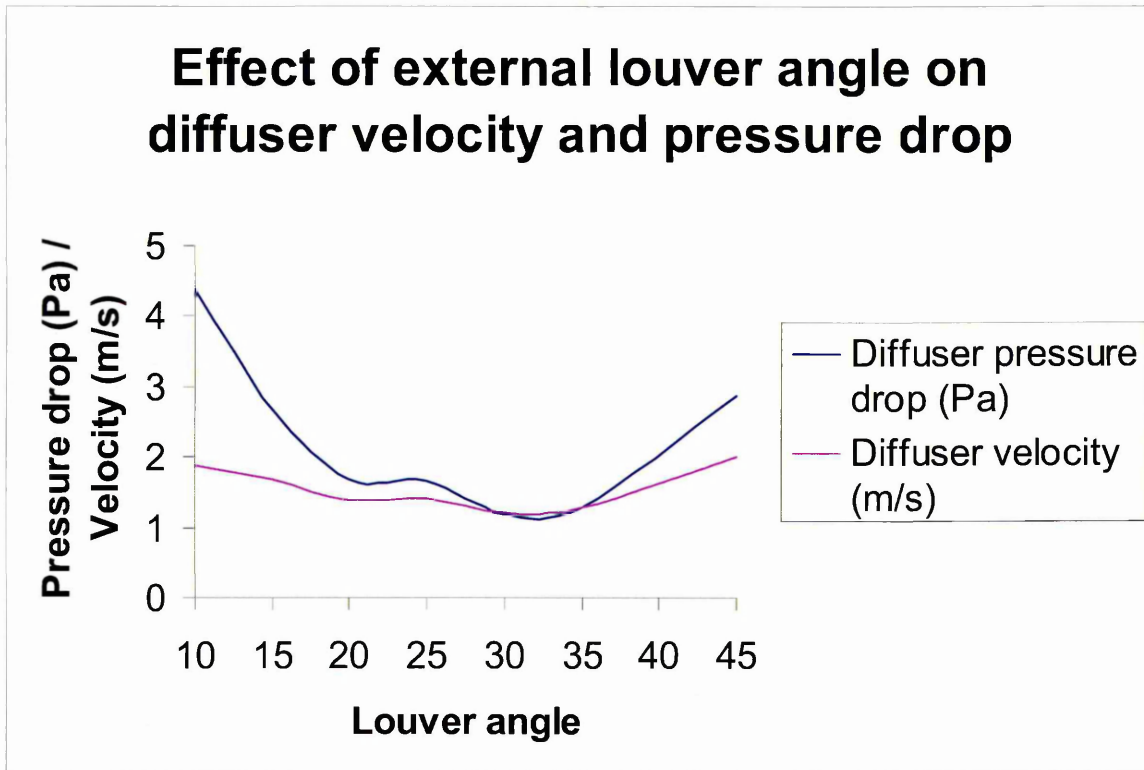
Figure 5-21 Effect of external louver angle variation on diffuser velocity and pressure

A third performance parameter, the internal air movement rate, showed little improvement through the incremental louver angle simulations. However, air movement rate compared to the louver angle in conjunction with the two remaining parameters, demonstrated clear advantage at the 35° intersection (Figure 5-22). The air movement rate has been multiplied by ten and then superimposed onto the graph for comparison with the line results.

Figure 5-22 Effect of external louver angle on wind vent performance

With the external louver angle of 35°, the internal air distribution shows a dramatic increase over the benchmark case. The air distribution velocity has increased by 45% over that of the benchmark model. The velocity contours confirm an increased internal air movement (Figure 5-23). Thus, the results confirmed that the optimum external louver angle is 35°.

2.07e-02	
1.97e-02	
1.86e-02	
1.76e-02	
1.66e-02	
1.55e-02	
1.45e-02	
1.35e-02	
1.24e-02	
1.14e-02	
1.04e-02	
9.32e-03	
8.28e-03	
7.25e-03	
6.21e-03	
5.18e-03	
4.14e-03	
3.11e-03	
2.07e-03	
1.04e-03	
0.00e+00	

Contours of Velocity Magnitude (m/s)

Dec 01, 2008
FLUENT 6.3 (3d, pbns, ske)
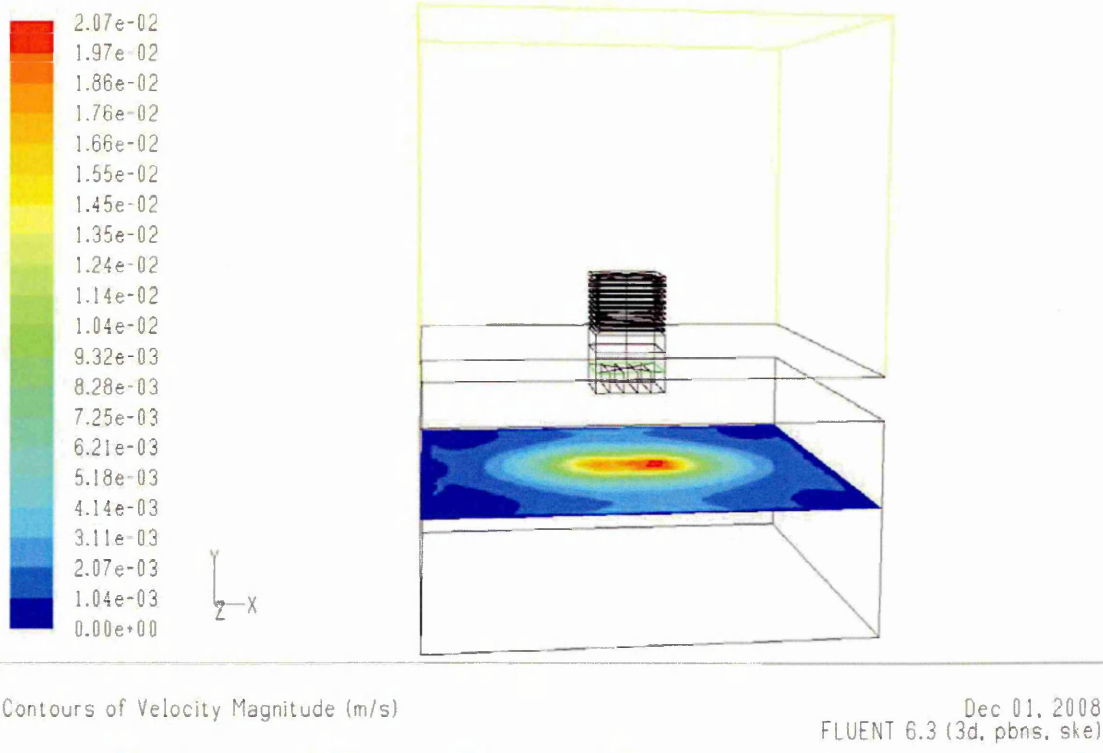
Figure 5-23 Velocity contours within the micro climate with an external louver angle of 35°

5.5 Number of external louvers

The benchmark wind vent contained eight active louvers. To determine the effect of the number of louvers on performance, four simulation models were created to reflect different number of external louvers. The number of louvers simulated were two, four, six and eight. The extremes of the range are shown in Figure 5-24.
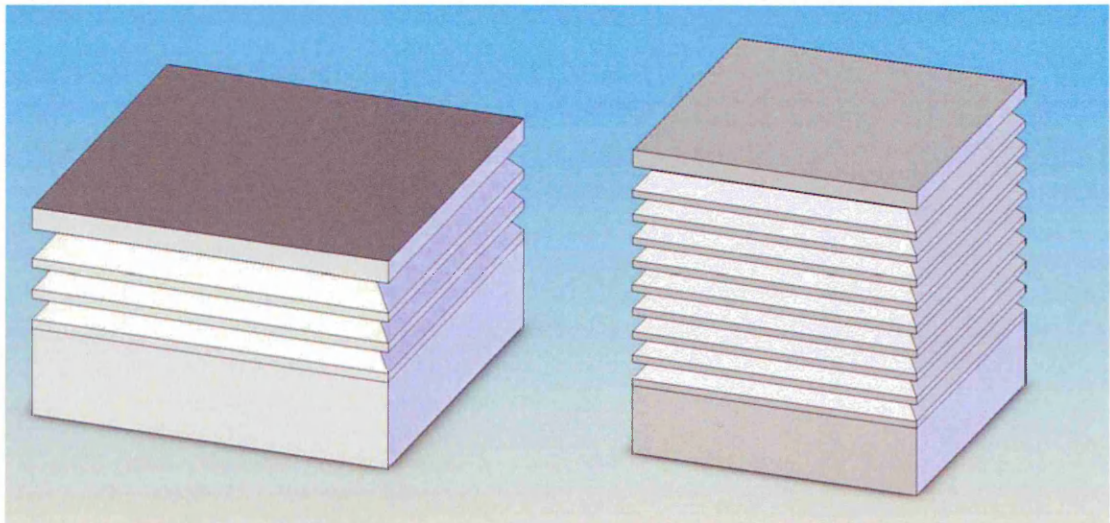
Figure 5-24 Range of simulation models, two to eight louvers, created to determine the effect of additional external louvers

115

The models were solved with an external wind velocity of 4.5m/s. The diffuser face was used to indicate the average velocity and pressure. The full results are shown in Table 5-9.

Table 5-9 Simulation results of varying the number of external louvers

Number of external louvers	Diffuser face velocity (m/s)	Diffuser face pressure drop (Pa)	Average internal air velocity (m/s)
2	0.22	0.03	0.34
4	0.42	0.13	0.35
6	0.52	0.21	0.34
8	0.57	0.25	0.34

From the results, increasing the number of external louvers leads to a direct increase in the diffuser face velocity and dynamic pressure. The internal air distribution is unaffected by the number of external louvers. The comparison of the simulation models is shown in Figure 5-25.
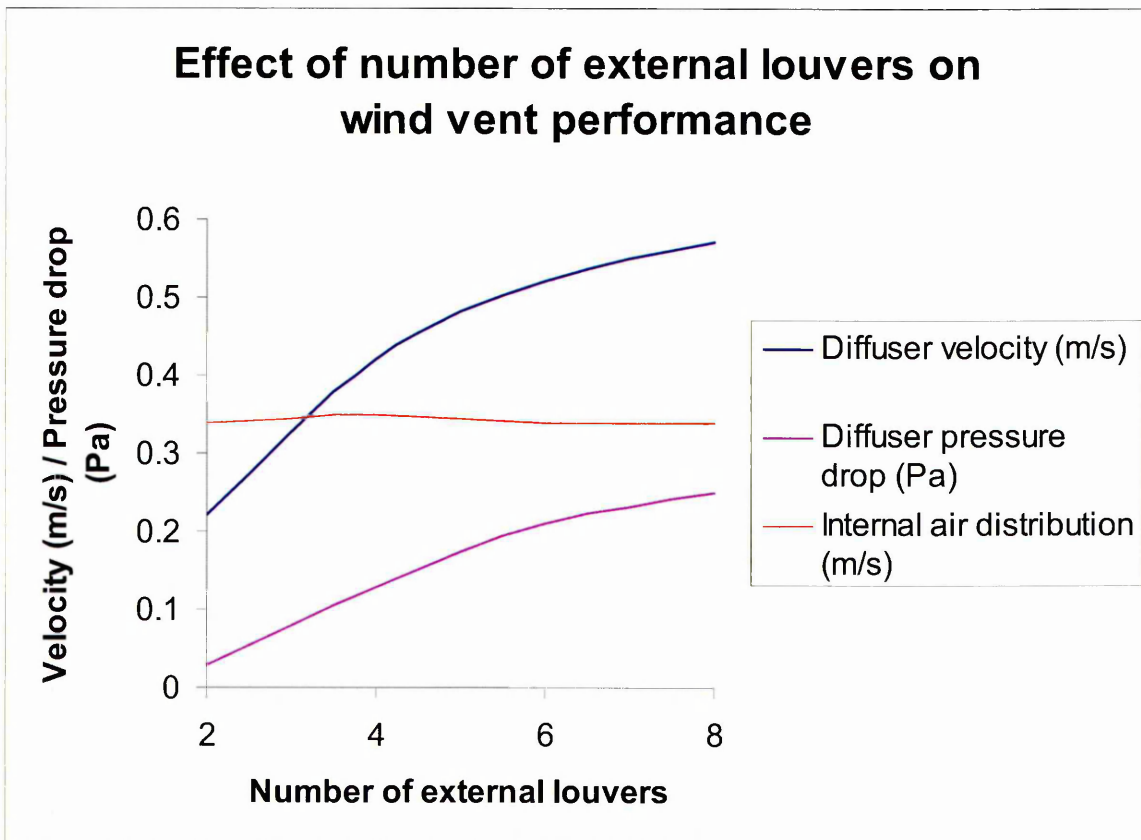
Figure 5-25 Effect of number of external louvers on the wind vent velocity and pressure

The results were as expected. As the effect of adding external louvers is to create a larger internal volume within the wind vent which will allow greater air-exchange between macro and micro-climate. The increased pressure is due to the added height of the wind vent creating a greater fluid head. This phenomena is encapsulated by Bernoullis equation (detailed in Chapter 3).

From this investigation, the optimum performance model is the eight louver model as it generates the greatest air-exchange rate across the diffuser face. However, the four louver model generates the same (nominally increased) internal air movement rate with a 35% decrease in air exchange, using half the material of an eight louver model (Figure 5-26), which would be desirable and hence a subjective optimum model.

Contours of Velocity Magnitude (m/s)

Dec 01. 2008
FLUENT 6.3 (3d, pbns, ske)
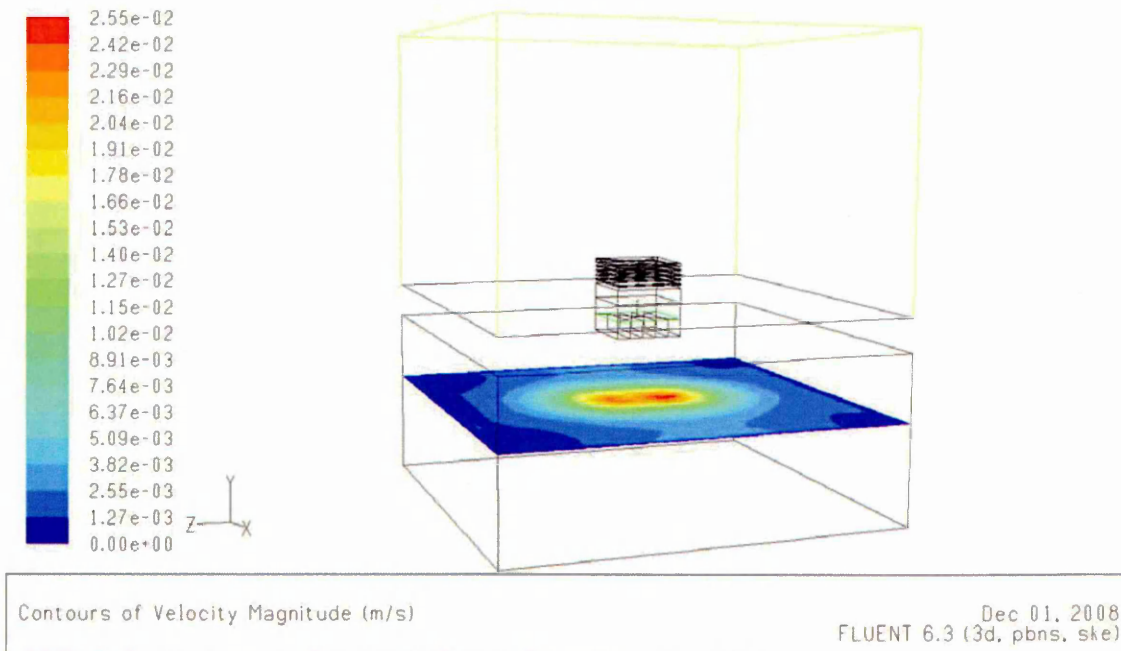
Figure 5-26 Velocity contours within the micro climate of the four louver simulation model

5.6 External louver spacing

The distance between external louvers was investigated to determine the effect on the overall performance of the wind vent. The benchmark case had 50mm

spacings between external louvers. Five new CFD models were created with variation of the distance between the external louvers. The new models had louver spacings of 10, 20, 30, 40, and 60mm (Figure 5-27).

Distance between the two arrows represents the louver spacing
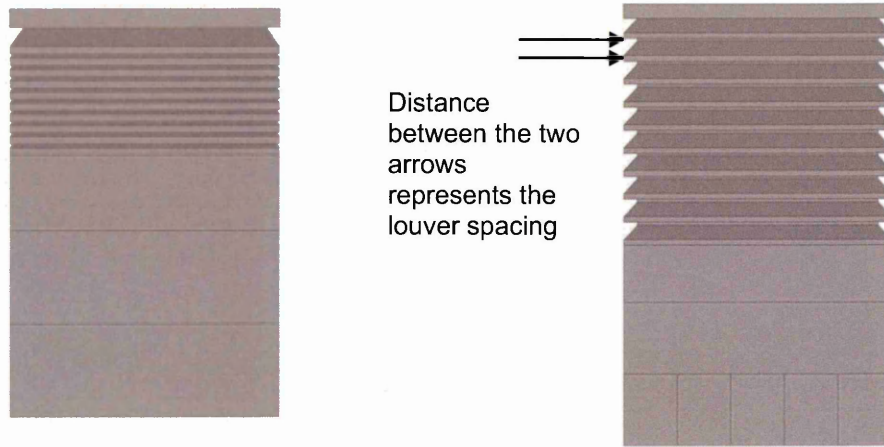
Figure 5-27 Limits of simulation models for external louver spacing (from 10 to 60mm).

The five simulation models were solved with an external wind velocity of 4.5m/s, all other geometry remained constant. Full results are shown in Table 5-10.

Table 5-10 Simulation results of the external louver spacing variation

Louver spacing distance (mm)	Diffuser face velocity (m/s)	Diffuser face pressure drop (Pa)	Average internal air velocity (m/s)
10	0.2	0.03	0.34
20	0.38	0.11	0.36
30	0.42	0.15	0.37
40	0.59	0.41	0.36
50	0.54	0.23	0.31
60	0.67	0.42	0.38

From the results, as the louver spacing increased the diffuser velocity and pressure also increased. At the benchmark case, 50mm, there was an anomaly within the data, both the velocity and pressure decreased from the 40mm case. Comparison of the 60 and 40mm case showed a similar diffuser pressure with a higher diffuser velocity in the 60mm case. This comparison showed that

although the air-exchange rate had increased, the pressure driving the flow through the wind vent had not. The internal air distribution similarly increased, in proportion to the increased louver spacing. This was as expected with a greater inlet and outlet area, allowing a greater suction effect within the micro-climate (detailed in Chapter 3). Comparison of the three performance indicators is shown in Figure 5-28.
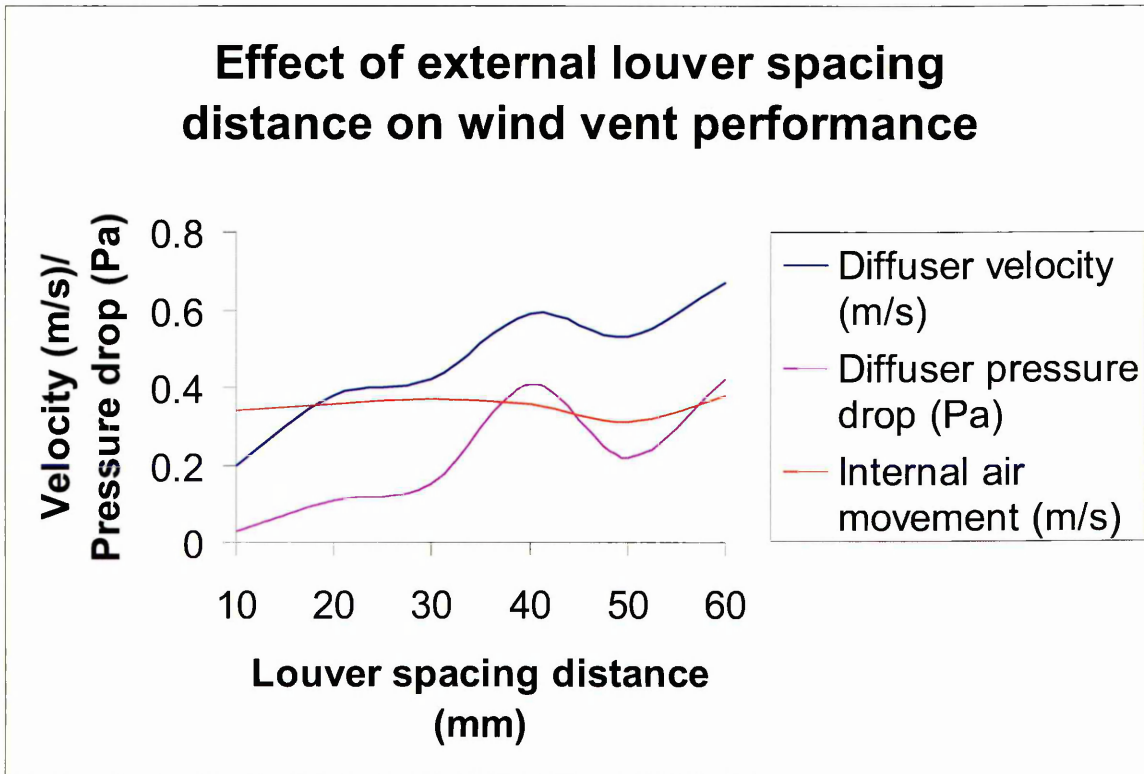
Figure 5-28 Effect of external louver spacing distance on the wind vent performance

The velocity and pressure trends have two peaks at 40mm and 60mm respectively. The internal air movement similarly has two peaks at 30mm and at 60mm. Comparing Table 5-10 and Figure 5-28, the results show that the optimum louver spacing is at 60mm. This is due to the combination of performance indicators being at the highest level at this geometrical configuration. However, the purpose of the external louver is to deflect prevailing rain whilst allowing air to enter. Therefore, increasing the louver spacing would in logical terms have an adverse effect on deflecting the rain

119

ingress. Hence, an subjective optimum setting for the spacing is to generate the maximum internal air movement rate or suction within the micro-climate, with the minimum louver spacing to prevent rain ingress. The subjective optimum louver spacing distance for this application is 30mm. Further analysis of the velocity contours confirmed this (Figure 5-29).

Contours of Velocity Magnitude (m/s)

Dec 01, 2008
FLUENT 6.3 (3d, pbns, ske)
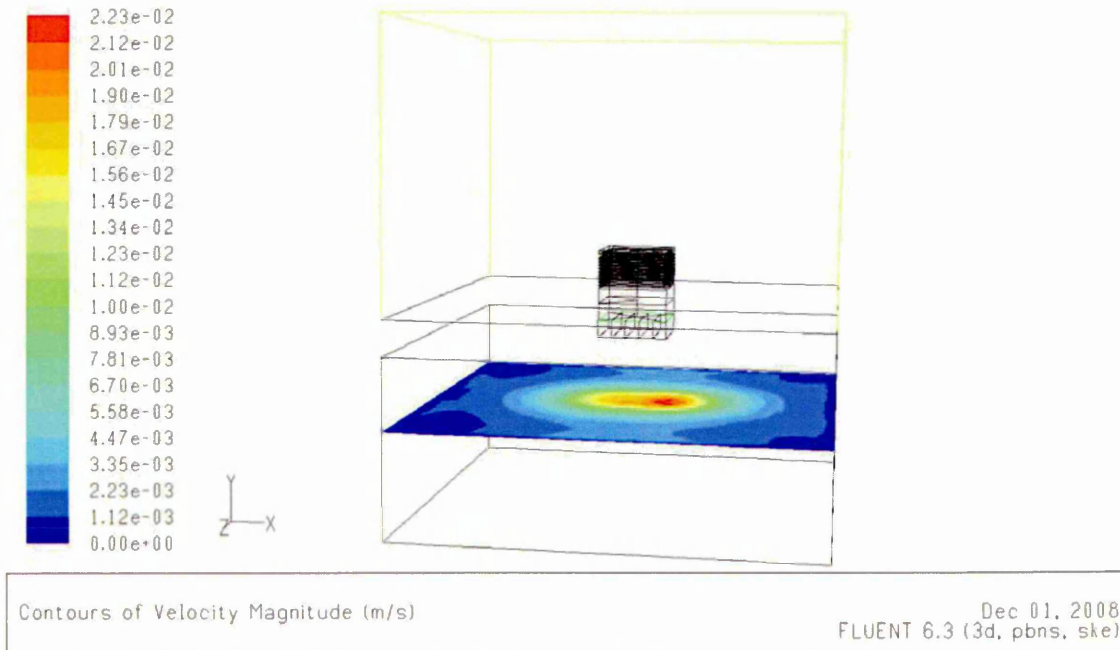
Figure 5-29 Velocity contours within the micro climate with an external louver spacing distance of 30mm

With an external louver spacing distance of 30mm, air exchange rate is lower than the benchmark with a 30% reduction. However, the internal air movement rate has increased by a comparative margin of 27%. The increased benefit to the wind vent is that the smaller louver spacing should aid the louver design effect of minimising rain ingress.

5.7 Internal cross dividers

To investigate the effect of internal cross-dividers on wind vent performance, two simulation models were built. The first model removed the cross dividers

from the wind vent. The second added an additional cross-divider to the bench

mark model giving a total of two cross dividers or eight faces (Figure 5-30).
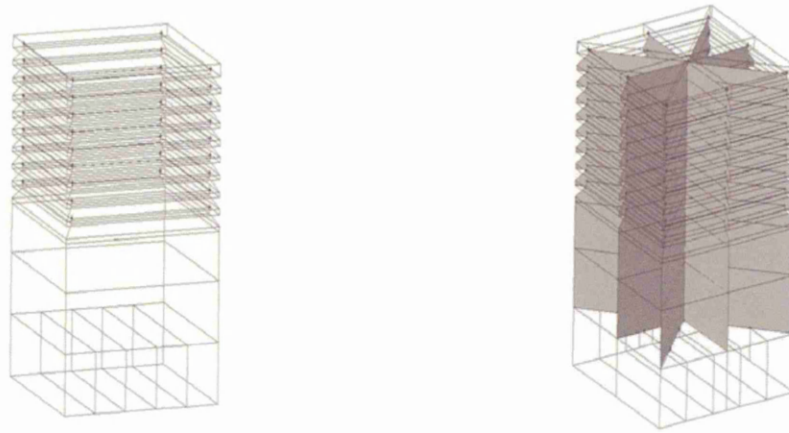
Figure 5-30 Range of simulation models built for internal cross dividers experimentation, from zero to two internal cross dividers

The simulation models were solved for an external wind velocity of 4.5m/s. The

complete results are shown in Table 5-11.

Table 5-11 Simulation results for internal cross divider experiments

Number of internal cross dividers	Diffuser face velocity (m/s)	Diffuser face pressure drop (Pa)	Internal air distribution (m/s)
0	0.02	0	0.36
1	0.57	0.25	0.34
2	0.7	0.38	0.34

The results showed that the cross-divider had a direct effect on both the velocity

and pressure on the diffuser face. This was as expected as the purpose of the

dividers is to direct external wind down-wards and into the micro climate. The

air distribution rate was not affected when comparing the benchmark case, one

cross-divider and the two cross-dividers. However, comparison of the zero

dividers case with the benchmark showed an increased air distribution rate with

the removal of the cross dividers (Figure 5-31). Removing the cross divider

caused the maximum suction effect (detailed in Chapter 3) of the wind vent to

move position from the diffuser face to the top of the wind vent. Due to the external wind having no direction (downwards), the airflow passes through the vent, termed passive stack. The net result is that the increased suction head of the device leads to an increased internal air movement rate.
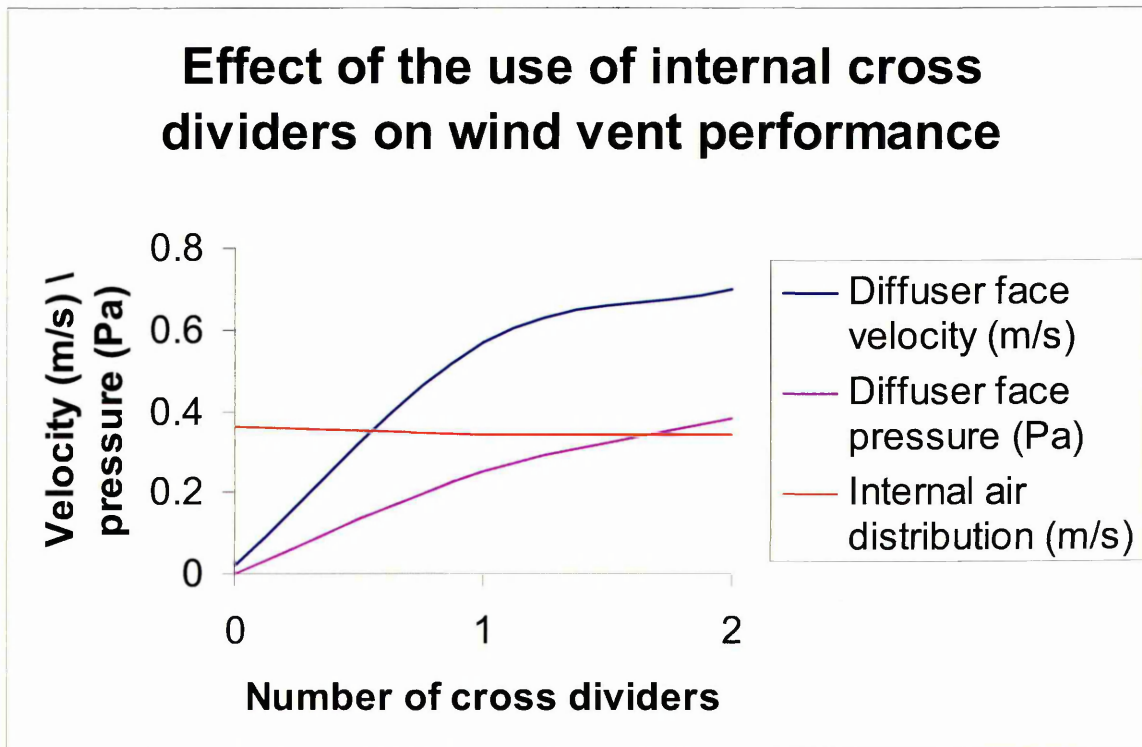
Figure 5-31 Effect of internal cross dividers on the wind vent performance

The results show that an increase in the cross dividers leads to a proportional increase in diffuser velocity and pressure. Increased velocity and pressure demonstrates a greater air-exchange rate within the micro-climate. The internal distribution remained unchanged from the benchmark case. The zero dividers case improved the internal air movement rate. However, the delivered velocity and pressure are significantly reduced by 95%. The wind vent is used to deliver and exchange air at the most efficient rate, thus the optimum design is the two cross-dividers case shown in Figure 5-32.

| 5.37e-02 |
| 5.10e-02 |
| 4.83e-02 |
| 4.56e-02 |
| 4.30e-02 |
| 4.03e-02 |
| 3.76e-02 |
| 3.49e-02 |
| 3.22e-02 |
| 2.95e-02 |
| 2.69e-02 |
| 2.42e-02 |
| 2.15e-02 |
| 1.88e-02 |
| 1.61e-02 |
| 1.34e-02 |
| 1.07e-02 |
| 8.06e-03 |
| 5.37e-03 |
| 2.69e-03 |
| 0.00e+00 |

Contours of Velocity Magnitude (m/s)

Dec 01, 2008
FLUENT 6.3 (3d, pbns, ske)
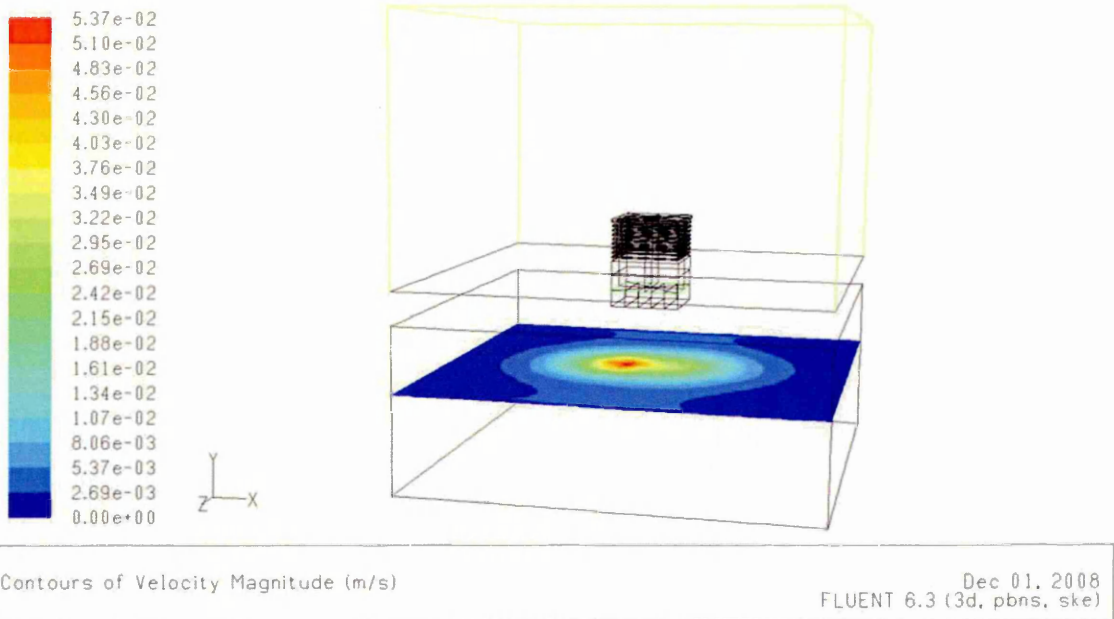
Figure 5-32 Velocity contours within the micro climate with two internal cross dividers

5.8 Internal fan

Simulation results showed that the suction effect drives the internal air distribution velocity. Therefore, to improve this rate an artificial suction rate was investigated. Using a fan within the wind vent to draw in external air and drive it into the micro-climate was simulated. A fan was created using a 0.5m diameter face, and the boundary condition fan. A range of fan pressures 20, 40, 60, 80 and 120Pa, matched to a commercially available product [Remco (2007)] were simulated. Three different fan locations were used namely top, middle and bottom (Figure 5-33).

Figure 5-33 The three fan positions used in the simulation models

5.8.1 Fan located at top position

Figure 5-34 depicts the velocity vector plot of the flow with the fan in top position. The flow was drawn into the fan, tunnelled centrally through the wind vent, into the micro-climate, allowing exhaust or spent air to exit via the bottom blades of the wind vent. The flow induced by the fan within the device, allows the exhaust air to exit via two areas either side of the fan-controlled air-jet entering the room.

Velocity Vectors Colored By Velocity Magnitude (m/s)   Dec 10, 2007
FLUENT 6.2 (3d, segregated, ske)
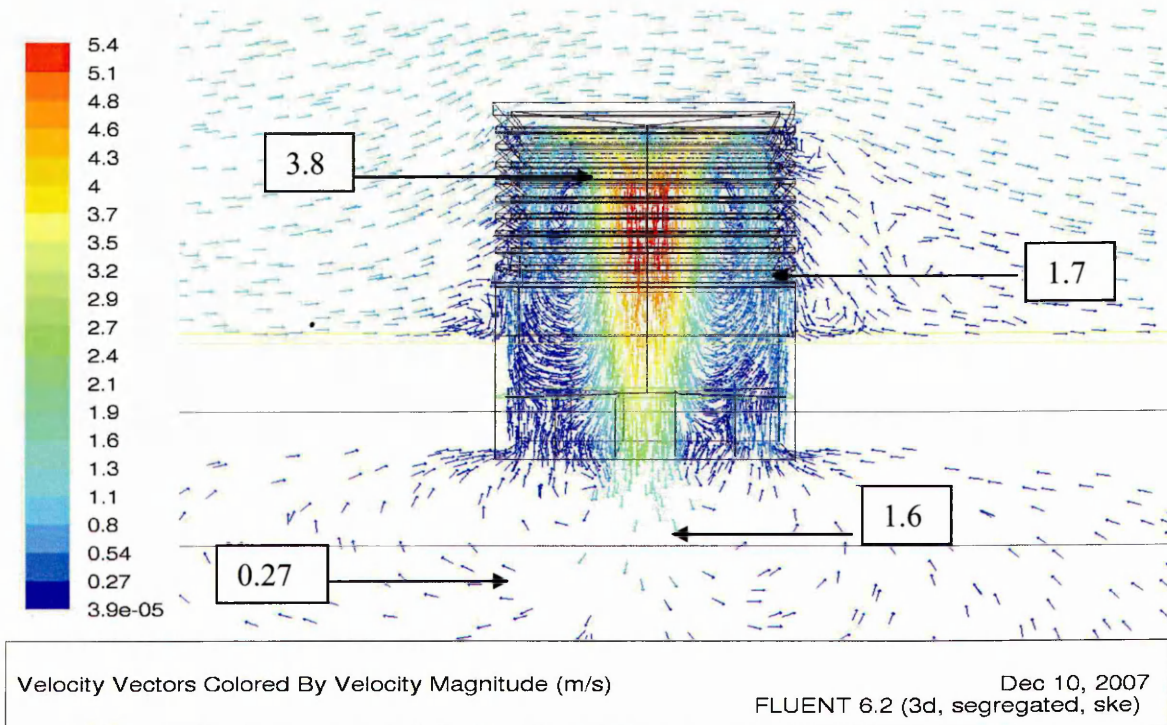
Figure 5-34 Fresh airflow path with fan in top position with 20Pa induced fan pressure

5.8.2 Fan located at middle position

The middle position showed the flow to be separated in the left hand quadrant due to the effect of the fan creating eddies and restricting the natural flow path (Figure 5-35). Additionally there was no clear path for the exhaust air to exit back to atmosphere. Without a clear area for the exhaust air to exit through the vent, the air is re-circulated around the room by the effective fan pressure. Consequently, in the middle position, the fan is no longer supplying the fresh air from the left hand quadrant, thus minimising the make-up air.

Velocity Vectors Colored By Velocity Magnitude (m/s)   Dec 10, 2007
                                                    FLUENT 6.2 (3d, segregated, ske)
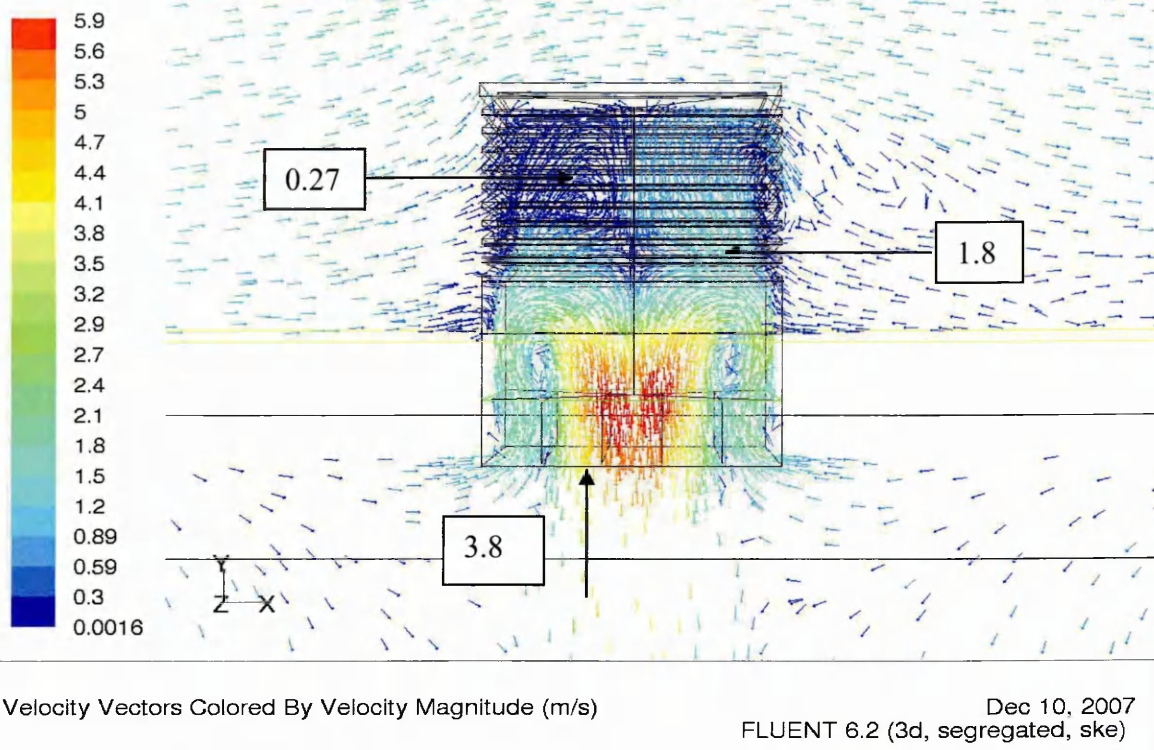
Figure 5-35 Fresh airflow path with fan in middle position with 20Pa induced fan pressure

5.8.3 Fan located at bottom position

Figure 5-36 depicts the effect of the fan in the bottom position. Results showed

that in this position, both quadrants demonstrate significant flow separation due

to eddies causing restriction to the natural flow path. In this position, the

exhaust air from the micro-climate has no clear path to exit the wind vent.

Without a clear area for the exhaust air to exit through the vent, it is re-

circulated around the room by the effective fan pressure. In the bottom position,

the fan is no longer supplying the fresh air from either quadrant. This

configuration has decreased the fresh-air supply capabilities of the device from

the previous fan positioning.

Velocity Vectors Colored By Velocity Magnitude (m/s)   Dec 10, 2007
FLUENT 6.2 (3d, segregated, ske)
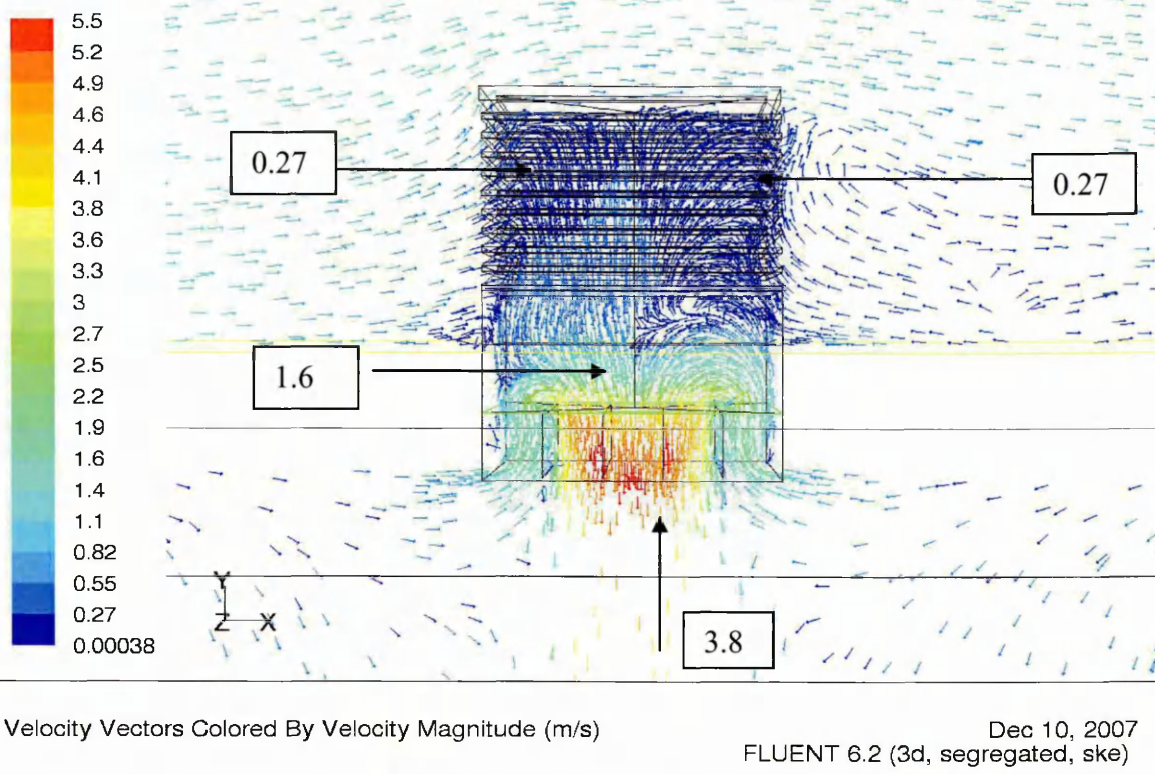
Figure 5-36 Fresh airflow path with fan in bottom position with 20Pa fan pressure

The three simulation models were solved for the full range of pressures (20 -

120Pa) with the results presented in Tables 5-12, 5-13 and 5-14.

Table 5-12 Simulation results for the fan located in the top position

Fan pressure (Pa)	Diffuser face velocity (m/s)	Average internal air velocity (m/s)
20	0.37	0.27
40	1.45	0.38
60	1.81	0.47
80	2.1	0.54
100	2.36	0.6
120	2.59	0.66

Table 5-13 Simulation results for the fan located in the middle position

Fan pressure (Pa)	Diffuser face velocity (m/s)	Average internal air velocity (m/s)
20	2.22	0.59
40	3.01	0.81
60	3.56	0.96
80	4.15	1.11
100	4.68	1.25
120	5.16	1.37

126

Table 5-14 Simulation results for the fan located in the bottom position

Fan pressure (Pa)	Diffuser face velocity (m/s)	Average internal air velocity (m/s)
20	2.23	0.55
40	3.18	0.79
60	3.75	0.95
80	4.31	1.09
100	4.83	1.22
120	5.32	1.34

The results showed that a fan located in the middle or bottom positions generates the largest velocities both across the diffuser face and also within the micro-climate. These higher velocities are due to the re-circulation rate within the micro-climate. The micro-climate has a smaller volume than the macro-climate. Hence, the re-circulation rate is vastly increased when compared to a mixed circulation of the fan in the top position (Figure 5-37).
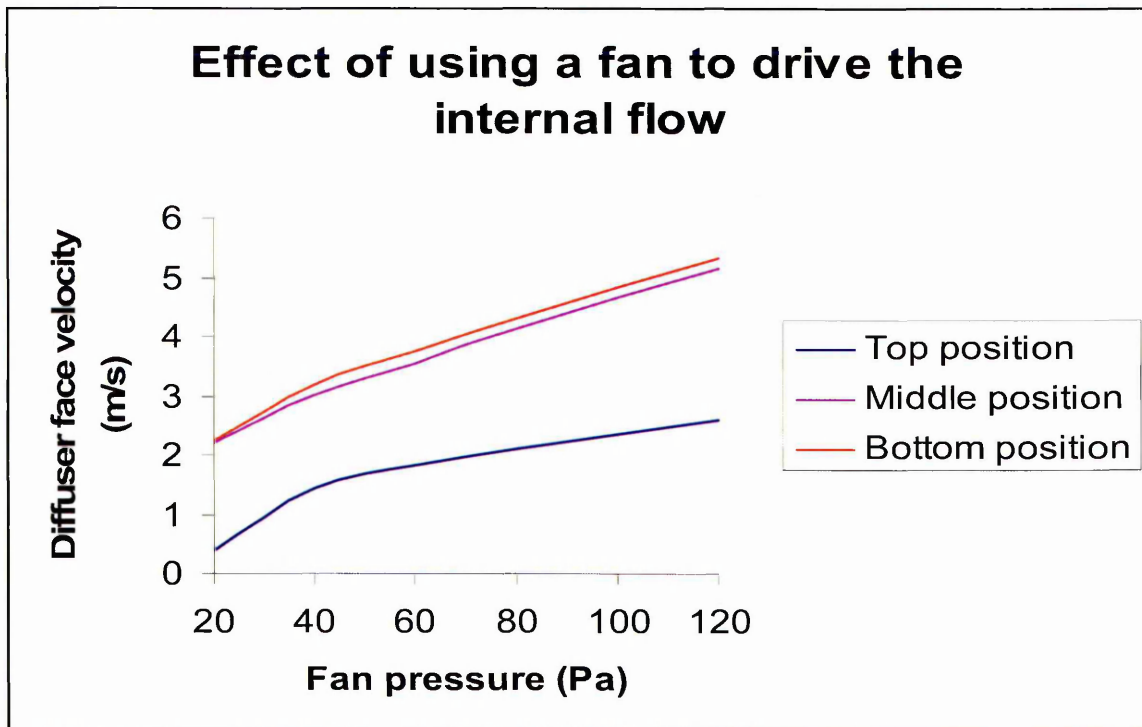
Figure 5-37 Effect on diffuser velocity of the three fan positions

Therefore, a fan located at the middle and bottom positions were discounted for this application, as the fresh air supply was severely restricted. The results of a fan located at the top position showed that a relatively low powered fan of 20Pa

is sufficient to match the benchmark internal air distribution at the UK average external wind velocity of 4.5m/s (Figure 5-28). The 20Pa fan produces 0.27m/s, whilst the benchmark case produces 0.31m/s a difference of 14%.

Contours of Velocity Magnitude (m/s)

Dec 01, 2008
FLUENT 6.3 (3d, pbns, ske)
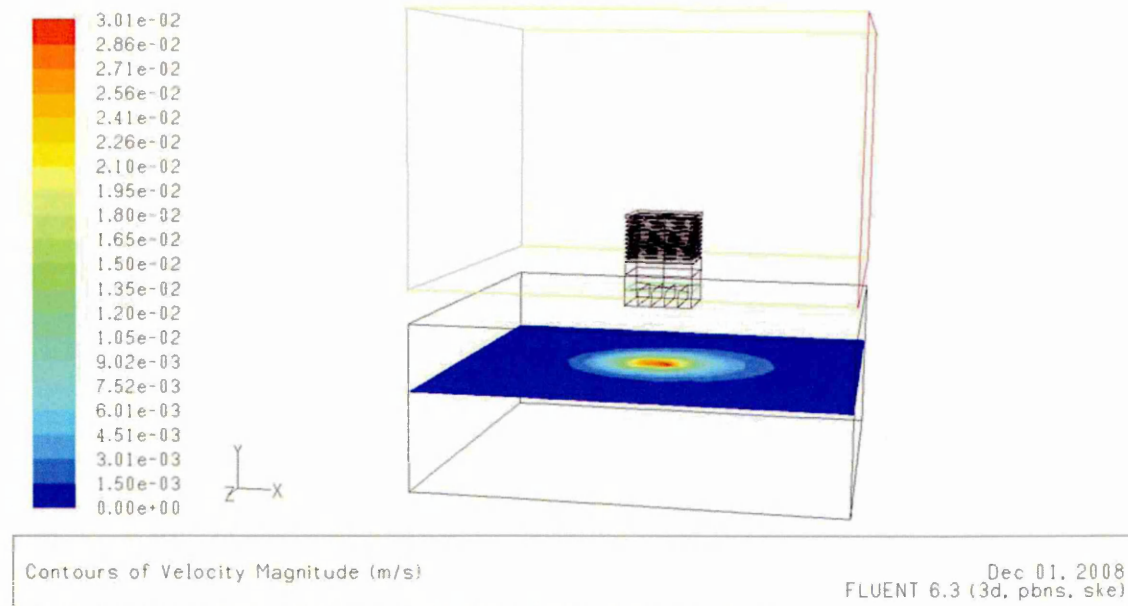
Figure 5-38 Velocity contours within the micro climate for a 20Pa fan in the top position

5.9 Optimum external geometry configuration

Following the previous investigations, where key external geometrical optimisation has been identified, a final simulation model was built to investigate their combined effects on the wind vents performance. The external geometry was selected to be replicated in far-field testing (see Chapter 7). Internal geometry variation could not be replicated in far-field testing. This was due to the internal geometry representing the structure and integrity of the wind vent. The optimum configuration consisted of four louvers, spaced at a distance of 30mm apart, using a 35° louver angle (Figure 5-39). This configuration represented the most desirable combination based on each components contribution to the device. Thus in cases where an increase in velocity would introduce a detrimental effect (such as rain ingress) the subjective optimum has been used.
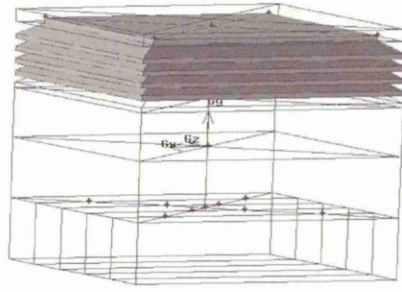
Figure 5-39 Simulation model to represent the optimum geometrical configuration

The optimum configuration was solved for a range of external wind velocities of 1, 2, 3, 4, 4.5 and 5m/s. The full results are shown in Table 5-15.

Table 5-15 Simulation results for optimum external geometry configuration

Velocity inlet speed (m/s)	Diffuser face velocity (m/s)	Diffuser face pressure drop (Pa)	Average internal air velocity (m/s)
1	0.07	0	0.07
2	0.14	0.02	0.14
3	0.2	0.03	0.22
4	0.28	0.06	0.3
4.5	0.32	0.08	0.33
5	0.37	0.1	0.37

The results were compared to the benchmark case with counter-current flow. The results showed that both velocity and pressure were significantly lower than the benchmark. The velocity was 43% lower at the maximum external wind speed simulated (5m/s). The pressure was 70% lower at the same external wind speed of 5m/s (Figure 5-40). The optimum configuration provided less air-exchange between macro and micro-climate.
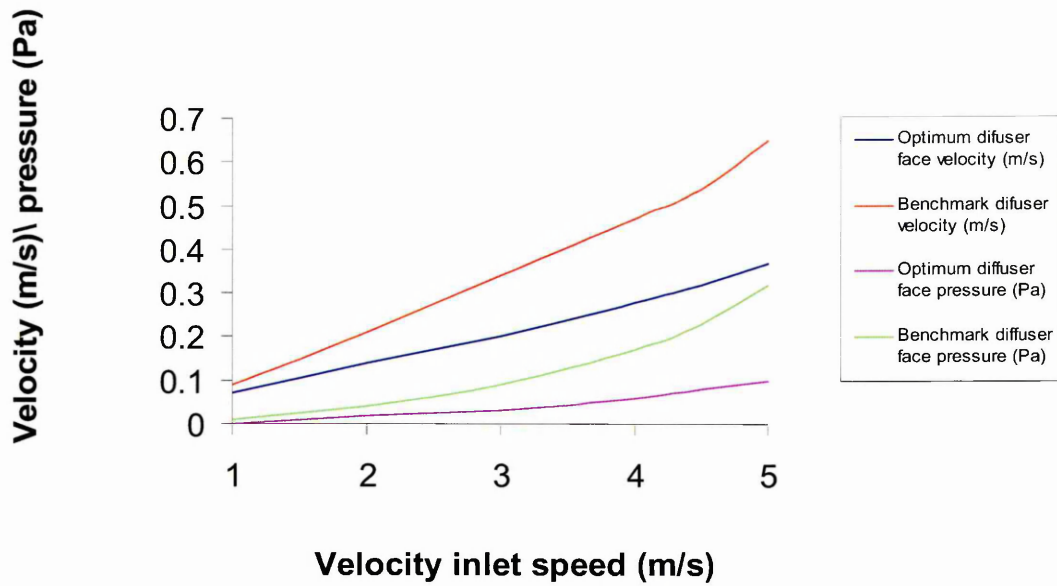
Figure 5-40 Comparison of the optimised wind vent performance with the bench mark wind vent

The internal air distribution rate for the optimum case is similar to the benchmark with a nominal improvement. The optimum geometry gave a 10% increase in internal air distribution at the highest external velocity simulated (5 m/s) in comparison to the benchmark case (Figure 5-41).
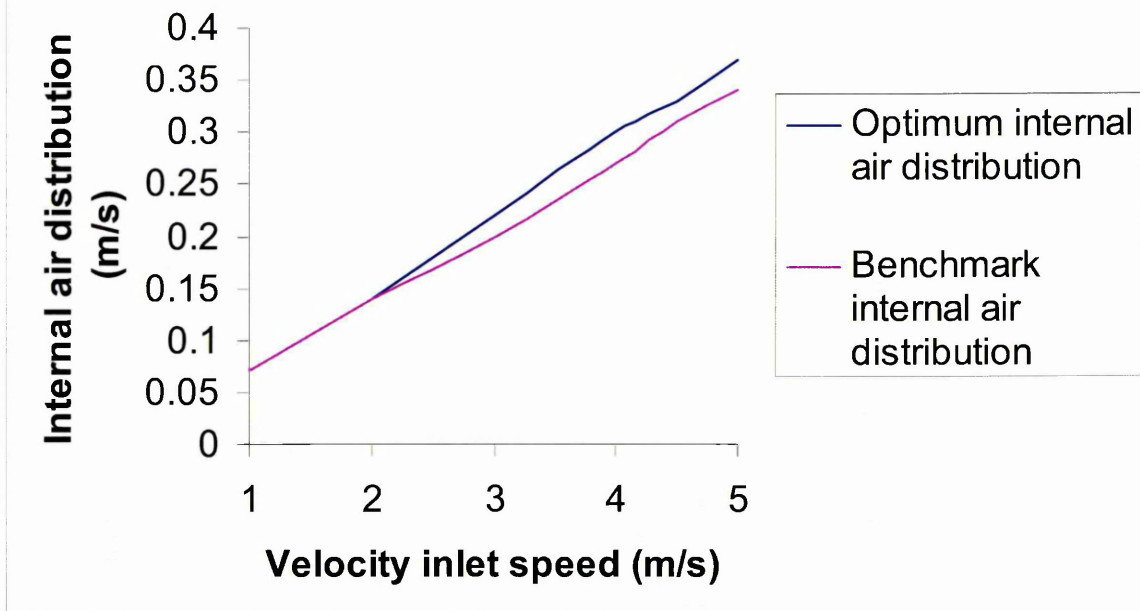
Figure 5-41 Comparison of the optimum external geometry with the benchmark internal air distribution

The optimum case provided greater air distribution within the room. This was as expected as previous investigations showed the suction effect had moved closer to the micro-climate. The results showed that the optimum external geometry when combined did not represent the optimum wind vent performance. However, the performance had been improved by the addition of internal geometrical variation not simulated in this investigation. Matched internal and external geometry is necessary for the desired performance parameters for each individual case. Moreover, this investigation has shown that the internal air distribution rate was improved by optimisation of the external geometry, using 50% less material for the wind vent construction (50% less external louvers), shown in Figure 5-42.

3.34e-02	
3.18e-02	
3.01e-02	
2.84e-02	
2.67e-02	
2.51e-02	
2.34e-02	
2.17e-02	
2.01e-02	
1.84e-02	
1.67e-02	
1.50e-02	
1.34e-02	
1.17e-02	
1.00e-02	
8.36e-03	
6.69e-03	
5.01e-03	
3.34e-03	
1.67e-03	
0.00e+00	

Contours of Velocity Magnitude (m/s)   Dec 01, 2008
                                                    FLUENT 6.3 (3d, pbns, rngke)
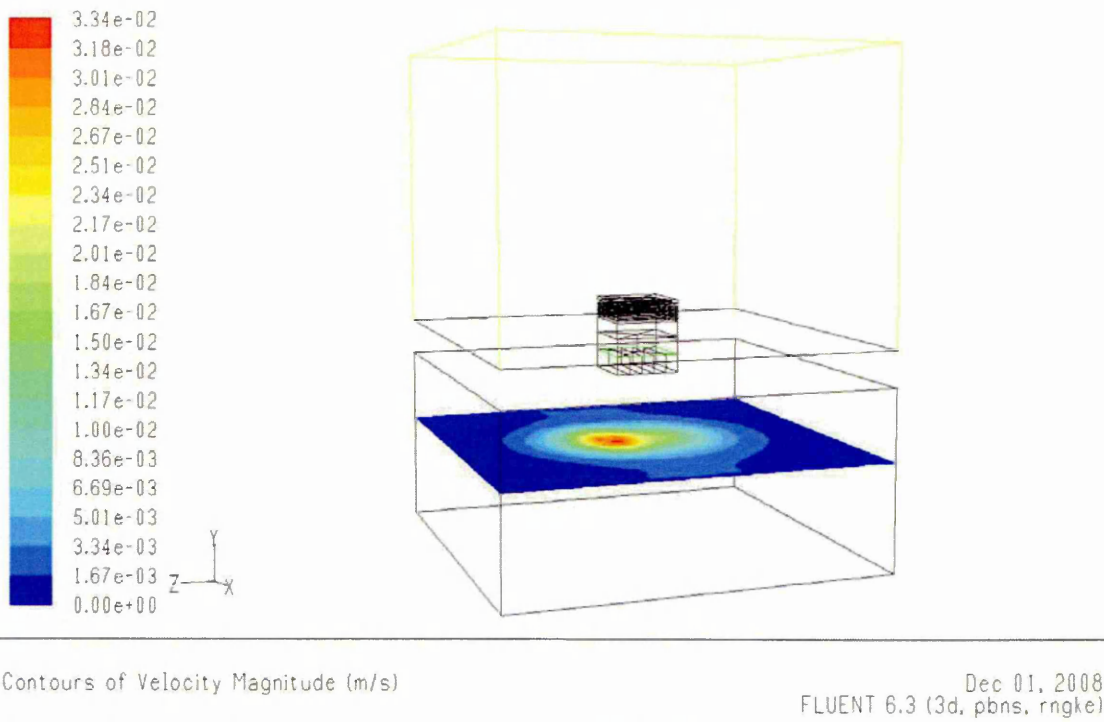
Figure 5-42 Velocity contours within the micro climate for the optimum external geometry with an external inlet speed of 4.5 m/s

5.10 Summary

This chapter presented eight CFD investigations with a total of 47 different simulation models built. Three performance parameters have been stipulated and used to evaluate the wind vent performance. The results have been presented in tabular, graphical and velocity contour form. A standard wind vent has been benchmarked with systematic geometrical variations used to ascertain their effect on the wind vent performance. The optimum simulation case has been presented in each experiment with a combined external geometry model compared to the benchmark case.

Chapter 6   Experimental set-up

6.1 Introduction

As part of this study, full scale experimental testing was undertaken to verify
and validate the CFD simulation work carried out. This chapter presents the
experimental representation of the macro-climate, micro-climate, wind vent and
test equipment used. The location of the test facilities was, where possible,
matched to the simulation model. For the purpose of this study, the wind vent
was a bespoke design to enable geometrical variation within the overall
structure. The following is a description of the individual components with the
complete assembly shown in Figure 6-12.

6.2 Macro-climate

The test facility was located within a four-story, flat-roofed building in the Psalter
lane campus of Sheffield Hallam University (Figure 6-1).
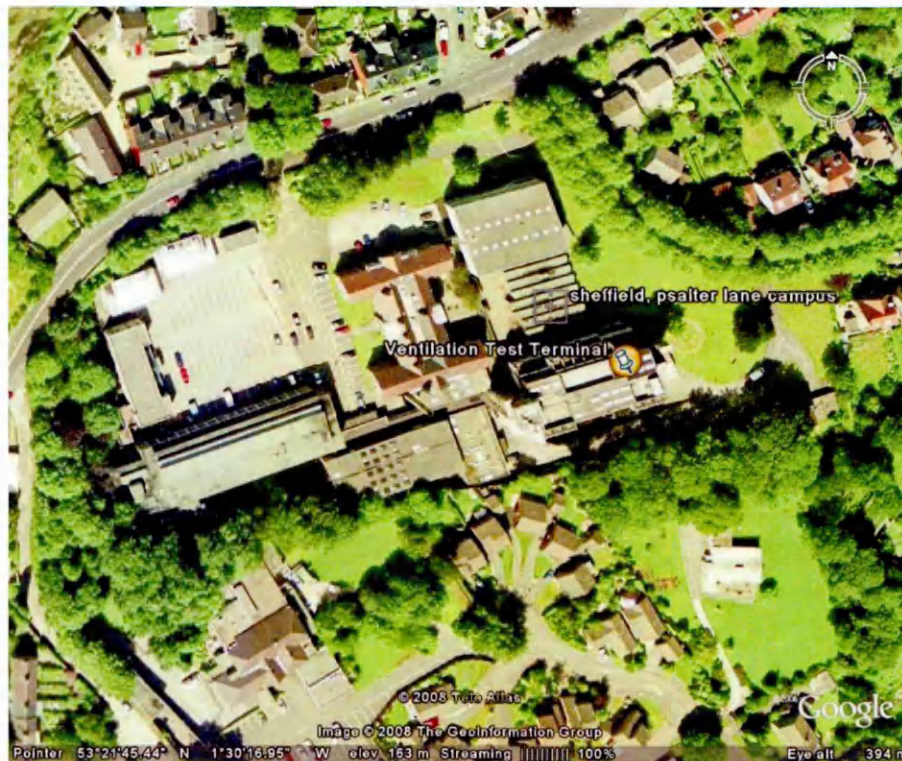
Figure 6-1 Location of macro-climate

This area provided an unobstructed airflow around the building. The flat roof was easily accessible, which facilitated the variation of the wind vent terminal geometry. The building stands 15m high, with a clearance of approximately 2m from the building facades.

The micro-climate was situated above a cluster of classrooms, on the fourth and top floor of the building, in C block. The classroom was ventilated via roof lights which were manually operated. A small classroom room 404A was assigned as a micro-climate. The roof light was removed and replaced with the bespoke wind vent. The location is shown in Figure 6-2.

Figure 6-2 Location of wind vent test terminal on allocated building

The wind vent was located to ensure an unobstructed airflow around the terminal. The roof contained no obstacles above the height of the roof lights used to ventilate the other classrooms within this block (Figure 6-3).

135

Room
404A
roof light

Figure 6-3 Illustration of roof obstructions relevant to the wind vent installation

To record the climatic data surrounding the terminal, during the experimental testing, a multi-test probe attachment of the weather station (Section 7.5.3) was placed on the roof (Figure 6-4).

Figure 6-4 Weather station probe located on the roof

The probe was located at a height of 0.5m above the roof of the wind vent and a distance of 1.5 away from the face of the device. This was to alleviate

distortion of the airflow path caused by the wind shearing over the wind vent roof and a return of airflow from the face.

6.3 Wind vent test terminal

To facilitate experimental variables, a bespoke wind vent was designed and built at Midtherm Engineering. The individual components were all modified to allow for ease of adjustment and removal if required. It was envisaged that the overall height of the structure would be reduced by removing standard blades to monitor the airflow present. This was incorporated into the bespoke design. The main components of the overall assembly were terminal roof or top hat, cross-dividers structure, louver blades, internal spacer, control damper unit and egg crate grille or diffuser.

6.3.1 Terminal roof

The terminal roof was designed to overhang the structure. Hence, in times of reduced louver numbers the internal structure was afforded shelter from external conditions, mainly in the form of driving rain (Figure 6-5).
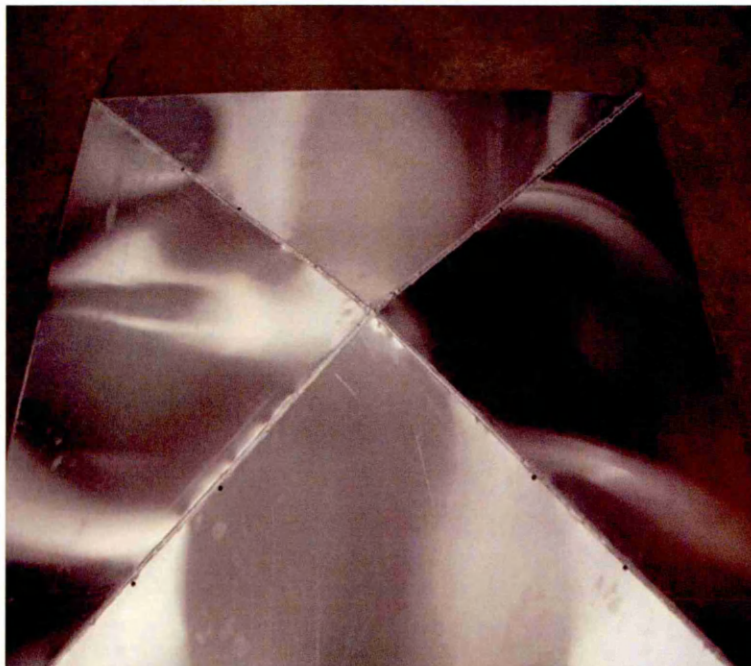
Figure 6-5 Terminal roof or top hat

The top hat was attached to the cross divider structure by eight 50mm cross-thread screws. The hat was lined with 50mm acoustic foam (Appendix B), to reduce any noise caused by rain hitting the sheet metal. The overall dimensions of the top hat were 1.4 x 1.4m with a height of 0.1m.

6.3.2 Cross-divider structure

To ensure rigidity in the assembly a cross-divider structure was designed to provide the main support to the terminal. The cross-dividers were encased by a stainless steel frame fixed in position by both rivets and weld (Figure 6-6). To reduce any breakthrough noise from the macro-climate to the micro-climate the cross-dividers were lined with the same acoustic foam as the top hat.

Stainless steel frame

Cross-dividers

Hole for attaching top hat
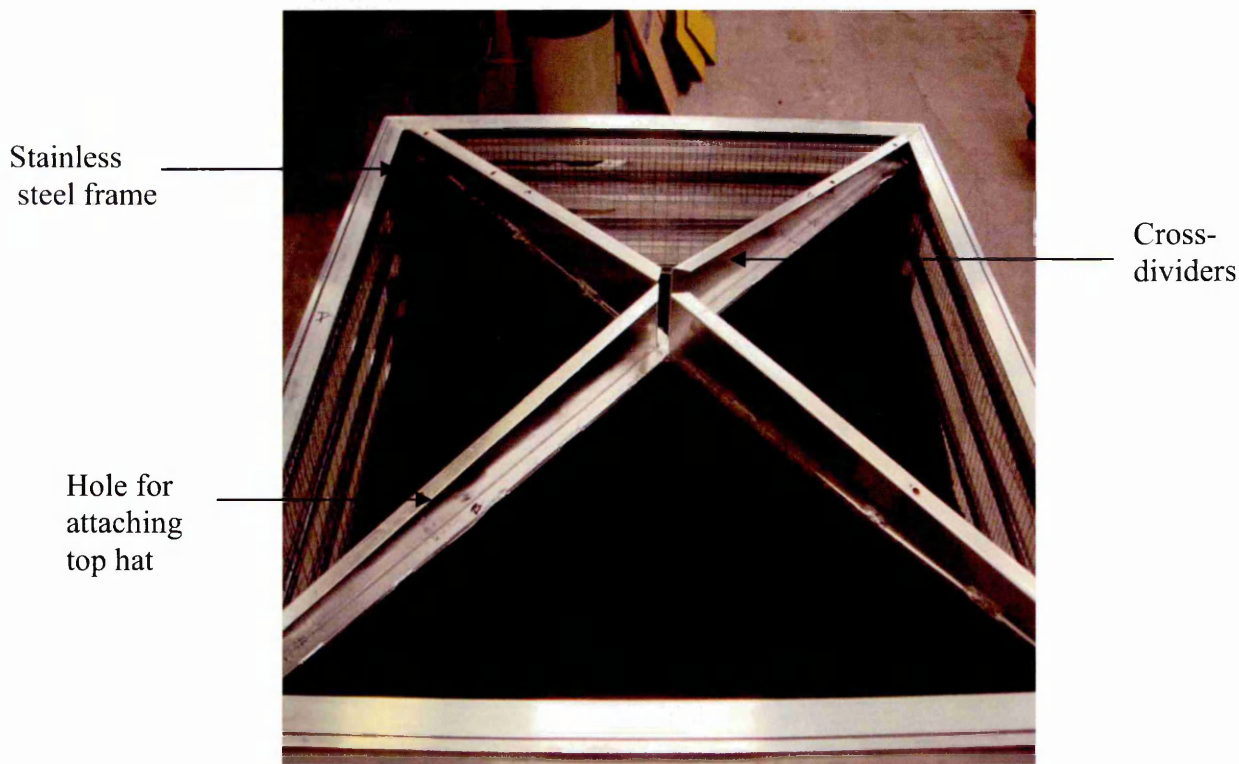
Figure 6-6 Cross divider structure

The external louvers were not individually attached to the cross-divider structure. Each louver slid over the structure and connected to the other louvers via

external stainless steel spacing bars. Four 50mm cross thread screws were used to fix each louver in place at the desired spacing. The overall dimensions of the structure were 1 x 1m with a height of 1m.

6.3.3 Louver blades

Two types of louver blades were manufactured. The louvers were distinguished by the pitch angle of the extrusion with respect to the vertical edge from the horizontal. The louver angles manufactured were 35° and 45° respectively (Figure 6-7). Each louver had a height of 100mm and a depth of 50mm.
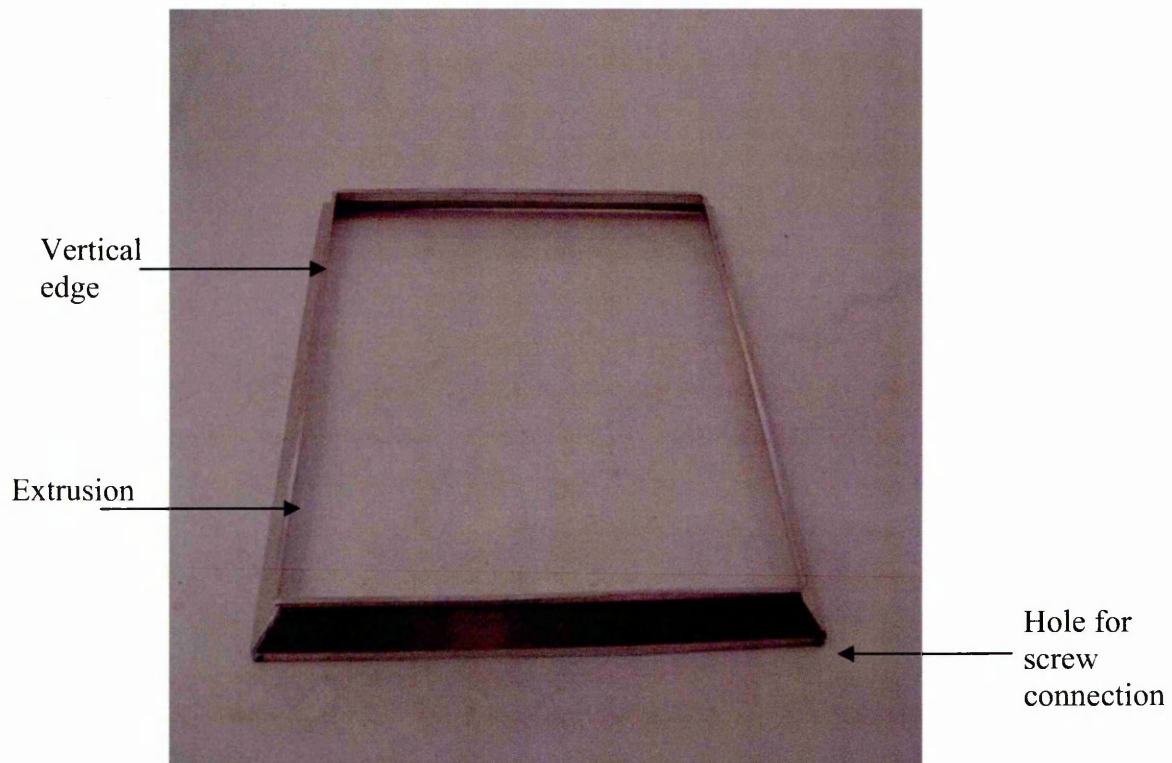
Figure 6-7 Individually manufactured louver blade

In total there were 18 louvers, nine of each extrusion angle. One louver was fixed to the cross-dividers and used to link the structure to the spacer. Therefore, this louver did not allow airflow through. Thus, there were eight opening louvers within the structure. To connect the louvers together, spacing bars were used at

139

each corner with holes spaced according to the required distance between the
louvers and the number of louvers required (Figure 6-8).
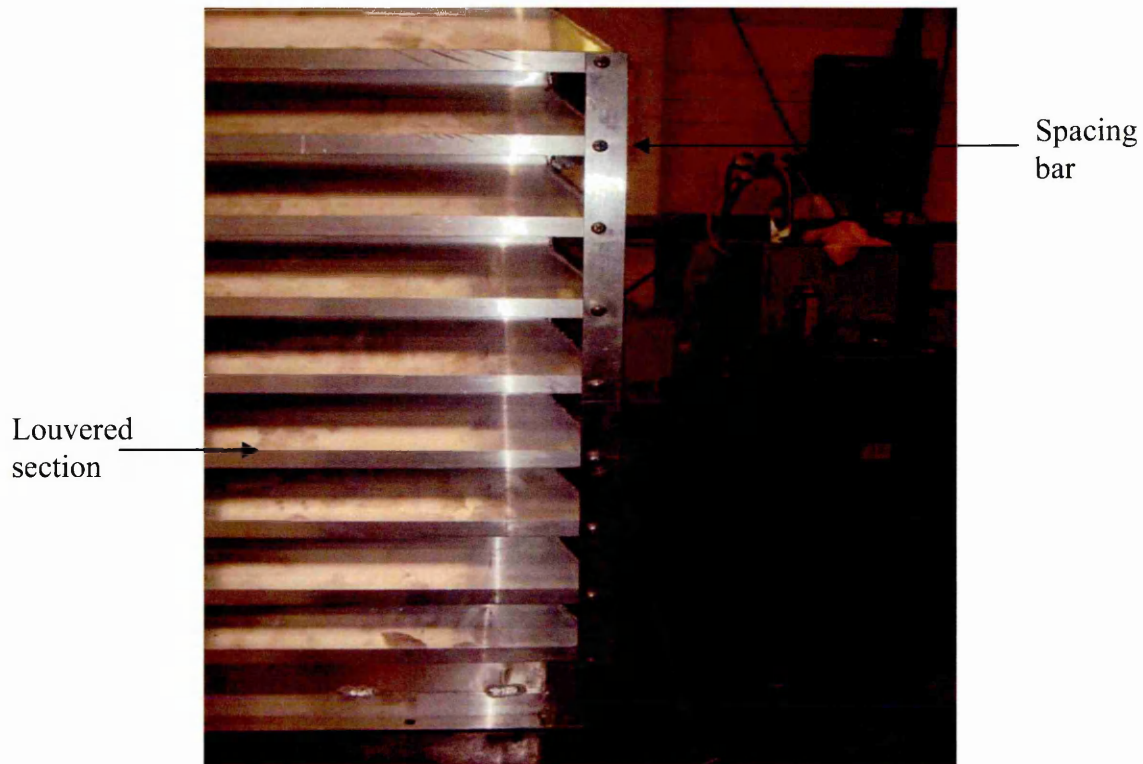
Figure 6-8 Louvered section connected by a spacing bar

The cross-divider structure and louvered section were connected to a spacing
piece which acted as a conduit between wind vent and micro-climate. The
structure was situated on top of a flange, which was in position for the existing
sky light on the roof.

6.3.4 Internal spacer

The internal spacer connected the wind vent to macro-climate via a damper unit
and egg-crate grille. The walls of the spacer were lined using acoustic foam
(Appendix B). The spacer was attached to the wind vent by the same roof light
flange and bolted together using the holes illustrated in Figure 6-9. The spacer

sat between the existing roof light flange and the classroom ceiling at a depth of 0.35m with a cross-section of 1 x 1m.
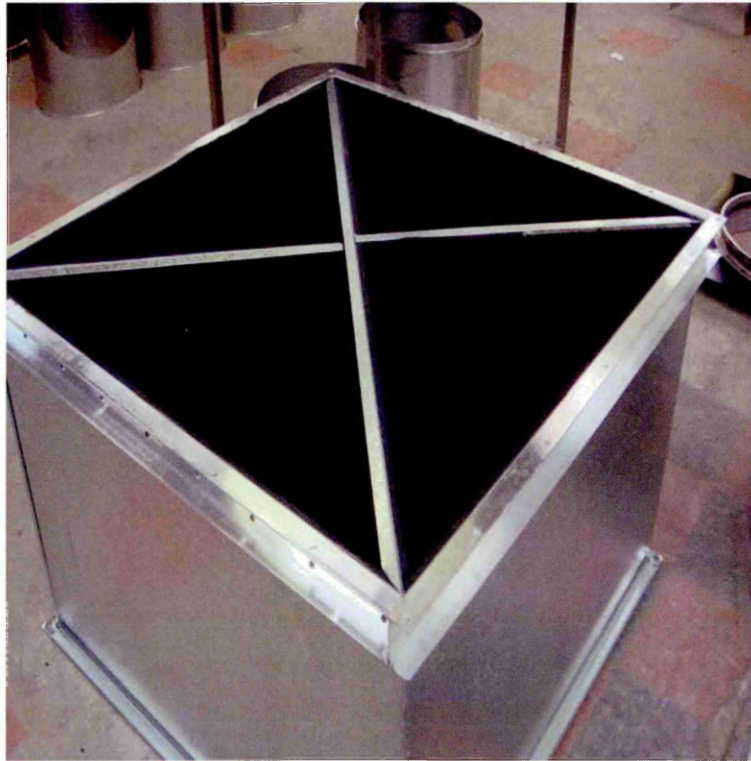
Figure 6-9 Manufactured spacer to join wind vent to the microclimate

The spacer acted as the final conduit between macro and micro-climate and the control mechanism was attached to it.

6.3.5 Control damper unit

The control damper unit was used to control the delivery rate of fresh air and the expulsion rate of spent air. The unit was attached to the spacer using four 30mm bolts. For the purpose of this study a manual damper unit was used. Thus, allowing the position of the damper blades to be fixed according to the required resistance to flow for each experiment (Figure 6-10). The dimensions of the unit were 1 x 1 x 0.25m.

Figure 6-10 Manual damper control unit

A further component, the egg-crate grille was used to diffuse or distribute the delivered flow around the micro-climate volume.

6.3.6 Egg-crate grille

The final component of the bespoke assembly was the egg-crate grille. This component was used to distribute the delivered flow rate more evenly within the micro-climate (Figure 6-11). The grille was attached using 16, 10mm cross-thread screws directly to the control damper unit. The overall dimensions of the grille were 1 x 1 x 0.01m.

Figure 6-11 Egg crate grille or diffuser

142
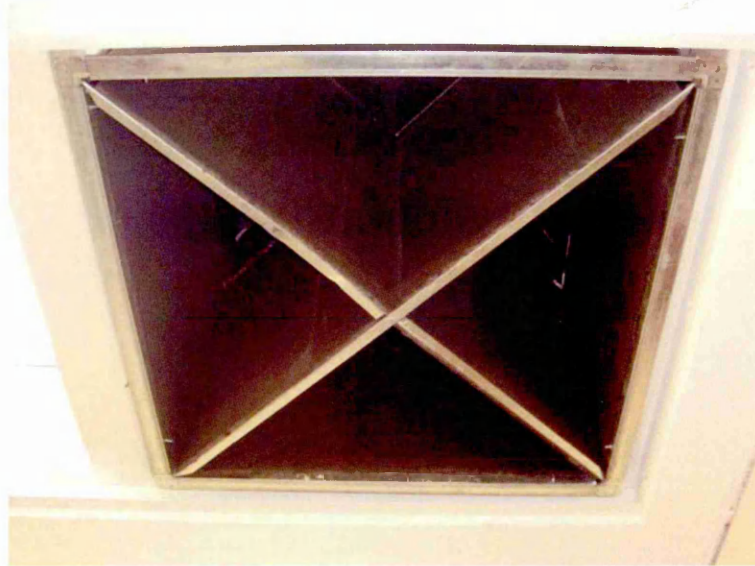
Figure 6-13 Spacing unit in position

The internal assembly of the wind vent namely, the spacer, control damper unit and the egg-crate grille were fixed to the wind vent via the existing roof light flange (Figure 6-14).

Figure 6-14 Finished internal assembly of the wind vent

6.3.8 Construction of the wind vent

Unless otherwise stated, each component of the wind vent was manufactured in sheet metal and bespoke for the purpose of this investigation. All fixings were standard rivet and weld. The damper unit was a commercially available unit with the control mechanism removed for manual operation. The egg-crate grille was

a stock item. The acoustic foam lining and the expanding foam are standard components. Full details of the standard components used and the engineering drawings for the bespoke wind vent are in Appendix B.

6.3.9 Adjustability of the wind vent terminal

The wind vent had three main methods of adjustment to allow for multiple variants for experimental investigation. The louver blade section allowed for the distance between louvers to be changed according to the size of the spacer bar used (Figure 6-15). The spacer bars were manufactured in five sets with different distances between the holes namely 20, 30, 40, 50 and 60mm.

Distance between holes was varied for each set of spacer bars
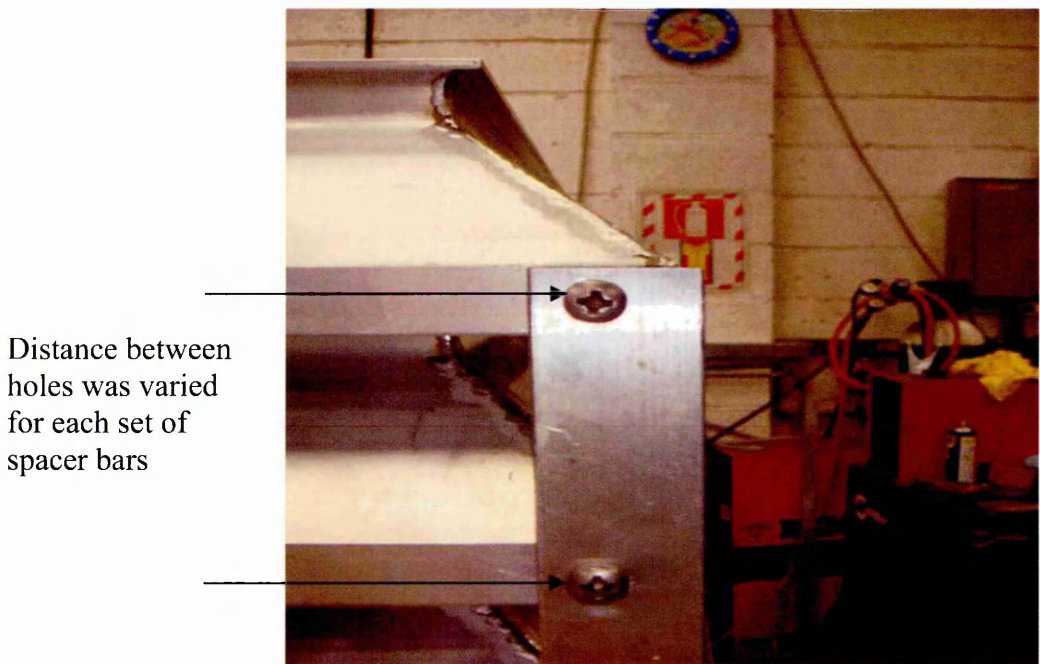
Figure 6-15 Spacer bar employed to provide adjustability between louvers

The second method for adjusting the terminal was by blanking off the internal duct work. Thus, controlling the number of opening louvers. To facilitate this, four blanking plates were manufactured (Figure 6-16).
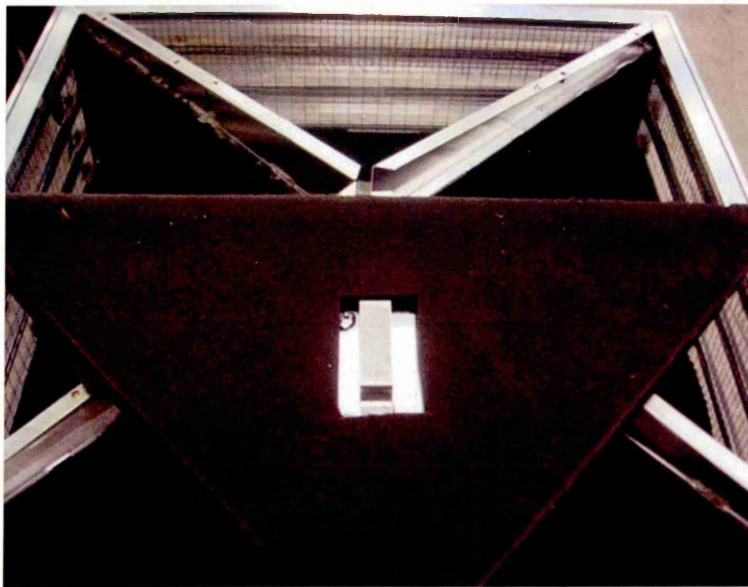
Figure 6-16 Blank plate manufactured to provide opening area adjustability within the wind vent

The blanking plates were used to seal the internal duct from external wind and effectively reduce the opening area without the need to reduce the overall structure height (Figure 6-17).
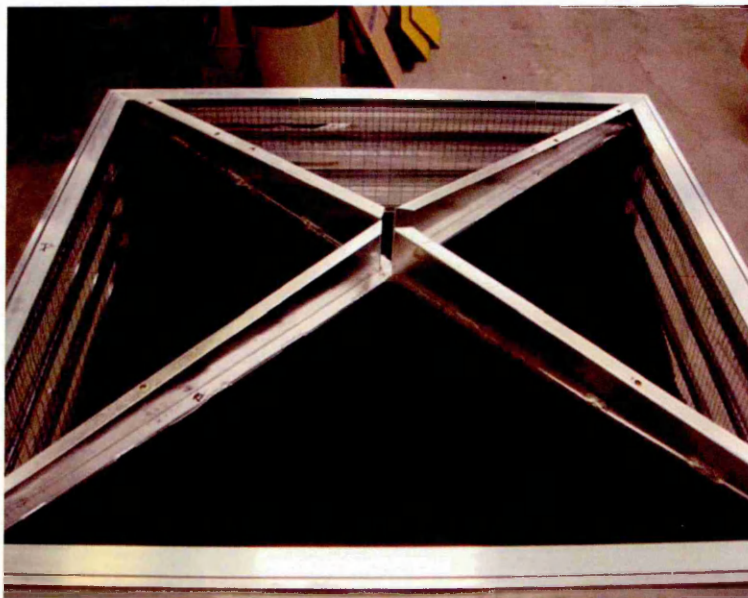
Figure 6-17 Internal duct sealed using blank plates

The final method of adjustability was the removal and replacement of the louvers. Two sets of louvers were manufactured. Two different external louver angles were available to monitor their effect on airflow.

6.4 Micro-climate

The micro-climate was selected to accurately reflect the simulation models. The simulation model had room dimensions of 6 x 6 x 2.5m with a volume of 90m^3. The experimental test room had a volume of 80m^3 with the dimension of 4.3 x 6 x 3.1m.

6.4.1 Location of sample points

The wind vent was located centrally within the micro-climate. Marked on the floor, a test grid was used to locate the position of the nine sample points required for comparison with the simulation model vertex. The positions of the sample points were evenly distributed within the floor area to mimic the vertices distribution within the simulation model. The exact position of the sample points is shown in Figure 6-18.
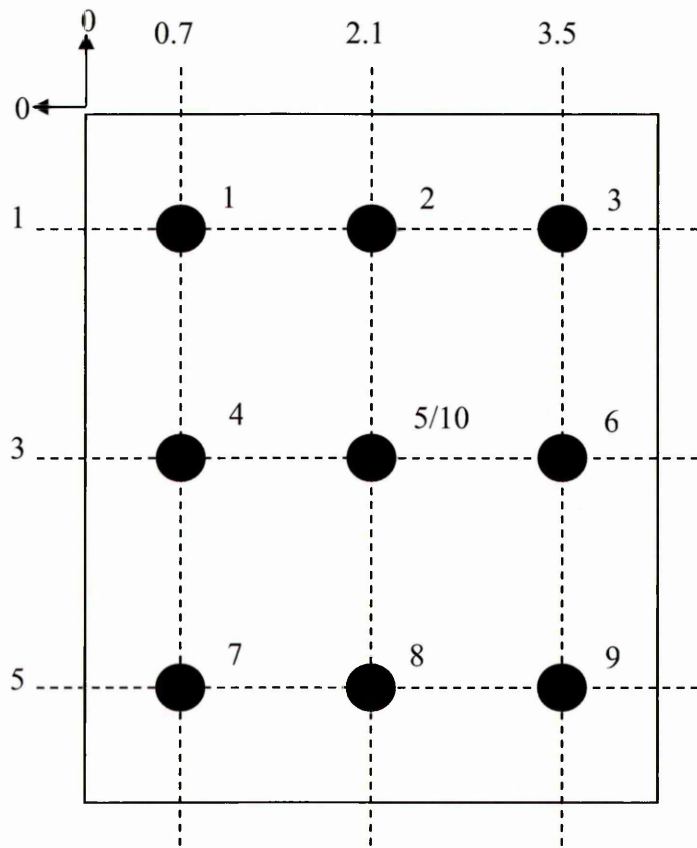
Figure 6-18 Exact position of sampling points located on the floor, all dimensions in m.

The centre of the wind vent was located directly above the sample point with coordinates (2.1, 3). This sample position has two sample points differentiated by the vertical distance at which the sample was taken. The vertical distance for the points one to nine was 1.5m with point ten taken at 2.75m which was the diffuser level.

6.4.2 Data recorder

To record the climatic data of both the macro and micro-climate in synchronisation, a multi-probe data recorder was placed within the micro-climate. This was located on a wall and recorded all relevant climatic data such as temperature, wind speed, rainfall, humidity and daylight hours. The data was stored locally prior to weekly download (Figure 6-19).
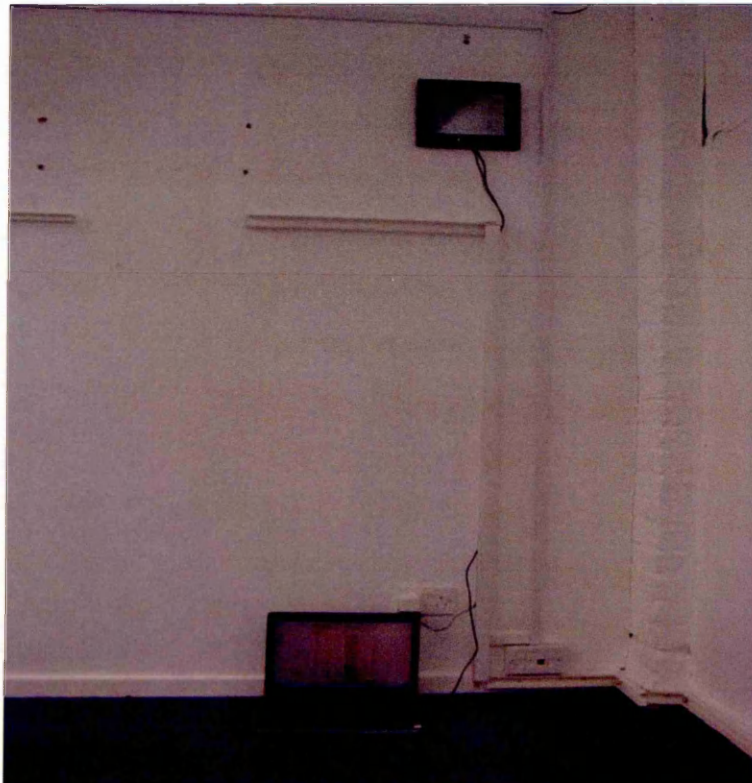
Figure 6-19 Data recorder with download facility located within the micro climate

6.5 *Experimental test equipment*

The purpose of the experimental testing was to determine the internal velocity within the micro climate and the effect of the geometrical variations on wind vent performance. To determine the internal velocity and also the airflow path within the room, the following test equipment was used:

- Velocity meter

- Velocity probe

- Weather station

- Smoke generator

- Solid state LASER

6.5.1 Velocity meter

The Testo 435-4 is a single instrument that can measure all of the key parameters needed to determine Indoor Air Quality (IAQ) and the efficient installation and maintenance of Ventilation and Air Conditioning (VAC) systems. The key parameters are air velocity, CO_2, relative humidity and air temperature. A range of thermal probes, vane probes and pitot tubes are available for the Testo 435-4 to allow measurements to be taken of airflow at various points in a micro-climate. The meter allows users to allocate measured values to measurement locations. This instrument also offers the ability to switch between two user profiles, namely duct measurement and IAQ. Due to the small internal velocities anticipated for this investigation, the thermal velocity probe was selected to be used in conjunction with the duct measurement profile of this meter. The thermal probe (6.5.2) measures flow speed, volume flow, air humidity and air temperature in one sequence. The duct measurement profile calculates the mean velocity over user defined time and area inputs. The time

(seconds) and area inputs (circle, rectangle, area,) are fully adjustable [Testo (2008)]. The meter is shown in Figure 6-20.

Figure 6-20 Test 435-4 multifunction measuring instrument

When connected to the thermal velocity probe, the meter took a time-averaged sample of the velocity which was user defined and matched to the weather station timed average of three minutes. The reading was compared to a user defined floor area of 26m^2 to give a definitive reading.

6.5.2 Thermal velocity probe

The Testo 435-4 meter was connected to a thermal velocity probe. The thermal velocity probe consists of a constant current hot-wire anemometer with a 12mm diameter probe head and 745mm telescopic length. The hot-wire anemometer measures a fluid velocity by recording the heat convected away by the fluid. The core of the anemometer is an exposed hot wire either heated up by a constant current or maintained at a constant temperature (Figure 6-21). In either case, the heat lost to fluid convection is a function of the fluid velocity.
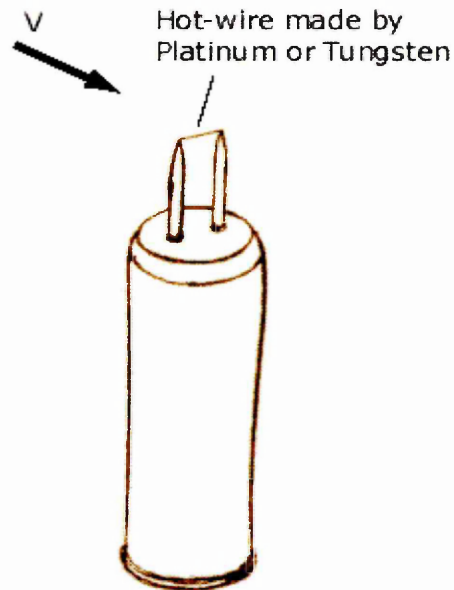
Figure 6-21 Typical hot-wire anemometer [Engineering fundamentals (2008)]

By measuring the change in wire temperature under constant current or the current required to maintain a constant wire temperature, the heat lost can be obtained. The heat lost can then be converted into a fluid velocity in accordance with convective theory. For a hot-wire anemometer powered by a constant current, the velocity of flow is a function of the temperatures of the wire and the fluid. If the flow temperature is measured independently, the fluid velocity can be reduced to a function of wire temperature alone. In turn, the wire temperature is related to the measured wire resistance. Therefore, the fluid velocity can be related to the wire resistance [Engineering fundamentals (2008)].

This probe was selected as it is sensitive to very small internal velocities, which were present during this investigation. "Thermal velocity probes have a very small intrinsic error. This means that thermal probes are mainly suitable for the measurement of low air velocities, as the uncertainty of measurement increases linearly as the air velocity rises" [Testo (2008)]. The probe was attached to a tripod to obtain the sample heights required (Figure 6-22).

151

Figure 6-22 Velocity probe connected to tripod and test meter

6.5.3 Weather station

The LaCrosse weather station is a facility with instruments and equipment to make observations of atmospheric conditions, in order to provide information to make weather forecasts and to study the weather and climate. The measurements taken include temperature, barometric pressure, humidity, wind speed, wind direction and precipitation amounts [LaCrosse (2008)]. The weather station is shown in Figure 6-23.
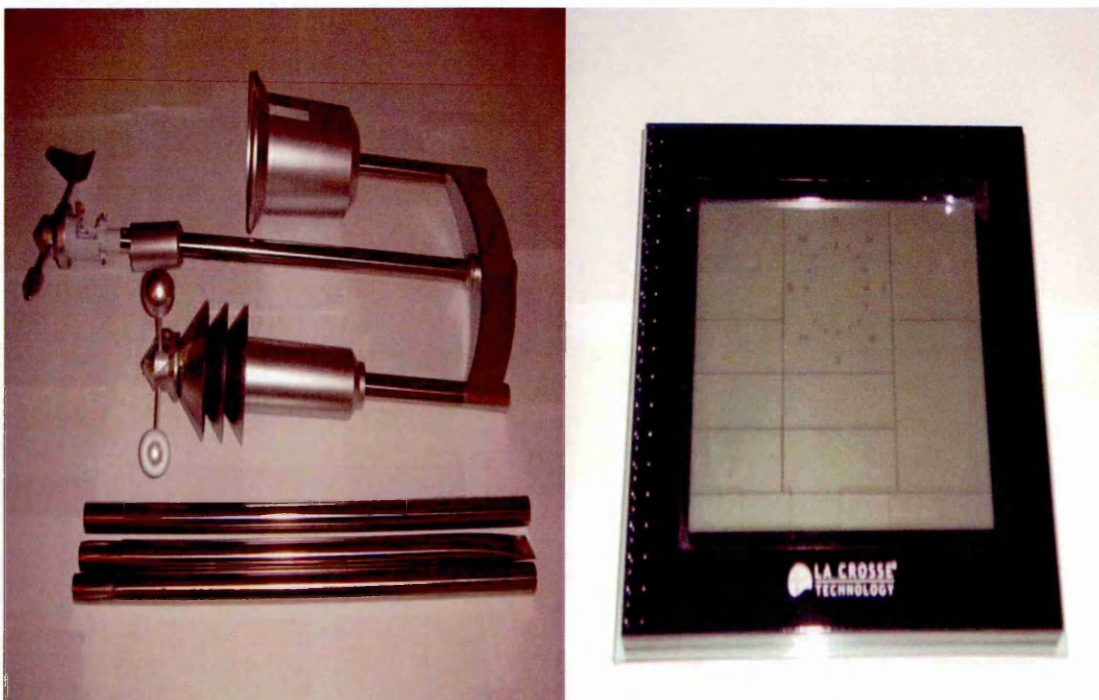
Figure 6-23 LaCrosse weather station WS2500

Automated observations were taken and averaged every three minutes. The observations were recorded and stored for a maximum ten day period prior to download. For the purpose of this investigation, the primary usage was the anemometer for wind speed, wind vane for wind direction and the data logging facilities. Cup anemometers use their rotation which varies in proportion to the wind speed to generate a signal. The design features three cups mounted on a small shaft. The rate of rotation of the cups can be measured by:

- Mechanical counters measuring number of rotations
- Electrical or electronic voltage changes (AC or DC)
- A photoelectric switch

The mechanical type anemometers indicate the wind flow in distance. The mean wind speed is obtained by dividing the wind flow by time of three minutes. For remote sites, this type of anemometer has the advantage of not requiring a mains power source. The response and accuracy of a cup anemometer are determined by its weight, physical dimensions and internal friction. Typical accuracy values for cup anemometers are ± 2% [Manwell *et al.* (2003)].

Wind direction is measured using a wind vane. A conventional wind vane consists of a broad tail that the wind keeps on the downwind side of a rotating vertical shaft. A counter weight placed at the upwind end is used to provide balance at the junction of the vane and shaft. Friction at the shaft is reduced with bearings and so the vane requires a minimum force to initiate movement. Wind vanes produce signals by contact closures (as in this case) or by potentiometers. The accuracy obtained from potentiometers is higher than that

from contact closures. However, this is balanced against a much higher cost [Manwell *et al.* (2003)].

The outdoor sensors of the LaCrosse weather station are combined into a single multi-functional device which was located on the roof. The data was transmitted using wireless signals to the weather station display. The indoor sensors were all contained within the weather station display screen. The samples were averaged and recorded over a three minute period.

6.5.4 Smoke generator

For flow visualisation within the micro-climate, a smoke generator was used to fill the micro-climate in order to monitor the fresh air displacement. A smoke generator also called a fog machine is a device which emits a dense vapour that appears similar to fog or smoke. Most smoke machines create the smoke by either vaporising a water and glycol-based or glycerin-based fluid. Some smoke machines use dry ice to produce a fog of carbon dioxide. For glycerin-based smoke as in this case, the fluid is injected into a heated block and evaporates quickly. The resulting pressure forces the vapour out of the nozzle. Upon coming into contact with cool outside air the vapour forms a fog. The smoke generator used was an Antari Z-series II, with type FLG liquid. The Z-series II has an 800 watt heater which generates a continuous flow of 1.42 m^3/s with a tank capacity of 0.8L [Antari (2008)] as depicted in Figure 6-24.
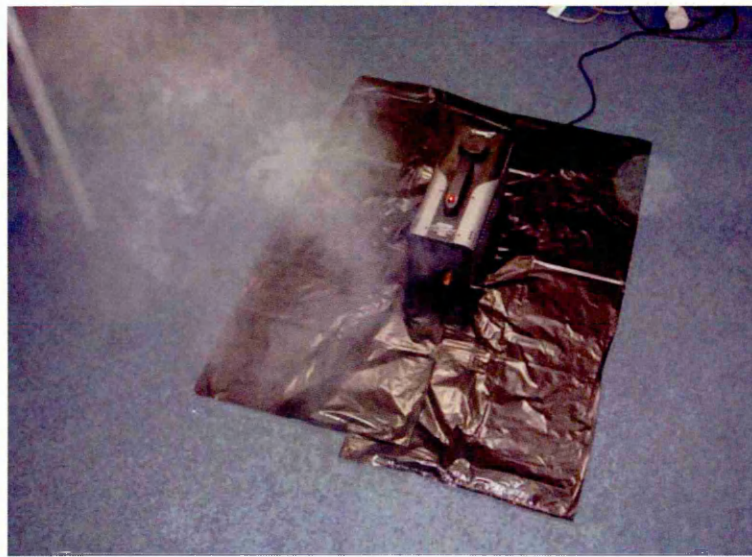
Figure 6-24 Antari z -series II smoke generator

6.5.5 Laser

A Light Amplification by Stimulated Emission of Radiation (LASER) was used to generate a 2 dimensional thin light sheet. The sheet was used to differentiate between fresh air supply entering and stale air exiting the micro-climate. A LASER is a device that emits light (electromagnetic radiation) through a process called stimulated emission. LASER light is usually spatially coherent which means that the light either is emitted in a narrow low-divergence beam, or can be converted into one with the help of optical components such as lenses. The coherence of typical LASER emission is distinctive. Most other light sources emit incoherent light which has a phase that varies randomly with time and position.

A LASER consists of a gain medium inside a highly reflective optical cavity as well as a means to supply energy to the gain medium. The gain medium is a material with properties that allow it to amplify light by stimulated emission. In its simplest form a cavity consists of two mirrors arranged such that light bounces back and forth each time passing through the gain medium. Typically one of the

155

two mirrors, the output coupler is partially transparent. The output LASER beam is emitted through this mirror (Figure 6-25). The process of supplying the energy required for the amplification is called pumping. The energy is typically supplied as an electrical current or as light at a different wavelength [Csele (2004)].
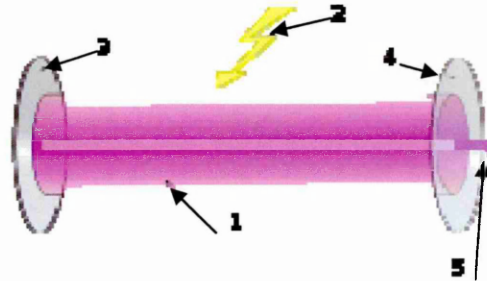
Figure 6-25 Illustration of the principle components of a laser [Csele (2004]]

Principal components:

1. Gain medium

2. Laser pumping energy

3. High reflector

4. Output coupler

5. Laser beam

This study used a DPSS Quantum Excel LASER (Figure 6-26).
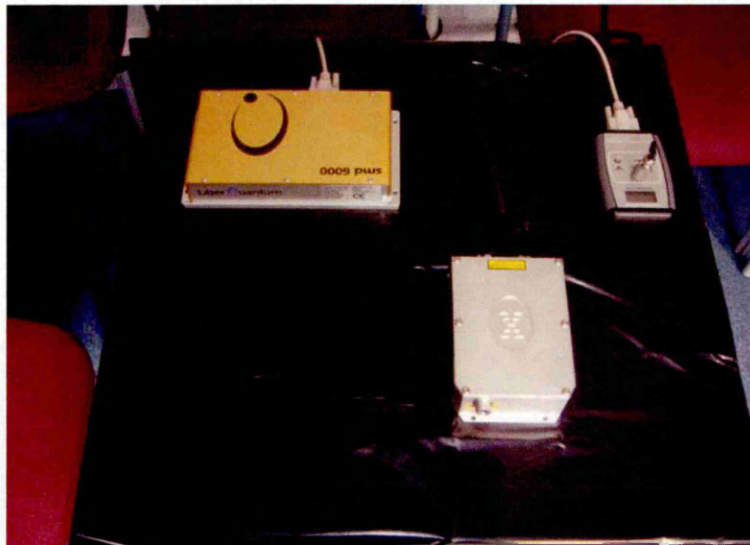
Figure 6-26 LASER quantum smd 6000

The excel produced a high power green beam up to 2W with a direct 30kHz modulation [Laserquantum (2008)]. This generated a sharp 2D screen across the micro-climate.

6.5.6 Accuracy specifications of test equipment

The equipment described in this chapter was matched to give accurate information to facilitate comparison with simulation data. Table 6-1 provides the manufacturers technical specification for each of the parameter sensors used in this study.

Table 6-1 Technical specifications of test equipment used

Parameter	Range	Resolution	Accuracy
External wind velocity	0 - 49 m/s	0.1 m/s	0.1%
External wind direction	0 - 355°	5°	1.5%
Internal velocity	0 - 20 m/s	0.01 m/s	0.15%

All the equipment was calibrated prior to use according to the manufacturers instructions.

6.6 Experimental test procedure

To ensure reproducibility for comparison of experimental results the same test procedure was used for each experiment. The duration of the test was the same for each experiment as detailed:

- At the diffuser sample point 10, a velocity reading was taken using the velocity probe, meter, and tripod set at a height of 2.75m. The sample

was taken and averaged over a three minute period with the result and start/finish times recorded.

- Starting at sample point 1 (Figure 6-18) and working in numerical order the above procedure was carried out for the nine sample points at a height of 1.5m.

- The procedure was carried out for five consecutive days to obtain a clear pattern of results.

- Following the fifth day of sampling, the data from the LaCrosse recorder was downloaded. The external conditions were recorded against the start/finish times of the sampling at three minute averaged data.

6.7 Summary

This chapter presented the geographical location of the test facility. The sampling and monitoring equipment used for the experimental section of this study has been detailed. The dimensions, components and set-up of the three main areas of the study namely macro-climate, micro-climate and wind vent were described in detail. Technical specifications and accuracy of the parameter sampling equipment were provided. The test procedure and duration of each experiment was presented.

Chapter 7   Experimental results

7.1 Introduction

The full scale bespoke wind vent (detailed in Chapter 6) has been subjected to extensive far-field experimental testing. Due to the unpredictability of the external wind conditions the testing period for each experiment was a minimum of five days. Five experiments were carried out on the wind vent namely benchmark, number of external louvers, distance between the external louvers, 35° angle louvers and an optimum configuration. Each variant of the wind vent was subjected to the test procedure (detailed in Chapter 6) with the results presented in this chapter.

7.2 Benchmark testing

The benchmark experiment consisted of a square 1 x 1m wind vent with eight opening louvers (as detailed in Chapter 6) shown in Figure 7-1. The control dampers remained fully open for each experiment.

Figure 7-1 The wind vent benchmark experimental setup

Initial testing of the benchmark wind vent was carried out via smoke testing for flow visualisation of the unit. To visualise the fresh air entering the micro-climate, it was first filled with smoke. The displacement effect of fresh air entering was observed using a LASER sheet (detailed in Chapter 6), shown in Figure 7-2.
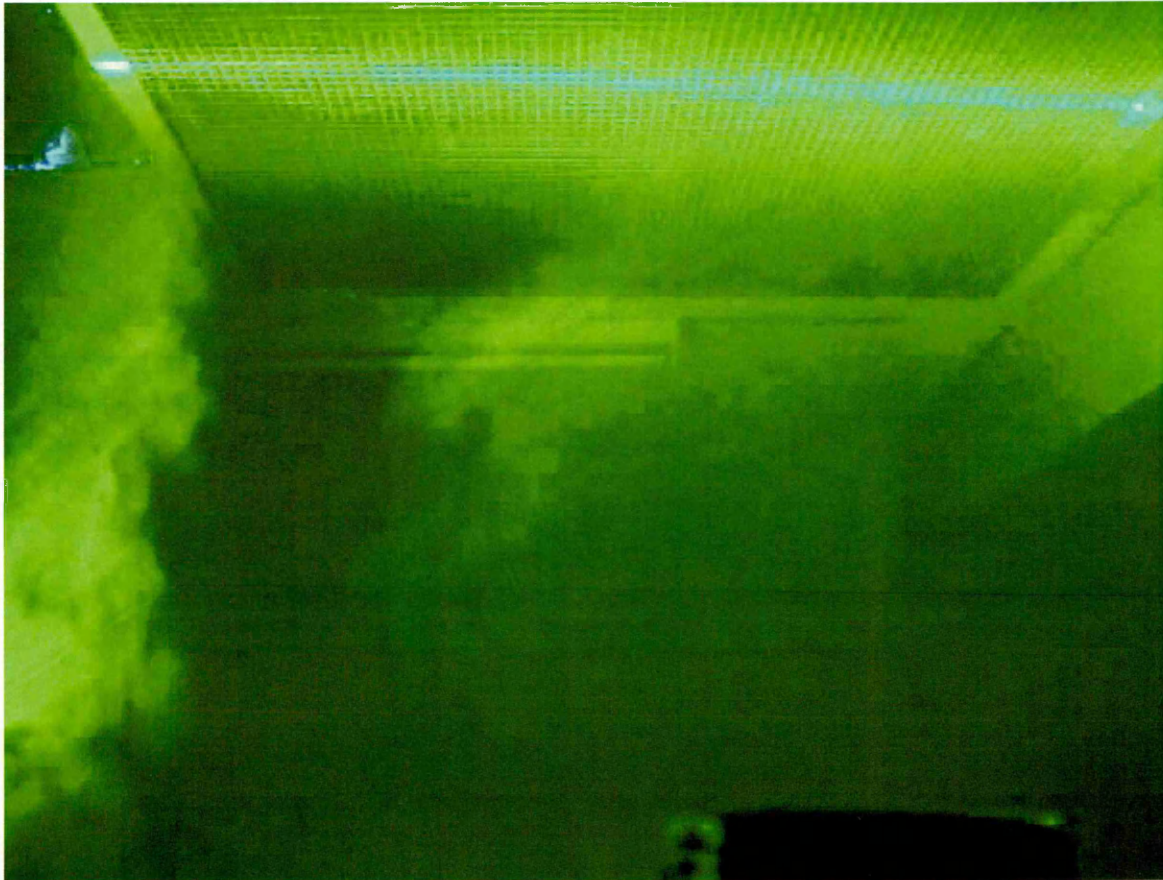
Figure 7-2 Flow visualisation of the benchmark experimental setup

Fresh air was observed entering the micro-climate through the left hand side of the diffuser displacing the smoke within the room (Figure 7-3). At this stage the fresh air was entering the micro-climate. However, the smoke was not exiting as it had not yet circulated.
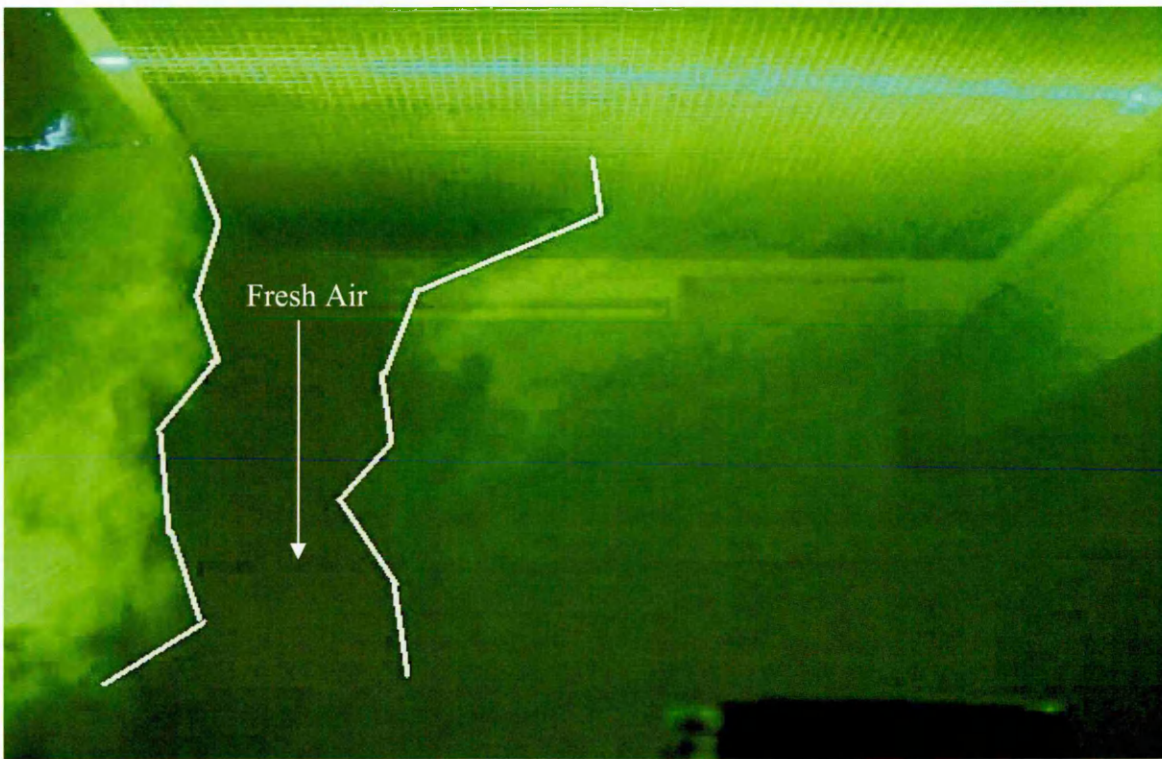
Figure 7-3 Annotated picture of the fresh air entering the micro climate via the left hand side of the diffuser

As the fresh air entered the micro-climate it began to displace the smoke. As the flow developed it circulated the room and exited via the right hand side of the diffuser (Figure 7-4).
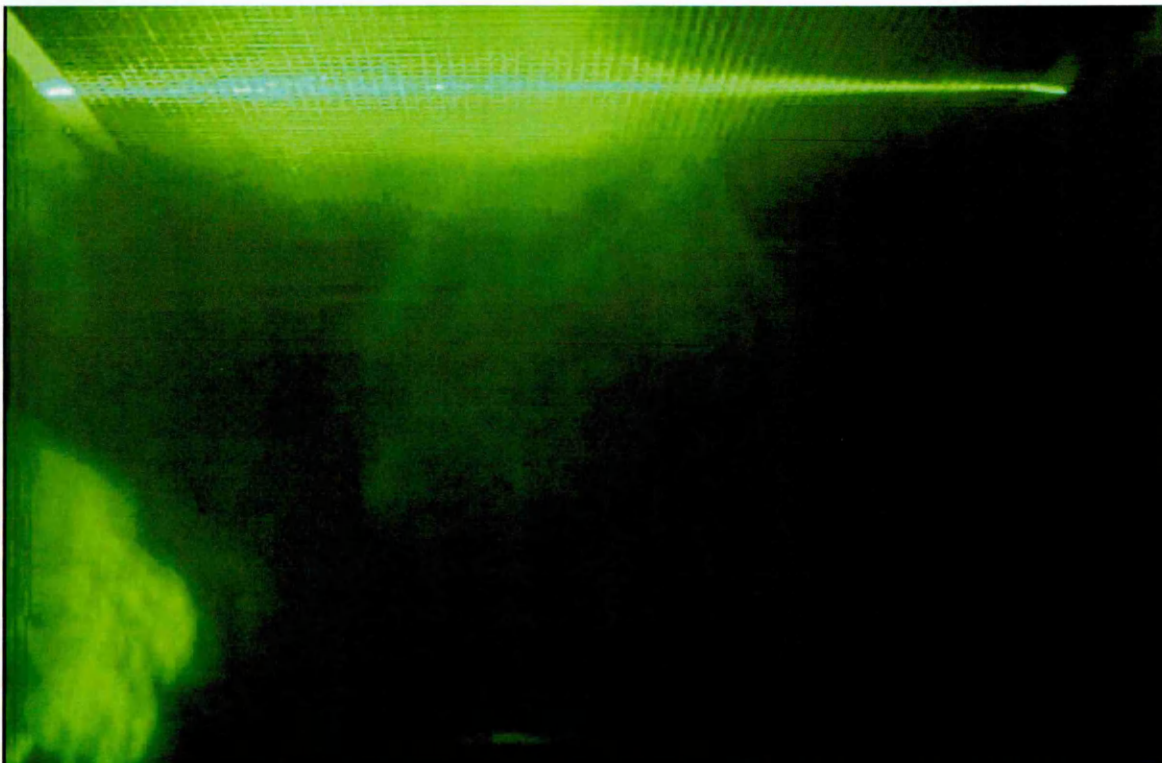
Figure 7-4 The displacement effect of fresh air within the micro-climate.

As the flow was now fully developed the four quadrants were working to both draw in fresh external air and exhaust stale air from the room (Figure 7-5).
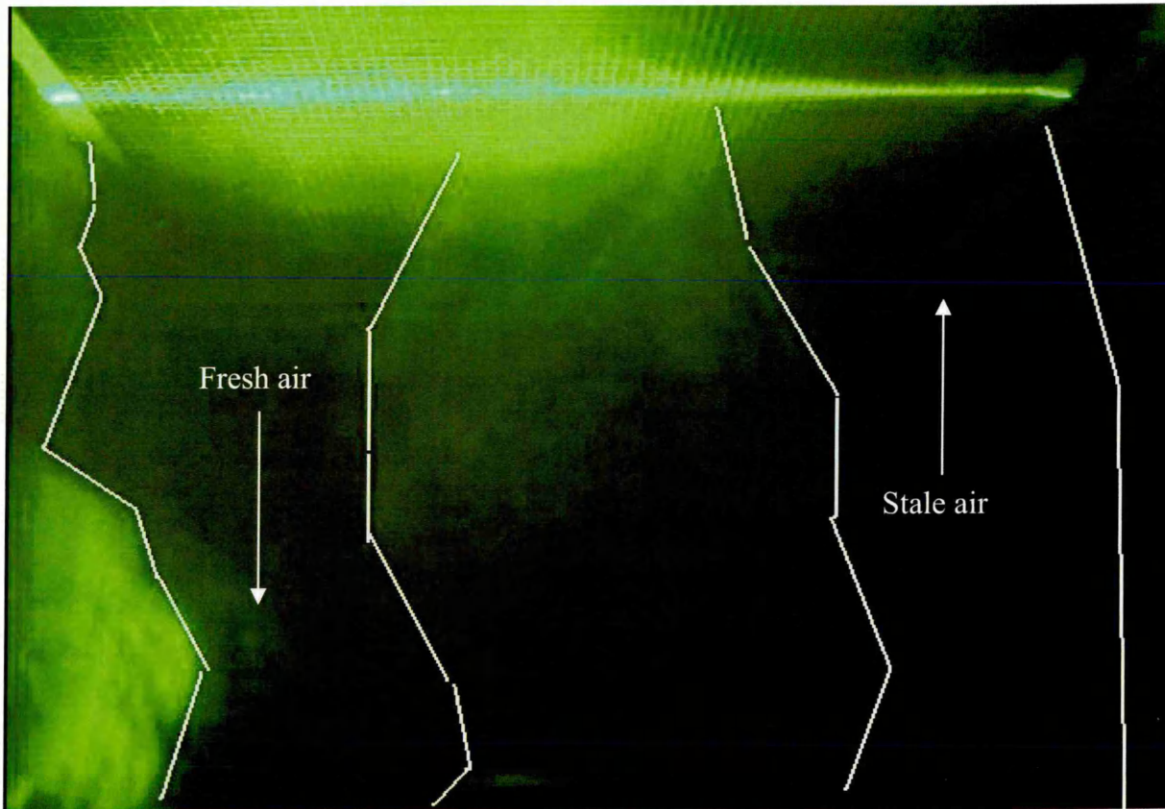
Figure 7-5 Annotated picture of the displacement effect of the wind vent

The benchmark geometry was monitored for five days, with the experimental test procedure repeated each time. The external wind conditions changed with such frequency that only averaged results gave a clear pattern of the flow. It became apparent that the corner sample points were unreliable. This was due to the close proximity of two connecting walls, with the heat transfer between the two creating an undesirable convection effect on the readings. Therefore, the four corner sample points were omitted from the results shown in Table 7-1.

Table 7-1 Averaged results for the benchmark experiment

Sample point	External velocity (m/s)	Internal velocity (m/s)
10	4.35	0.27
2	3.4	0.03
4	4.4	0.01
5	4.1	0.05
6	3.6	0.03
8	4	0.03

Standard deviation (σ) values for table: External velocity = 1.7m/s, Internal velocity (points 2,5,6,7,8) = 0.02m/s, diffuser (point 10) = 0.1m/s.

From the results over the course of the experiment the average external velocity was 4m/s. As expected the highest internal velocity was at the diffuser. The second highest internal velocity was at sample point five which was situated directly below the diffuser point. This was due to the control dampers being in the fully open position. Consequently, the flow was not redirected around the micro-climate. The results are represented in Figure 7-6, for comparison with later experiments.
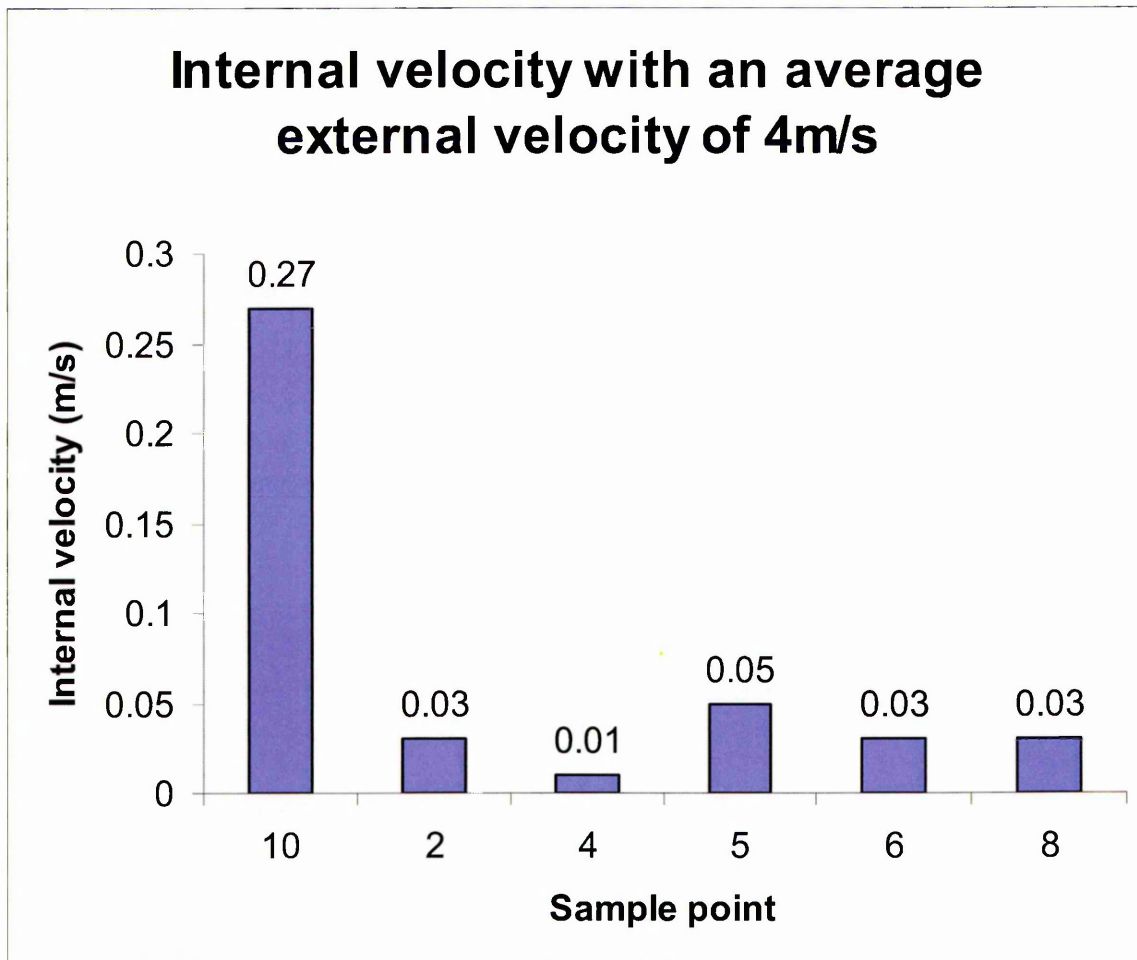
Figure 7-6 Experimental results of the benchmark wind vent with an external velocity of 4m/s

7.3 Number of external louvers

To investigate the effect of varying the number of external louvers in the wind
vent, three different experimental set-ups were used. The three set-ups were six
louvers, four louvers and two louvers (the benchmark contained eight louvers).
To achieve these set-ups the internal blanking pieces were placed at the
appropriate louver level and sealed in place (Figure 7-7). Thus, the number of
opening external louvers was reduced.
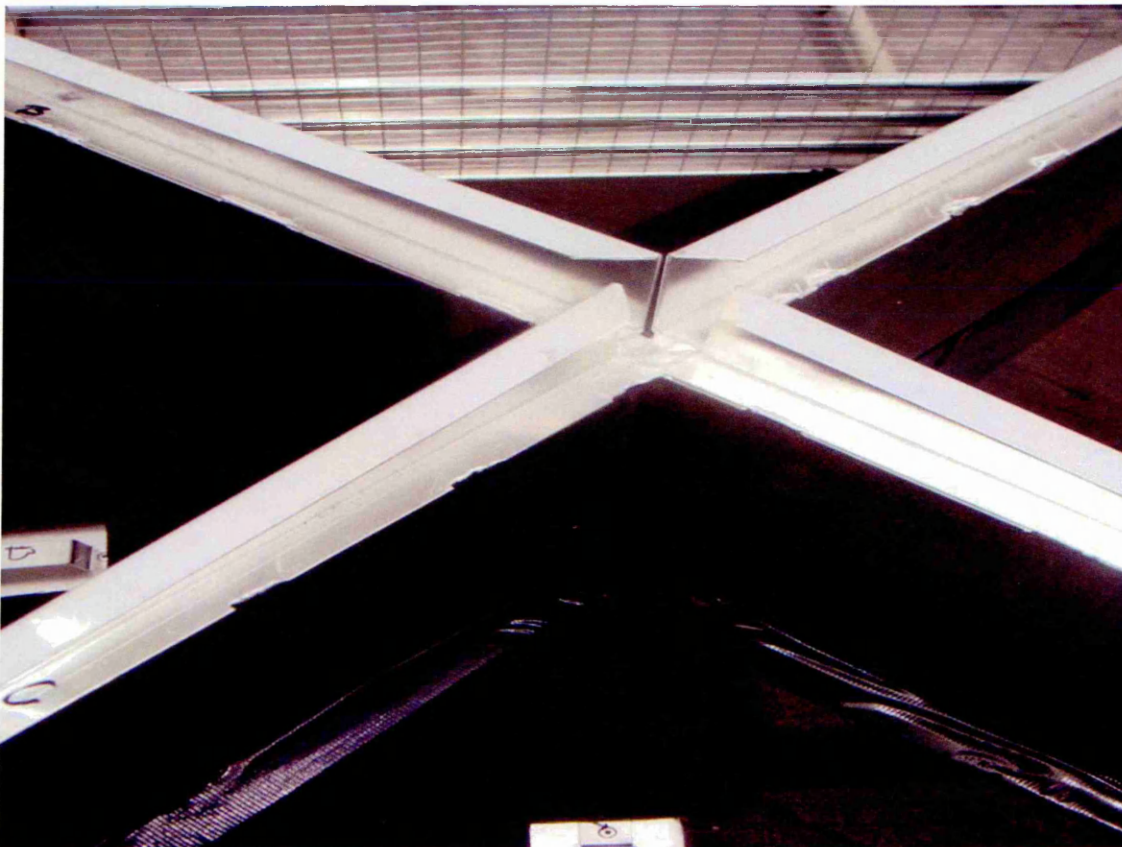
**Figure 7-7 Experimental set-up using blanking piece to vary the number of opening
external louvers**

7.3.1 Six external louvers

The six-opening external louvers set-up was monitored for five days with the
averaged experimental results shown in Table 7-2.

Table 7-2 Averaged results for the six louvers experimental set-up

Sample point	External velocity (m/s)	Internal velocity (m/s)
10	4.2	0.18
2	4	0.02
4	4.1	0.01
5	4.8	0.08
6	3.8	0.01
8	4.3	0.01

Standard deviation (σ) values for table: External velocity = 1.3m/s, Internal velocity (points 2,5,6,7,8) = 0.03m/s, diffuser (point 10) = 0.06m/s.

From the results, the maximum velocity was at the diffuser sample point ten, with the second highest at sample point five. The results follow the same trend as the benchmark case. The average external wind speed across the five days was 4m/s and the results are represented for comparison in Figure 7-8.

Figure 7-8 Average internal velocity results of the six external louver experimental set-up

7.3.2 Four external louvers

The four-opening external louvers geometry was monitored for five days with the averaged experimental results shown in Table 7-3.

Table 7-3 Averaged results for the four louvers experimental set-up

Sample point	External velocity (m/s)	Internal velocity (m/s)
10	4.4	0.17
2	5.3	0.02
4	5.3	0.01
5	4.7	0.03
6	4.8	0.01
8	4.6	0.03

Standard deviation (σ) values for table: External velocity = 1.7m/s, Internal velocity (points 2,5,6,7,8) = 0.01m/s, diffuser (point 10) = 0.09m/s.

The results show similar trends to the previous experiments. From the results, reducing the number of external louvers has reduced the internal velocity. It should be noted that the average external wind speed across the five days was 5m/s, which is higher than the previous set-up of six louvers. Allowing for the higher wind speeds, the four louver set-up still produced lower internal velocities. The results are represented in Figure 7-9.
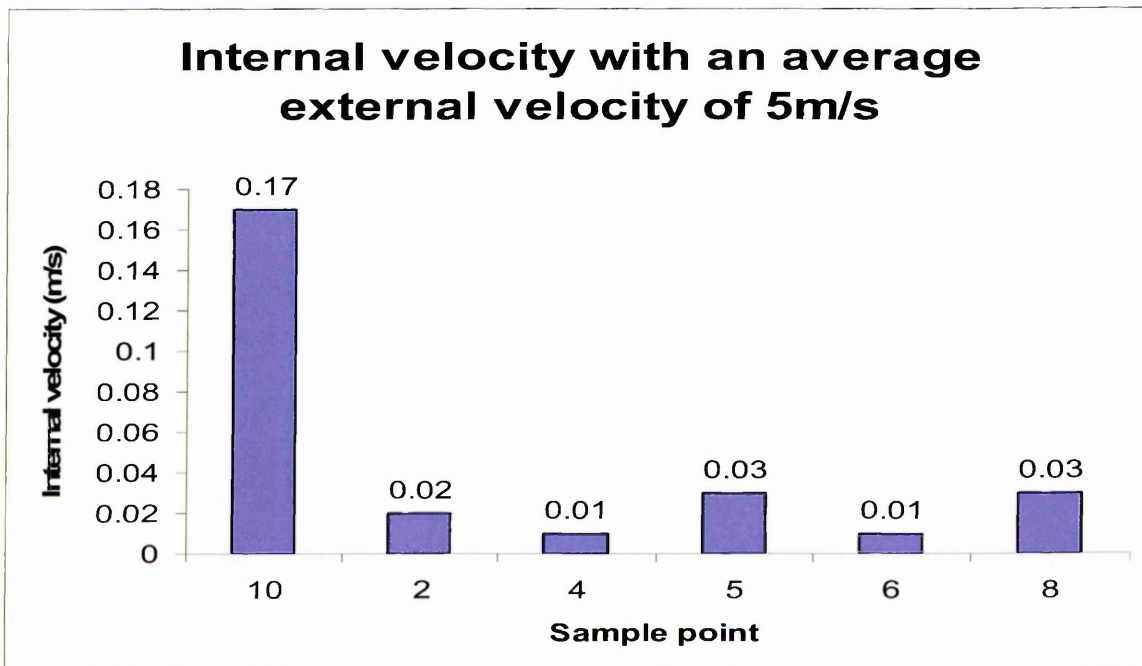
Figure 7-9 Average internal velocity results of the four external louver experimental set-up

7.3.3 Two external louvers

The two-opening external louvers geometry was monitored for five days with the averaged experimental results shown in Table 7-4.

Table 7-4 Averaged results for the two louvers experimental set-up

Sample point	External velocity (m/s)	Internal velocity (m/s)
10	7.8	0.07
2	8.9	0.03
4	8.6	0.02
5	8.2	0.04
6	7.8	0.03
8	8.2	0.04

Standard deviation (σ) values for table: External velocity = 2.3m/s, Internal velocity (points 2,5,6,7,8) = 0.02m/s, diffuser (point 10)m/s = 0.03m/s.

The results show a reduction in the internal velocity compared to the previous experimental set-ups of six and four louvers. At sample point five there is an increased internal velocity in comparison to the previous four louver case. However, the external velocity is much higher with 8.2m/s in this case compared to 4.7m/s in the four louvers case. The average external velocity across the five days was 8m/s, which is much higher than any of the previous experiments. The results are represented in Figure 7-10.
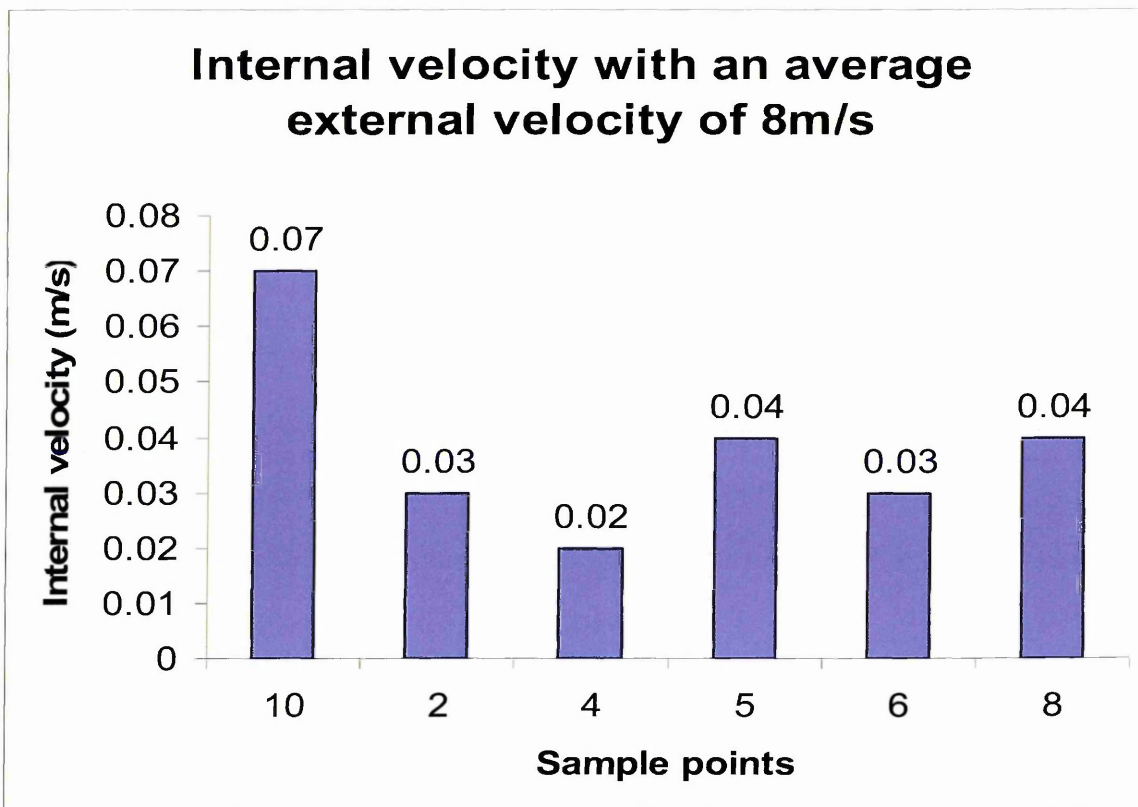
Figure 7-10 Average internal velocity results of the two external louver experimental set-up

Allowing for this higher external velocity, the two louver case follows the trend of a reduced internal velocity in-line with a reduction in the amount of louvers. Due to the variation of the external wind speed it was not possible to draw a direct comparison between the three cases. However, the results showed that a reduction in the number of louvers resulted in a reduction of internal velocity. To demonstrate this, the six louver case is compared with that of the benchmark case (eight louvers). Both cases had an average external velocity of 4m/s, the results are represented in Figure 7-11.
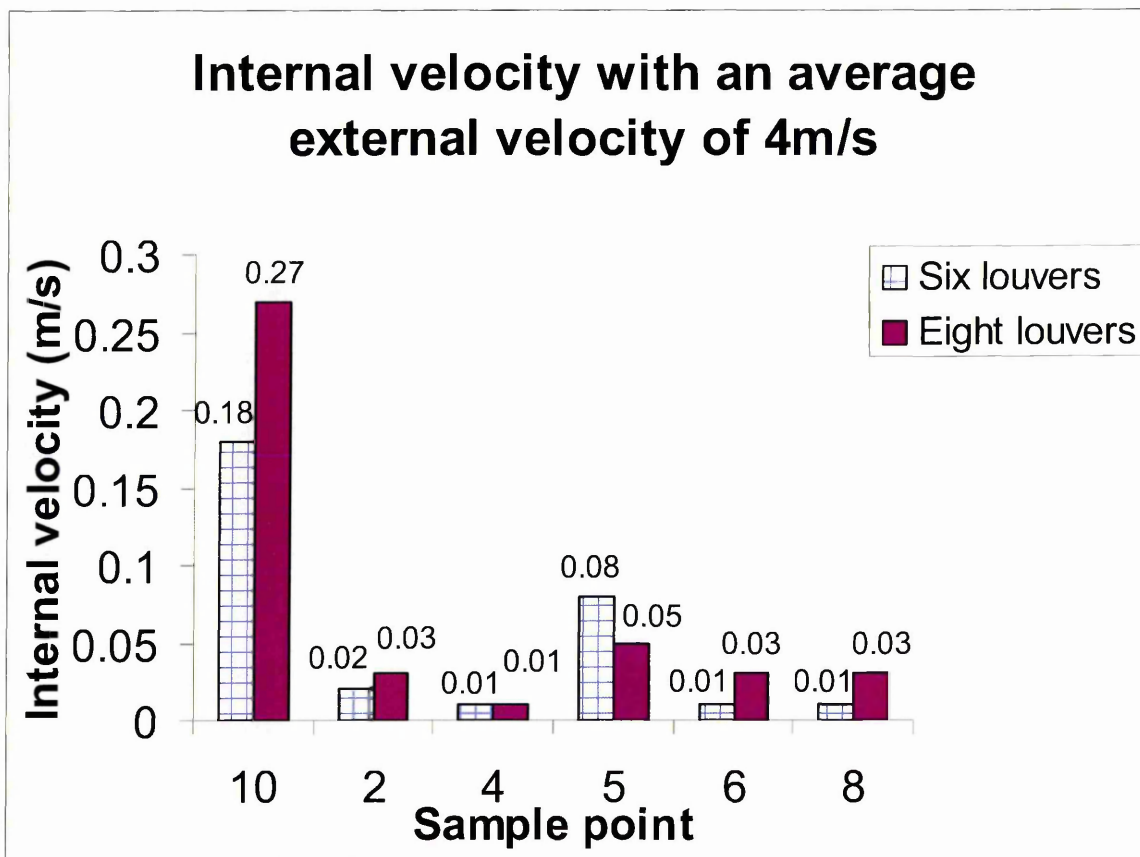
Figure 7-11 Comparison of the six louver experimental set-up with the benchmark case

From Figure 7-11, it is shown that a reduction in external louvers reduces the internal velocity. At sample point five, the six louver set-up provided a greater internal velocity. However, this was due to a higher external velocity of 4.8m/s in comparison to 4.1m/s. The full results are shown in Tables 7-1 and 7-2.

7.4 Distance between external louvers

To investigate the effect of varying the distance between the external louvers, three different experimental set-ups were used. The three set-ups were achieved by using spacer bars at the four corners of the wind vent (described in Chapter 6). Reducing the distance between the louvers had an undesirable effect of reducing the overall height of the louver section (Figure 7-12). Hence, the internal blanking piece was used at the top louver to alleviate any additional

airflow. The three louver spacings tested were 20, 30 and 60mm, with the

benchmark case having 50mm louver spacings.

Figure 7-12 Experimental set-up for the investigation into the effect of varying the spacing between external louvers, 20mm spacing shown.

7.4.1 External louver spacing of 60mm

The external louver spacing of 60mm was monitored for five days with the

averaged experimental results shown in Table 7-5.

Table 7-5 Averaged results for the 60mm spacing experimental set-up

Sample point	External velocity (m/s)	Internal velocity (m/s)
10	5	0.21
2	4.3	0.03
4	4.8	0.06
5	4.7	0.12
6	4.5	0.07
8	5.3	0.05

Standard deviation (σ) values for table: External velocity = 2.3m/s, Internal velocity (points 2,5,6,7,8) = 0.04m/s, diffuser (point 10)m/s = 0.04m/s.

The results show that the maximum velocity is at sample point ten, with the second highest at sample point five. These results follow the same trend as the benchmark case. The external wind speed averaged across the five days was 5m/s. The results are represented in Figure 7-13.
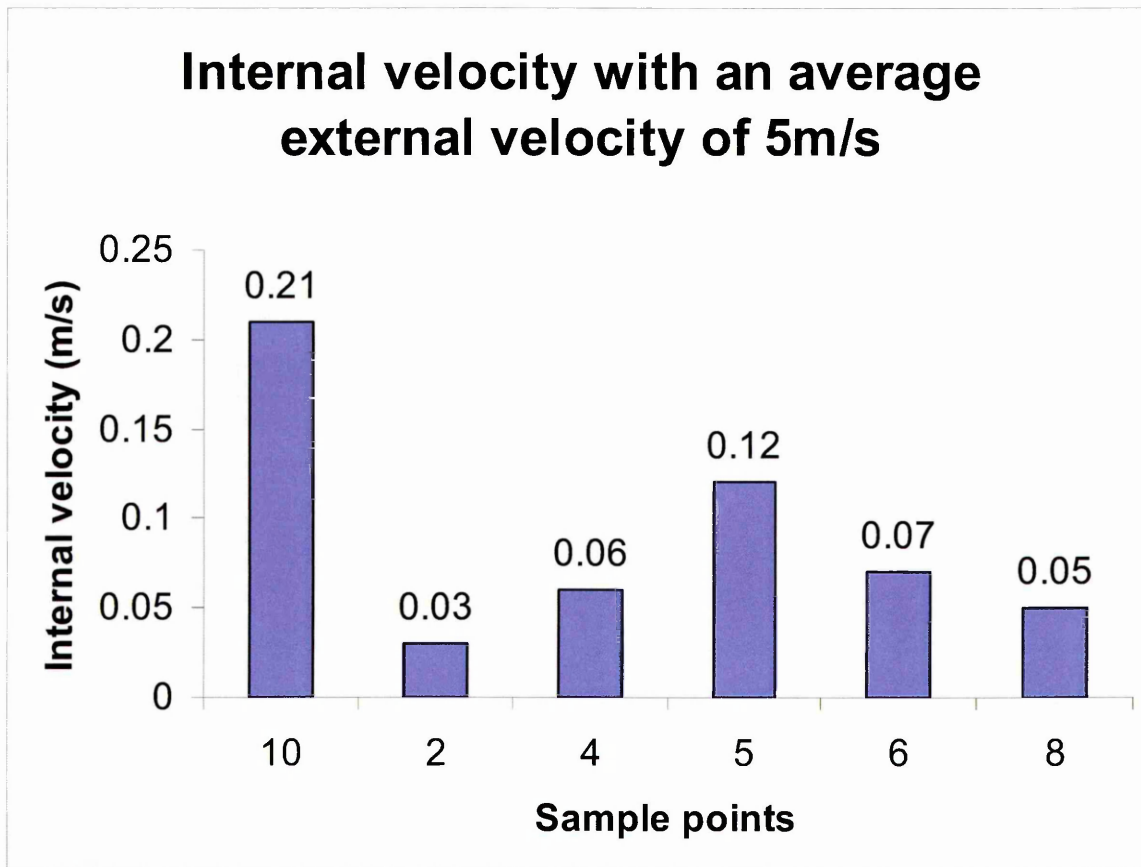
Figure 7-13 Average internal velocity results of the 60mm external louver spacing experimental set-up

7.4.2 External louver spacing of 30mm

The external louver spacing of 30mm was monitored for five days with the averaged experimental results shown in Table 7-6.

Table 7-6 Averaged results for the 30mm spacing experimental set-up

Sample point	External velocity (m/s)	Internal velocity (m/s)
10	7.1	0.15
2	7.3	0.02
4	7.2	0.02
5	6.9	0.04
6	6.7	0.03
8	4.9	0.02

Standard deviation (σ) values for table: External velocity = 1.5m/s, Internal

velocity (points 2,5,6,7,8) = 0.01m/s, diffuser (point 10)m/s = 0.05m/s.

From the results, the reduction in louver spacing has produced a lower internal

velocity. The average external velocity across the five days was 7m/s which is

higher than the previous 60mm spacing experimental set-up. Despite this higher

external velocity, the internal velocity is still lower than the 60mm spacing set-up.

The results are represented in Figure 7-14.
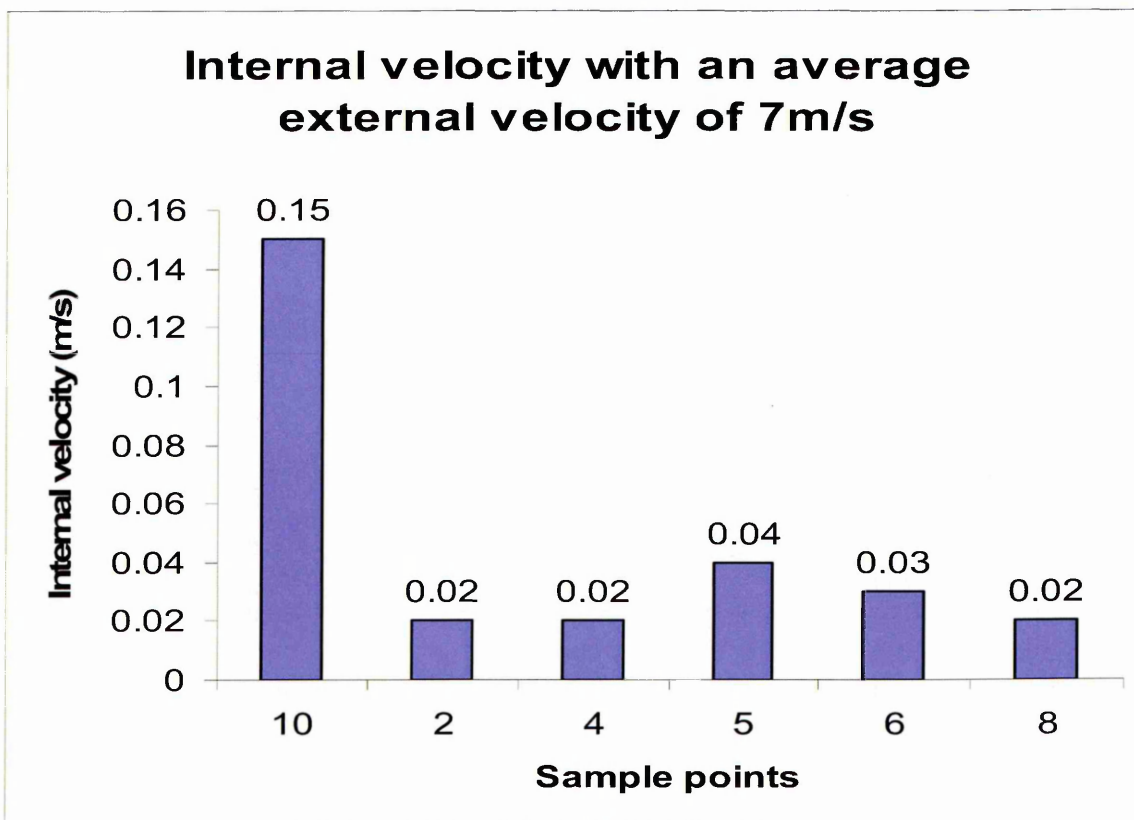
Figure 7-14 Average internal velocity results of the 30mm external louver spacing experimental set-up

7.4.3 External louver spacing of 20mm

The external louver spacing of 20mm was monitored for five days with the averaged experimental results shown in Table 7-7.

Table 7-7 Averaged results for the 20mm spacing experimental set-up

Sample point	External velocity (m/s)	Internal velocity (m/s)
10	8.7	0.13
2	6.5	0.01
4	6.9	0.03
5	6.9	0.05
6	6.1	0.02
8	6	0.02

Standard deviation (σ) values for table: External velocity = 3.3m/s, Internal velocity (points 2,5,6,7,8) = 0.02m/s, diffuser (point 10)m/s = 0.03m/s.

From the results, the internal velocity across diffuser sample point 10 is reduced when compared to the previous experimental set-up of 30mm spacing. The average external velocity across the five days was 7m/s. The results are represented in Figure 7-15.
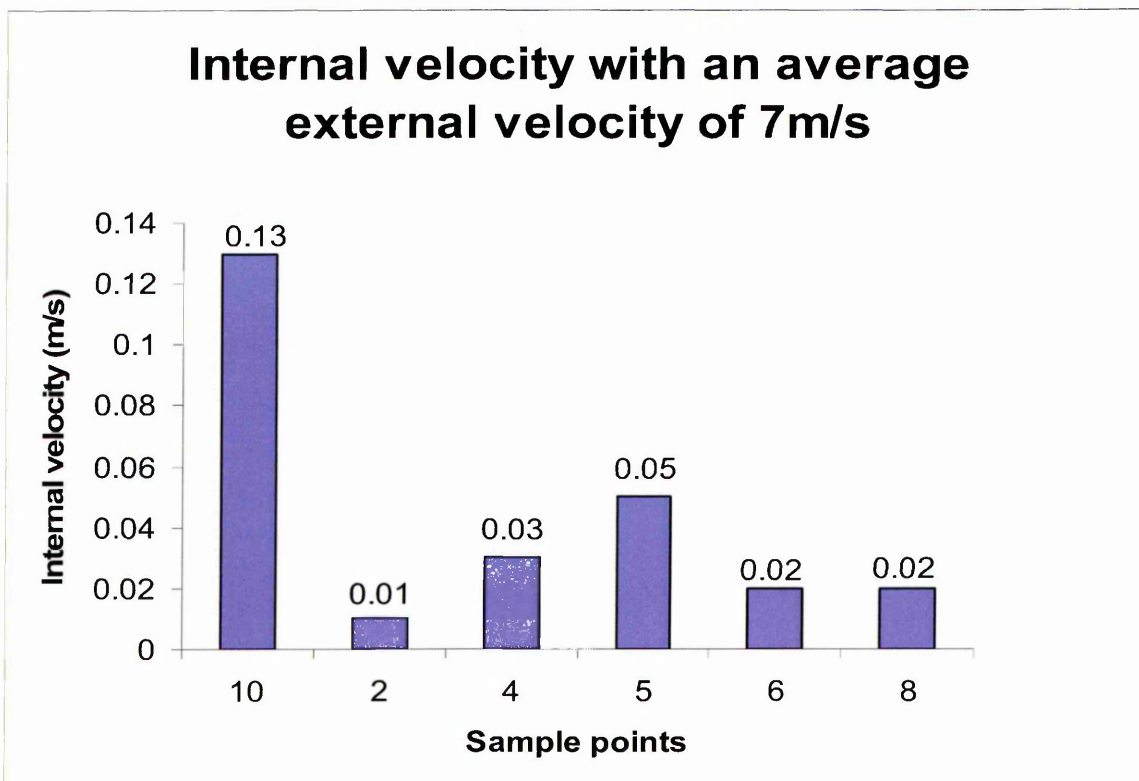
Figure 7-15 Average internal velocity results of the 20mm external louver spacing experimental set-up

The two cases of 30 and 20mm external louver spacing, share the same average external velocity of 7m/s. A direct comparison between the two is shown in Figure 7-16.
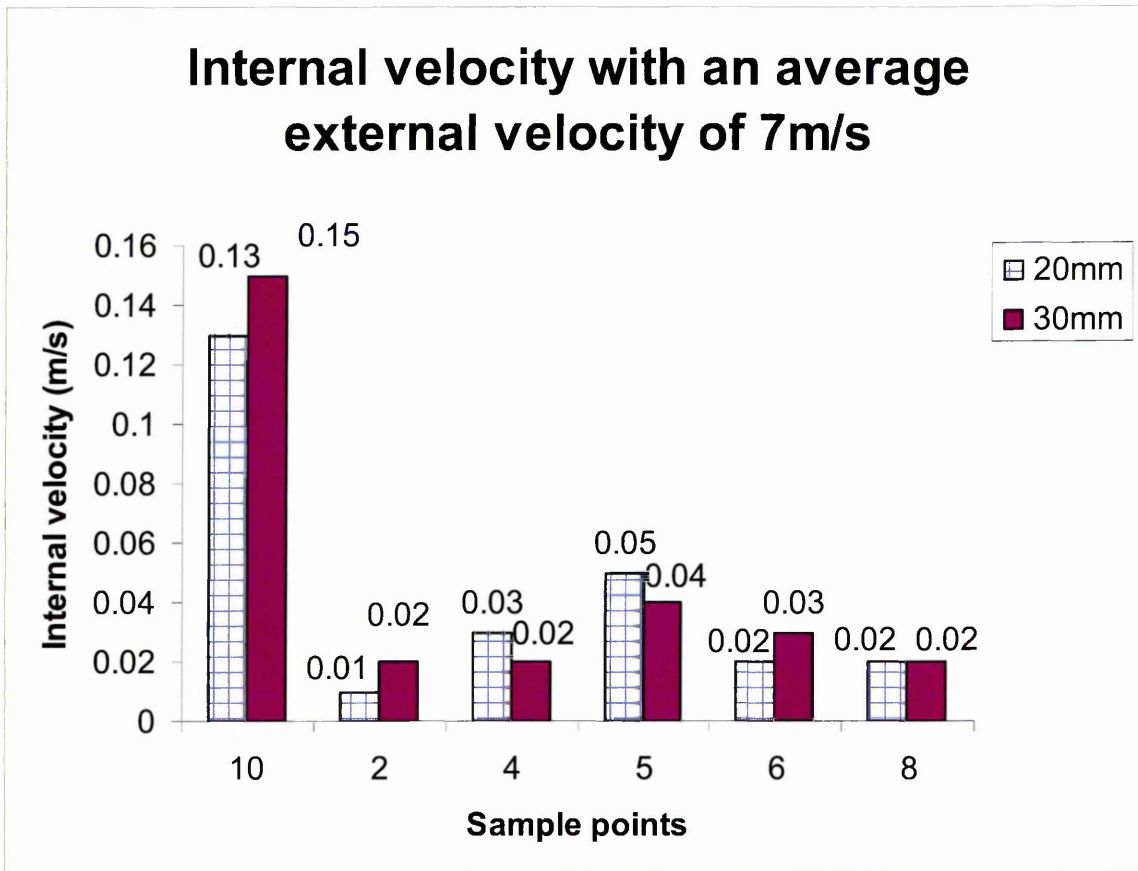
Figure 7-16 Comparison of the 30 and 20mm external louver spacings

From Figure 7-16, the reduction in spacing from 30 to 20mm had little overall effect on the internal velocity. Sample point ten showed a reduced velocity which indicated a reduction in air-exchange within the wind vent. The results were as expected. Reducing the spacing reduced the opening area of the wind vent which restricted the airflow through the terminal.

7.4.4 External louver angle of 35°

To investigate the effect of the external louver angle on the internal velocity of the wind vent, a new set of louvers were used. From the CFD simulation results (see Chapter 5) the optimum external louver angle was determined as 35°. A

set of eight external louvers were manufactured with an external louver angle of 35° and attached to the wind vent (Figure 7-17). All other geometrical parameters remained the same as the benchmark including the louver spacing.

Figure 7-17 Experimental wind vent with 35° louvers

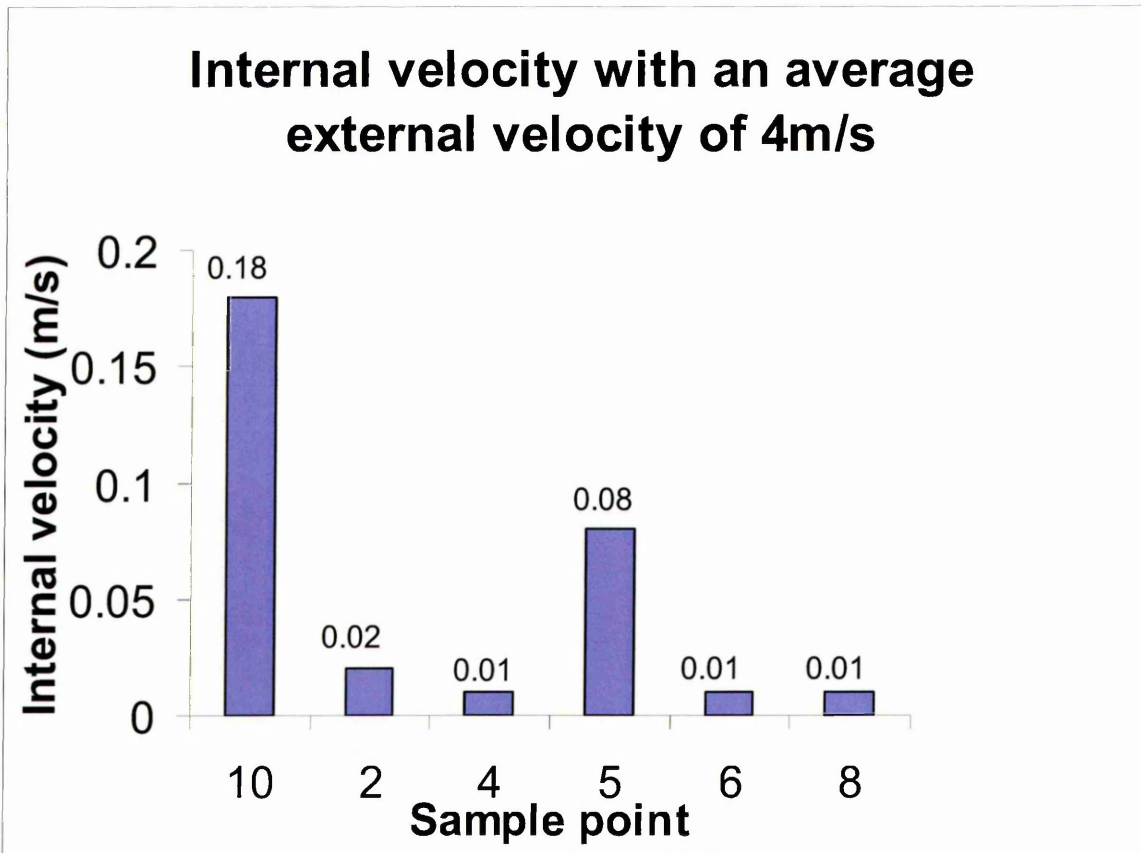The external louver angle experimental set-up was monitored for five days with the averaged experimental results shown in Table 7-8.

Table 7-8 Averaged results for the external louver angle experimental set-up

Sample point	External velocity (m/s)	Internal velocity (m/s)
10	3.5	0.27
2	3.6	0.02
4	3.6	0.05
5	3.1	0.05
6	3.2	0.04
8	2.5	0.04

Standard deviation (σ) values for table: External velocity = 1.0m/s, Internal velocity (points 2,5,6,7,8) = 0.02m/s, diffuser (point 10)m/s = 0.08m/s.

The averaged external wind speed across the five days was 3m/s. The results are represented in Figure 7-18.
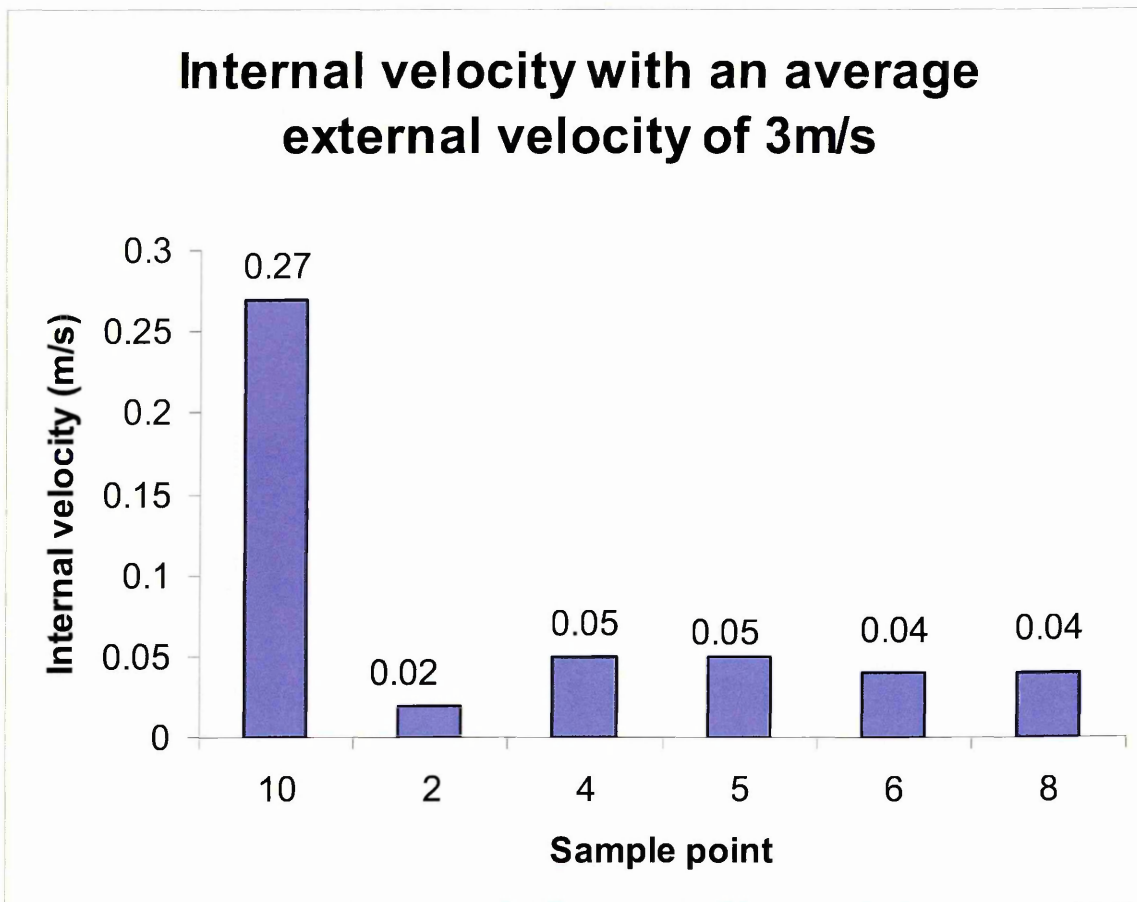
Figure 7-18 Average internal velocity results of the 35° external louver angle

From the results, the external louver angle at 35° has matched the performance

of the benchmark case at 45° (Figure 7-19). Both sample points ten and five are

equal in each experimental set-up, with 0.27m/s at point ten and 0.05m/s at

point five. However, the average external wind speed is lower in the 35°

experiment, with an average of 3m/s compared to 4m/s of the benchmark case.

Therefore, the 35° louver increased the internal velocity in comparison to the

benchmark. This result concurs with that of the CFD simulation.
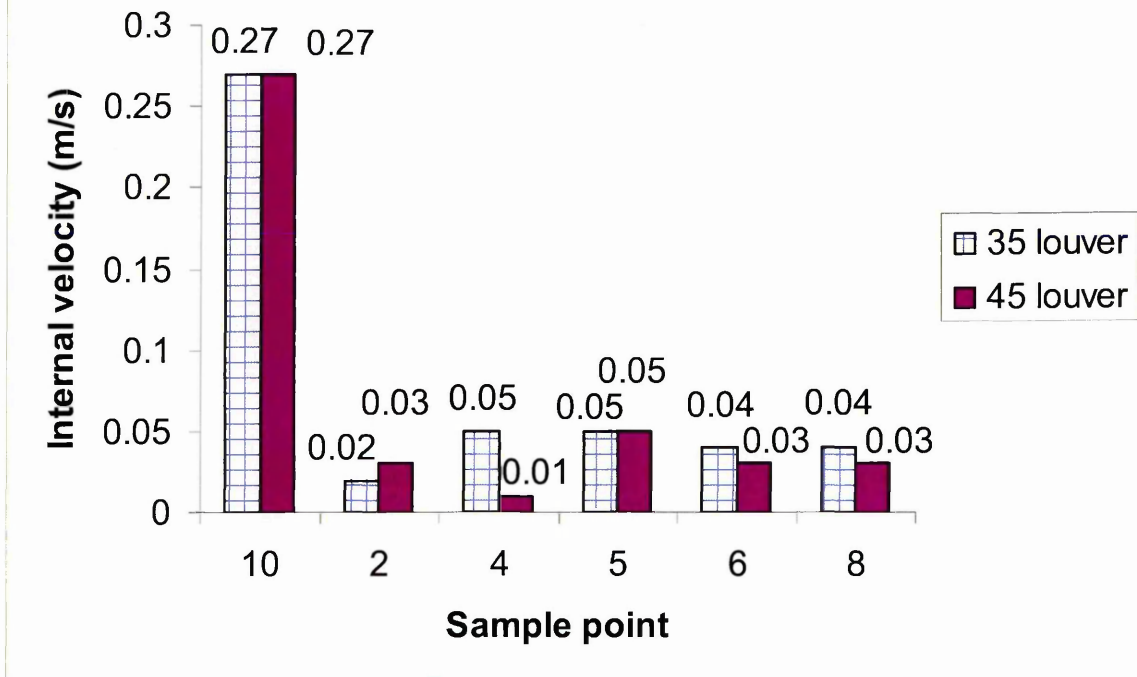
Figure 7-19 Comparison of the 35° louver angle with the benchmark case

7.5 *Optimum geometrical configuration*

The optimum geometrical configuration was devised from the CFD simulation

and experimental work. The optimum wind vent comprised of four external

louvers, 30mm louver spacing and a louver angle of 35°. The optimum

experimental configuration (Figure 7-20) is the same as the optimum CFD

simulation configuration.

Figure 7-20 Experimental set-up of the optimum configuration

The optimum geometrical configuration set-up was monitored for five days with the averaged experimental results shown in Table 7-9.

Table 7-9 Averaged results for the optimum configuration experimental set-up

Sample point	External velocity (m/s)	Internal velocity (m/s)
10	4.5	0.24
2	3.5	0.01
4	3.8	0.02
5	3.5	0.05
6	3.9	0.02
8	3.3	0.02

Standard deviation (σ) values for table: External velocity = 1.1m/s, Internal velocity (points 2,5,6,7,8) = 0.02m/s, diffuser (point 10)m/s = 0.06m/s.

The average external wind speed across the five days was 4m/s. The results are represented in Figure 7-21.
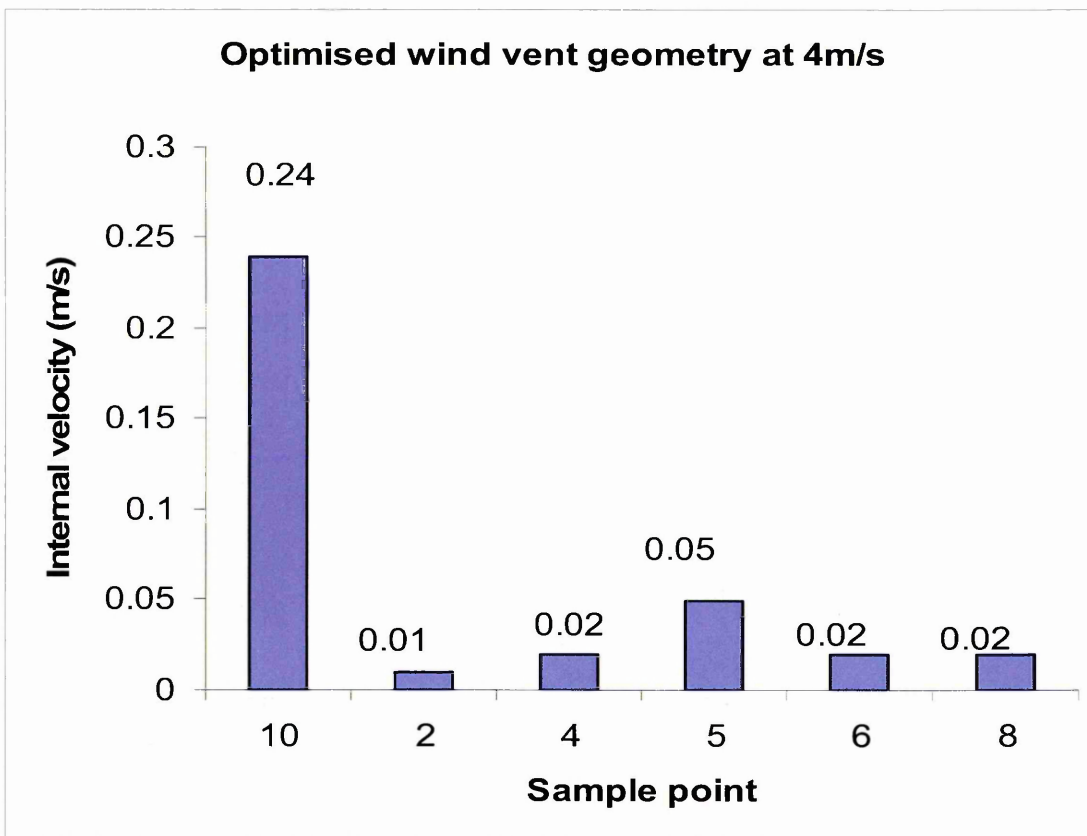
Figure 7-21 Average internal velocity results of the optimum geometrical configuration

The external velocity in the optimum case was 4m/s. Therefore, a direct

comparison with the benchmark case was made (Figure 7-22).
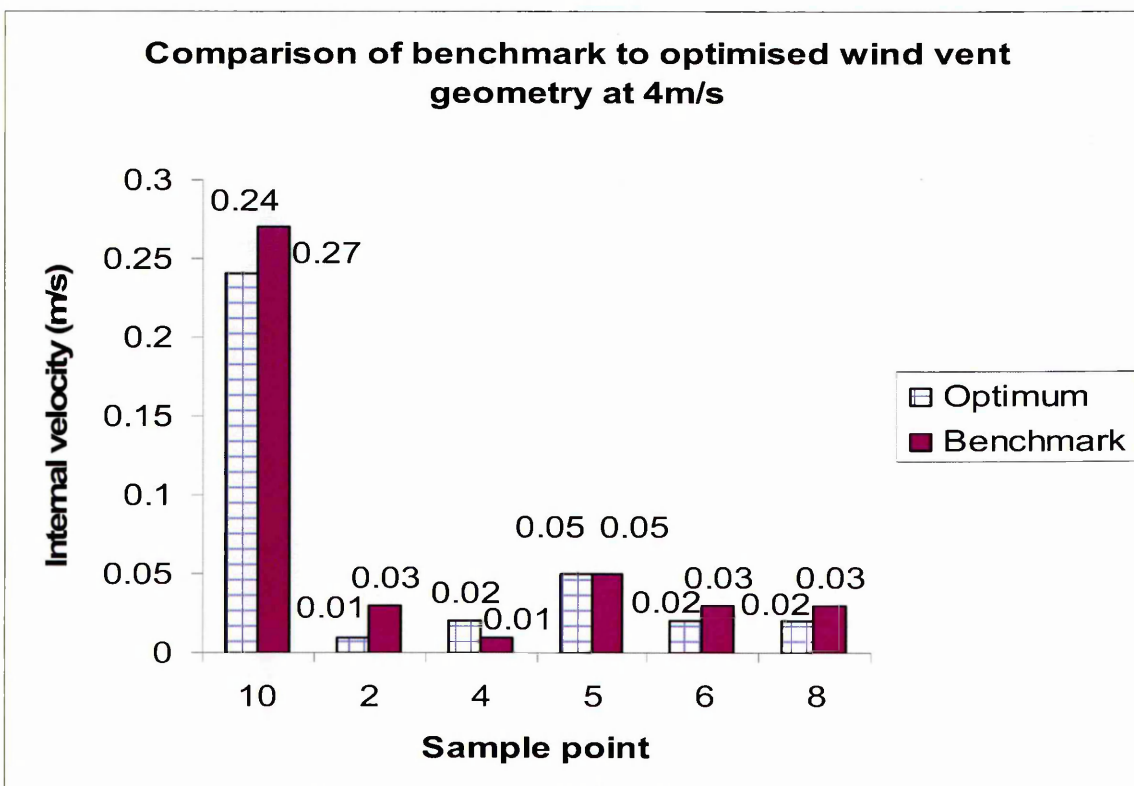
Figure 7-22 Comparison of the optimised wind vent geometry with the benchmark

From Figure 7-22, the optimised geometrical configuration did not out perform the benchmark wind vent. The results showed a marginal advantage in the internal velocity produced by the benchmark in the range of 11 - 20%. However, this range must be considered in the context of the small velocities experienced as the maximum velocity deviation at any sample point was 0.03m/s. The experimental results showed that singular geometrical variation can improve the wind vent performance. Applying the geometrical variations in conjunction did not produce an increase in performance. However, the experimentally optimised geometry achieved a similar performance to that of the benchmark wind vent, whilst reducing the number of components and materials used in its construction. The experimental results concur with those of the CFD simulations.

7.6 Summary

This chapter presented five experimental investigations using far-field testing. Each investigation was carried out using a pre-determined test procedure (described in Chapter 6). The results of the investigations were presented in both tabular and chart form. Comparisons were drawn between experiments and presented in chart form. The systematic investigation led to a distinct geometrically optimised wind vent. The optimised wind vent was investigated and compared to the benchmark case. The results of the optimised against the benchmark geometry were discussed and presented in chart form.

Chapter 8   Validation of the CFD model

8.1 Introduction

There are three approaches to the study of natural ventilation namely empirical models, experimental measurements and CFD simulations. The empirical models in this study were derived from experimental measurements (see Chapter 3). The CFD models must be validated to provide confidence in their accuracy [Hills, 2006]. To validate the CFD simulations, the computed results are compared with the experimental data following a method proposed by Chen *et al.* (2004). To validate the simulated flow, the experimental flow visualisation is compared for the benchmark geometry. To validate the simulation results, different external velocities (2, 4 and 5m/s) and geometries were used namely the benchmark and optimum geometries. The sample points referred to in the validation are shown in Figure 6-18. To evaluate the error range and trends, a comparison is made between this study and other published work.

8.2 Flow visualisation

The flow visualisation of the simulated results is described in detail in Chapter 5. The experimental flow visualisation is described in detail in Chapter 7. The two flow visualisations are compared for the benchmark case. Only the benchmark case is considered. As the geometrical variations carried out affect the rate not the method of air-exchange. This comparison is made as a qualitative evaluation of the results as described by Srebric and Chen (2002A).

8.2.1 Benchmark case

The simulation results showed the external velocity from the macro-climate entering at the left-hand side of the wind vent (Figure 8-1). The air velocity was higher at this side of the wind vent due to the prevailing external velocity. The

external velocity is driving the air into the micro-climate. The right-hand side of the wind vent showed the exhaust air (from the micro-climate) exiting. The air velocity was lower at this side of the wind vent due to it being drawn by the suction effect (detailed in Chapter 5). The suction effect is much lower than the driving effect of the external velocity.

| 5.44e+00 |
| 5.17e+00 |
| 4.90e+00 |
| 4.62e+00 |
| 4.35e+00 |
| 4.08e+00 |
| 3.81e+00 |
| 3.54e+00 |
| 3.26e+00 |
| 2.99e+00 |
| 2.72e+00 |
| 2.45e+00 |
| 2.18e+00 |
| 1.90e+00 |
| 1.63e+00 |
| 1.36e+00 |
| 1.09e+00 |
| 8.16e-01 |
| 5.44e-01 |
| 2.72e-01 |
| 0.00e+00 |

Path Lines Colored by Velocity Magnitude (m/s)   Jul 06, 2007
                                          FLUENT 6.2 (3d, segregated, ske)
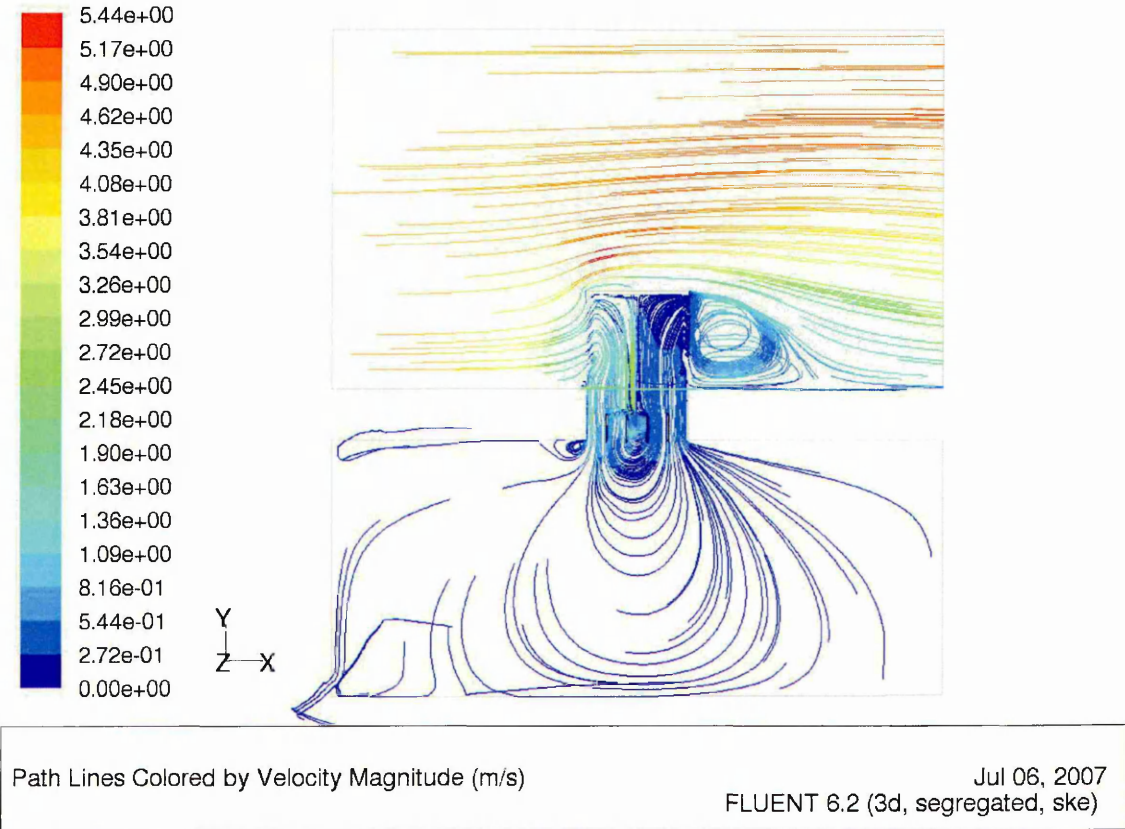
Figure 8-1 Simulation flow results for the benchmark geometry illustrated using velocity vectors

The experimental flow visualisation showed fresh air entering the wind vent at the left-hand side (Figure 8-2). The fresh air entered at a higher velocity due to the external driving velocity. The higher velocity at the point of entry was visible due to the amount of smoke being displaced at this side of the wind vent.
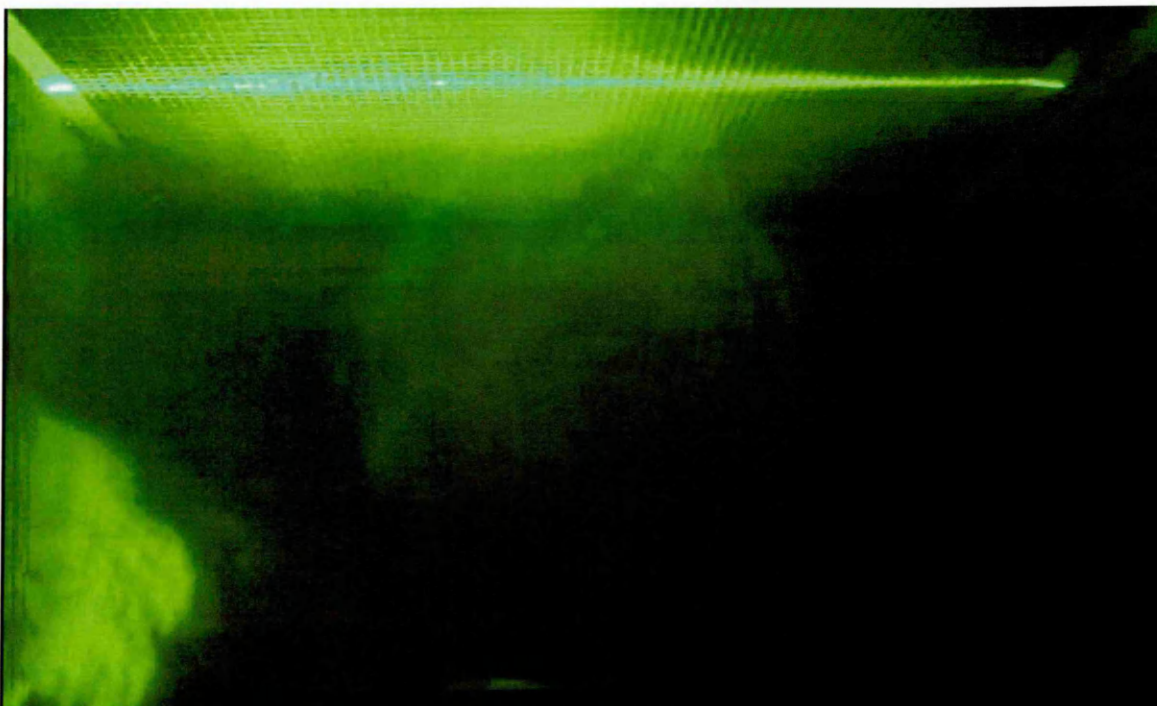
Figure 8-2 Experimental flow visualisation for the benchmark geometry

The right-hand side of the wind vent showed the stale air exiting at a lower velocity due to the suction effect. The lower velocity was indicated by the lack of smoke movement around this area of the wind vent. The two effects in tandem are displayed more clearly in Figure 8-3.
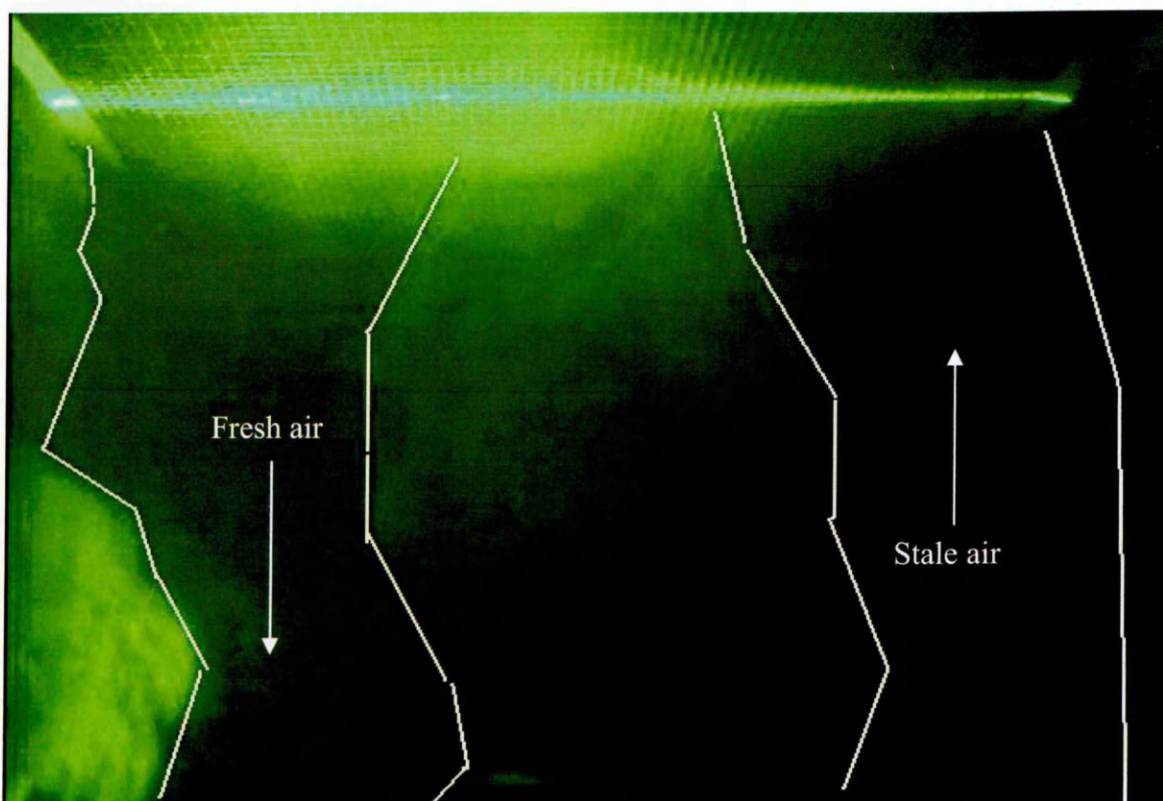
Figure 8-3 Annotated picture of the displacement effect of the wind vent

The flow pattern in the simulation model is the same as the flow pattern recorded in the experimental test. The method of air-exchange is the same in both cases. Therefore, the simulation flow is considered validated.

8.3 Numerical analysis

To determine the accuracy of the simulated numerical results they have been compared to the experimental readings. The simulation volume (micro-climate) differs marginally to the experimental volume. Therefore, both sets of results have been normalised. To normalise the results they have been divided by the maximum internal velocity at sample point five (shown in Figure 6-18). The data at diffuser sample point ten remained unchanged as it is unaffected by the control volume. The CFD results were systematically compared to the experimental data as proposed by Chen and Srebric (2002B). The benchmark case was compared with two different external velocities. The benchmark and optimum geometries were also compared.

8.3.1 Benchmark case with external velocity at 4m/s

The experimental results (Chapter 7) used averaged data to determine the effectiveness of geometrical variations. To validate the model, only experimental data which is comparable to 4m/s with a tolerance of ± 0.5m/s has been used. The two sets of normalised data for the benchmark geometry are shown in Table 8-1.

Table 8-1 Normalised results for the benchmark geometry

Sample point	CFD result	Experimental result	Difference (m/s)
2	0.22	0.28	0.06
4	0.22	0.14	0.08
5	0.02	0.07	0.05
6	0.22	0.28	0.06
8	0.1	0.14	0.04
10	0.2	0.27	0.07

From Table 8-1, the difference was within the range 0.04 - 0.08m/s. Diffuser sample point ten which is unaffected by the size of the control volume, has a difference margin of 0.07m/s. The trends are represented in Figure 8-4.
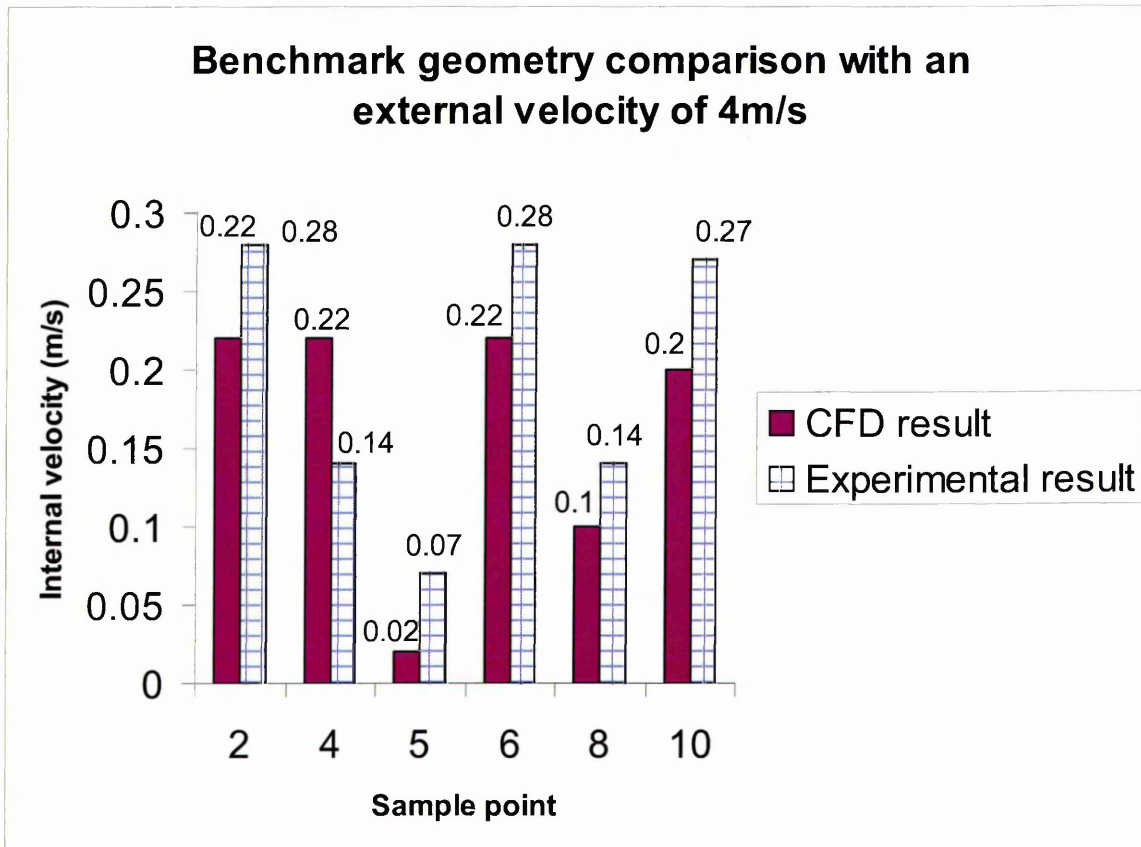
Figure 8-4 Comparison of the benchmark geometry CFD results against experimental data

From Figure 8-4, at most sample points, five out of six, the experimental result is greater than that of the CFD simulation. The trends for both the CFD and experimental data are in good agreement. The comparison showed a low difference range and the trends to be in good agreement. Hence, the CFD simulation was considered validated for this geometry with an external velocity of 4m/s.

8.3.2 Benchmark case with external velocity at 2m/s

To determine the accuracy of CFD simulation results at lower external velocities, the same geometry was used with an external velocity of 2m/s. The same

tolerance of ± 0.5m/s was applied to the experimental data used. The two sets of normalised data for the benchmark geometry are shown in Table 8-2.

Table 8-2 Normalised results for the benchmark geometry

Sample point	CFD result	Experimental result	Difference (m/s)
2	0.33	0.25	0.08
4	0.22	0.25	0.03
5	0.01	0.04	0.03
6	0.22	0.25	0.03
8	0.44	0.5	0.06
10	0.09	0.15	0.06

From Table 8-2, the difference was within the range 0.03 - 0.08m/s. This range was similar to the previous case with an external velocity of 4m/s. The difference at diffuser sample point ten was 0.06m/s. This had increased from the previous case but is still within the range 0.03 - 0.08m/s. The trends are shown in Figure 8-5.
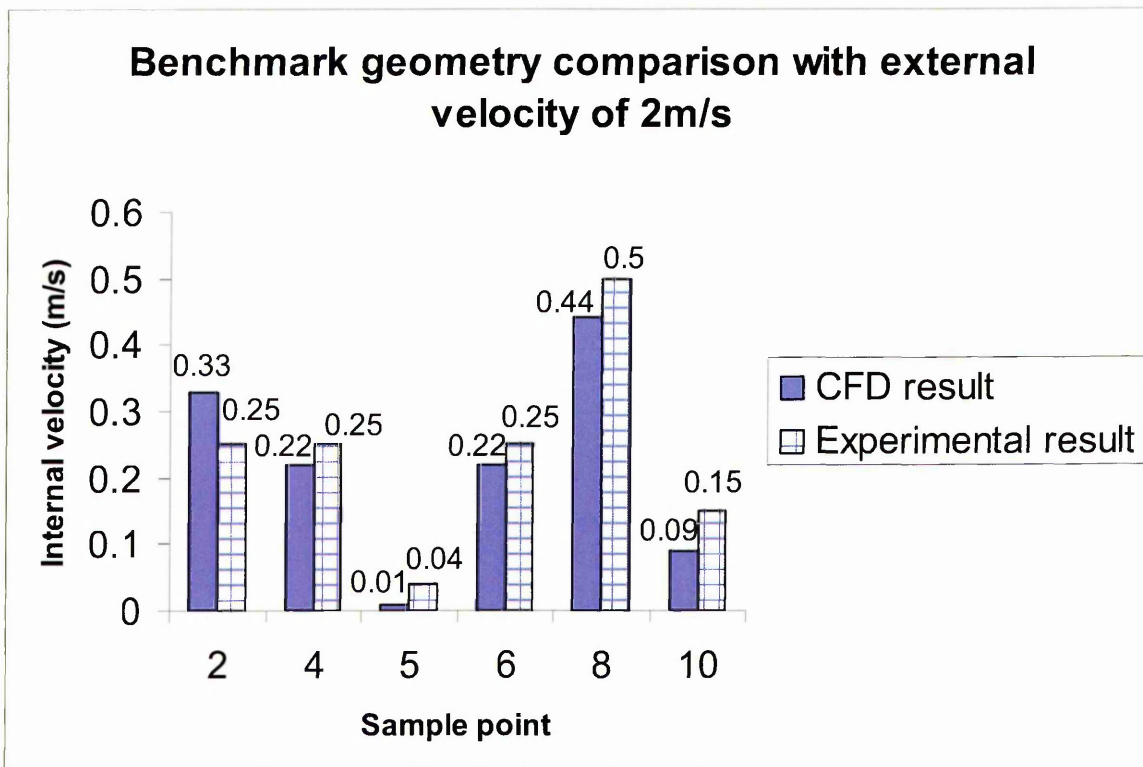
Figure 8-5 Comparison of the benchmark geometry CFD to experimental data

From Figure 8-5, at most sample points, five out of six, the experimental result was higher than that of the CFD simulation. This trend was repeated from the

previous case of 4m/s. The trends for both the CFD and experimental data are in good agreement. The comparison showed a low error margin and the trends in good agreement. Hence, the CFD simulation was considered valid for this geometry with an external velocity of 2m/s. Both the trends and the difference range were in agreement in the two cases with varying external velocities. Therefore, accuracy of the CFD simulations was unaffected by the external velocity.

8.3.3 Optimum case with an external velocity of 5m/s

The accuracy of the CFD results was unaffected by the external velocity. To determine the effect of geometrical variation on the simulation accuracy, the optimum case was analysed. An external velocity of 5m/s was used with the same tolerance on experimental data. The two sets of normalised data for the benchmark geometry are shown in Table 8-3.

Table 8-3 Normalised results for the optimum geometry with an external velocity of 5m/s

Sample point	CFD result	Experimental result	Difference (m/s)
2	0.15	0.13	0.02
4	0.2	0.13	0.07
5	0.02	0.08	0.06
6	0.25	0.25	0
8	0.2	0.25	0.05
10	0.23	0.24	0.01

From Table 8-3, the difference was within the range of 0 - 0.07m/s. The difference at diffuser sample point ten was 0.01m/s. The difference range was similar to that of the previous two cases. The trend is represented in Figure 8-6.
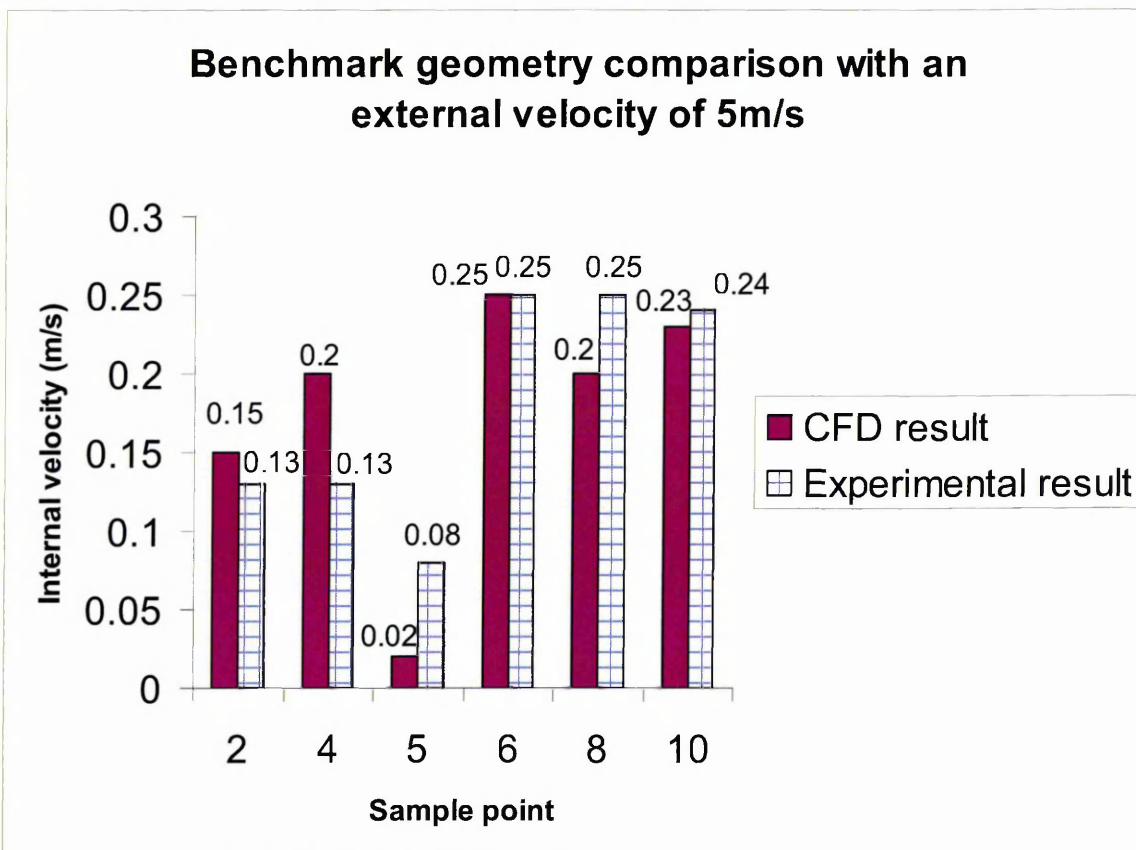
Figure 8-6 Comparison of the optimum geometry CFD results against experimental data

From Figure 8-6, at most of the sample points, four out of six, the experimental data is higher than or equal to the simulation result. The trends followed the same path as the previous two cases. Additionally, the maximum difference is marginally, 0.01m/s, lower than the previous case. Variation of the geometry had no effect on the accuracy of the CFD result.

8.4 Comparison to similar studies

The trends were consistent across all three cases. According to Chen and Serbric (2002) "as long as the trends that are predicted are consistent, the less-than-perfect accuracy should be acceptable". In this study the difference range was within the range 0 - 0.08m/s across all the three cases. The range must be considered within the context of this work. To evaluate the accuracy of the range, it was compared to other published work within the same field of

investigation. Elmualim (2006) used CFD and experimental investigations to evaluate the performance of a wind vent. The wind vent was of similar construction to the benchmark geometry used in this investigation. The CFD simulation results were compared to Elmualim (2006) results to establish the trend. The error range of the Elmualim investigation was evaluated against the range found in this study.

8.4.1 Comparison of simulation results

The wind vent used in the Elmualim (2006) investigation was of the same construction as the benchmark case. However, the scale of the Elmualim wind vent was 50% smaller than that of the benchmark geometry. To make an accurate comparison the two sets of results have been normalised. The method of normalisation is the same used throughout this investigation. The same sample point, the diffuser sample point 10 has been used. The results are shown in Table 8-4.

Table 8-4 Normalised simulation results for the two studies

External velocity (m/s)	Elmualim result (m/s)	Hughes result (m/s)	Difference (m/s)
1	0.14	0.21	0.07
2	0.43	0.42	0.01
3	0.63	0.59	0.04
4	0.86	0.79	0.07

From Table 8-4, the difference range was within 0.01 - 0.07m/s. This range is in-line with the range found during the validation investigation of this study. The trend is represented in Figure 8-7.

Figure 8-7 Comparison of the normalised simulation results for the two studies

From Figure 8-7, the trends are the same between the two studies. The CFD simulation results follow the same trend as both the experimental work of this investigation and the simulation work of the Elmualim investigation.

8.4.2 Comparison of simulation results against experimental work

The experimental work used in the Elmualim (2006) study was based on wind tunnel experiments. The CFD results of the benchmark geometry were compared to the wind tunnel investigations of Elmualim. The normalised results are shown in Table 8-5.

Table 8-5 Normalised results for the CFD comparison to wind tunnel experimentation

External velocity (m/s)	Elmualim result (m/s)	Hughes result (m/s)	Difference (m/s)
1	0.25	0.21	0.04
2	0.54	0.42	0.12
3	0.78	0.59	0.19
4	0.89	0.79	0.10

From Table 8-5, the difference was within the range 0.04 - 0.19m/s. This range is far higher than the 0 - 0.08m/s range shown in this investigation. The trend is represented in Figure 8-8.
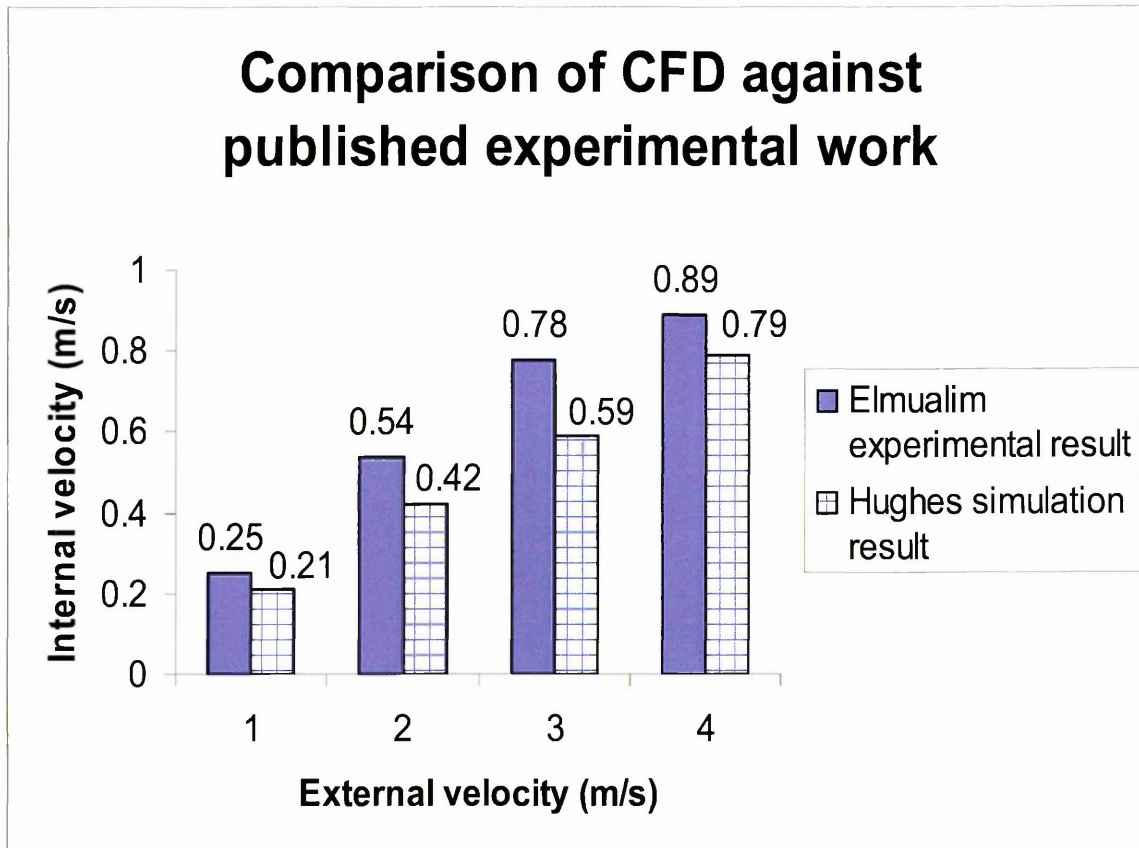
Figure 8-8 Comparison of simulation result against wind tunnel testing results

From Figure 8-8, the trend is the same for both sets of normalised results. The trends followed the same path in both the CFD and the experimental comparison. Therefore, the trends were correct for the simulation results in this study.

8.4.3 Comparison of error range

The trends were the same across simulation and experimental work in both this study and in comparison to Elmualim (2006B) investigations. To evaluate the error range, a comparison was made between the Elmualim error range and the

error range of this study. The results of Elmualim`s simulation and experimentation work are shown in Table 8-6.

Table 8-6 Comparison of Elmualim simulation and experimental data

External velocity (m/s)	Simulation result (m/s)	Experimental data (m/s)	Difference (m/s)
1	0.14	0.25	0.11
2	0.43	0.54	0.11
3	0.63	0.78	0.15
4	0.86	0.89	0.03

From the Table, the error was within the range of 0 - 0.15m/s. The error trend is represented in Figure 8-9. This study found a range of 0 - 0.08m/s. Therefore, the error range in this investigation was within acceptable limits.
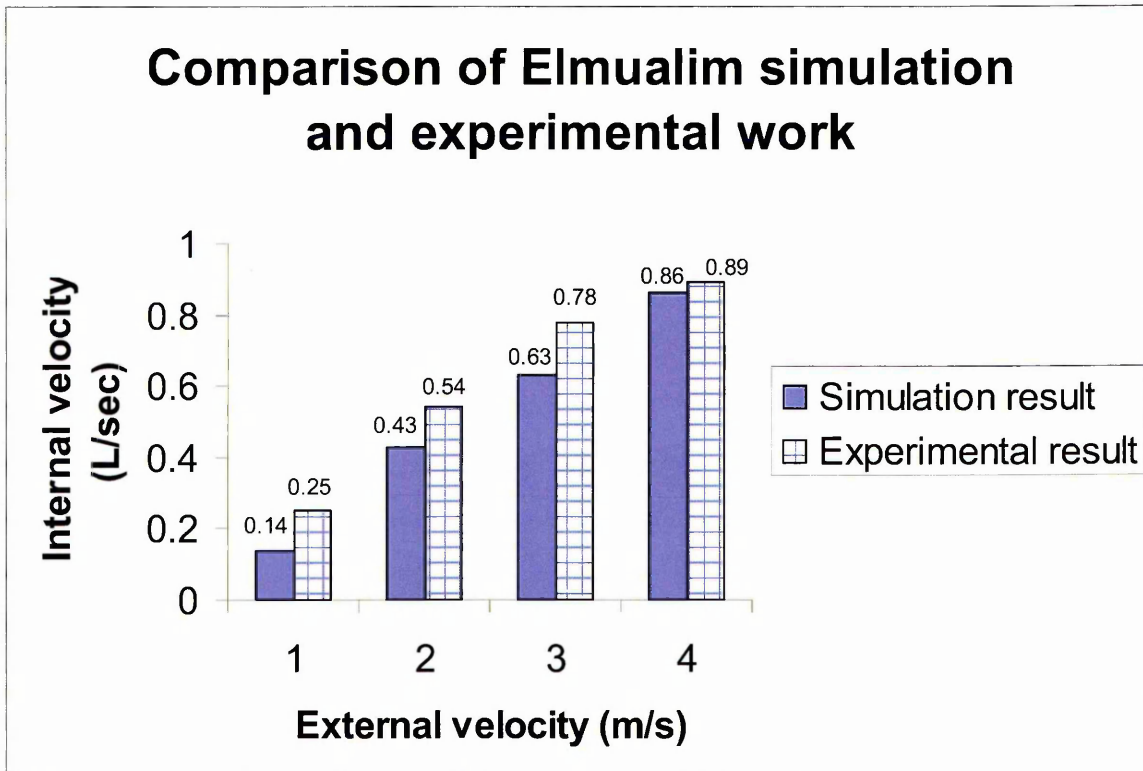
Figure 8-9 Comparison of Elmualim simulation and experimental results

From Figure 8-9, the trend followed the same path as this investigation. In the Elmualim investigation the wind tunnel experimentation over-predicts the result in comparison to the simulation. This is in-line with this investigation where the experimental data over-predicts the simulation. This was due to the CFD model

not incorporating the full physical characteristics of the experimental model. The CFD model did not incorporate an air leakage rate, hence the airtight CFD simulation consistently over-predicts the experimental results.

The Elmualim wind tunnel experiments used a fan to generate the external wind. The location of the fan, without the use of a flow screen, resulted in a non-uniform air velocity profile. The far-field experimentation of this study used a uniform velocity profile, which resulted in a more accurate validation.

The Elmualim investigation explained the CFD error by the lack of geometry in the simulation model. The CFD model omitted the louver, control dampers and diffuser geometry. These problematic areas of geometry were treated as single faces with a discharge coefficient used (described in Chapter 3). This explained the variation between the two sets of error trends.

8.5 Summary

The CFD simulation results have been validated against experimental results. The results have been compared through flow and numerical analysis. The difference range was found to be 0 - 0.08m/s. The accuracy was shown to be independent of external velocity and geometrical variation. The trends were shown to be consistent across all cases. The difference range and trends were evaluated against other published work in the same area. Agreement between the trends of the two studies was demonstrated. The accuracy of this investigation was shown to be within acceptable limits. This chapter has validated the simulation results used in this study.

Chapter 9   Conclusions and recommendations

9.1 Conclusions

The objectives of this study were clearly defined in Chapter 1. This study has achieved its objectives through systematic numerical and experimental investigations. The objectives met are summarised as follows:

- The wind vent is capable of meeting British Standards Institution (1991) guidelines for fresh air delivery. The recommended rates and the wind vents capabilities were fully detailed in Chapter 6.

- The key geometrical components have been identified as the external louver angle, the distance between the louvers and the number of external louvers. An optimised wind vent has been numerically and experimentally investigated. The optimised wind vent has shown a similar, but not increased performance to the benchmark case. This investigation has shown that the optimum geometrical configurations when investigated in conjunction do not provide the optimum performance (Chapters 5 and 7).

- This investigation has used full scale far-field testing to collect high quality data. The data was collected over a sustained period to ensure accuracy and repeatability. This data was analysed and used to validate the CFD simulations. The comparison between the experimental data and simulation work demonstrated good agreement with accuracy within the range of 0 - 0.08m/s (Chapter 8).

- The CFD models were verified as accurate through experimental work and comparison to other published research in this field. The accuracy level was shown to be independent of geometrical variation and external velocities. The range of accuracy in other published research was shown to be in the range of 0 - 0.15m/s. This investigation improved on this

accuracy with a range of 0 – 0.08m/s and validated the use of CFD for the study and analysis of wind vent device (Chapter 9).

This study has shown that the optimised wind vent did not provide the anticipated performance increase. This was due, in part, to the geometrical optimisation process being constrained by consideration of additional criteria some of which were subjective in nature. For example, while the CFD results showed that an increased louver spacing provided an increased velocity, maintaining a smaller spacing was thought advantageous since it was perceived that this would reduce possible rain and noise ingress. Similarly, the use of four louvers as opposed to eight was judged desirable since the associated reduction in materials usage was judged to increase cost efficiency; the CFD results, however, showed that a reduction in louvers marginally decreased the velocity. Another constraint on the geometries considered here related to the materials considered - manufacturing considerations imposed a geometry based on louvers constructed from sheet steel. Thus the optimision of the wind vent undertaken here was, in fact, partially constrained by certain subjective / externally imposed issues rather than being a true collection of peak performance parameters. Notwithstanding this reservation, this work has shown that the wind vent geometry may be carefully selected and matched to meet any user specific requirements or regulations, hence making the device more accessible to the UK market.

Through the course of this investigation, it became apparent that there are other factors which influence the specific performance of a wind vent. These are rain ingress, breakthrough noise and thermal comfort. These factors are addressed

in the further work section of this chapter. To make a complete assessment of the suitability of the wind vent as an eco-technology for the UK these outstanding factors need to be thoroughly investigated.

9.2 Contribution to knowledge

The Literature review (Chapter 2) identified gaps in the knowledge of this subject area. The following summarises the contribution this investigation has made to the knowledge of natural ventilation and in particular wind vent device:

- Extensive far-field experimental data was provided for the wind vent. Systematic geometrical optimisation was experimentally tested. A methodology for comparing averaged far-field results to simulation results has been developed (Chapters 5 and 7).

- CFD models have been validated using far-field testing for the wind vent device. The level of accuracy using far-field testing to validate the CFD models has been demonstrated. A higher level of accuracy has been shown in comparison to other experimental validation techniques (Chapter 8).

- An empirical method for estimating the flow through wind vent device has been developed. The empirical method utilises two coefficients found through experimentation in this investigation (Chapter 3).

- This investigation has shown that the performance of the wind vent can be optimised through geometrical variation. The optimum geometrical

variation was identified for each section of the wind vent in isolation. The optimum geometrical variations when combined do not provide the optimum wind vent performance (Chapters 5 and 7).

- The geometry of the wind vent was systematically examined. The contribution of each section of geometry to the performance of the device has been established. The effect of geometrical variation on the flow and air movement from the wind vent has been demonstrated (Chapters 5 and 7).

- 47 CFD simulation models were built incorporating the full geometry of the wind vent device. A methodology for dynamically modifying fluid volumes has been devised (Chapter 4).

The optimised geometry found through this investigation is subject to patent application number 0809311.4. A copy of the full application is in Appendix C.

9.3 Recommendations for further work

This study highlighted that combined changes to the wind vent geometry did not deliver the anticipated performance increase when compared to isolated geometrical variation. Due to the high level of correlation between the experimental readings and the simulation model, further investigations could be carried out using the CFD model only, with a high degree of confidence. This methodology could therefore be used to investigate combined changes in order to further refine the wind vent. Experimental testing would therefore only be applied to validate and support a CFD optimised wind vent. This would

significantly reduce the experimental costs and workload when pursuing the optimum configuration for any given application.

Three further areas have been identified that require investigation. The three areas are rain ingress, breakthrough noise and thermal comfort. These areas are specialist subjects and require further investigation. This investigation addressed each of these points briefly.

9.3.1 Rain ingress

The wind vent uses external louvers to guide the fresh air into the micro-climate. However, the air may contain water droplets. The mass of these particles may hinder the performance of the wind vent in terms of occupancy comfort. Further investigation is required into the effect of geometrical variation on rain ingress. The effect of climatic conditions on the breakthrough rain needs to be clearly identified. The simulation work needs to be validated using a climatic wind tunnel and far-field testing. This would allow the wind vent to be evaluated against current BSI standards [British Standards Institution (2001)].

9.3.2 Breakthrough noise

A wind vent as opposed to a mechanical ventilation system, introduces an uncontrollable noise factor. Mechanical systems are sealed units with a noise rating according to the manufacturer's specification. The wind vent has no seal and exposes the micro-climate to external noise sources. In addition, the internal noise generated is transmitted to the external macro-climate. Work was carried out on the test wind vent by the BSRIA. Their investigation found that

201

the wind vent increased ambient noise levels by 3.2dB. The full report is in Appendix D. Further investigation is required to evaluate the effect of geometrical variation on the ambient noise level. A purpose built sound chamber is required for this level of investigation. The wind vent needs to be rated according to current BSI standards [British Standards Institution (1997)].

9.3.3 Thermal comfort

The wind vent provides fresh air to the micro-climate. The level of fresh air required is based on legislation and occupants' requirements. The latter relates to occupants' perception of the rate required. Occupants perception of fresh air requirement is based on their personal comfort level. Thermal comfort is a specialised subject area and requires further investigation. There are numerous factors influencing the thermal gain within the micro-climate. The main factors are solar gain, internal equipment levels, number of occupants, materials of construction and activity levels of the occupants. The Chartered Institute of Buildings Service Engineers (CIBSE) has produced many documents on the subject of thermal comfort. CIBSE (2005) evaluates the effect of building materials and equipment on a buildings thermal envelope.

These values need to be incorporated into a simulation model to evaluate the performance of the wind vent. In addition, the buoyancy effect caused by thermal gain needs to be established.

References

AHMED, A.K (2004). Feeling the breeze on Arabian nights. Fluent News, Spring 2004 pg13.

AHMED, R., S. (1998). Computational fluid dynamics. In: HUCHO, W. H. (ed.). *Aerodynamics of road vehicles.* Fourth ed., USA, SAE International, 765-836.

ALLARD, F., GHIAUS, Y. and MANSOURI, Y. (2003). Natural ventilation for health, comfort and energy efficiency. In: *ENCAC-COTEDI 2003,* 5-7 November 2003. 5-25.

ANDERSON, J.D. Jr (2007). *Fundamentals of Aerodynamics.* 4th ed. UK, McGraw-Hill.

Antari. *Smoke generator.*[online] Last accessed 14 th October 2008 at: http://www.antari.com/Company%20Profile/Z-Series%20II/Z-800II/z-800-II.html

ARSEN, T. S. and HEISELBERG, P. Single-sided natural ventilation driven by wind pressure and temperature difference. *Energy and buildings,* In Press, Corrected Proof .

AXLEY, J.W. (2001) Application of natural ventilation for US commercial buildings, NIST, Washington, DC.

AYAD, S. S. (1999). Computational study of natural ventilation. *Journal of wind engineering and industrial aerodynamics,* **82** (1-3), 49-68.

BABUSKA, I., ZIENKIEWICZ, O.C, GAGO, J. and OLIVIERA, E.R.A. (eds) (1986). *Accuracy Estimates and Adaptive Refinements in Finite Element Computations.* Chichester:wiley.

BASKAYA, S. and GILCHRIST, A. (1996). Buoyancy-induced flow through a narrow chamber containing an internal heat source: Comparison of experimental measurements and numerical simulations. *Institution of mechanical engineers,* **210** 489-498.

Battle McCarthy Consulting Engineers (1999). *Wind towers, Detail in Building. Academy Editions.* Great Britain, Wiley.

BBC News Online (2007), Brown outlines `eco town` plan. Last updated 13/5/07 http://news.bbc.co.uk/1/hi/uk_politics/6650639.stm. Last accessed 5/5/08.

BBC News Online (2007), First zero-emission home unveiled, last updated 11/6/07 http://news.bbc.co.uk/1/hi/business/6735715.stm. Last accessed 10/5/08/

BONE, V. (2007), Making your home a green house. BBC News, online http://news.bbc.co.uk/1/hi/uk/6653687.stm. Last accessed 7/5/08.

BRITISH STANDARDS INSTITUTION 1991. BS5925:1991: *Ventilation principles and designing for natural ventilation.* London, British Standards Institution.

BRITISH STANDARDS INSTITUTION 1997. BSEN717-1: *Acoustics-rating of sound insulation in buildings and small building elements.* London, British Standards Institution.

BRITISH STANDARDS INSTITUTION 2001. BSEN13030 2001:*Ventilation for buildings testing of louvers for rain ingress.* London, British Standards Institution.

BUILDING SERVICES RESEARCH INFORMATION ASSOCIATION (2005). Wind-Driven Natural Ventilation Systems, A BSRIA Guide.

BUILDING AND BUILDINGS, ENGLAND AND WALES (2007). *The Energy Performance of Buildings (Certificates and Inspections)(England and Wales)Regulations 2007.* 991 .

CHEN, Q. and SREBRIC, J. (2002A). An example of verification, validation, and reporting of indoor environment CFD analyses (RP-1133). *ASHRAE transactions,* **108** (2), 185-194.

CHEN, Q. and SREBRIC, J. (2002B). A procedure for verification, validation, and reporting of indoor environment CFD analyses. *HVAC&R research,* **8** (2), 201-216.

CHEN, Q. (2004). Using computational tools to factor wind into architectural environment design. *Energy and buildings,* **36** (12), 1197-1209.

CHEN, Q and JIANG, Y. (2003). Buoyancy-driven single sided natural ventilation in buildings with large openings. *International journal of heat and mass transfer,* **46** (6), 973-988.

CHUNG, T. J. (2002). *Computational fluid dynamics.* New York, Cambridge.

CHARTERED INSTITUTE BUILDING SERVICES ENGINEERS (2005). *Natural ventilation in non-domestic buildings* AM10. UK, CIBSE.

CLARK, R. P., BAKER, C. R. and GLOVER, D. D. (1974). Room ventilation by natural convective airflows. *Proceedings of the Institution of mechanical Engineers,* **3** (1), 17-19.

CLOVER, C. (2007). Buildings will have to display energy rating.[online] *The Daily Telegraph,* 30 March 2007. Article from Telegraph Media Group Ltd. Last accessed on 5th July 2007 at:
www.telegraph.co.uk/core/content/buidingsmustdisplayenergyrating.html

CSELE, M. (2004). *Fundamentals of Light Sources and Lasers*, Wiley.

Data Dubai, (2007). Wind tower. [online image]. Last accessed 3 September 2008 at: www.datadubai.com

deGIDDS,W. and PHAFF, H. (1982) Ventilation rates and energy consumption due to open windows:A brief overview of research in The Netherlands, *Air Infiltration Review,* vol 4, pp4-5.

Department for Education and Skills Briefing framework for secondary school projects *Ventilation of school buildings.* Building Bulletin 101, May 2005.

Department for Education and Skills Briefing framework for secondary school projects. Building Bulletin 98, April 2004.

Department of Housing and Development (circa 2002). Buoyancy ventilation [online image]. Last accessed 1st September 2008 at: www.hud.gov/ventilation

DRORI, U. and ZISKIND, G. (2004). Induced ventilation of a one-story real-size building. *Energy and buildings,* **36** 881-890.

Dyer Environmental (circa 2001). Single sided ventilation [online image]. Last accessed 25th October 2008 at: http://www.dyerenvironmental.co.uk/day_ventilation.gif

ELMUALIM, A. A. (2006A). Verification of design calculations of a wind Catcher/Tower natural ventilation system with performance testing in a real building. *International journal of ventilation,* **4** (4), 393-404.

ELMUALIM, A. A. (2006B). Dynamic modelling of a wind catcher/tower turret for natural ventilation. *Building services engineering research and technology,* **27** (3), 165-182.

ELMUALIM, A. A. (2006C). Effect of damper and heat source on wind catcher natural ventilation performance. *Energy and buildings,* **38** (8), 939-948.

ELMUALIM, A. A. (2006D). Failure of a control strategy for a hybrid air conditioning and wind catchers/towers system at bluewater shopping malls in Kent, UK. *Emerald insight,* **24** (11/12), 399-411.

ELMUALIM, A. A. and AWBI, H. B. (2003). Post occupancy evaluation of a building employing windcatchers for summer ventilation [online]. *Emerald,* **21** (13/14), 17/7/07. at: www.emeraldinsight.com.

Energy Comfort 2000 (1998). Natural ventilation and cooling strategies in new office designs. In: Energy Comfort 2000 conference, Netherlands.

Energy report Ltd, (circa 2005). Energy rating system. [online image]. Last accessed 10th August 2008 at: www.energyreport.co.uk/energy_performance_certifivates_commercial.html

Engineering fundamentals (2008), Hot wire anemometers.[online], Last accessed 25/11/08 at: http://www.efunda.com/designstandards/sensors/hot_wires/hot_wires_theory.cfm.

EVOLA, G. and POPOV, V. (2006). Computational analysis of wind driven natural ventilation in buildings. *Energy and buildings,* **38** 491-501.

FLUENT (2006). *Fluent user manual 6.2* [Computer Program]. Adobe.

FLUENT (2006). *Gambit user manual.* [computer program]. Adobe.

GHIAUS, C. and ALLARD, F. (eds.) (2005). *Natural ventilation in the urban environment.* UK, Earthscan.

GRACA, C. G., LINDEN, F. P. and BROOK, M. (2005). Design of the natural ventilation system for the new san diego childrens museum. In: *Ninth International IBPSA Conference,* August 15-18, 2005. Canada, Building Simulation, 349-356.

GRATIA, E., BRUYERE, I. and DE HERDE, A. (2004). How to use natural ventilation to cool narrow office buildings. *Building and environment,* **39** (1), 1157-1170.

HAMDAN, M. H. (1998). A note on computational uncertainty. *Applied mathematics and computation,* **94** (2-3), 285-291.

High performance commercial building facades (circa 2007). Stack ventilation image [online image]. Last accessed on 26th October 2008 at: http://gaia.lbl.gov/hpbf/picture/casestudy/gsw/gswsec.jpg

HILLS, Richard G. (2006). Model validation: Model parameter and measurement uncertainty. *Journal of heat transfer,* **128** (4), 339-351.

HOMES, J. M. and MCGOWAN, S. *Simulation of a Complex Wind and Buoyancy Driven Building.* ARUP, Unpublished .

HOUGHTON, E. L. and CARPENTER, P. W. (2003). *Aerodynamics for engineering students.* 5th ed., Elsevier.

Hugh Pearmen, (circa 2005).Blueswater shopping centre. [online image]. Last accessed 1st September 2008 at: www.hughpearmen.com

HUGHES, B. R. and GHANI, S. A. A. A. (2008). Investigation of a wind vent passive ventilation device against current fresh air supply recommendations. *Energy and buildings,* **40** (9), 1651-1659. .

HUGHES, B. R. and ABDUL GHANI, S. A. A. A.(2009). Numerical investigation into the effect of wind vent dampers on operating conditions. *Building and environment,* **44** (2), 237-248 .

HUNT, G. R. and LINDEN, P. F. (1999). The fluid mechanics of natural ventilation - displacement ventilation by buoyancy - driven flows assisted by wind. *Building and environment,* **34** 707-720.

Iklim Ltd, (circa 2000). Air handling unit. {online image}. Last accessed 5th August 3008 at: http://www.iklimnet.com/expert_hvac/ahu.html

NEWTON, I. (1995). *The principia.* New York, Prometheus Books.

JIANG, Y., ALLOCCA, C. and CHEN, Q. (2004). Validation of CFD simulations for natural ventilation. *International journal of ventilation,* **2** (4), 359-370.

KAMINSKI, D. and JENSEN, M. (2005). *Introduction to thermal and fluid engineering.* Wiley International Edition ed., USA, John Wiley and Sons.

LaCrosse technology. *weather station.* [online] Last accessed 1st October 2008 at: http://www.lacrossetechnology.com/2317/index.php

LAMB, H. H. (1968). Britains climate, its variability and some of its extremes. *Institution of mechanical engineers part 3: Energy,* **182** 80-106.

Laser Quantum. *Laser products.* [online] Last accessed on 17th October 2008 at: http://www.laserquantum.com/lasers/excel.html

LETAN, R., DUBOVSKY, V. and ZISKIND, G. (2003). Passive ventilation and heating by natural convection in a multi-storey building. *Building and environment,* **38** (2), 197-208.

LUI, L. and MAK, C. M. (2007). The assessment of the performance of a windcatcher system using computational fluid dynamics. *Building and environment,* **42** (3), 1135-1141.

LI, Y. and DELSANTE, A. (2001). Natural ventilation induced by combined wind and thermal forces. *Building and environment,* **36** 59-71.

LOMAS, Kevin J. (2007/2). Architectural design of an advanced naturally ventilated building form. *Energy and buildings,* **39** (2), 166-181.

London Metropolitan University (circa 2005). BRE headquarters image [online image]. Last accessed 1st September 2008 at: www.learn.londonmet.ac.uk

MANWELL, J, McGOWAN,J and RODGERS, A (2003). *Wind Energy Explained.* UK, Wiley.

Midtherm engineering. *Wind vent.* [online] Last accessed 1st November 2008 at: http://www.midtherm.co.uk/mideng/index2.htm

MONTAZERI, H. and AZIZIAN, R. Experimental study on natural ventilation performance of one-sided wind catcher. *Building and environment,* In Press, Corrected Proof .

MONGOMERY, D.C. (2005) Design and Analysis of Experiments. 6th ed. UK, Wiley.

ODEN, T. J., WU, W. and LEGAT, V. (1995). An *hp* adaptive strategy for finite element approximations of the Navier-Stokes equations. *International journal for numerical methods in fluids,* **20** 831-851.

ODEN,J.T, STROUBOULIS, T. and DEVLOO, P. (1986). Adaptive finite element methods for the analysis of inviscid compressible flow: I. Fast refinement/unrefinement and moving mesh methods for unstructured meshes. *Comp.Meth.Appl.Mech.Eng.,*59, no.3, 327-62.

PAPAEFTHIMIOU, D. V., KATSANOS, C.O, VRACHOPOULOS, G.M, FILIOS, A.E, KOUKOU M.K and LAYRENTI, F.G (2007). Experimental measurements and theoretical predictions of flowfield and temperature distribution inside a wall solar chimney. *Institution of mechanical engineers:Part C,* **221** 33-41.

PRIYADARSINI, R., CHEONG, K. W. and WONG, N. H. (2004). Enhancement of natural ventilation in high-rise residential buildings using stack system. *Energy and buildings,* **36** 61-71.

PTC (2008). *Pro Engineer wildfire* [computer program]. Adobe

Remco Ltd. (2007). *Products list-fan.* [online]. Last accessed 15 October 2007 at: http:// www.remco.co.uk/products/axial/page39.htm

ROACHE, P. J. (1997). Quantification of uncertainty in computational fluid dynamics. *Annual review of fluid mechanics,* **29** 123-160.

Roger Wilde (circa 2005). Inland revenue building [online image]. Last accessed 25th October 2008 at:
http://www.rogerwilde.com/images/glass_blocks/inland_revenue_nottingham.jp g

SANTAMOURIS, M. and ALLARD, F (2002). *Natural ventilation in buildings A design handbook.* London, James and James.

SHUN, S. and AHMED, A. N. (2007). Utilizing wind and solar energy as power sources for a hybrid building ventilation device. [online]. *Renewable energy,* (In Print),.

SU, Y., RIFFAT, S., LIN, Y.L, KHAN, N. (2008) Experimental and CFD study of ventilation flow rate of a monodraught™ windcatcher. *Energy and buildings,* In Press, Corrected Proof .

Testo Ltd (2008). *Products list-velocity meter.* [online].Last accessed 15 September 2008 at: http://www.testo.co.uk/online/abaxx-?$part=PORTAL.GBR.ProductCategoryDesk&$event=show-from-menu&categoryid=1690454

MEHTA, U.B. (1991) Some aspects of uncertainty in computational fluid dynamics results, J. Fluid Eng.:Trans. ASME 113 538-543.

United States centennial of flight commission (circa 1999). Angle of attack image [online image]. Last accessed on 14th October 2008 at: www.centennialofflight.gov

Urban Living,(circa 2000). Young families tired of surburbia. [online image]. Last accessed 1st September 2008 at: http://www.92101urbanliving.com/blog/uncategorized/young-familiestierd-of-suburbia/117/

YANG, T. (2004). CFD and Field Testing of a Naturally Ventilated Full-Scale Building. PhD, University of Nottingham.

Bibliography

AFSHAR F., ALLAN, C., NORTON, J. and DARDIE, M.R. (1974) Oman: Problems and Potentials of Indigenous Building. *Development Workshop Report. London: Architectural Association School of Architecture*

AYNSLEY, R. (1999). Unresolved issues in natural ventilation for thermal comfort. In: *First International One Day Forum on Natural and Hybrid Ventilation,* September 1999. International Energy Agency,.

BADESCU, V. and SICRE, B. (2003). Renewable energy for passive house heating. part I. building description. *Energy and buildings,* **35** (1), 1077-84.

BADESCU, V. and SICRE, B. (2003). Renewable energy for passive house heating. II. model. *Energy and buildings,* **35** (1), 1085-96.

BADESCU, V. and STAICOVICI, M. D. (2006). Renewable energy for passive house heating: Model of the active solar heating system. *Energy and buildings,* **38** 129-141.

BENHAM, P, CRAWFORD, R and ARMSTRONG, C (1996). *Mechanics of Engineering Materials Second Edition.* UK, Prentice Hall.

BLOCKEN, B. and CARMELIET, J. (2004). Pedestrian wind environment around buildings: Literature review and practical examples. *Journal of thermal envelope and building science,* **28** (2), 107-159.

CHEN, D. Z., LI, Y. and MAHONEY, J. (1999). Modelling ventilation flows using a fine-bubble technique. In: *First International One Day Forum on Natural and Hybrid Ventilation,* September 1999. International Energy Agency,.

Department for environment food and rural affairs [online]. Last accessed on September 8 2007 at: http://www.defra.gov.uk/.

EASTOP, T.D and McCONKEY, A (1993). *Applied Thermodynamics for Engineering Technologists.* UK, Prentice Hall.

FATHY, H. (1986). *Natural energy and vernacular architecture, principles and examples with reference to hot arid climates.* London, University of Chicago press.

HUGHES, T. (2000). *The Finite Element Method: Linear Static and Dynamic Finite Element Analysis.* New York, Dover publications.
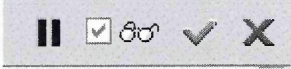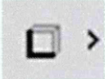
LAI, C.M (2003). Experiments on the ventilation efficiency of turbine ventilators used for building and factory ventilation. *Energy and buildings,* **35** 927-932.

LAMIT, L. (1998). *Basic Pro/ENGINEER in 20 Lessons.* USA PWS publishing.

LIDDAMENT, M.W.(1996). A Guide to Energy Efficient Ventilation. *Air Infiltration and ventilation Centre,* United Kingdom.

SHIGLEY, J, MISCHKE, C and BUDYNAS, R (2003). *Mechanical Engineering Design seventh Edition.* USA, McGraw Hill.

Procedure for Creating Fluid Volume Using Pro-Engineer

1   Create⟶ New part

2   Insert⟶ Share data⟶ Copy Geometry (from desired part)

3   Location ⟶ Default

4   Surface Ref ⟶ Define, Select desired surfaces to be copied*
           * Hold CTRL key for multiple surfaces

5   Edit ⟶ Fill ⟶ Ref ⟶ Define (Pick Top Datum)

6   Create an Entity From Edge, [□ >] button⟶ Single, Hold control button
           and pick the edges*
           * Tilt the Model for better view

7   Press tick

8   Edit ⟶ Fill ⟶ Ref, click on plane, then;
           Insert ⟶ Model Datum ⟶ Plane, Pick top datum and an Edge (Hold
           CTRL)

9   Ok ⟶ Sketch ⟶ [□ >] ⟶ Single, Hold control button and pick the
           edges*
           * Tilt the Model for better view

10   Click Fill (1) ⟶ and an edge ⟶ Edit ⟶ Merge

11   Repeat step 10 for fill (2)

12   Edit ⟶ Solidify (Solidify the two fills)

13   Now check the geometry;

           Click wire Frame on and check the connectivity
           Purple = Not solid
           Yellow = Porous
           White = Solid

14   File ⟶ Save as ⟶ step

Model generation procedure (Pro-engineer Wildfire)

1   Modify original part, then regenerate

2   Re-generate copied part (solidified part)

3   Re-generate assembly (solidified assembly)

4   Save a copy ➡ stp. ➡ name it ➡ ok

Gambit import procedure

1   Import step file ➡ check; Heal, Make tolerant ➡ uncheck; stand alone
     faces, edges

2   Create a volume around assembly by copying vertices, make volume $2m^3$

3   Subtract each assembly volume from each other

4   Split assembly volumes from new surrounding volume

5   Create 2 large faces as cross-dividers

6   Split each assembly volume with cross-divider faces

7   Name each external face of the wind vent volume as "Wall"

CFD governing equations

Mass conservation equations

For the fluid element, (illustrated in Figure A-1), the rate of increase of its mass is

equal to the net rate of flow of mass into the controlled volume.
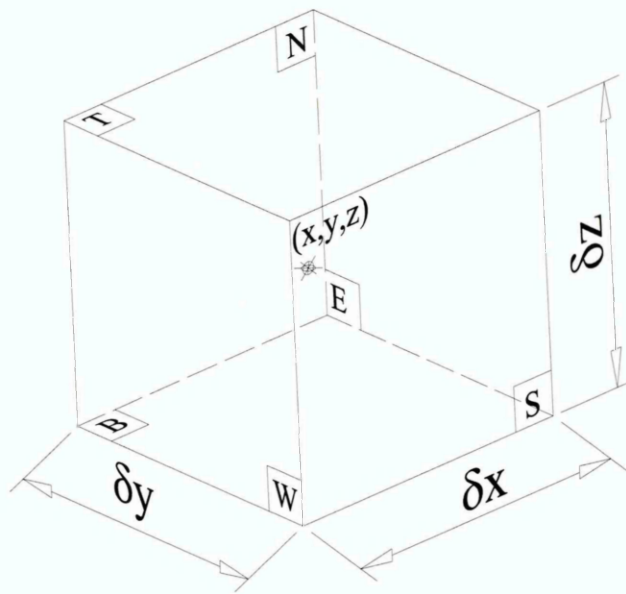
Figure A-1 Fluid element for conservation laws [www.fluent.com]

This yields:

$$\frac{\partial \rho}{\partial t} + \frac{\partial(\rho u)}{\partial x} + \frac{\partial(\rho v)}{\partial y} + \frac{\partial(\rho w)}{\partial z} = 0 \qquad (A\text{-}1)$$

Or written in vector notation:

$$\frac{\partial \rho}{\partial t} + div(\rho \mathbf{u}) = 0 \qquad (A\text{-}2)$$

Equation A-2 is the unsteady, three-dimensional mass conservation, (or continuity equation) at a point in a compressible fluid. For an incompressible fluid, the density ρ is constant and equation A-2 becomes:

$$div\mathbf{u} = 0 \qquad (A\text{-}3)$$

Or in longhand notation:

$$\frac{\partial u}{\partial x} + \frac{\partial v}{\partial y} + \frac{\partial w}{\partial z} = 0 \qquad \text{(A-4)}$$

1.1.1 Momentum equations

Newton's second law states that the rate of change of momentum of a fluid particle equals the sum of the forces on the particle. The rates of increase of x-, y- and z-momentum per unit volume of a fluid particle are given by:

$$\rho\frac{Du}{Dt} \qquad\qquad \rho\frac{Dv}{Dt} \qquad\qquad \rho\frac{Dw}{Dt} \qquad\qquad \text{(A-5)}$$

There are two types of forces on fluid particles:

- Surface forces: pressure forces and viscous forces.

- Body forces: gravity force, centrifugal force, Coriolis force and electromagnetic force.

The body forces overall effect is defined by the source S_{Mx}, S_{My} and S_{Mz} of the x-component, y-component and z-component of the momentum equation.

The x-component of the momentum equation is given by:

$$\rho\frac{Du}{Dt} = \frac{\partial(-p + \tau_{xx})}{\partial x} + \frac{\partial \tau_{yx}}{\partial y} + \frac{\partial \tau_{zx}}{\partial z} + S_{Mx} \qquad \text{(A-6)}$$

The y- component of the momentum equation is given by:

$$\rho\frac{Dv}{Dt} = \frac{\partial \tau_{xy}}{\partial x} + \frac{\partial(-p + \tau_{yy})}{\partial y} + + \frac{\partial \tau_{zy}}{\partial z} + S_{My} \qquad \text{(A-7)}$$

The z-component of the momentum equation is given by:

$$\rho \frac{Dw}{Dt} = \frac{\partial \tau_{xz}}{\partial x} + \frac{\partial \tau_{yz}}{\partial y} + \frac{\partial(-p + \tau_{zz})}{\partial z} + S_{Mz}$$
(A-8)

1.1.2 Navier-Stokes equations for a Newtonian fluid

The governing equations contain - as further unknowns - the viscous stress component τ_{ij}. Useful forms of the conservation equations for fluid flows are obtained by introducing a suitable model for the viscous stress τ_{ij}. In many fluid flows, the viscous stresses can be expressed as functions of the local deformation rate (strain rate). In three-dimensional flows, the local rate of the deformation is composed of the linear deformation rate and the volumetric deformation rate. There are three linear elongating deformation components:

$$e_{xx} = \frac{\partial u}{\partial x} \qquad e_{yy} = \frac{\partial v}{\partial y} \qquad e_{zz} = \frac{\partial w}{\partial z}$$
(A-9)

There are also six shearing linear deformation components:

$$e_{xy} = e_{yx} = \frac{1}{2}\left(\frac{\partial u}{\partial y} + \frac{\partial v}{\partial x}\right) \quad e_{xz} = e_{zx} = \frac{1}{2}\left(\frac{\partial u}{\partial z} + \frac{\partial w}{\partial x}\right) \quad e_{yz} = e_{zy} = \frac{1}{2}\left(\frac{\partial v}{\partial z} + \frac{\partial w}{\partial y}\right)$$
(A-10)

The volumetric deformation is given by:

$$\frac{\partial u}{\partial x} + \frac{\partial v}{\partial y} + \frac{\partial w}{\partial z} = div\mathbf{u}$$
(A-11)

Substitution of these stress equations into the momentum equations (A-6, A-7, A-8) yields the so-called "Navier-Stokes" (NS) equations, named after the two 19th century scientists who derived them independently.

The x-component of NS equation is given by:

$$\rho \frac{Du}{Dt} = -\frac{\partial p}{\partial x} + div\,(\mu gradu\,) + S_{Mx}$$

(A-12)

The y-component of NS equation is given by:

$$\rho \frac{Dv}{Dt} = -\frac{\partial p}{\partial y} + div\,(\mu gradv\,) + S_{My}$$

(A-13)

The z-component of NS equation is given by:

$$\rho \frac{Dw}{Dt} = -\frac{\partial p}{\partial z} + div\,(\mu gradw\,) + S_{Mz}$$

(A-14)

1.1.3 k-ε transport equation

The two-equation k-ε model is the default turbulence model in FLUENT and it was used to carry out the computational work reported in this study. The k-ε model focuses on the mechanisms that affect the turbulent kinetic energy. In this model, the eddy viscosity is computed from additional semi-empirical transport equations (partial differential equations) for the velocity and length scales of turbulence. The turbulent kinetic energy (k) is used as: a form of the velocity scale (ϑ), and its dissipation rate (ε) as a length scale (l):

$$\vartheta = k^{\frac{1}{2}} \qquad\qquad l = \frac{k^{\frac{3}{2}}}{\varepsilon}$$

(A-15)

The eddy viscosity is specified as follows:

$$\mu_t = C_\mu \rho \vartheta\, l = \rho C_\mu \frac{k^2}{\varepsilon}$$

(A-16)

Where C_μ is a dimensionless constant. The standard model uses the following transport equations for k and ε:

$$\frac{\partial(\rho k)}{\partial t} + div(\rho k \mathbf{U}) = div\left[\frac{\mu_t}{\sigma_k} grad k\right] + 2\mu_t E_{ij}.E_{ij} - \rho\varepsilon \tag{A-17}$$

$$\frac{\partial(\rho\varepsilon)}{\partial t} + div(\rho\varepsilon \mathbf{U}) = div\left[\frac{\mu_t}{\sigma_\varepsilon} grad\varepsilon\right] + C_{1\varepsilon}\frac{\varepsilon}{k}2\mu_t E_{ij}.E_{ij} - C_{2\varepsilon}\rho\frac{\varepsilon^2}{k} \tag{A-18}$$

The equations contain five adjustable constants C_μ, σ_k, σ_ε, $C_{1\varepsilon}$ and $C_{2\varepsilon}$. The default FLUENT standard k-ε model uses values for the constants that are arrived by comprehensive data fitting for a wide range of turbulence flows, [Fluent, 2006]:

$$C_\mu = 0.09 \qquad \sigma_k = 1.00 \qquad \sigma_\varepsilon = 1.30 \qquad C_{1\varepsilon} = 1.44 \qquad C_{2\varepsilon} = 1.92 \tag{A-19}$$

No attempt was made in this study to modify these coefficients. Therefore, all the computational work carried out and reported in this study is based on the previous coefficient values.

SIMPLE ALGORIYTHM

Using the continuity equation to correct the pressure values obtained from the momentum equations, it is possible to devise a stable model when used on a double staggered grid; one for velocity substitutions and another for pressure:

$$p = p^* + p' \tag{A-20}$$

Where p' is the previous pressure value and p* is the new pressure suggested at the node considered:

$$u = u^* + u' \qquad v = v^* + v' \qquad w = w^* + w' \qquad \text{(A-21)}$$

A number of substitutions are carried out using the discretised governing equations, giving new values for the pressure (p*). Under-relaxation is used to dampen the excessive shoots in the pressure values calculated (to deter divergence). The new (usable) pressure value becomes:

$$p^{new} = p^* + \alpha_p p' \qquad \text{(A-22)}$$

Where α_p is; the pressure under-relaxation factor, (where $0 < \alpha_p < 1$). The velocities components are also under-relaxed. The iteratively improved velocity components u^{new}, v^{new} and w^{new} are obtained from:

$$u^{new} = \alpha_u u + (1 - \alpha_u)u^{(n-1)} \qquad \text{(A-23)}$$

$$v^{new} = \alpha_v v + (1 - \alpha_v)v^{(n-1)} \qquad \text{(A-24)}$$

$$w^{new} = \alpha_w w + (1 - \alpha_w)w^{(n-1)} \qquad \text{(A-25)}$$

Where: α_u, α_v and α_w are; the u- v- and w-velocity under-relaxation factors with values between 0 and 1. Therefore u, v and w are the corrected velocity components without relaxation, and, $u^{(n-1)}$, $v^{(n-1)}$ and $w^{(n-1)}$, represents their values obtained in the previous iteration. The choice of under-relaxation factors α is essential for cost effective simulations. A large value of α leads to oscillatory or even divergent iterative solution; and a value which is too small will cause extremely slow convergence.

INTERNAL ADJUSTABLE LID
TO ACT AS FALSE TOP

INTERCHANGEABLE
CROSS DIVIDERS

REMOVABLE FIXED BANK OF BLADES
TO SLIDE OVER INTERNAL FRAME
TO BE SUPPLIED IN 2 No BLADE ANGLES
45 AND 35 DEGREE.
BANKS OF BLADES TO BE SUPPLIED IN PITCHES
OF 10MM, 20MM, 30MM AND 60MM INCREMENTS.

INTERCHANGEABLE
BLANKING PLATES

35 DEG BLADES @ 10MM PITCH

35 DEG BLADES TO BE SUPPLIED
IN BANKS OF 8 (MULTIPLES OF 2) FOR
INDIVIDUAL TESTS. CROSS DIVIDER SECTIONS
AND BLANKING PLATES TO BE SUPPLIED
TO SUIT No OF BLADE PITCHES TO BE TESTED

REMOVABLE TOP SECTION

45 DEG BLADES @ 60MM PITCH

45 DEG BLADES TO BE SUPPLIED
IN BANKS OF 2,4,6 AND 8 FOR
INDIVIDUAL TESTS. CROSS DIVIDER SECTIONS
AND BLANKING PLATES TO BE SUPPLIED
TO SUIT No OF BLADES TO BE TESTED

rocon
foam products ltd

CLASS 'O' FOAM DATA SHEET

CAA Spec. 8/FAA 25   CHAR 1-3

Random Incidence Sound Absorption Coefficient – Foam (BS3638 1987)

Frequency Hz	125	250	500	1K	2K	4K	NRC
12mm Thick	0.08	0.14	0.22	0.32	0.40	0.53	0.27
25mm Thick	0.16	0.29	0.42	0.56	0.69	0.76	0.49
50mm Thick	0.23	0.49	0.70	0.88	0.92	1.02	0.75

Noise Reduction Coefficient (arithmetic average of values at 250, 500, 1K and 2K HZ)

Additional Options:

Available with self adhesive backing and die cut to drawing.

A range of facings are also available for laminating to the foam including a class 'O' film.

Rocon Foam Products limited reserves the right to update information regarding class 'O' foam without prior notice. Every effort will be made to inform all customers of any changes to specifications.

MARCH 2007.

CLASS 'O' FOAM DATA SHEET

Class 'O' acoustic foam can be used in preference to Mineral Wool/Glass Fibre insulation materials, as it will not shed fibres or release particulate matter, yet still offers comparable acoustic perfrormance and the necessary fire specification performance.

Physical Properties – Foam

Density in Kg/m^3 to BS4443	80 (min) to 100
Thermal Conductive W/MK	0.048
Working Temperature Range	-30' C / + 100' C
Classification to BS3379	A
Hardness (Newtons) to BS4443	40-180
Tensile Strength Kpa Min BS4443	70-75
Elongation at Break % Min BS4443	150
Compression Set % Max BS4443	12-13%
Standard Colour	Black (Grey & White available)

Typical Flammability Properties – Foam;

Building Regulations 1985 Para A8 (b) Doc B		Class 'O'
BS476 Part 6	Fire propagation index (1)	8.5
	Sub index 1.1	2.7
	Sub index 1.2	4.5
	Sub index 1.3	1.3

BS476 Part 7	Class '1'
BS476 Part 5	Non Ignition
BS7175 Section 2 No;-7 CRIB	Pass
BS6853 Part B 5.3	< 5
BS5652 Part 2 No;-5 CRIB	Pass
FTS 15 4 X No;-7 CRIBS (For material thickness >27mm	Pass
FMVSS302 Self Extinguishing	Pass
Oxygen Index L01	50
Smoke Maximum Obscuration % BS511	60

ISO 9001
REGISTERED FIRM

Unit 14, Shrub Hill Industrial Estate, Tolladine Road, WORCESTER WR4 9EL
Tel: (01905) 26616 or 26498 Fax:(01905) 612319
V.A.T No: 670483722   Co. Reg. No: 3016977

2

Product Data Sheet

Product:	**WINDVENT TERMINAL**	
Material:	*Terminal:*	Aluminum (2mm thick) fully welded outer casing with bird mesh on inlet louvers. Construction is from fully welded corrosion resistant aluminium, fitted with internal acoustic material.
	External Finish:	Powder Coated to any RAL colour.
	Internal:	Bird mesh/cross dividers/acoustics
Application:	The terminal can be used in a number of ways as detailed below: • Natural Ventilation System • Passive Stack System • As an architecturally attractive way to disperse stale air from within the building using stack effect. • Vertical Balanced Flues	
Sizes:	400mm to 3000mm Square or Round (Dia.) For pitched or flat roof heights from 1m to 3m. Large custom built terminal work can be undertaken tailor-made to the customers particular requirements.	
Installation:	The terminal is designed to mount on either a builders kerb or a factory made upstand.	
Guarantee:	Guaranteed against material and workmanship defects for 12 months.	
Quality:	Manufactured to ISO 9001 (Certificate No. 5458)	
Product Picture:		
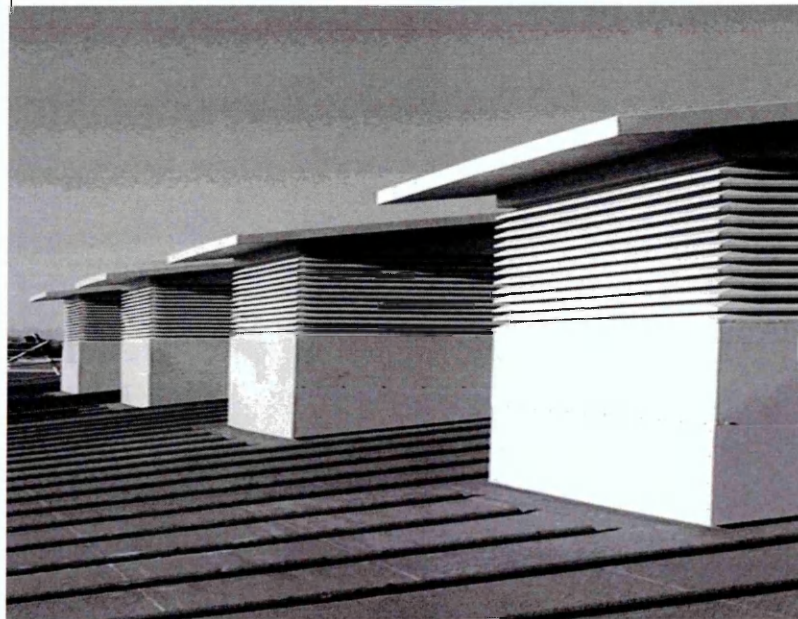
WINDVENT SYSTEMS

Function

The Midtherm "Windvent" is a natural ventilation system operating on established aerodynamic principles. As air flows around the terminal itself, positive and negative pressure areas are generated. On the positive side air enters the louvres of the terminal and is directed down through the internal vanes into the room below. The negative pressure on the leeward side of the terminal, induces air to leave the louvres, and stale air from the room below rises and is expelled from the terminal. This process is aided by stack effect, i.e. as cool air enters the windward side of the unit it descends into the room below, and the warm stale air rises in the ducts facing the leeward side.

Terminal Specification

The units are constructed from fully welded corrosion resistant type 1050 AH14 pure aluminium of 2-3mm thickness and highly resistant to weathering and to chemical attack.
Internal cross dividers are also manufactured from corrosion resistant aluminium. The units are manufactured in accordance with BS EN ISO 9001 and to suit most architectural requirements. Airways are protected by incorporating anti-bird mesh. The units are powder coated to any of the extensive RAL range or clear lacquered.

Main Body size: 800mm x 800mm reducing to 600mm x 600mm
Overall Height: 1050mm
Height above roof: 620mm

Insulation/acoustics

Class 'O' type 12.5mmTHK acoustic foam is used in preference to mineral wool/glass fibre insulation materials, as it will not shed fibres or release particulate matter, yet offers comparable acoustic performance and the necessary fire performance. Data sheets are available and can be issued on request.

Windvent Controls

The 24v Siemans Actuator is incorporated into a multi blade ES Aeroseal damper controlled by room temperature sensor.
The fully programmable main control unit(s) can incorporate many bolt on facilities, however these particular control panels selected conform to your client specification with night time cooling facility, Including heating system relay/interlock and fire alarm relay.

Features:

- Room temperature sensor with inbuilt set-point and display
- Master system override selector (open/auto/close)
- Drive up to 6 dampers from 0-10v modulating output
- Optional 7 day time-switch
- Fire alarm relay/interlock and heating system relay.

Optional Features:

- Room humidity sensor
- Room air quality sensor
- Rain (precipitation) sensor and powder supply
- Wind speed sensor
- Room override unit
- Linear actuators (24vac open/close – 150Nm stroke 100/200/300mm)
- Remote control

Windvent Dampers

Series Aeroseal for system air balancing and shut off having aerodynamic double skin type 1.4016 (430) ferritic stainless steel 50mm wide x 0.4mm thick blades with synthetic trailing edge blade seals and stainless steel side seals.
Housed within a galvanised casing being suitable for system with a temperature range of 0 ^{0}C through to +70 ^{0}C.

Optional blade construction type 1.4404 (316) Austenitic stainless steel can be offer on request for additional cost.

Fire Rated Duct

The fireproof product has been tested and assessed by BRE LPC in accordance with BS 476-24 'Fire tests on building material structures – methods for determination of the fire resistance of ventilation duct'.
The 2-hour fire resistance is for stability, integrity and insulation in equal measure being: stability 120 mins, integrity 120 mins and insulation 120 mins.

The fire proof slabs are fixed to the galvanised (vertical) ductwork by means of welded pins. Theses are generally spaced at 350mm maximum centres along the length of the duct and at 500mm maximum centres across the width and depth. Pins are required on all four sides of the vertical duct. When faced with difficult site circumstances fire proof slab materials can be bonded using glue.

30 May 2008

By email attachment and post

Mr Graham Hulse
Sheffield Hallam University
Enterprise Centre
City Campus
Sheffield
S1 1WB

Your ref: TGH100596
Our ref: MMN/JAH/P220064

Dear Graham

Re: **UK Patent Application No. 0809311.4**
        Building Ventilator
        In the Name of Sheffield Hallam University
        Inventors: Ben Hughes and Saudi Ghani

Following the filing of the above application I enclose a copy of the official filing receipt and specification as filed. The application has been given the number 0809311.4 and a filing date of 16 May 2008.

I confirm having filed the request for combined search and examination at the UK IP Office. As indicated previously, the application was filed to be directed to three separate inventive concepts namely i) the angle of inclination of the blades, ii) the distance between the blades and iii) the position of the optional fan. I confirm having filed three separate search requests to ensure all claims of the application are searched. In this case we anticipate the results of the search and the examination report will issue in around 4 to 6 months time. I will report to you with this in due course.

Please note, the application was filed with informal drawings. Please provide your instructions for me to proceed with obtaining formal drawings to replace those currently on file.

A description of *either* any feature relating to the invention which is not described specifically in the application (*eg* any modification, additional detail or example) *or* a specific combination of technical features which is not described specifically in the application (*eg* in the context of a preferred embodiment) may need to be incorporated into a supplementary patent application. Failure to file the supplementary patent application *before* the feature or combination of features is disclosed to a third party may make it impossible to secure valid patent protection for an invention relying on or incorporating the feature or combination of features. Failure to file the supplementary patent application on or before 16 May 2009 would make it impossible to retain the benefit of the UK filing date.

If you are interested in seeking protection for your invention outside the UK, a patent application in the country of interest must be filed on or before 16 May 2009 *if* the benefit of the UK filing date is to be retained. Failure to file an application on or before that date would make it impossible to retain the benefit of the UK filing date and might make it impossible to secure patent protection in that country at all. A number of routes exist for filing patent applications outside the UK and I would be happy to discuss them with you.

Please do not hesitate to contact me if you have any questions or require any further information. In the meantime, I enclose our invoice relating to fees outstanding on this file.

Kind regards.

Yours sincerely

Martin Neilson
for Urquhart-Dykes & Lord LLP

cc: Ben Hughes

Cardiff Road
Newport
South Wales
NP10 8QQ
United Kingdom

Telephone +44 (0) 8459 500505
Minicom +44 (0) 8459 222250
Fax   +44 (0) 1633 817777

DX 722540/41 Cleppa Park 3

Website www.ipo.gov.uk

Urquhart-Dykes & Lord LLP
Tower North Central
Merrion Way
LEEDS
UK
LS2 8PA

RECEIVED

2 6 MAY 2008

URQUHART-DYKES & LORD LLP
LEEDS

DIARY ENTRY : 22-May-2008

Date 16/05/08⁹   Initials ORB.
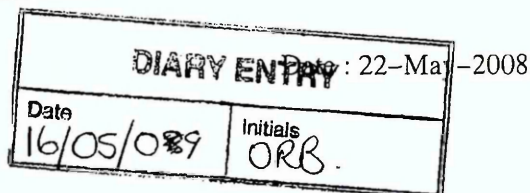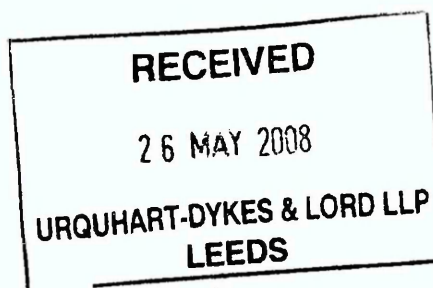
Your Ref. : MMN/JAH/P220064

PATENT APPLICATION NUMBER 0809311.4

We have received your request for grant of a patent and recorded its details as follows :

Filing Date*	:	16–May–2008
Earliest Priority Date	:	
Applicant(s)/contact point	:	Sheffield Hallam University

Application Fee Paid	:	Yes	
Description (number of pages)	:	16	
	:		
Claims (number of pages)	:	5	
Drawings(number of pages)	:	13	
Abstract (number of pages)	:	1	
Statement of inventorship (Form 7)	:	No	Must be submitted by 16–Sep–2009
Request for search (Form 9A)	:	Yes	
Request for examination (Form 10)	:	Yes	
Priority documents	:	None	
Other attachments received	:		

Please quote the application number in the heading whenever you contact us about this application.

If you have any queries about the accuracy of this receipt please phone the Document Reception Manager on +44 (0) 1633 814570. For all other queries, please phone our Central Enquiry Unit on 08459 500 505 if you are calling from the UK, or +44 1633 813930 if you are calling from outside the UK. Or email enquiries@ipo.gov.uk.

* This filing date is provisional. We may have to change it if we find during preliminary examination that the application does not satisfy section 15(1) of the Patents Act 1977 or if we re–date the application to the date when we get any later filed documents.

The notes shown below explain the time limits by which any requirements need to be met. However if you do not have a representative acting for you, we will send you a letter within the next four weeks to explain the next steps in the application process.

a. *If the application fee has not been paid, or if any of the claims, abstract and search request have not been filed, the time available for filing them is:-*

(i) if there is no earliest priority date shown on this receipt, you have until 12 months from the filing date quoted overleaf.

(ii) if an earliest priority date is shown on this receipt, you have until 12 months from that date *or* 2 months from the filing date quoted overleaf, whichever is later.

b. *Whenever the date of filing relies on a reference to an earlier application, the respective times available for filing the description and the certified copy of the earlier application on which the date of filing relies (accompanied by a translation into English, if the copy of the earlier application is not in English) are:-*

(i) for the description, the same time as given in Note a. above.

(ii) for the certified copy of the application on which the date of filing relies, you have until 4 months from the filing date quoted overleaf.

c. *A Patents Form 7 (Statement of inventorship and of right to grant of a patent) is required if any applicant named is not an inventor **or** there is an inventor who is not named as an applicant **or** any named applicant is a corporate body. Where a form 7 is required, the time available for filing is:-*

(i) if there is no earliest priority date shown on this receipt, you have until 16 months from the filing date quoted overleaf.

(ii) if an earliest priority date is shown on this receipt, you have until 16 months from that date.

d. In certain circumstances you may be able to request the extension of a particular time limit, for instance by paying a late fee. Further information can be obtained from our Central Enquiry Unit, whose contact details are shown overleaf.

BUILDING VENTILATOR

The present invention relates to a ventilator for a building, and in particular although not exclusively, to a passive and passive assisted ventilation stack.

5

Most modern buildings require a ventilator system to provide a supply of fresh air to the building interior.   Also, ventilation systems provide a means of regulating the internal temperature of a building where occupants, equipment and solar heat contribute to the internal temperature of the building and if unregulated would lead to overheating.

10

Legislation in most jurisdictions establish minimum fresh air requirements for the interior of buildings depending upon intended usage and occupancy levels.

Typically, most commercial large buildings utilise electricity driven air conditioning
15   systems that both circulate air within the building and provide internal air temperature control.

In response to climate change, attributed largely to the amount of greenhouse gas emissions globally, national and international legislation has imposed emission limitations
20   in an attempt to combat global warming.   Accordingly, certain jurisdictions such as the United Kingdom have introduced regulations on the energy performance of buildings. All buildings in the United Kingdom will eventually have an energy rating including an annual carbon emission rating.

25   This increased awareness of the carbon footprint of buildings, has led to the re-examination of the energy performance and suitability of all working systems associated with the building that consume energy.   Air conditioning is one of the greatest energy consumers in buildings, and therefore provides potential to make a dramatic impact on the building's overall energy rating.   Therefore a ventilation system that requires no energy input is an
30   attractive option for modern construction.

There are two main categories for ventilation strategies, namely mechanical and natural. Mechanical ventilation is the most commonly used form as it offers on demand and controllable delivery rates. Examples of mechanical ventilation include convention air conditioning that utilises refrigeration and a fan to drive airflow circulation around the

5   system and the interior of the building.

Natural ventilation relies on the external wind conditions to deliver the required fresh air supply. A natural ventilation stack device sits at the top of the building or room and acts as both an inlet and extract. As warm air rises and exits the room via the stack, a negative

10   pressure is created in the room which acts to draw-in an external fresh air supply. The flow of air through the device is further assisted by the windward and leeward pressures exerted on it by the external wind speed. The rate at which the flow is delivered to the receiving room is controlled by mechanical dampers and a static ceiling diffuser.

15   Natural ventilation systems may be further categorised into two groups, namely passive and active. A passive stack applies no mechanical force to induce the flow through the device. An active stack utilises a mechanical force to create or direct the flow through the system. The active stack ensures the required air supply rates will be achieved. However, this stack does not offer the level of energy consumption savings of the passive

20   system.

GB 2432207 discloses an active stack ventilation arrangement that utilises a fan positioned at the bottom of the ventilator to draw air into the building interior.

25   Whilst advantageous over conventional air conditioning systems the inventors have identified a number of disadvantages with existing natural ventilation assemblies of the kind identified above.

Accordingly, the present invention provides a natural ventilator configured to supply fresh

30   air into the interior of a building and importantly to allow stale air to exit the building interior without requiring mechanical or electrically driven components.

A hybrid device which offers the mechanical assistance of an active stack without compromising the energy consumption level of a passive stack is provided and is referred to as a passive-assisted stack. This hybrid device utilises a fan positioned within the natural ventilator, the fan being operable only when required to assist the flow of air

5   between the building exterior and interior via the ventilator.

According to a first aspect of the present invention there is provided a building ventilator comprising: a frame mountable at an opening in a roof of a building, the frame defining a duct to convey air between an exterior and an interior of the building; a plurality of vent

10   blades mountable at an external facing region of the frame such that the blades are mounted at the exterior of the building and are stacked above one another to form a louver, each blade having a leading edge to be external facing relative to the duct and a trailing edge to be internal facing relative to the duct; wherein each blade between the leading edge and trailing edge is inclined relative to a horizontal plane at an angle in the range 30 to 40°.

15

The inventors have discovered that by altering the angle of inclination of the individual blades of the louver, the velocity and pressure performance and importantly the rate of air flow into and out of the building interior is improved and optimised with regard to the circulation of clean air from the building's exterior to its interior.

20

Preferably, each blade is inclined relative to the horizontal at an angle in the range 32 to 38°. More preferably, this angle of inclination is within the range 34 to 36° and optimally is 35°.

25   Optionally, the ventilator comprises internal walls extending in the longitudinal direction between the external and internal facing ends of the frame to partition the air flow duct and to guide air flow through the ventilator.

The ventilator frame and louver may comprise any shape and configuration to suit the

30   requirements of the building. For example, the cross sectional profile, in the horizontal plane, of the frame and louver sections of the ventilator may define a circle, oval, square or rectangle. Preferably, the frame is cuboid in particular rectangular or square cuboid

comprising four walls being open at a top and adjacent bottom face. The frame is arranged in the ventilator with the top face being external facing and the bottom face being interior facing.

5   Preferably, the ventilator blades are joined at each end to adjacent blades, in the same plane, to define the edges of a rectangle and/or square. This quad blade structure may be formed as a modular arrangement or as a unitary blade arrangement in which the four blades are inclined upwardly towards a central plane within the square or rectangle. The quad blade arrangement may be mounted at the exterior facing top face of the cuboidal

10   frame above its four walls to define a louver having four sides comprising a plurality of blades arranged on top of one another extending over each face.

Optionally, the ventilator may comprise a cover member to sit above the uppermost blade and block the exterior facing end of the duct defined by the upper region of the louver.

15

Optionally, each blade may comprise a flange positioned at the leading and trailing edge and projecting transverse to the blade. With the blades aligned in position to be inclined at an angle 30 to 40° relative to a horizontal plane, each flange may extend substantially vertically.

20

Preferably, the ventilator comprises a stack of four to six blades arranged on top of one another, the blades comprising a single blade or quadrant of blades having four sides in the same plane. Preferably, the ventilator comprises four blades and in particular four quadrant blade sets. As will be appreciated, the ventilator may comprise any number of

25   vent blades to suit the requirements of the building with regard to fresh are delivery rates and wind noise.

According to a second aspect of the present invention there is provided a building ventilator comprising: a frame mountable at an opening in a roof of a building, the frame

30   defining a duct to convey air between an exterior and an interior of the building; a plurality of vent blades mountable at an external facing region of the frame such that the blades are mounted at the exterior of the building and are stacked above one another to form a louver,

each blade having a leading edge to be external facing relative to the duct and a trailing edge to be internal facing relative to the duct; wherein the distance in the vertical direction between adjacent blades at the their respective leading edge regions is in the range 25 to 35 mm.

5

Preferably, the vertical distance between adjacent blades is 27 to 33 mm. More preferably, the vertical distance between adjacent blades is 30 mm.

According to a third aspect of the present invention there is provided a building ventilator

10   comprising: a frame mountable at an opening in a roof of a building, the frame having an exterior facing end and an interior facing end to define a duct there between to convey air between an exterior and an interior of the building; a plurality of vent blades mountable at the exterior facing end of the frame, the blades mounted above one another to form a louver; and a fan mounted within the louver region of the device defined by the stack of

15   blades substantially between a lowermost blade and an uppermost blade in the vertical direction.

Preferably, the fan is mounted within the louver region of the device towards the blade positioned furthest from the external facing end of the frame in the vertical direction.

20   More preferably, the fan is mounted within the louver region of the device substantially in the same horizontal plane as the blade positioned furthest from the external facing end of the frame in the vertical direction. The fan may be mounted centrally within the louver region of the device in the horizontal plane.

25   According to a specific implementation, the ventilator is devoid of internal partition walls within the duct extending in the vertical direction between the external and internal facing ends.

Preferably, the ventilator comprises control means to provide manual and/or automatic

30   control of the fan. The ventilator may also comprise an electric motor configured to drive the fan with the control means coupled to the electric motor. Optionally, the control

means may be coupled to a suitable wind gauge and is operative in response to the wind speed detected by the wind gauge.

A specific implementation of the present invention will now be described, by way of
5   example only, and with reference to the accompanying drawings in which:

Figure 1 is a perspective view of a building comprising a ventilator according to a specific implementation of the present invention;

Figure 2 is a more detailed illustration of the ventilator of the present invention as detailed in Figure 1;

10   Figure 3 is a cross sectional side elevation view of the ventilator of Figure 2;

Figure 4a is a side elevation view a vent blade that defines the louver of Figure 3;

Figure 4b is a perspective view of the vent blade of Figure 4a;

Figure 4c is a cross sectional side elevation view of two adjacent vent blades positioned on top of one another in the vertical direction defining a portion of the louver of
15   Figure 3;

Figure 5 is a side perspective view of the ventilator of Figure 3;

Figure 6 illustrates a perspective view of the ventilator of Figure 3 further comprising a fan assembly located within the louver section of the ventilator of Figure 5;

Figure 7 illustrates the different regions and directions of pressure and velocity
20   measurement through the ventilator of Figure 3;

Figure 8 is a graph of pressure versus blade angle at various regions of the ventilator of Figure 7;

Figure 9 is a graph of velocity versus blade angle at various regions of the ventilator of Figure 7;

25   Figure 10 is a graph of pressure versus velocity in the vertical direction through the centre of the ventilator of Figure 3;

Figure 11 is a graph illustrating the overall performance of blade angle on the air flow rate through the ventilator of Figure 7;

Figure 12 illustrates the affect on the air flow path through the ventilator of Figure
30   3 by a fan positioned at an upper region of the ventilator;

Figure 13 illustrates the affect on the air flow path through the ventilator of Figure 3 by a fan positioned at a middle region of the ventilator;

Figure 14 illustrates the affect on the air flow path through the ventilator of Figure 3 by a fan positioned at a bottom region of the ventilator;

Figure 15 illustrates the fresh air delivery rates provided by the ventilator with the fan at the top, middle and bottom positions as illustrated in Figures 12 to 14.

5   Figure 16 is a graph of velocity/pressure against a distance of separation of the vent blades for the ventilator of Figure 3.

A natural ventilator provided by the inventors is optimised to supply fresh air into the interior of a building whilst minimising energy consumption.   The present invention

10   provides both a passive and a passive-active system configured to maintain airflow rates into the building interior in the event of reduced wind speed at the exterior of the building.

Figure 1 illustrates a building 100 comprising roof 101 separating an exterior region 103 from the building interior 104.   A ventilator 102 is positioned at an opening 105 formed in

15   the roof 101.

Figure 2 illustrates ventilator 102 comprising a louver region 201 comprising a plurality of vent blades 202 stacked on top of one another in the vertical direction.   The vent blades are positioned on top of and extend from a frame 200 mounted in the opening 105 formed

20   within roof 101.   A cover 204 is positioned at an uppermost region of ventilator 102 to cover the internal duct formed within the ventilator 102 defined by louver blades 202 and ventilator frame 200.   According to the specific implementation, frame 200 comprises four substantially planar panels 203 connected together at adjacent edges to form a hollow cuboid.

25

Referring to figure 3, an upper open face 305 of frame 200 is external facing relative to building interior 104.   The adjacent open bottom face 304 is positioned facing the building interior 104 with frame panels 203 extending through opening 105.   The louver blades 202 extend from the external facing open end 305 of frame 200 positioned external 103 to the

30   building interior 104.   Accordingly, frame 200 and louver blades 202 define an internal air flow passageway extending vertically through the ventilator comprising internal louver duct 300 positioned directly above duct 302 defined by frame 200.

Optionally, one or a plurality of internal partition walls 301 may be positioned within the frame duct 302 and/or louver duct 300 to guide the airflow through the ventilator and into the building interior 104.

5

Referring to figures 4a to 4c, each louver blade 202 comprises an inclined, substantially planar region 400 extending between an uppermost flange 401 and a lowermost flange 402, each flange 401, 402 extending over the upper and lower edges of the inclined blade region 400 respectively, when the blade is aligned substantially in the horizontal plane as

10   illustrated in figures 3 and 4A. Each flange 401, 402 is allied substantially vertically when blade 202 is aligned horizontally with each flange 401, 402 extending transverse to the inclined blade region 400. Uppermost flange 401 comprises an uppermost edge 410 and a lowermost edge 411 in contact with the uppermost edge of the inclined blade region 400. The lowermost flange 402 comprises a lowermost edge 409 and an uppermost edge 412 in

15   contact with a lowermost edge of the inclined blade region 400.

Each blade 202 comprises four inclined blade regions 403, 406, 407, 408 as illustrated in figure 4b. Each blade region is bordered by upper and lower flanges 401, 402 as illustrated in figure 4a. Each of the four blade regions 403, 406, 407, 408 and the

20   associated flanges 401, 402 are connected at their respective ends to form a square or rectangular quadrant, with each side represented by each of the four inclined blade regions.

Referring to figures 4a and 4c, each inclined blade region 400 is inclined, relative to a horizontal plane 417 by an angle θ. According to the specific implementation, θ is in the

25   region of 30 to 40°, 32 to 38° and 34 to 36° and optimally substantially 35°.

As illustrated in figure 3, each louver blade 202 is arranged on top of one another in a vertical direction above frame 200 to form the louver. In this orientation, each blade 200 is separated from a neighbouring blade, in a vertical direction by distance d. Distance d is

30   defined as the distance between the lowermost edge 409 of flange 402 of an upper blade A and the upper edge 412 of flange 402 of a neighbouring lower blade B. Distance d corresponds to the available space, in the vertical direction through which air may flow

from exterior 103 into the louver interior 300. Where each blade 202 is devoid of upper and lower flanges 401, 402 respectively, distance d corresponds to the distance between the lowermost surfaces 413 of an upper blade to the uppermost surface 414 of a lower blade.

5

Referring to figure 4c, each blade 202 comprises a leading edge 416 being external facing and a trailing edge 415 arranged internally to define louver duct 300. According to the quadrant blade arrangement of 4b, each blade comprises four leading edges and four trailing edges.

10

Alternatively, where each blade 202 is devoid of upper and lower flanges 401, 402, respectively, distance d corresponds to the distance between the leading edges of each blade A and B.

15 Referring to figure 5, louver 201 comprises an uppermost blade 500 positioned furthest from frame 200 in the vertical direction. A lowermost blade 501 sits directly on top of the uppermost open face 305 of frame 200. The present invention is configured to utilise any number of louver blades positioned intermediate 502 between upper blade 500 and lower blade 501. Ventilator 102 comprises four blades and in particular four blade quadrants

20 illustrated in figure 4b stacked on top of one another directly above frame 200.

The present invention also relates to a hybrid natural and mechanical ventilator referred to a passive-assisted natural ventilator. The hybrid ventilator utilises a low energy fan driven by a low voltage battery (not shown). The battery may be charged by a solar panel (not

25 shown) positioned at/or on top of cover 204. Alternatively the fan or battery may be coupled to a mains supply. Figure 6 illustrates a passive-assisted ventilator arrangement comprising a fan 600 having fan blades 605, the fan and blades being mounted internally within ventilator 102. Through experimental investigation, the inventors have determined that fresh air delivery rates through ventilator 102 into building interior 104 are optimised

30 with fan 600 positioned at an uppermost region the ventilator and in particular at or towards the uppermost fan blade 500 at region 601 in a vertical direction through ventilator

102. Fan 600 is positioned substantially centrally within a blade quadrant of figure 4b in the horizontal plane.

5 Frame 200 may be divided into three regions in the vertical direction, an uppermost region 602 positioned directly below lowermost fan blade 501; a lowermost region 604 and an intermediate region 603 positioned between upper and lower regions 602, 604 respectively, in the vertical direction. According to the present invention, control dampers (not shown) may be housed within lowermost frame region 604 to provide control of the airflow velocity and direction through the ventilator and into the building interior 104.

10

The inventors undertook a numerical investigation using computational fluid dynamics to determined air pressure and current velocity and in particular fresh air delivery rates through the ventilator. Figure 7 illustrates the various regions through the ventilator for which statistical airflow behaviour was investigated. In order to obtain a clear pattern of

15 the pressure and velocity profiles within the ventilator, six regions were investigated with regions 700 to 704 representing pressure and velocity in the horizontal plane at various regions spaced apart in a vertical direction through the ventilator. The pressure and velocity was also determined in the vertical plane 705 extending through the louver duct 300 and frame duct 302 referring to figure 3. Plane 700 is positioned at the top of the vent

20 in close proximity to the uppermost fan blade 500. Plane 701 is positioned at the top of the frame in close proximity to its uppermost open face 305. Plane 701 is positioned at the top of a vertex build up in the ventilator referred to as the trailing edge stall with plane 702 positioned at the bottom of this vertex. Planes 703 and 704 are positioned at the either side of the dampener region 604 in a vertical direction with plane 704 positioned in

25 close proximity to the bottom open face 304 of frame 200. The results of the pressure and velocity investigation, illustrated in figures 8 to 11, correspond to the various regions through the ventilator in which data was analysed as detailed in figure 7.

The present invention is designed to provide optimum 'comfort levels' within building

30 interior 104. This is achieved via an investigation into the variation of air velocity, pressure and density through various regions of the ventilator in response to variation of the angle θ, distance d and position of fan 600 in a vertical direction through ventilator

102. Figures 8 to 11 detail the effects of blade angle variation; figures 12 to 15 illustrate the effect of fan position within the ventilator and figure 16 illustrates the effects of louver spacing.

5 **Louver Blade Angle**

The effect of varying the blade angle on the pressure and velocity through the ventilator was determined to achieve the optimum blade angle for maximum comfort levels and in particular fresh air delivery rates into the building interior 104.

10

Referring to figure 8, air pressure data 800 was obtained at region 703; air pressure data 801 was obtained at region 704; air pressure data 802 corresponds to the pressure drop across the dampener region 604; air pressure data 803 corresponds to pressures at region 700.

15

Referring to figure 9, air velocity data 900 was obtained at region 703; air velocity data 901 was obtained at region 704; air velocity data 902 corresponds to the 'comfort level' representing the average airflow movement velocity within room interior 104; air velocity data 903 was obtained at region 700.

20

Referring to figure 10 data 1000 correspond to the air pressure verses blade angle in the vertical plane 705 with data 1001 corresponding to the air velocity in the vertical plane 705. Figure 11 illustrates the overall performance of the ventilator with data 1001 corresponding to the 'comfort level' and data 1000 and 1001 corresponding to that of

25 figures 8 and 9.

The purpose of investigation was to establish maximum air movement within a controlled volume which represents a small classroom. Utilising eight different computational fluid dynamics (CFD) models, the angle of the blades was increased by 5° each model, for a

30 range of 10° - 45°. The external wind velocity was set at 4.5 m/s, as this is the UK average wind speed.

Previous work has shown the critical role of damping on occupants' comfort levels. Accordingly data was obtained at planes 703 and 704 placed either side of the damping unit. In order for the dampers to operate effectively the pressure drop across them must be at a minimum, thus enable the unit to control accurately the rate of flow. Figure 8 show

5   the two trends of data 800 and data 801 are at their closest over a range of 28° - 37°.

Referring to figure 9, in order for the dampers to work effectively, it is desirable for the velocity drop across data 900 and data 901 to be at a minimum. This range is as expected, due to pressure and velocity being proportional, across the same values of 28° - 37°.

10

Figure 10 illustrates the average velocity and pressure across the vent against the attack angle of the blade. As the pressure inside the ventilator decreases the velocity will increase, as effectively any flow restriction is reduced. From figure 10 it is evident that at the points of intersection, the flow and pressure is at the optimum for the ventilator's

15   performance. The two points of intersection of data 1000 and 1001 are 28° and 35° respectively.

However the purpose of optimising the ventilator performance ultimately is to provide optimum comfort levels inside the occupancy area. Therefore in order to assess this

20   performance, the comfort level within the area must be shown in tandem with the ventilator's pressure and velocity profiles.

Figure 11 illustrates the scaled comfort level, pressure and velocity against the blade angle. The comfort level is scaled by a factor of ten in order for it to fit the velocity and pressure

25   profiles for comparison, this does not affect the results in any way. The plots show clearly that at the second point of intersection, 35°, the comfort level within the occupied area is at its peak.

Therefore the overall performance of the ventilator peaks at the 35°angle. Comparison of

30   the data at 35° with the benchmarked 45° blade angle shows a 45% increase in occupants' comfort level, and a 42% reduce in the trailing edge stall pressure produced. It is clear

that reduction in trailing edge stall is proportional to the increase in occupant's comfort level.

From the results it is evident that by altering the blade angle, the velocity and pressure performance is improved to desirable levels to achieve optimum occupant comfort levels. This investigation confirms that a blade angle of 35° provides optimum performance at the given parameters.

The investigation also established that the reduction in trailing edge stall is proportional to the increased velocity distribution within the occupied space. This connection is established as the removal of such restrictive pressure allows a free flow through the ventilator, and is pivotal to the operation of the control mechanism, namely the damper unit.

Ventilator Fan Position

The location of fan 600 within ventilator 102 was examined. It has been found that even at low pressure, the air supply rate through the ventilator is excessive which would cause control dampers located within region 604 to work harder in order to dampen the airstream into the building interior 104. The effects of increasing the use of the control dampeners increases the energy consumption of ventilator 102 which is undesirable.

Figure 12 illustrates the ventilator 102 with fan 600 positioned at an upper region of the ventilator in close proximity to uppermost fan blades 500. Fan 600 is operative to assist the airflow current in a downward direction 1200 though the internal duct of the ventilator 300, 302. The airflow stream 1201 continues out of the bottom face 304 and into building interior 104 and then circulates 1202 through interior 104 and exits this interior 1203 as the airflow current circulates between exterior 103 and interior 104. Importantly, due to the creation of the airflow profile within the ventilator 100 by fan 600 positioned at uppermost louver blade 500, stale air 1203 from interior 104 is capable of exiting the ventilator via flow path 1205 between louver blades 202.

Figure 13 illustrates the ventilator of figure 12 with fan 600 positioned at a more central region corresponding to region 602 illustrated in figure 6. In this arrangement, fan 600 creates a strong airflow stream 1300 and 1301 in a substantially vertically direction into interior 104. Stale air 1302 re-enters the ventilator via open face 304. However, this stale

5   air 1302 is then directed 1303 into the airflow suction path created by fan 600 to be reintroduced into interior 104 via airflow path 1300. This diversion of the airflow path 1303 is caused by the airflow currents created within the louver region due to this mid fan position.

10   Figures 14 illustrates a similar arrangement to figures 12 and 13 albeit with fan 600 positioned at a lowermost part of ventilator 102 corresponding to region 604 of figure 6. In this position, a strong airflow current is created 1400, 1401 in a vertical direction within interior 104. Stale air 1402 then re-enters the ventilator via open face 304 and is redirected at 1405 into the suction airflow path created by fan 600. As with the

15   arrangement of figure 13, stale air 1303, 1405 is presented from escaping from the ventilator 1205 (referring to figure 12) due to the turbulence created within the louver region 201 by the relative fan position.

The fan position also has an affect upon the airflow at environment 103 into louver duct

20   300. Referring to figure 12, with fan 600 at an uppermost position, clean air is capable of flowing into the ventilator 1204 over the entire height of the blade stack. In contrast, and referring to figures 13 and 14, the fresh air supply 1304, 1403 into the ventilator is perturbed by the eddy currents created within ventilated duct 300. With fan 600 positioned at its lowest most orientation of figure 14, the fresh air supply is prevented from

25   entering the ventilator 1404 due to the turbulence within louver duct 300. In the orientations of figures 13 and 14, there is no clear area through which the exhaust air may exit the ventilator and according it is re-circulated within interior 104 by the effective fan pressure.

30   Figure 15 illustrates the total fresh air delivery rates supplied by ventilator 102 for the three fan positions of figures 12, 13 and 14. Data 1500, 1501 and 1502 correspond to fan 600

positioned at the top (figure 12), middle (figure 13) and bottom (figure 14), of ventilator 102, respectively.

The British Standard (BS) minimum fresh air delivery rates are specified as 0.8 L/sec per

5   m² and 5 L/sec per occupant. The occupancy level for this investigation was 20 occupants which is the recommended level for a small classroom. According to the present investigation, when the external wind velocity is 1m/s ventilator 102 does not meet the criteria for the amount of fresh air per occupants and therefore the passive ventilator 102 requires assistance.

10

A total of 18 CFD models were created covering a pressure range of 20 - 120 Pa, in three different locations. The results show that in each of the three locations of figures 12 to 14, a fan pressure of 20Pa assists the external wind velocity (1 m/s) to achieve the BS criterion.

15

The fan in the top position of figure 12 creates the smallest increase in fresh air supply from 4.5 to 18.5 L/sec per occupant at a fan pressure of 20 Pa. The flow visualisation of these results (figure 15) shows that the fan draws in fresh air whilst allowing the receiving room's exhaust air to exit via two channels 1205 either side of the fan.

20

The fan in the middle and bottom positions of figures 13 and 14, respectively, shows very similar results in terms of fresh air supply rate. Both give considerable improvements of 111 and 11.5 L/sec respectively. The flow visualisation of these results show that for the middle fan position (figure 13) the fresh air (external) is restricted in one quadrant, and the

25   exhaust air (room internal) has no natural path 1303 to exit ventilator 102. Figure 14 illustrates that at the bottom fan position, the restriction is in both quadrants 1405 and again there is no return path for the exhaust air.

The flow delivery rate results of figure 15 for the middle and bottom fan position show that

30   although the rate at which the air is delivered into the room has increased, little fresh air is drawn into the room. Instead, the air is being re-circulated by the fan in these two positions and therefore the ventilator does not meet the fresh air delivery rate requirements.

From the results, it was clear that a low voltage fan would need to produce a minimum pressure of 20 Pa to achieve the BS required minimum ventilation rates. The fan should be located in the top position to ensure fresh air is drawn in at low external wind speeds (1

5 m/s) and delivered to the receiving room without restricting the exhaust air flow path.

Louver Blade Separation Distance

By changing the external distance of separation between the closest regions of adjacent

10 louver blades 202 (distance d) illustrated in figures 4c and 5, the rate at which fresh air is delivered into the building interior is affected. The undesirable affects of increasing the louver blade spacing are twofold:

  i breakthrough noise from external sources enters the ventilator 102 and hence the building interior 104; and

15 ii rain ingress, wind may be driven into the ventilator duct 300 and into building interior 104.

The objective therefore is to optimise louver spacing to give the lowest possible distance to reduce breakthrough noise and rain ingress whilst acceptable fresh air delivery rates are

20 provided through the ventilator. Figure 16 illustrates experimental results with data 1600 corresponding to the velocity of air through the ventilator, data 1602 corresponds to the pressure of air through the ventilator and data 1601 corresponds to the 'comfort level' being the air movement rate within the building interior 104.

25 As illustrated in figure 16, a maximum 'comfort level' is observed for a louver spacing (d) of 30 mm. Importantly, reducing the louver spacing has therefore been found to match the observed air movement rate within interior 104 in addition to reducing breakthrough noise and the likelihood of rain ingress into ventilator 102.

30

Claims:

1.   A building ventilator comprising:

a frame mountable at an opening in a roof of a building, the frame defining a duct to convey air between an exterior and an interior of the building;

5   a plurality of vent blades mountable at an external facing region of the frame such that the blades are mounted at the exterior of the building and are stacked above one another to form a louver, each blade having a leading edge to be external facing relative to the duct and a trailing edge to be internal facing relative to the duct;

wherein each blade between the leading edge and trailing edge is inclined relative

10   to a horizontal plane at an angle in the range 30 to 40°

2.   The ventilator as claimed in claim 1 wherein the angle of inclination is in the range 32 to 38°.

15   3.   The ventilator as claimed in claim 1 wherein the angle of inclination is in the range 34 to 36°.

4.   The ventilator as claimed in claim 1 wherein the angle of inclination is in the range 35°.

20

5.   The ventilator as claimed in any preceding claim comprising internal walls mounted within the frame, the internal walls configured to partition the duct in the longitudinal direction between the interior and exterior of the building.

25   6.   The ventilator as claimed in any preceding claim wherein the frame is cuboid shaped comprising four walls extending between an open top face and an open bottom face, the top face arranged to be facing the exterior of the building and the bottom face arranged to be facing the interior of the building.

30   7.   The ventilator as claimed in claim 6 wherein the blades are mounted on the top face and extend externally of the building away from each of the four walls of the frame.

8.   The ventilator as claimed in any preceding claim wherein the blades are linear.

9.   The ventilator as claimed in claim 7 wherein four blades are arranged in the same plane and are joined at each end to a neighbouring blade to define the edges of a rectangle.

10.   The ventilator as claimed in claim 7 wherein four blades are arranged in the same plane and are joined at each end to a neighbouring blade to define the edges of a square.

11.   The ventilator as claimed in any preceding claim wherein the blades are stacked vertically above one another and the frame.

12.   The ventilator as claimed in any preceding claim further comprising a cover member configured to sit above an uppermost blade and block an external facing end of the duct.

13.   The ventilator as claimed in any preceding claim wherein each blade comprises a flange extending from the leading and trailing edge, each flange orientated transverse to the plane of the blade.

14.   The ventilator as claimed in any preceding claim wherein the blades are mounted above one another to form a louver, the louver comprising between four to six blades.

15.   The ventilator as claimed in any preceding claim wherein the blades are mounted above one another to form a louver, the louver comprising four blades.

16.   The ventilator as claimed in any preceding claim wherein a distance in the vertical direction between adjacent blades is in the range 25 to 35 mm.

17.   The ventilator as claimed in any preceding claim wherein a distance in the vertical direction between adjacent blades is 30 mm.

18. The ventilator as claimed in any preceding claim comprising a fan mounted within the louver region of the device defined by the stack of blades substantially towards the blade positioned furthest from the external facing end of the frame.

5 19. A building ventilator comprising:

a frame mountable at an opening in a roof of a building, the frame defining a duct to convey air between an exterior and an interior of the building;

a plurality of vent blades mountable at an external facing region of the frame such that the blades are mounted at the exterior of the building and are stacked above one

10 another to form a louver, each blade having a leading edge to be external facing relative to the duct and a trailing edge to be internal facing relative to the duct;

wherein the distance in the vertical direction between adjacent blades at the their respective leading edge regions is in the range 25 to 35 mm.

15 20. The ventilator as claimed in claim 19 wherein the distance between adjacent blades is in the range 27 to 33 mm.

21. The ventilator as claimed in claim 19 wherein the distance between adjacent blades is 30 mm.

20

22. The ventilator as claimed in any one of claims 19 to 20 wherein the louver comprises four blades positioned above one another.

23. The ventilator as claimed in any one of claims 19 to 22 wherein the frame is

25 cuboid shaped comprising four walls extending between an open top face and an open bottom face, the top face arranged to be facing the exterior of the building and the bottom face arranged to be facing the interior of the building.

24. The ventilator as claimed in claim 23 wherein the blades are mounted on the top

30 face and extend externally of the building away from each of the four walls of the frame.

25. A building ventilator comprising:

a frame mountable at an opening in a roof of a building, the frame having an exterior facing end and an interior facing end to define a duct there between to convey air between an exterior and an interior of the building;

a plurality of vent blades mountable at the exterior facing end of the frame, the blades mounted above one another to form a louver; and

a fan mounted within the louver region of the device defined by the stack of blades substantially between a lowermost blade and an uppermost blade in the vertical direction.

26.   The ventilator as claimed in claim 25 wherein the fan is mounted within the louver region of the device towards the blade positioned furthest from the external facing end of the frame in the vertical direction.

27.   The ventilator as claimed in claims 25 or 26 wherein the fan is mounted within the louver region of the device substantially in the same horizontal plane as the blade positioned furthest from the external facing end of the frame in the vertical direction.

28.   The ventilator as claimed in any one of claims 25 to 27 wherein the fan is mounted centrally within the louver region of the device in the horizontal plane.

29.   The ventilator as claimed in any one of claims 25 to 28 wherein the duct is devoid of internal partitions extending in the vertical direction between the exterior and interior facing ends.

30.   The ventilator as claimed in any one of claims 25 to 29 further comprising electronic control means to provide manual and/or automatic control of the fan.

31.   The ventilator as claimed in any one of claims 25 to 30 wherein the fan comprises an electric motor.

32.   The ventilator as claimed in any one of claims 25 to 31 wherein the frame is cuboid shaped comprising four walls extending between an open top face and an open

bottom face, the top face arranged to be facing the exterior of the building and the bottom face arranged to be facing the interior of the building.

Abstract

A natural ventilator for a building configured to supply optimum rates of fresh air into a
building interior.   The ventilator is optimised with regard to spacing between vent blades
of the louver and the angle of inclination of each blade relative to a horizontal plane.   An
active-passive natural ventilator is also provided comprising a low power fan to assist the
rate of fresh air delivery through the ventilator.   The position of the fan within the
ventilator is optimised with the fan positioned at an uppermost region and internal of the
louver.

Figure 6

Report

www.bsria.co.uk

Acoustic Testing of Midtherm Windvent Terminal

Report 51914A
April 2008

Carried out for: **Midtherm Engineering Ltd**
New Road
Netherton
Dudley
West Midlands
DY2 8SY

Compiled by: Andrew Coulson

Quality Approved: *Colin Pearson*

SUMMARY

An acoustic test of a Wind-Driven Natural Ventilation System was conducted on behalf of Midtherm Engineering Ltd at Sheffield Hallam University, Psalter Lane Campus. The objective was to identify the effects on sound level in a room from installing such a device. It was found that the ventilation system raised the noise level 3.2dBA above ambient levels.

CONTENTS

APPENDICES

TABLES

FIGURES

1   INTRODUCTION

An acoustic test at Sheffield Hallam University was conducted by Andrew Coulson of BSRIA on 11th April 2008. The objective was to measure the effect of installing a Wind-Driven Natural Ventilation System on noise breakthrough from outside.

This report presents the sound level data in decibels recorded during the survey. The effect of the Ventilation System on sound level is also highlighted and discussed.

The following BSRIA publication provides useful background information:

PARKER J, TEEKARAM A. Wind –Driven Natural Ventilation Systems. BG 2/2005. BSRIA. 2005. ISBN 0 86022 647 6.

1.1   GENERAL METHODOLOGY

The ventilation device had been installed on the roof of a building on Psalter Lane Campus, part of Sheffield Hallam University. This provided ventilation to a room on the upper level of the building. For the purposes of this test it was necessary to simulate the effect of no ventilation device being present. In order to achieve this the damper was closed and the ventilator terminal section sealed with insulation material for alternate half hour periods. (See **Figure 1**)

Figure 1: Showing how the terminal was sealed with insulation material

A sound level meter, CEL-480 Version 2.1 serial number 032770, with octave-band measuring capability was used to monitor the sound level in the room, the total measuring time being 5 hours. Firstly, the sound level in the room was measured with the Ventilation System in full operation and the dampers set to the fully open position. (See **Figure 2**)

Figure 2: Shows the unobstructed terminal

The sound level meter was then calibrated at 113.6dB and placed in the centre of the room 1.5m above the floor (See **Figure 3**). The device was set to monitor the full octave band range in a time period of 5 minutes. This process was repeated for 30-minutes.

Figure 3: Shows the set up of the sound level meter in the room

The damper was then closed (See **Figure 4**) and the ventilator terminal section sealed (as in **Figure 1**).

Figure 4: Shows the ventilation system with the damper in the closed position

With the sound level meter in the same position in the room another set of measurements was taken for 30 minutes.

The process was repeated 4 times with the position of the sound level meter in the room varied. For the final 30-minute measurement only the ventilation dampers were closed, with no insulation being applied to the terminal section. All detector positions with their corresponding measurement numbers are shown in **Figure 5** below.

Figure 5: Shows the various detector positions with corresponding measurement numbers in the room. (All dimensions are in cm)
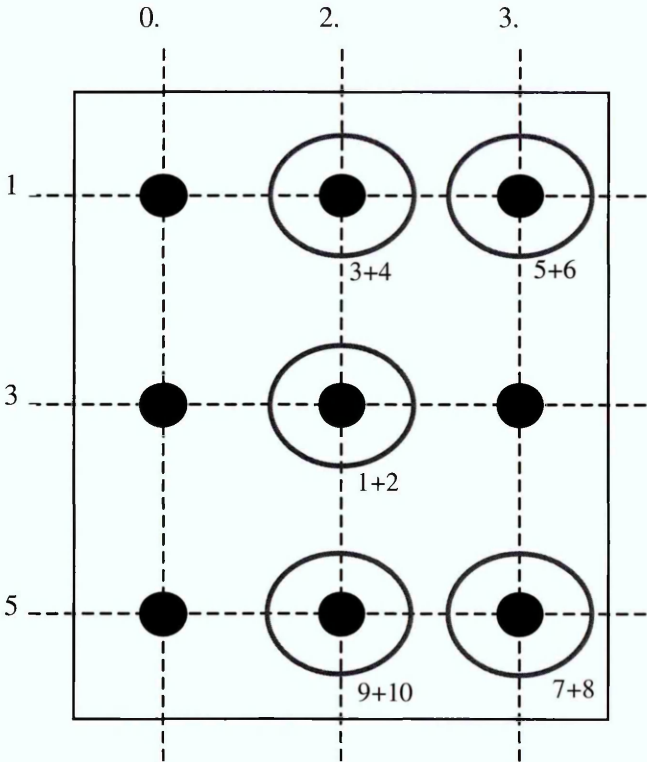
1.1.1 A-weighting

The A-weighting curve is one of a set of four, defined in various standards relating to sound level measurement as A, B, C, and D. Curves A, B and C are for low, medium and high loudness sounds. D is specifically for measuring very loud aircraft noise.

The A-weighing curve is based on the 40-phon equal-loudness contour for typical human hearing, being a rough approximation of that curve after inversion to indicate gain rather than level. 40 phon is the sort of level likely to exist in a normal quiet environment similar to the conditions involved in this test.

1.1.2 Equivalent sound level Leq

The dominant characteristic of environmental noise is that it is not steady-at any particular location the noise usually fluctuates considerably from quiet at one instant to loud the next. Thus, one cannot simply say that the noise level at a given location or that experienced by a person at that location is "so many decibels" unless a suitable method is used to average the time-varying levels.
Equivalent Sound Level is formulated in terms of the equivalent steady noise level which in a stated period of time would contain the same noise energy as the time-varying noise during the same time period. This is most relevant to the realms of human hearing.

2 RESULTS AND DISCUSSION

Table 1 presents the average sound level difference in dBA Leq between consecutive 30-minute measurements. The final sound level difference was calculated by taking the mean of all the differences. During the test some of the measurements were affected by rainfall. In order to prevent any anomalies they were eliminated from the results. In this case the average sound level difference was found to be 3.2dBA. This means that installing a Ventilation System should result in a 3.2dBA increase above normal sound levels.

Another comparison can be made by averaging the sound level at each frequency band. This is presented in **Graph 1**. This illustrates how the sound level is increased across the frequency range. As expected, the sound level with the damper closed and terminal sealed is lower than with the damper open.

For the final measurement only the damper was closed. This highlighted the possibility of sound level reduction after installation of a Ventilation System device by simply closing the damper.

Table 2 shows a sound level difference of 4dBA. This shows that for conditions involving no rainfall and wind speeds averaging 6m/s sealing the terminal causes no further sound reduction and that closing the dampers effectively negates the presence of the wind catcher.

Table 1: Shows the sound level difference between consecutive measurements

Measurement Number	Sound Level (dBA Leq)	Difference
1	32.3	2.8
2	29.5	
3	33.2	3.5
4	29.7	
5	30.8	3.6
6	27.1	
7	33.6	2.2
8	31.4	

Graph 1: A comparison of average sound level at each frequency band
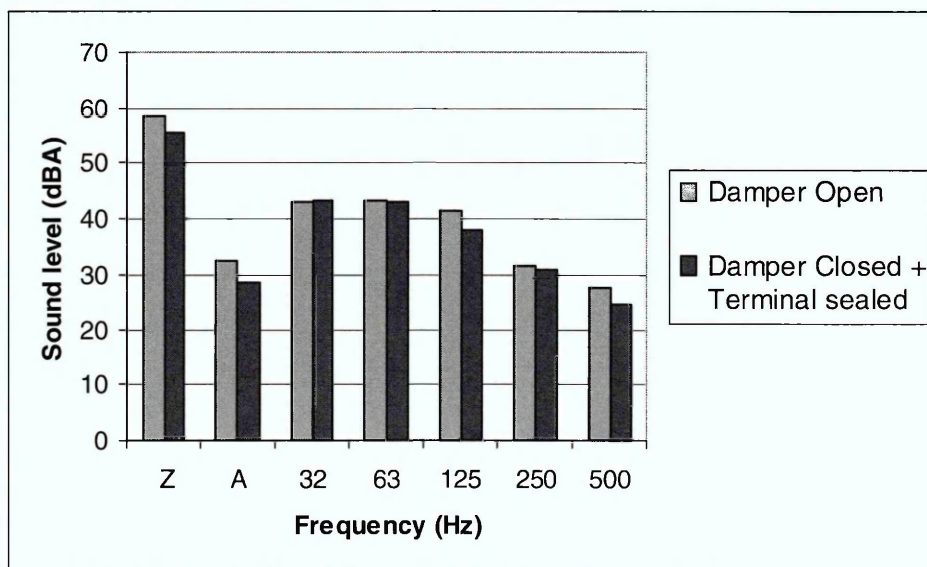
Table 2: Shows the sound level difference between damper open and damper closed conditions

Measurement Number	Sound Level (dBA Leq)	Difference
9	32.6	4.0
10	28.6	

2.1.1 External noise level

The external noise level was not measured for the full duration of the test, but is likely to have been between 58 and 62dBA at the inlet to the ventilator. It would have been about 2dB higher at street level

APPENDICES

Appendix: A   Test Summary

Measurement Number	Time	Cover on/off	Note A weighted reading dB	Calibration (dBA)	Wind speed	Wind direction
1	10:10	Off	32	113.6	6.5	SSE
2	11:02	On	29.5	113.6	4.6	N
3	11:47	Off	38.4	113.6	4.5	ESE
4	12:30	On	30	113.6	4.7	S
5	13:10	Off	32	113.6	5	SSW
6	13:50	On	27	113.6	5.6	NE
7	14:30	Off	33	113.6	6	SW
8	15:09	On	31	113.6	6.7	S
9	15:48	Off	32	113.6	4.2	WNW
10	16:23	On	28	113.6	7.7	WSW

TEST CERTIFICATE

Issued By BSRIA Instrument Solutions

Date of Issue 18 March 2008

Certificate Number
TR07175

Page 1 of 3 Pages
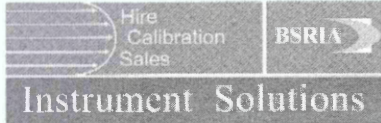
BSRIA Instrument Solutions
Old Bracknell Lane West, Bracknell, Berkshire RG12 7AH UK
Tel: +44 (0) 1344 459314 Fax: +44 (0) 1344 714868
e mail: info@bis.fm   website: www.bis.fm

COPY

Customer : BSRIA Instrument Solutions
Old Bracknell Lane West, Bracknell
Berks RG12 7AH

Date Received : 19 November 2007

Instrument -	System ID :	200550	Job Number : H14853
	Description :	Environmental Noise Meter	Ref. Number : 200550
	Manufacturer :	CEL	
	Model Number :	480.C1 Kit	
	Serial Number :	032770	Last Certificate Number : TR06969
	Procedure Version :	5F17V2/T	Last Calibration Date : 11/02/2008

Environmental Conditions

Temperature :   23"C +/- 4"C
Relative Humidity :<70% +/- %

Mains Voltage :   240V +/- 10V
Mains Frequency : 50Hz +/- 1Hz

Comments

Unless otherwise stated all readings are made at 1kHz Lin.

Pre Amplifier S/N = 4/02225057

Ambient Conditions. Baro Pressure 1013.2 mbar. Temperature 21.4 °C

2510

Traceability Information

Instrument description	Serial number	Certificate number	Cal. Date	Cal. Period
Bruel & Kjaer 4226 Acoustic Calibrator	1551580	15419	28/09/2006	104

Tested By : A. Lennard   **Date of Test :** 18 March 2008

This certificate provides traceability of measurement to recognised National Standards, and to the units of measurement realised at the National Physical Laboratory or other recognised National Standards laboratories.
Copyright of this certificate is owned by the issuing laboratory and may not be reproduced except with the prior written approval of the issuing laboratory.
This certificate complies with the requirements of BS EN ISO 10012:2003.

TEST CERTIFICATE

Test Title	Tolerance	Applied Value	Reading	% Of Spec.
CONTENTS				
Sound Level Meter	---	---	Pass	
Batteries, AA, x8	---	---	Pass	
CEL-284/2 Calibrator	---	---	Pass	
Batteries, PP3, x2	---	---	Pass	
Software Disc, x2	---	---	Pass	
Comms Lead	---	—	Pass	
Power Supply	---	---	Pass	
Wind Muff	---	---	Pass	
Tripod	---	---	Pass	
Case	---	---	Pass	
Manual	---	---	Pass	
Certificate	---	---	Pass	
ELECTRICAL SAFETY				
Power Supply	---	---	Pass	
Inspection Results And Power Supply Functional Test.				
Sound Level Meter	---	---	Pass	
Sound Calibrator	—	---	Pass	
Power Supply, Test	---	---	Pass	
Battery Check	---	---	Pass	
SOUND LEVEL METER DEFAULT SETUP				
Default Fact Setup	---	---	Pass	
Date / Time Set	---	---	Pass	
Backlight = 5secs	---	---	Pass	
Microphone = Free	---	---	Pass	
Memory Cleared	---	---	Pass	
CALIBRATION CONFIRMATION				
Calibration Check	---	---	Pass	

Uncertainties

Sound Level   ±0.5 dB
An additional uncertainty of 1 least significant digit shall also apply.

TEST CERTIFICATE

Test Title	Tolerance	Applied Value	Reading	% Of Spec.

CALIBRATION RESULTS, SOUND LEVEL METER

Broad Band Mode

Range, 30 to 100dB	1.1dB	94.0dB	94.0dB	0%
Range, 40 to 110dB	1.1dB	94.0dB	94.1dB	9%
Range, 50 to 120dB	1.1dB	114.0dB	114.1dB	9%
Range, 60 to 130dB	1.1dB	114.0dB	114.0dB	0%
Range, 70 to 140dB	1.1dB	114.0dB	114.1dB	9%

A WEIGHTING, FAST RESPONSE, 50 - 120dB RANGE

94dB @ 125Hz	1.5dB	77.9dB	78.0dB	7%
94dB @ 4kHz	1.6dB	95.0dB	94.9dB	6%

C WEIGHTING, FAST RESPONSE, 50 - 120dB RANGE

94dB @ 125Hz	1.5dB	93.8dB	93.8dB	0%
94dB @ 4kHz	1.6dB	93.2dB	94.4dB	75%

OCTAVE MODE, 40 to 110dB Range

31.5Hz	1.5dB	94.0dB	93.9dB	7%
62.5Hz	1.5dB	94.0dB	94.0dB	0%
125Hz	1.5dB	94.0dB	93.9dB	7%
250Hz	1.4dB	94.0dB	93.9dB	7%
500Hz	1.4dB	94.0dB	94.0dB	0%
1kHz	1.1dB	94.0dB	94.1dB	9%
2kHz	1.6dB	94.0dB	94.5dB	31%
4kHz	1.6dB	94.0dB	94.3dB	19%

Above tolerances are those as stated in IEC61672 For a Type 1 Sound Level Meter.

TEST RESULTS, ACOUSTIC CALIBRATOR

CEL-284/2 Calibrator	1.1dB	114.0dB	114.0dB	0%

------------------------ END OF DATA ------------------------

COPY

Uncertainties

Sound Level   ±0.5 dB
An additional uncertainty of 1 least significant digit shall also apply.

List of Tables